The role of brown algal cell walls in morphogenesis and development

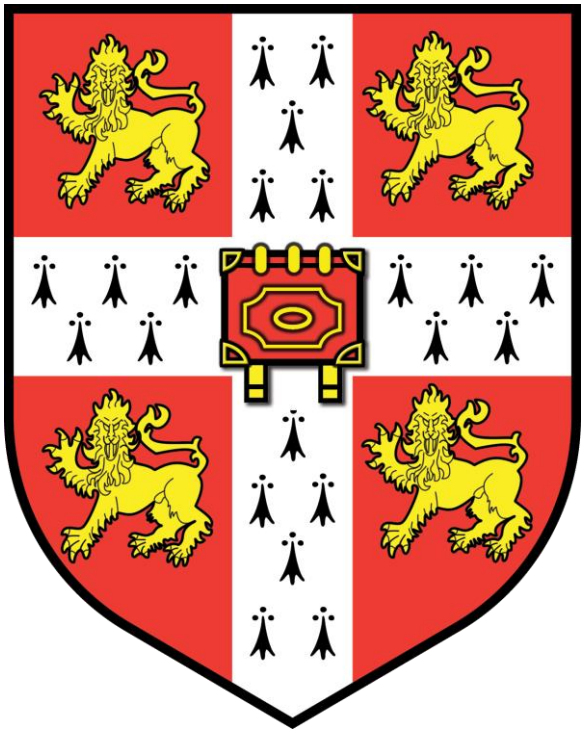

Marina Linardić

Downing College

April 2018

This dissertation is submitted for the degree of Doctor of Philosophy

Summary

Name: Marina Linardić

Thesis title: The role of brown algal cell walls in morphogenesis and development

Morphogenesis in walled organisms represents a highly controlled process by which the variability of shapes arises through changes in the structure and mechanics of the cell wall. Despite taking different evolutionary paths, land plants and some brown algae exhibit great developmental and morphological similarities.

In two brown algal model systems: the *Sargassum muticum* apex and the *Fucus serratus* embryo, I have used a combination of imaging techniques, growth analyses, surgical and pharmacological treatments, as well as molecular, biochemical and mechanical approaches to characterise the growth patterns and the cell wall contribution to shape change.

To understand how the adult algal body is formed, I examined the branching strategy (phyllotaxis) in *S. muticum*. My results suggest that in *S. muticum* the spiral phyllotactic pattern and the apical cell division pattern are not linked. The phytohormone auxin and the biochemical changes of the cell wall do not seem to be correlated with the bud outgrowth, contrary to observations in plants. In summary, these results suggest *Sargassum* convergently developed a distinct growth mechanism with similar shape outcome as observed in plants.

This dissertation is one of the first attempts to explore cell wall mechanics in brown algal development and its correlation with underlying cell wall biochemistry utilising the *Fucus* embryo as a known system. The results suggest a correlation between the wall mechanics and alginate biochemistry with the growing and non-growing regions of the embryo. In addition, altering cell wall deposition or composition has a strong effect on embryo rhizoid elongation and is, in certain cases, accompanied by significant increase in cell wall stiffness and reduction of alginate epitopes. Furthermore, preliminary results exploring

transcriptomic changes during development indicate differential expression of particular alginate biosynthesis enzymes (mannuronan C5 epimerases) during development, suggesting alginate conformational modifications might be stage specific.

These results contribute to the current knowledge addressing the importance of cell walls in brown algal development using novel tools and approaches. Understanding developmental processes in brown algae will provide a better insight how similar morphogenetic traits are established using different body-building mechanisms.

This dissertation is the result of my own work and includes nothing which is the outcome of work done in collaboration except where specifically indicated in the text.

I further state that no substantial part of my dissertation has already been submitted, or, is being concurrently submitted for any such degree, diploma or other qualification at the University of Cambridge or any other University or similar institution except as declared in the Preface and specified in the text.

It does not exceed the length limit of 60,000 words set by the Degree Committee for the Faculty of Biology.

- Marina Linardić, 2018

Acknowledgments

Firstly, a big thank you to my supervisor Dr Siobhan Braybrook – for giving me the opportunity to explore the interesting developmental side of brown algae and for all the support through the ups and downs during this three-year long process.

To Prof Alison Smith – thank you for all the useful discussions and your support in the final moments of my PhD.

Thank you to the whole Braybrook group: Louis, Giulia, JJ, Rozi, Firas, Marco, Tom, Joanna and Adi – for all the valuable discussions (scientific and non-scientific), help in the lab and always-needed short coffee breaks.

Science is best made in collaboration – I would like to thank the Phycomorph members for all the valuable discussions, advice and suggestions during workshops and conferences I attended. To Anna – thank you for all the help with the RNA sequencing analysis.

To Downing College – thank you for all the financial support during my studies. It was a great honour to be a recipient of a studentship that honours two great minds in the field of algal research, Ralph Lewin and Felix E Fritsch.

To the Cambridge bunch: Nadine, Claire, Tessa, Thomas, João, Fabricio, Chris, Clément and Tom – thank you for the amazing three years I have shared with you in this beautiful place, all the many adventures we had (and will have!), all the tears and laughter along the way. You all hold a special place in my heart.

To my Biokolektiva: Petra, Zrinka, Maja, Sanya and Franka – this is what all those all-nighters were leading to. Thank you for being here for me along the way.

To Mateja, Stela and Karmen – thank you for such a genuine friendship and support in every aspect of my life.

And finally, to my family, Zoran, Nikica and Ivana – these past three years, and all the moments that led me to where I am today, would not have been possible if it weren’t for your unconditional love and support.

Table of Contents

List of Figures

List of Tables

List of abbreviations

10dAF	10 days after fertilisation
2, 4-D	2, 4- Dichlorophenoxyacetic acid
24hAF	24 hours after fertilisation
72hAF	72 hours after fertilisation
AC	apical cell
AFM	atomic force microscopy
AGP	arabinogalactan protein
AIR	alcohol insoluble residue
ANOVA	analysis of variance
ASW	artificial seawater
BAM	brown algal monoclonal (antibody)
BLAST	Basic Local Alignment Search Tool
BSA	bovine serum albumin
cDNA	complementary DNA
CesA	cellulose synthase A
DMSO	dimethyl sulfoxide
DNA	deoxyribonucleic acid
EGTA	ethylene glycol-bis(β-aminoethyl ether)-N,N,N',N'-tetraacetic acid
ELISA	enzyme linked immunosorbent assay
FITC	fluorescein isothiocyanate
FRAP	fluorescence recovery after photobleaching
G	guluronic acid
GMD	GDP- mannose 6-dehydrogenase
IAA	indole-3-acetic acid
LR	London resin

M	mannuronic acid
MPI	mannose-6-phosphate isomerase
MC5E	mannuronan C5 epimerase
NAA	1-Naphthaleneacetic acid
NCBI	National Center for Biotechnology Information
PBS	phosphate buffered saline
PMM	phosphomannomutase
qPCR	quantitative polymerase chain reaction
RNA	ribonucleic acid
ROI	region of interest
RT	room temperature
RT-PCR	reverse transcription polymerase chain reaction
TMM	trimmed mean of M-values
TPM	transcripts per million transcripts
UV	ultraviolet

Publications

Linardic M, Braybrook S A (2017) Towards an understanding of spiral patterning in the *Sargassum muticum* shoot apex**.** Sci Rep. 7: 13887, DOI:10.1038/s41598-017-13767-5

The published paper was co-written by M. Linardic and S. Braybrook. All experiments were performed by M. Linardic.

Torode TA, **Linardic M**, Kaplan JL, Braybrook SA (2018) AFM-based analysis of cell wall mechanics in macroalgae. In: Methods in Macroalgae, Eds. Charrier, B and Reddy CRK. CRC Taylor & Francis.

M. Linardic performed AFM experiments and analysis for *F. serratus* embryos and reviewed the manuscript.

Chapter 1. Introduction

Morphogenesis represents a set of highly controlled processes by which the shapes of organisms arise. The formation of shapes constitutes an extremely interesting phenomenon, since the presence of similar shapes might be found in very distant evolutionary lineages (e.g. plants and brown algae). This might imply a shared mechanism between these lineages to achieve similar structural solutions using a different approach to defined growth. The basis of growth has been of interest in the field of developmental biology. A morphogen-based growth has been explored in plant systems (Reinhardt et al., 2003a). In addition, a physical basis of plant growth has recently been investigated. This discusses the relationship between cellular shape changes, the corresponding pattern of stresses in the tissues, and morphogenesis. It seems that, in plant organisms at least, the mechanical perception of growth can regulate morphogenesis patterns (Sampathkumar et al., 2014). Because of these interesting phenomena, the exploration and correlation of morphological homoplasy in developmental decisions of brown algae and plants presents an interesting question to address.

1.1. Brown algae – independent evolution of multicellularity

Brown algae are a group of multicellular photosynthetic organisms which mostly inhabit marine environments. They can be found in the intertidal belt and upper littoral regions of colder waters, particularly in the Northern Hemisphere, where they represent one of the most important marine habitats acting as shelter, nursery and hatchery for many marine animals (e.g. kelp forests; Leblanc et al., 2011; Steneck et al., 2002). For example, kelp forest ecosystems together with all the associated biota (animals and epiphytes) represent one of the most diverse ecosystems on the planet (Mann, 1973).

The brown algal lineage currently has 2098 species classified in 285 genera and 20 orders (de Reviers et al., 2007; Guiry and Guiry, 2017). In the past few

decades, phylogenetic studies of brown algae have tried to resolve the evolutionary relationships between different orders of this group (Fig. 1.1A). Studies of specific conserved sequence data have shown that orders such as Dictyotales, Sphacelariales and Syringodermatales diverged early in evolution. However, ten orders (e.g. Ectocarpales, Laminariales, Fucales; Silberfeld et al., 2010) were clustered closely together without the ability to distinguish between their phylogeny. Their likely polytomic nature (phylogenetic node with multiple branching points) is referred to as brown algal crown radiation (BACR; de Reviers and Rousseau, 1999). The question of the divergence of the BACR orders has been addressed recently and the majority of relationships within this group have been investigated (Silberfeld et al., 2010; Fig. 1.1B). This study looked into evolutionary paths in the BACR orders with a higher resolution; 72 taxa and 10 genes analysed. However, only four clades could be distinguished within 10 orders examined: Desmarestiales clade, Sporochnales/Scytothamnales/ *Bachelotia* clade, Ectocarpales/Laminariales clade and Fucales/Nemodermatales/ Tilopteridales/Ralfsiales clade. The parenchymatous organization (where the initial meristematic cell or group of cells produces the body through its divisions) is likely to have appeared in a common ancestor of parenchymatous BACR species. This hypothesis is valid for all the species besides Fucales; both of the model species in this thesis belong to two families of this order, Fucaceae and Sargassaceae. To date, it is not possible to determine whether the apical organisation in the Fucales was secondarily gained as a homoplasic characteristic or from a BACR ancestor.

While the evolutionary history of the brown algae is still questioned today, it is firmly established that they are very distant from other walled, photosynthetic, organisms such as the Viridiplantae (land plants and green algae). They are estimated to have appeared around 200 million years ago (Silberfeld et al., 2010). The distance between brown algae, Viridiplantae and red algae is best illustrated by considering the origin of their photosynthetic capacity: land plants, green and red algae appeared after a primary endosymbiotic event took place (combining a free living cyanobacterium and heterotrophic eukaryote) whereas a secondary endosymbiotic event (red alga engulfed by an ancestral unicellular heterotrophic eukaryote) gave rise to the brown algal branch (Reyes-Prieto et al., 2007; Yoon et al., 2004). Brown algae represent one of the five major lineages (with red algae,

plants (including green algae), fungi and metazoans) that have developed a multicellular body organization, independently from other species (Charrier et al., 2012; Silberfeld et al., 2010). An independent evolutionary path makes the comparison of morphogenesis on a physical level highly interesting; while the phylogenetic branches are divergent between brown algae and plants, a similar physical set of rules might have to be maintained.

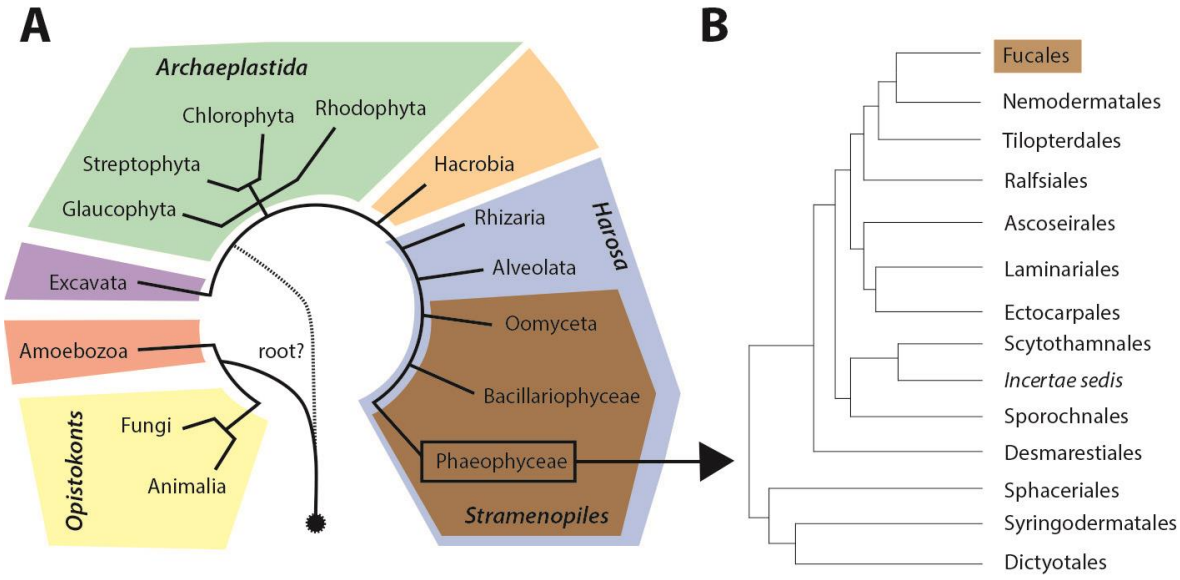

Figure 1.1. Evolutionary position of brown algae within the eukaryotic tree of life. (A) Phylogenetic relationships between Opisthokonta, Amoebozoa, Excavata, Archaeplastida, Hacrobia and Harosa (Stramenopiles–Alveolates–Rhizaria - SAR). Adapted from Charrier et al., 2012. (B) Relationships between 14 out of 20 brown algal orders. Order Fucales (highlighted in brown) contains both of the species examined in this thesis (*Fucus serratus* and *Sargassum muticum*). Adapted from Silberfeld et al., 2010.

1.2. Shape formation in brown algal lineage

Among all of the algal groups (green, red and brown), the brown algae have the biggest diversity in size and shape, from filamentous to 'complex' thalli (bodies) (Charrier et al., 2012). The thallus of a 'complex' alga (parenchymatous; e.g. Laminariales and Fucales) can be divided into 3 main regions. The holdfast represents an "anchor" of the alga, which attaches to the substrate (surface, such as rock or sand; Fig. 1.2A, C). This region serves purely as a means to keep the alga attached and does not have a root-like function, so is not involved in uptake of

nutrients/water. The stipe is the second structure and it serves as the ‘stem’ of the alga (Fig. 1.2A, B). The third part is the frond (blade/lamina; Fig. 1.2A, B). In Fucales, the frond changes into reproductive ‘tissue’ (receptacles) during the reproductive season which holds special bodies (conceptacles) filled with male and/or female gametes (Fig. 1.2D, E). Another addition in the frond that can be observed in several species are the air bladders – air filled structures with the role of maintaining the upward position of the algae whilst in the water column (Fig. 1.2F).

Complex multicellularity in parenchymatous brown algae comes from evolution of distinct growth patterning. This growth arises from specific cell divisions whose source can be located at the tip (as apical cell/meristem; e.g. *Fucales*, or a terminal cell, e.g. *Sphaceriales*; Katsaros, 1995; described in more detail in Chapter 2) or in the tissues themselves (localized or diffuse intercalary growth (Laminariales); Charrier et al., 2012). The morphologies observed in this lineage are highly plastic, which has resulted in multiple errors during taxonomical classifications in the past. Only with the development of molecular tools has this started to be resolved (Demes et al., 2009). The plasticity in the morphologies in the brown algal lineage comes from the ability of these individuals to adapt to the changes in their surrounding environments such as seasons (Falace and Bressan, 2006), temperature (Pereira et al., 2011), depth (Engelen et al., 2005) or community structure (Arenas et al., 2002).

The brown algae inhabit a very dynamic marine environment, which resulted in several structural adaptations to their bodies. Firstly, there does not seem to be a clear functional differentiation present within the brown algal cells, such as roots or vasculature found in plant systems. Aquatic life has advantages when it comes to nutrient uptake; there is no need to rely on localised supply of nutrients from the soil, nutrients can be taken up by the whole body from the surrounding water. Even though no true functional differentiation exists, brown algae have developed differentiated cell types. The most advanced example lies in the cells of ‘complex’ parenchymatous brown algae such as Fucales and Laminariales: an outer meristoderm (‘epidermis’), middle cortex and central medullar cells (represented in Chapter 2, Fig 2.5.; Katsaros and Galatis, 1988; Kaur and Vijayaraghavan, 1992; Moss, 1950).

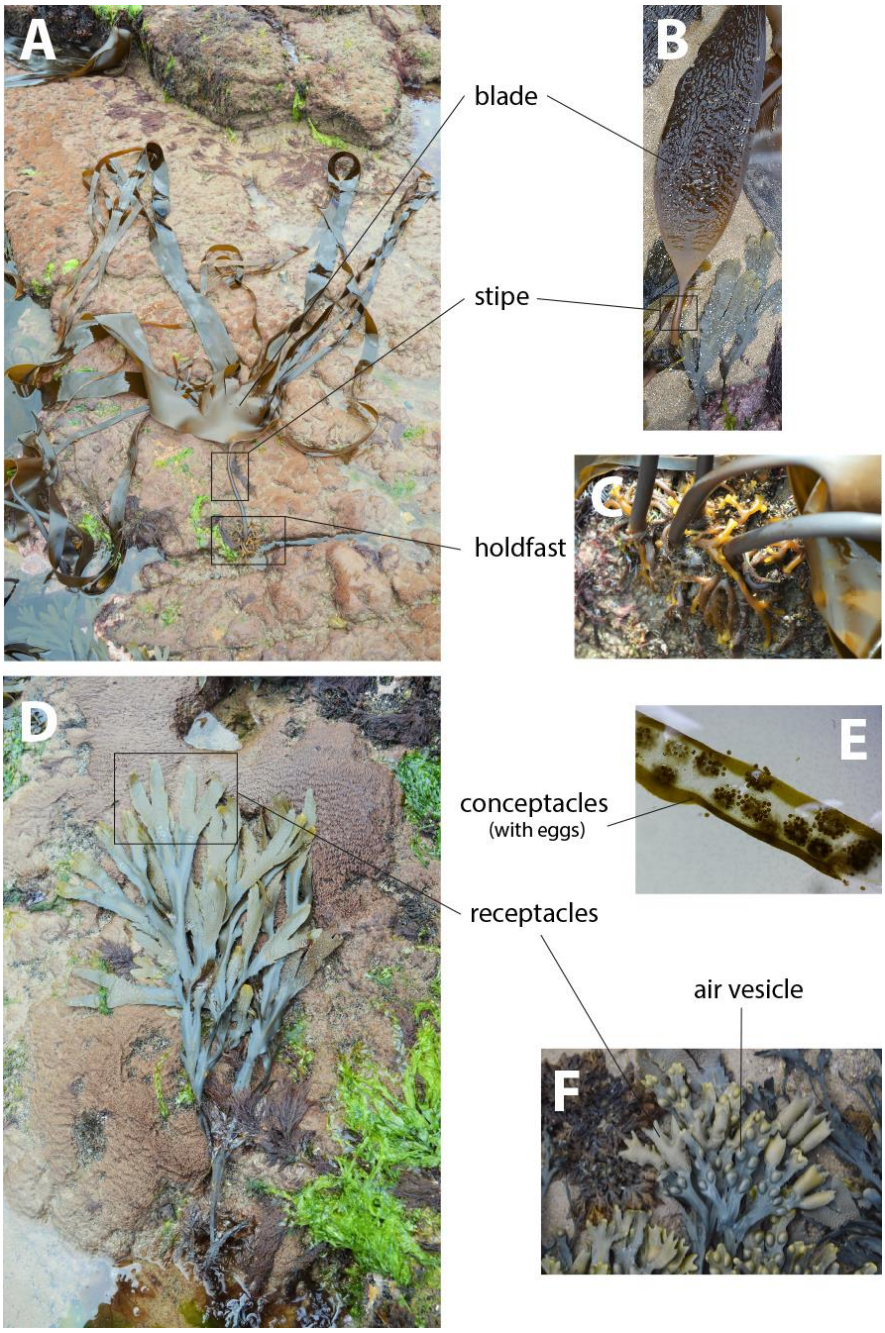

Figure 1.2. Structures found in complex brown algae. (A) *Laminaria digitata* and (B) *Saccharina latissima* have a holdfast (C) to attach to the rock substrate, a stem-like stipe and a blade. In *F. serratus* (D), during the reproductive winter period, tips of the blade transform into reproductive tissues (receptacles) holding reproductive structures (conceptacles) with gametes (e.g. eggs in females, E). (F) *F. vesiculosus* has air vesicles to help it stay upright in the water column.

.

As a second adaptation to marine environment, brown algae had to overcome the destructive effect of harsh marine conditions, such as strong wave action and predator grazing. To confront the environmental conditions, they have developed the ability to regenerate their tissues (by keeping the cellular totipotent ability). Some species, such as *Laminaria,* have been found to regenerate from induced callus tissue and protoplasts (Saga et al., 1978). Several studies have looked at mechanical wound responses and the following regeneration processes. In *F. vesiculosus*, cutting the region where the apical cell is located results in induction of branch formation on the distal cut surface (Moss, 1965). In a sister species, *F. distichus*, the same regenerative effect can be seen after mechanical wounding of tissues due to herbivorous snail grazing (Van Alstyne, 1989). Another example of the ability for mature tissues to regenerate comes from wounding experiments done on *Sargassum filipendula* and *F. vesiculosus* where the new branches can be formed from the inner medullary cells (Fagerberg and Dawes, 1976; Fulcher and McCully, 1969). This regeneration process indicates that brown algae can have the ability to re-initiate normal morphogenetic processes through maintaining cell totipotency and/or creation of new stem cells.

.

1.3. Brown algal cell walls - architecture

Although very distant from each other, brown algae and land plants share some common features such as multicellularity, photosynthetic ability and a cell wall. In these walled organisms, the process of morphogenesis is controlled by the activity of the extracellular matrix surrounding each cell (cell wall) and the intercellular turgor pressure. A biophysical theory of cellular growth in plants has been suggested by Lockhart (1965), who explained the growth through water uptake (turgor pressure increase) and the yielding of the cell wall. The yielding of the cell wall involves both rearrangement of already present wall polymers (through stretching) and new wall deposition (to maintain integrity). The resulting increase in cell volume reduces the turgor pressure and allows the uptake of new water, when the process of cell expansion repeats (wall extensibility and its relation to growth is reviewed in detail in Cosgrove, 2016).

The basic structures of algal and plant cell walls are similar: rigid and strong fibres are embedded in a gel-like matrix. In plants and algae, the load-bearing fibre elements are crystalline cellulose microfibrils, which are synthesized by membrane complexes that contain cellulose synthases (Mueller and Brown, 1980; Peng and Jaffe, 1976), but their similarity in composition ends there. The matrix polysaccharides are physically analogous, yet chemically divergent, between these two distant groups. In plants, two different groups of matrix polysaccharides exist – hemicellulose and pectin. Hemicelluloses are cellulose-binding polysaccharides which, together with cellulose microfibrils, form a network. Pectin represents a matrix in which this network is embedded, it pushes the microfibrils apart to ease their movements during cell growth and locks them in place when growth stops (for review see Cosgrove, 2005). In brown algae, the matrix polysaccharides are different: the cellulose binding polysaccharides are sulphated fucans, whereas alginate, the pectin functional analogue, forms a matrix in which all other polysaccharides are embedded (Fig. 1.3; Kloareg and Quatrano, 1988; Michel et al., 2010). The relative proportions of these three components in brown algal zygotes are around 60% alginate, 20% cellulose, and 20% sulphated fucans (Quatrano and Stevens, 1976). In plants, primary walls are composed of 15–40% cellulose, 30–50% pectin, and 20–30% hemicellulose (Cosgrove and Jarvis, 2012).

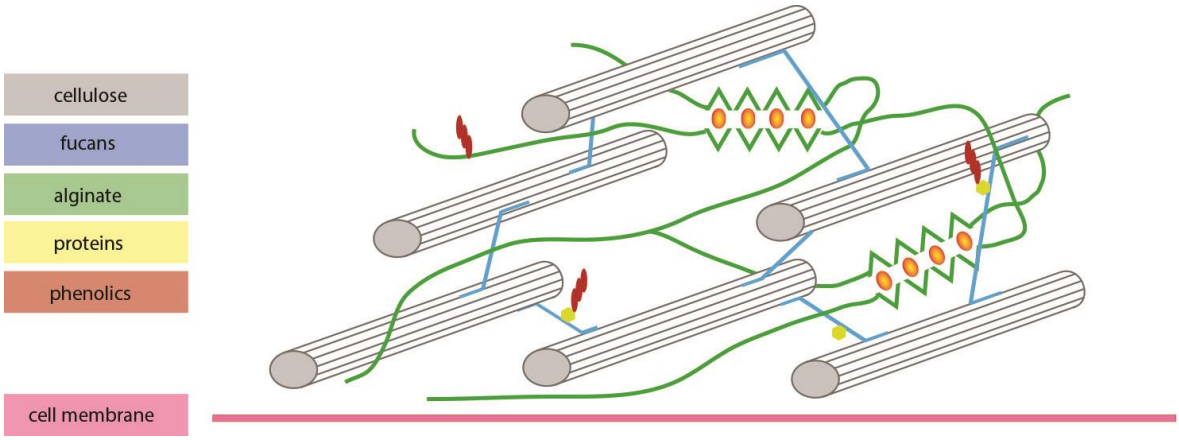

Figure 1.3. Brown algal cell wall architecture. Cellulose microfibrils embedded in alginate matrix tethered with sulphated fucans and phenolic compounds. Parts of alginate containing guluronic acid can crosslink with calcium ions and form “egg-box” linkages within the wall.

1.3.1. Alginate

Alginate is a gel-like cell wall component of brown algae (Kloareg and Quatrano, 1988), also synthesized by some bacterial genera, *Azotobacter* and *Pseudomonas* (Rehm and Valla, 1997).

1.3.1.1. Structure

Alginate is an unbranched polysaccharide consisting of variable amounts of (1->4) linked ß-D-mannuronic acid and its epimer α-L-guluronic acid (Hirst and Rees, 1965). These monomer residues are distributed within the alginate polymer in three different fractions: mannuronic acid (M-block), guluronic acid (G-block) or alternating mannuronic-guluronic acid residues (MG-block), with an equal proportion of the two monomers (Haug et al., 1966; Haug et al., 1967; Fig. 1.4A). Different binding of the two residues due to their conformation results in four different variations of orientations: M-M, M-G, G-M, and G-G. Because of these differences, the physical properties of these linkages are different. M-M bonds create a flat structure, whereas G-G bonds create a more compact structure (Fig. 1.4A). The M-G and G-M linkages create an in-between state. This results in M-G blocks being more flexible than G-G blocks, but also more flexible than the M-M blocks as well (Mørch et al., 2008).

In addition, the involvement of alginate residues in controlling mechanical properties of gels (and therefore cell walls) lies in their ability to interact with positively charged cations, such as Ca^{2+}. The linking conformation of the guluronic acid (G) residues allows the interaction between the negatively charged alginate and the calcium ions (Fig. 1.4B). The interaction results in cross-linking: four guluronic acid residues and a calcium ion are needed to form a compact linkage; multiple consecutive crosslinks can then form a structure referred to as the ‘egg-box’ (Grant et al., 1973; Fig. 1.4C). This makes the gels mechanically stiffer; it has been shown that the alginates containing higher amounts of guluronic acid residues form stronger gels (Draget et al., 1994). To some extent, the interactions with calcium ions can be formed between the alternating linkages of the mannuronic and guluronic acid (M-G, G-M), although with a lower affinity (Donati et al., 2005).

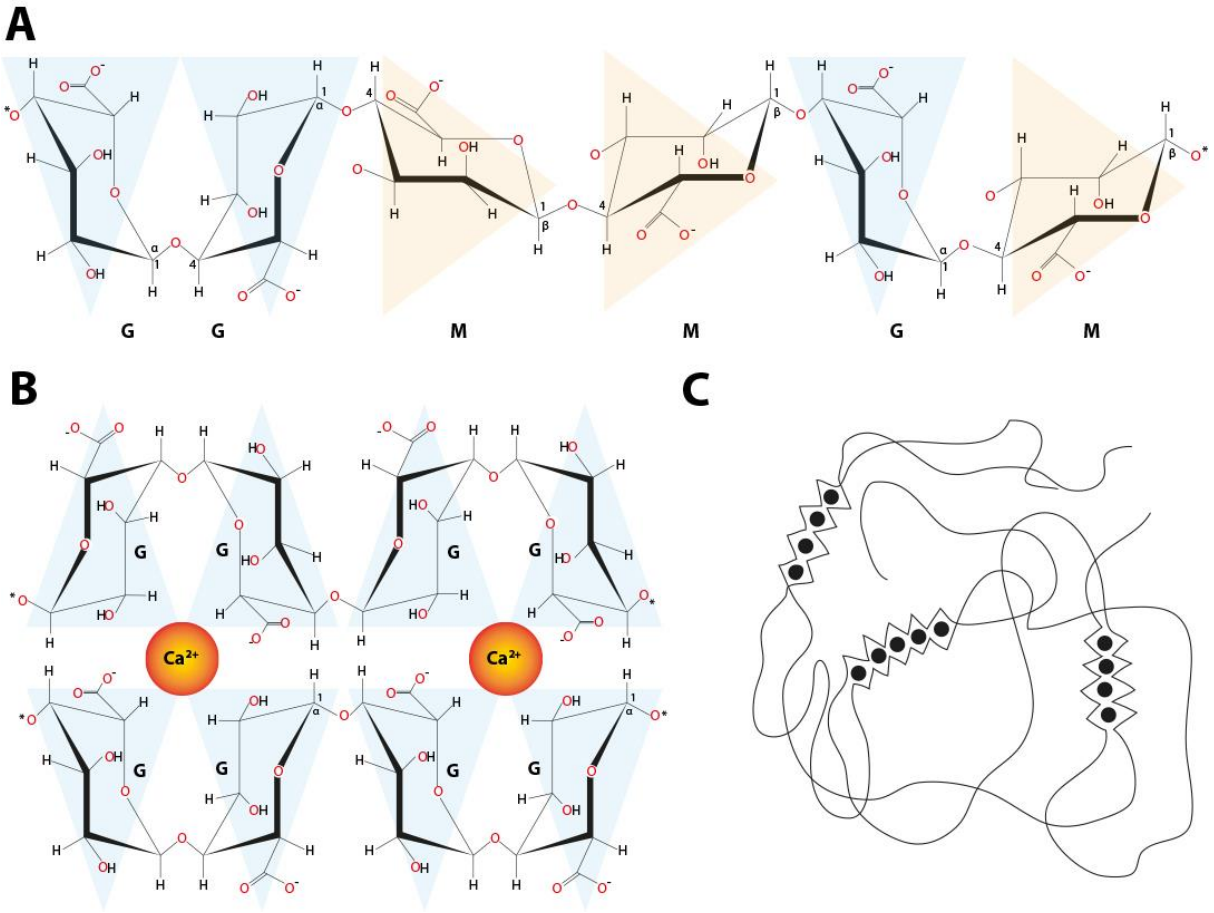

Figure 1.4. Alginate structure. (A) Structural configuration of an alginate chain with mannuronic acid (M; orange) and guluronic acid (G; blue) residues (B) Crosslinking of guluronic acid residues with calcium ions and a spatial schematic representation of the “egg-box” model (C; after Grant et al., 1973).

1.3.1.2. Alginate biosynthesis

It has been shown that alginates are synthesized intracellularly in a precursor form, after which they are delivered to the targeted place (cell surface) via vesicles originating from the Golgi apparatus (Vreeland and Laetsch, 1989).

The biosynthetic pathway of alginate is well known in the two bacteria, *Pseudomonas aeruginosa* and *Azotobacter vinelandii* (Rehm and Valla, 1997). The alginate pathway in brown algae is considered to be similar to these bacteria. However, homologues to a few enzymes present in the bacterial alginate biosynthesis chain have not been found in the genome of the brown alga *Ectocarpus* (AlgA and Alg8; Michel et al., 2010). The alginate biosynthesis process is as follows: fructose-6-phosphate is converted to mannose-6-phosphate. This mannose-6-

phosphate is then converted into mannose-1-phosphate, followed by GDP-mannose, and GDP-mannuronate. GDP-mannuronate is polymerized into poly-mannuronate (poly-M). The final step in the alginate biosynthesis involves a conformational change of the mannuronic acid residue into its epimer, guluronic acid (Fig. 1.5). This change is catalysed by a family of enzymes called mannuronan C5 epimerases (MC5Es; Haug and Larsen, 1969).

MC5E function has been well understood in bacterial systems, where one and seven MC5Es have been found in *Pseudomonas* and *Azotobacter*, respectively (Ertesvåg et al., 1999; Franklin et al., 1994; Hartmann et al., 2002a; Svanem et al., 1999). The epimerization function studies of these proteins have revealed that each enzyme has different patterns with respect to sequence distributions of M and G residues. In brown algae, a higher number of potential genes encoding these proteins have been found. Molecular analyses have revealed candidates for 31 genes in *Ectocarpus siliculosus* (Michel et al., 2010), 105 in *Saccharina japonica* (Ye et al., 2015), 6 in *Laminaria digitata* (Nyvall et al., 2003) and 31 in *Undaria pinnatifida* (Feng et al., 2015). The variety of potential epimerases found in the species of the brown algal lineage suggests that brown algae might have evolved the ability to 'tweak' the alginate structure to finer detail than what is observed in bacteria. However, the exact function of almost all of these epimerases remains unknown. Two of the currently known algal MC5Es have been functionally described: in *Saccharina japonica*, a recombinant epimerase (SjC5-VI) epimerises M to G alternately (Inoue et al., 2016). In *Ectocarpus siliculosus*, MEP13-C5 is thought to epimerase block MM regions, although its exact function is not completely clear (Fischl et al., 2016).

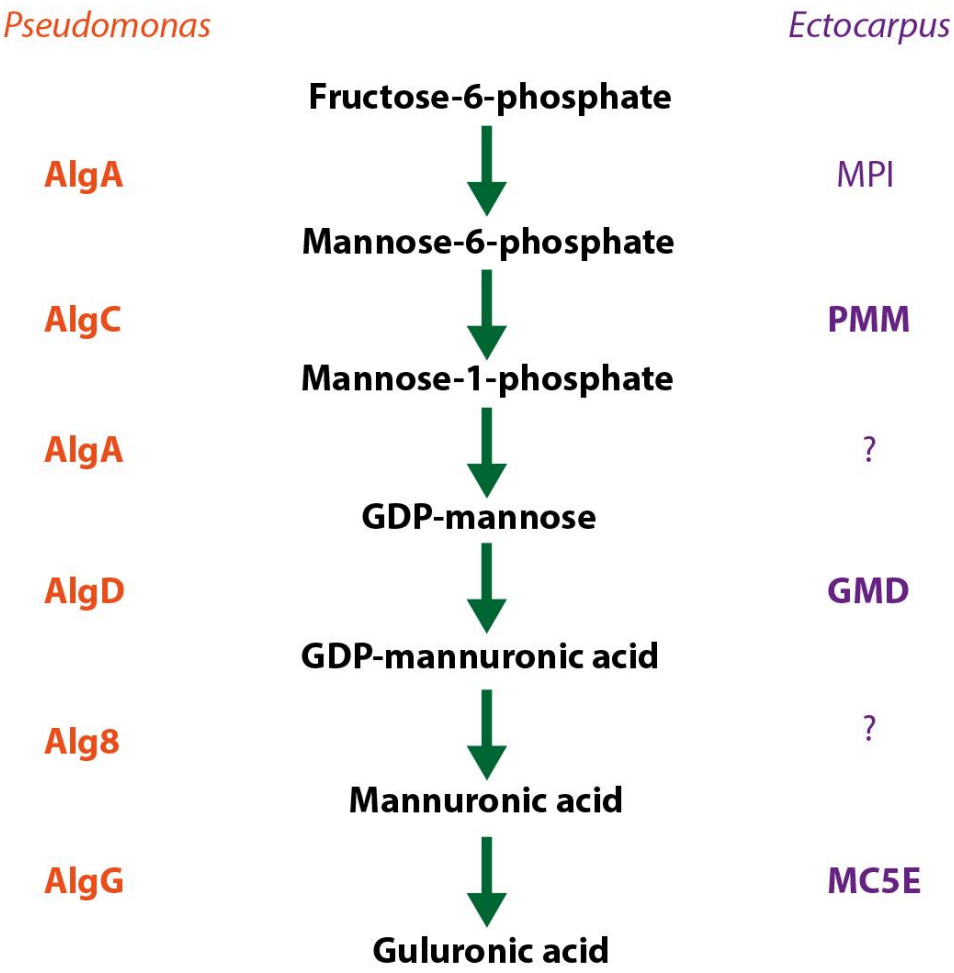

Figure 1.5. Alginate biosynthesis scheme. Pathways of biosynthesis in bacteria (*Pseudomonas aeruginosa*; orange) and corresponding gene homologues in brown algae (*Ectocarpus siliculosus*; purple). Genes marked in bold represent unambiguously identified genes, non bolded genes represent potential candidates. Homologues of AlgA and Alg8 are not found in the *Ectocarpus* genome (question marks). MPI: mannose-6-phosphate isomerase, PMM: phosphomannomutase, GMD: GDP- mannose 6-dehydrogenase, MC5E: mannuronan C5 epimerase. Adapted from Michel et al., 2010).

1.3.1.3. Biological role of alginates

In the cell wall structure of brown algae, alginate forms a gel matrix in which other polysaccharides are embedded, analogous to the pectin matrix of land plants. The state of the alginate gel is dependent on the MC5E activity which epimerises M residues into G residues (Haug and Larsen, 1969). G residues can then be cross-linked with divalent ions and result in a stiffer gel (Draget et al., 1994). Many examples found in tissues of brown algae in nature support this mechanical role of

alginate. Alginates rich in M and MG blocks have been found in blades exposed to waves, suggesting more flexibility is needed to counteract wave action (Kloareg and Quatrano, 1988). *Laminaria hyperborea* has high contents of guluronic acid in its stipe, while the blades have much lower guluronic acid content, potentially to allow them to be more flexible (Draget et al., 2005). The composition of alginates have been found to vary due to some factors, such as species examined, tissue type or the environment they inhabit (Craigie et al., 1984; Haug et al., 1974).

1.3.1.4. Application of brown algal alginates

Alginate is a commercially valuable chemical, used by many different industries (Draget and Taylor, 2011). It has been used in nanotechnology (Kovalenko et al., 2011; Zhao et al., 2012), in fuel and ethanol production (Enquist-Newman et al., 2013; Wargacki et al., 2012; Wei et al., 2013), encapsulation technology (Ertesvåg and Valla, 1998) and in the cosmetic and food industries as a thickening agent (Gómez-Díaz and Navaza, 2003; Podkorytova et al., 2007).

1.3.2. Sulphated fucans

Sulphated fucans (fucoidans) are a group of sulphated polysaccharides containing α-L-fucose residues, but can also contain mannose, xylose, galactose and uronic acid (Percival and Ross, 1950). They are present in all brown algae studied to date, but not in the other marine and freshwater algal groups (green, red) nor plants. Plants and other algae are not completely devoid of sulphated polysaccharides. Sulphated galactans have been found in red algae as well as marine angiosperms (Aquino et al., 2005; Pereira et al., 2005), whereas sulphated glucans, sulphated galactans and sulphated arabinogalactans have been found in green algae (Matsubara et al., 2000; Uehara et al., 1992). However, sulphated fucans remain unique to brown algae.

1.3.2.1. Structure

Being a group with a high amount of variability in their structure, sulphated fucans can be classified into three groups based on their backbone structure: fucoidans (homofucans), ascophyllans (xylofucoglucuronans) and galactofucans (glycurunofucoglycans). The homofucan backbone is composed of pure fucose, the

ascophyllan backbone is composed of uronic acid, whereas galactofucans have a galactose rich backbone (Fig. 1.6A, B and C; Kloareg and Quatrano, 1988).

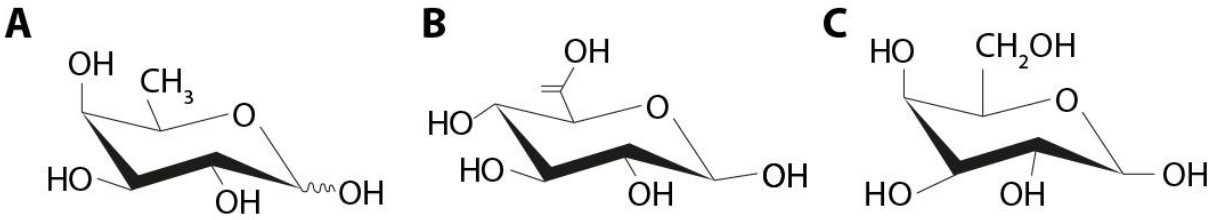

Figure 1.6. Chemical structure of 3 types of backbone residues in sulphated fucans. (A) fucose (B) uronic acid (C) galactose.

1.3.2.2. Biosynthesis of sulphated fucans

The exact biosynthesis of sulphated fucans in brown algae has not been investigated fully. It is suggested that GDP-L-fucose acts as a precursor. In cells, fucans are thought to be synthesized as a polyfucase carbohydrate and then sulphated (Quatrano and Crayton, 1973). The polymerisation and the sulphation are thought to be catalysed via fucosyltransferases and sulfotransferases, respectively (Michel et al., 2010). There is some evidence that the final sulphation step might be happening in the Golgi apparatus, before being transported to the wall (McCully, 1968). The modifications of the fucans are thought to be done via activity of glycosyl hydrolases and/or sulfatases (Michel et al., 2010). In the *Ectocarpus* genome, enzymes that might have the function to modify and synthesise sulphated fucans *de novo* have been suggested (Michel et al., 2010).

1.3.2.3. Biological role of sulphated fucans

Sulphated fucans are found in brown algae, as well as marine invertebrates (Mourão and Bastos, 1987; Mulloy et al., 1994). It is thought that sulphated fucan production correlates with the increased salinity exposure in some species of marine angiosperms (Popper et al., 2011). Furthermore, the depth at which the algae are found seems to have an influence on the amount of fucoidan found in the algal cell walls; the amount decreases as the depth increases, suggesting a role in desiccation protection (Black, 1954; Mabeau and Kloareg, 1987). In addition, sulphated fucans are known to play a role in the zygotic development in fucoid

species by affecting the adhesion to the substrate (Crayton et al., 1974) and could be involved in tethering other polysaccharides in the cell wall (Bisgrove and Kropf, 2001).

Sulphated fucans have a wide range of bioactive uses in animal medicine such as anti-coagulant and anti-thrombotic activity, response to inflammation and immune systems, anti-proliferative and anti-adhesive effect on cells and antiviral activity (reviewed in Boisson-Vidal et al., 1995).

1.3.3. Cellulose

Cellulose represents the third major component of the cell wall, however, unlike plants, only a small proportion of the brown algal wall is made of it, varying from 1 – 8 % of the dry weight (Cronshaw et al., 1958). In plants, the cellulose representation in dry weight is much higher, ranging from 15-40% (Cosgrove and Jarvis, 2012). This difference most likely reflects the environments these two groups inhabit; cellulose is a load-bearing component which gives strength to the plant body to stay upright, whereas brown algal bodies need to be more flexible (less stiff material like cellulose) due to the water action in their aqueous environments.

1.3.3.1. Structure of cellulose

Cellulose is a linear homopolysaccharide composed of β-D-glucopyranose residues, linked by (1 -> 4) glycosidic bonds (Purves, 1954). The ability of hydroxyl groups in cellulose to form molecular hydrogen bonds within or between different chains allows cellulose to form microfibril structures (Delmer and Amor, 1995).

1.3.3.2. Biosynthesis

Cellulose microfibrils are produced and deposited *in situ* by cellulose synthase complexes (CesA), which are localised in the plasma membrane (Peng and Jaffe, 1976). Glycosyl transferases (GTs; catalyse establishment of glycosidic linkages) have been found in the genome of brown alga *Ectocarpus* with 88 representatives (32 families). In one of the families, GT2, 9 enzymes have been found to consist of membrane proteins homologous to CesA and cellulose synthase-like (CSL) proteins from plants (Michel et al., 2010).

The action of forming microfibrils in the CesA complexes is different between plants and algae. These terminal complexes in plants form rosettes resulting in a cylindrical shape of cellulose microfibrils (Brown Jr., 1996). In contrast to plants, terminal complexes in brown algae do not form rosettes, but rather single rows comprising between 10 and 100 subunits, resulting in a ribbon shaped structure (Tamura et al., 1996). These ribbon-like structures have a thickness of around 2.6 nm and a variable length of 2.6 – 30 nm (Tamura et al., 1996). Another interesting difference between plant and brown algal cellulose biosynthesis lies in the positioning of terminal complexes as they move along the membrane. In plants, the complexes are guided by microtubules (Heath, 1974), whereas in brown algae it is thought that actin filaments have this role (Katsaros et al., 2002).

1.3.4. Phlorotannins

Besides the three aforementioned polysaccharides, the brown algal cell wall includes other structures, such as phlorotannins. Phlorotannins are a group of polymers formed of phloroglucinol (1,3,5-trihydroxybenzene) monomer units.

Vesicles within cells called physodes serve as a storage for most of the phenolics found in brown algae (Ragan, 1976). Phlorotannins are involved in a number of physiological process within brown algae such as chemical defence, protection against oxidative damage from UV radiation and interactions with other organisms (Henry and Van Alstyne, 2004; Targett and Arnold, 1998). In addition, they are an integral component of brown algal cell walls (Schoenwaelder, 2002). Phlorotannin concentrations have been found to vary from 0.5 -13% of the overall dry mass in brown algal species, depending on the geographical area (Targett et al., 1992).

Besides their biological role in brown algae, phlorotannins have been reported to have several bioactivities in animals such as antioxidant and anti-inflammatory (Kim et al., 2009; Wang et al., 2012), anti-carcinogenic (Kong et al., 2009), anti-HIV (Artan et al., 2008), anti-diabetic (Okada et al., 2004), as enzyme inhibitors (Shibata et al., 2002) as well as bactericides (Nagayama et al., 2002).

1.3.5. Cell walls in brown algae and plants – a mechanical role in shape formation

There has been discussion in the past years about how cell wall components affect cell growth in plants. Although the cellulose represents the load bearing component, it has been shown that pectin has an important mechanical role in plant growth (Braybrook and Peaucelle, 2013). The major type of pectin, homogalacturonan (HG) is a simple polymer of 1-4 linked α-D-galacturonic acid in which residues may be methyl-esterified. The degree of esterification determines the pectin's mechanical state as follows: when de-esterified, calcium ions (Ca^{2+}) can bind and cause the cross-linking of pectin, ultimately resulting in a more rigid cell wall (Fig. 1.7A). When esterified, pectin chains do not cross link with each other and the cell wall is less rigid. The indications for this have been found in a variety of plant systems; diffuse meristematic growth where the pectin chemistry relates to the active growth site (Braybrook and Peaucelle, 2013; Peaucelle et al., 2011), as well as tip growing pollen tubes where a similar pattern has been recognized (Chebli et al., 2012). The difference between these two forms of pectin likely plays a large role in determining where and when the growth will occur.

As previously mentioned, in brown algae, a similar situation might happen. Alginate is a simple polymer of β-D-mannuronic acid and α-L-guluronic acid. These two components always come in blocks, creating the so called M and G blocks (Haug et al., 1966; Haug et al., 1967). The G blocks have the ability to bind divalent cations (e.g. Ca^{2+}, Ba^{2+}, Sr^{2+}; Smidsrød et al., 1972), similarly to de-esterified pectin. M blocks, on the other hand, do not have this feature (Fig. 1.7B). Furthermore, alginate structure can be modified by post-polymerisation enzymatic modification (mannuronan C-5-epimerase (MC5E) turning M to G (Ertesvåg et al., 1995). Ionic binding by G blocks likely leads to gel rigidity in a manner similar to HG-Ca binding in plants (Draget et al., 2005; Fig. 1.7A, B).

Despite the differences in the cell wall composition, it might be that the gel-like matrix polysaccharides act in a similar manner to regulate growth in these highly divergent, multicellular brown algae. The similarities go further, as the overall mechanics of cell growth in plants and algae are the same, perhaps owing to their

similar wall structures. Internal turgor pressure is the main force that drives cell growth and the rate of growth is regulated by the cell wall itself. Furthermore, in diffuse growth, the orientation of the cellulose microfibrils determines the direction of growth, whereas the polarised deposition of wall material determines the tip growth (Baskin, 2005; Cosgrove, 2005; Kropf et al., 1998).

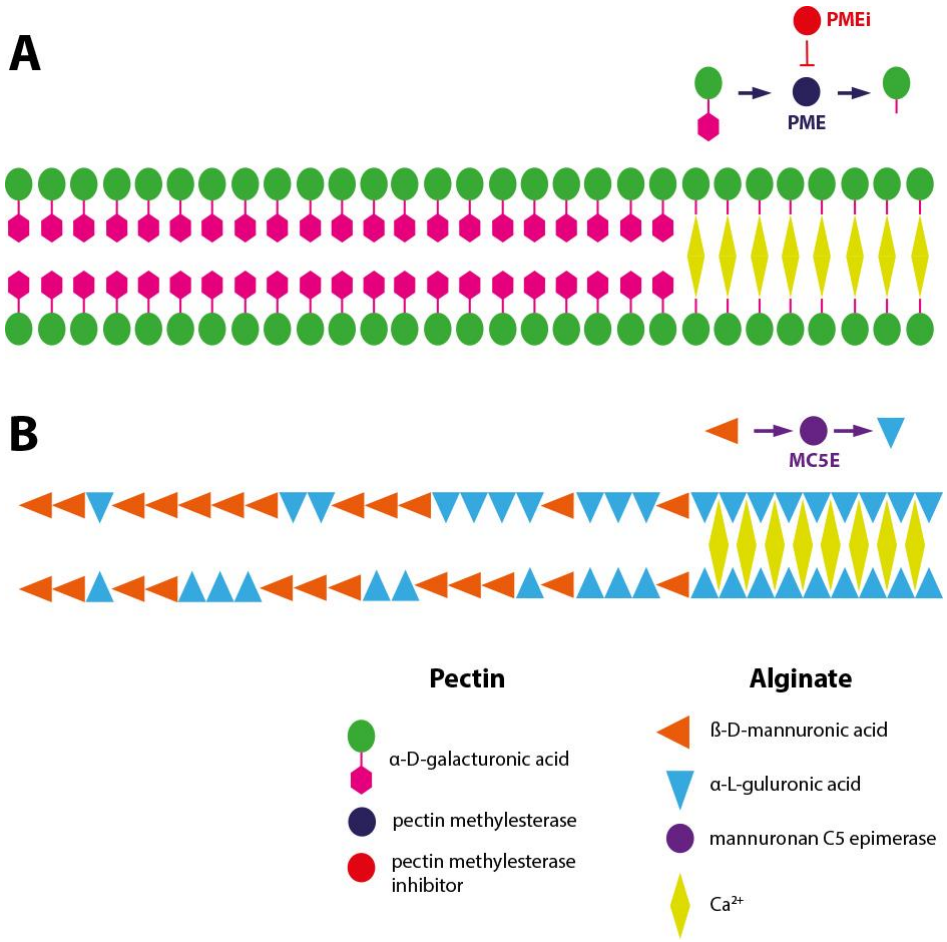

Figure 1.7. Mechanical link between the pectin and alginate structure. A) Pectin homogalacturonan is a chain formed of α-(1–4)-linked D-galacturonic acid. PME (pectin methyl esterase) removes methyl groups from the residues. They can then cross link with calcium ions (Ca^{2+}) and make the gel stiffer. PMEi inhibits the effect of PME which leads to methyl esterified residues. B) Alginate is a chain formed of M (mannuronic acid), G (guluronic acid) and MG (mannuronic and guluronic acid) blocks. Ca^{2+} can bind to the G blocks of the alginate making the gel stiffer.

1.4. Investigating properties of cell walls

The process of morphogenesis in walled organisms can occur through two processes: an increase in internal pressure, which overcomes the wall strength and

through a combination of modification of wall composition followed by a mechanical response (wall loosening). In order to understand how the two latter processes relate to each other, a combination of two methods can be applied: atomic force microscopy (AFM) for mechanical properties, and wall immunolocalisation for the spatial-biochemical properties.

1.4.1. Mechanical characterisation of cell walls

From a mechanical perspective, walled organisms are special in two aspects. The first relates to the cell wall, which acts as a mechanical barrier for growth. The second encompasses internal pressure, which pushes onto the cell wall and keeps the cells turgid. As such, morphogenesis in walled organisms relies highly on mechanical changes that occur on a cellular level. Only in the past decade, the mechanical aspects of growth have started to be explored. The methods used include ball tonometry, micro- and nano-indentation, depending on the area of indentation (ball tonometry 300 - 5000 µm, micro-indentation 1-11 µm, nano-indentation 10-40 nm; Milani et al., 2013). Atomic force microscopy (AFM) can be applied for both micro- and nano-indentation.

AFM-based indentation can be used to investigate different physical properties of a biological sample (such as elastic, plastic and/or viscoelastic properties). The experiments are performed by indenting the area of interest with a tip attached to a cantilever (Fig. 1.8A). Each indentation results in two force-indentation curves. Each curve pair describes the movement of the AFM cantilever, as it approaches, deforms and retracts (Fig. 1.8B). From this curve, an elastic modulus (Young's modulus, E_A) can be extrapolated. Young's modulus represents a coefficient that reports the material's elasticity. If a material has a high Young's modulus, it means the material is less elastic, hence stiffer. The process of calculating Young's modulus from indentation data involves fitting the obtained approach curve to a mechanical model. The model most currently used for curve fitting is the Hertzian model; developed for elastic homogeneous materials. Even though the cell wall does not behave as a purely elastic material, this modulus is the best qualitative method currently applicable.

In plants, AFM-based techniques have been used to explore the mechanics of different systems such as shoot apical meristems (Braybrook and Peaucelle, 2013; Milani et al., 2014; Peaucelle et al., 2011), roots (Fernandes et al., 2012) and pollen tubes (Chebli et al., 2012; Geitmann and Parre, 2004). To date, AFM has not been extensively used in exploring brown algae; the potential of this method has only recently been demonstrated in a brown algal model system *Ectocarpus siliculosus* (Tesson and Charrier, 2014).

There are several advantages to use an AFM-based technique to explore brown algal cell walls. The ability of the process to be performed in water is the first step towards applying these methods to an aqueous system, such as algae. Furthermore, *Ectocarpus*, as well as one of the systems used in this study (*F. serratus* embryo) have natural adhesive properties that keep them in place; a fixed sample is a necessity for these types of techniques due to their indenting nature.

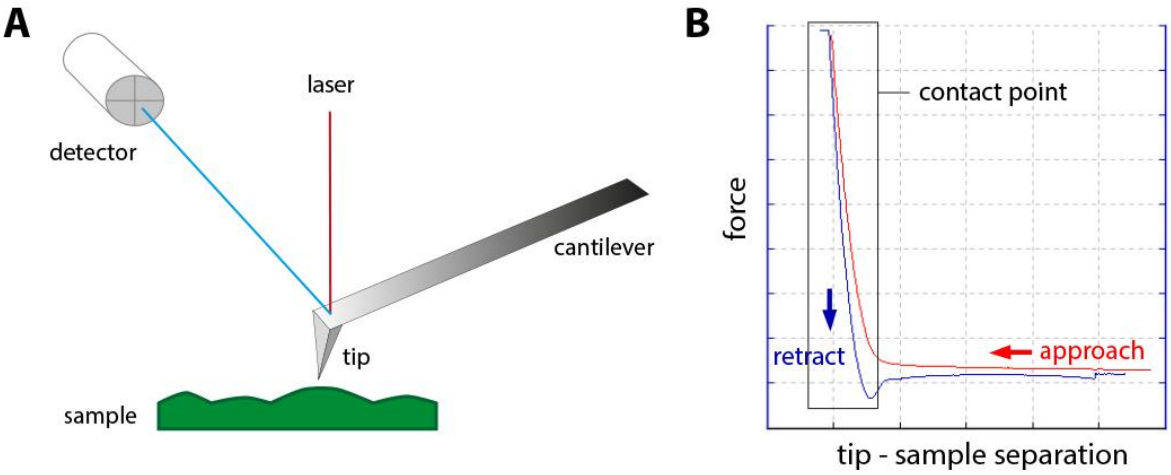

Figure 1.8. Basic process of atomic force microscopy method. (A) The microscope consists of a cantilever with an attached tip. When the cantilever touches the surface of the sample, it bends; this results in the deflection of the laser pointed at the cantilever. The reflected laser beam is detected by a photodiode detector. (B) The output of a single indentation results in two curves, the approaching and the retracting curve. As the tip approaches the surface, no contact is established yet (flat right portion of the red curve). When the tip hits the sample the contact point is established and the indentation begins until it reaches the set indentation force (black rectangle). After it has reached the given force, it starts the retraction, first decreasing the depth of indentation (still seen as in contact), and then moving away from the sample.

1.4.2. Spatial distribution of brown algal wall components

Immunolocalisation is a method based on the detection of specific targets called antigens (mostly proteins or polysaccharides) in biological samples by antibodies as probes. The fundamental ability of antibody production as a response of animal immune systems to foreign substances has been exploited in the field of biochemistry to develop new antibodies binding to a range of targets (epitopes).

In plants, a range of antibodies has been raised in the past to explore the role of both primary and secondary cell wall components in different aspects of cell and developmental biology (see review Knox, 2008). The immunolocalisation approach has been used to investigate potential correlation between pectin methyl esterification status and the mechanical properties (antibody 2F4 in meristems - Braybrook and Peaucelle, 2013; Peaucelle et al., 2008); antibodies JIM5 and JIM7 in pollen tubes - Chebli et al., 2012).

Recently, a range of antibodies have been raised against brown algal cell walls (Torode et al., 2015; Torode et al., 2016). A portion of these antibodies binds to the alginate fraction of cell walls, whereas the rest has been developed to bind to the sulphated fucan component (Appendix 1.). This enabled the exploration of a variety of questions related to the role of cell walls in brown algal development and biology that have started to be addressed (Torode et al., 2016).

1.5. Studying brown algal cell walls and morphogenesis – step towards understanding different evolutionary paths to shape formation

Brown algal species show the highest variation in shape morphologies across all the algal lineages. In addition, their evolutionary position on the tree of life makes them an interesting group to explore multicellularity and morphogenesis. It is fascinating that similar morphogenetic traits seem to have reappeared in very distant organisms during the evolution of eukaryotes; e.g. brown algae and plants. It seems

that different lineages have managed to find different convergent ways to produce similar body shapes, regardless of their phyletic legacy.

As organisms whose cells are encapsulated within the cell wall, the form of brown algae is largely determined by the shape of this wall and changes within are of fundamental importance during cell morphogenesis. Given the similarities in cell wall structures, one might expect that developmental patterns could be similar between plants and brown algae, regardless of their very distant evolutionary pathways. In contrast, similarities in specific aspects of cell biology (such as cell walls) might not directly involve similarities in other aspects of morphogenesis. Although very special, brown algal morphogenesis has scarcely been studied in the past. Therefore, exploring mechanisms of pattern formation and cell wall mediated shape change in this lineage could provide answers and more insight into different or similar evolutionary solutions to morphogenetic processes.

1.6. Aim of the study

The aim of the project is to explore potential mechanisms governing growth and morphogenesis in brown algae, with special focus on the cell wall role during this process. The project addresses these questions in two developmental aspects: apical growth driving pattern formation and early algal embryogenesis.

Apical growth and pattern formation

In Chapter 2, I explore the potential mechanisms of apical patterning and the role of cell wall in organ formation in a brown alga, *Sargassum muticum*. It exhibits interesting spiral phyllotactic pattern (positioning of new organs) in its apex, which is strikingly similar to many plant species. *Sargassum* was chosen as the best system to address these questions because of the aforementioned interesting morphology, as well as its availability on the UK coast and the ability to use them for *in vitro* experimentation. To understand how branching occurs in a brown algal species, I look into the link between the phyllotactic pattern and the meristem cell

divisions, potential changes in the cell wall biochemistry and mechanics during branch outgrowth as well as the possible role of a phytohormone auxin in the patterning.

Embryogenesis

Chapters 3 and 4 explore the process of embryogenesis in a brown alga *Fucus serratus*. The fucoid zygote has been used before as a model system to address several fundamental developmental questions. Its development starts free from the mother tissue and its fertilisation can be finely orchestrated *in vitro* resulting in a large number of fertilised eggs. In addition, it is present along the coast of the United Kingdom. All these addressed characteristics represent major reasons why this species was chosen to address the questions interesting for this project. Chapter 3 concentrates on characterising the embryogenesis process in *F. serratus,* with special attention to describing novel insights into the cell wall mechanics and biochemistry and a specific type of growth observed, tip growth. Chapter 4 explores in more depth the relationship of tip growth with cytoskeleton, calcium and cell wall and their effects on growth and cell wall properties.

Chapter 2. Towards an understanding of spiral patterning in the *Sargassum muticum* shoot apex

The majority of Chapter 2 was published in Scientific Reports (2017); for details see 'Publications' page (p. xv). Results not included in the published MS are denoted in the Materials and Methods section with *.

2.1. Summary

In plants and parenchymatous brown algae the body arises through the activity of an apical meristem (a niche of cells or a single cell). The meristem produces lateral organs in specific patterns, referred to as phyllotaxis. Two different control mechanisms have been proposed: one is position-dependent and relies on morphogen accumulation at future organ sites; the other is a lineage-based system which links phyllotaxis to the apical cell division pattern. Here I examine the apical patterning of the brown alga, *S. muticum*, which exhibits spiral phyllotaxis (137.5° angle) and an unlinked apical cell division pattern. The *Sargassum* apex presents characteristics of a self-organising system, similar to plant meristems. In contrast to complex plant meristems, I was unable to correlate the plant morphogen auxin with bud positioning in *Sargassum*, nor could I predict cell wall softening at new bud sites. The data suggest that in *S. muticum* there is no connection between phyllotaxis and the apical cell division pattern, indicating that a position-dependent patterning mechanism may be in place. The underlying mechanisms behind the phyllotactic patterning appear to be distinct from those seen in plants.

2.2. Introduction

In developmental biology, fate decisions (such as where to place a new organ) often exhibit characteristics of emergent phenomena. Such decisions are often made based on a position-dependent patterning system where the position of a cell within a tissue or organ specifies its fate and a signal (or morphogen) acts as an instructive agent (Scheres, 2001). An alternative mechanism depends on cell lineage, although this seems less prevalent in walled organisms such as plants (Scheres, 2001). When one examines the processes behind aerial organ positioning in plants, phyllotaxis, two major theories emerge: in some early diverging land plants, phyllotactic patterning is attributed to patterned divisions at the meristematic apical cell; in Spermatophytes (seed plants), paterns are attributed to a morphogen-based mechanism. The latter is considered as position-dependent patterning and the former as lineage-dependent.

Early diverging land plants, such as mosses and ferns, maintain a single apical cell which acts as a stem cell for the apex (Nägeli, 1845a; Nägeli, 1845b; Schüepp, 1926). In mosses, the pattern of leaf production may be seen as lineage-dependent as it follows the apical cell patterning directly (Harrison et al., 2009; Renzaglia et al., 2000). In horsetails and fern apices, the arrangement of the leaves is independent of the division pattern in the apical cell (Bierhorst, 1977; Golub and Wetmore, 1948). These latter two examples hint at a position-dependent patterning mechanism which takes place post apical-cell division. Further evidence for a self-organising and robust patterning mechanism in ferns comes from experiments where apical cell ablation does not lead to growth arrest, but instead to a new apical cell establishment and subsequent spiral phyllotaxis about the new centre (Cutter and Voeller, 1948; Wardlaw, 1949). Work in ferns from Wardlaw (1949) and in flowering plants from Snow & Snow (1935) explored positional patterning mechanisms which were both physical (tissue tension) and morphogen (the phytohormone auxin) based; however, no further modern explorations have been conducted in these species to our knowledge.

In Spermatophytes the meristematic activity in the shoot apex is attributed to an organised group of cells. This niche serves as a reservoir for production of cells which then give rise to the lateral organs (Meyerowitz, 1997; Steeves and Sussex,

1989). Phyllotactic patterning occurs independently from division patterns within the meristematic niche and evidence exists for a position/morphogen-based patterning mechanism: organs emerge due to local auxin accumulation (Reinhardt et al., 2003a). Auxin moves through plant tissues via specific efflux and influx transport proteins, which have been found to be involved in phyllotaxis regulation. Auxin is thought to be transported upwards into the meristem through the epidermis. The newly forming primordia in the meristem act as sinks – they accumulate auxin, creating a local auxin maxima, resulting in a defined pattern of its distribution, which corresponds to the observed leaf phyllotactic pattern (Reinhardt et al., 2003a)**.** This auxin accumulation is then followed by the softening of tissues at specific positions at the shoot apex (Braybrook and Peaucelle, 2013; Milani et al., 2014). Stochastic fluctuations in auxin concentration can lead to coordinated polarisation of auxin transporters and result in a self-organising pattern of organs (Jönsson et al., 2006). Ablation of the meristematic niche leads to re-establishment of a new niche and organised phyllotaxis lending weight to a robust self-organising mechanism rooted in the morphogen auxin (Reinhardt et al., 2003b; Steeves and Sussex, 1989).

Plants are not the only organisms to display spiral organ arrangement. Two genera of parenchymatous multicellular brown algae, in the order Fucales, arrange their organs in spirals: *Sargassum* and *Cystoseira* (Church, 1920; Peaucelle and Couder, 2016). Other members of the order tend to display dichotomous branching (e.g. *Fucus sp.*). The body of parenchymatous brown algae is built through the meristematic activity of an apical cell (Fritsch, 1945; Katsaros, 1995). In the Fucales, the apical cell presents as three or four sided in transverse view and divides from these faces (Clayton et al., 1985; Kaur, 1999; Klemm and Hallam, 1987; Moss, 1967; Moss, 1969; Nizamuddin, 1967; Yoshida et al., 1983). In some cases, the apical cell is thought not to divide but rather to stimulate the cells around to do so (Moss, 1967). In *Cystophora*, it has been proposed that the division pattern of the apical cell drives the observed branching pattern of the thallus, similar to the lineage-dependent theory for moss (Klemm and Hallam, 1987). In *Fucus*, if the apical cell is removed growth of the branch ceases (Moss, 1967), indicating a less robust patterning mechanism than seen in spermatophytes, ferns and lycophytes. As such, the literature indicates that phyllotactic patterns in parenchymatous brown algae may be lineage-dependent. Furthermore, it remains unclear whether phytohormones

(auxin as the primary candidate) play a role in brown algal phyllotaxis. Auxin has been detected by GC-MS in the brown alga *Ectocarpus siliculosus* and some genes in the auxin biosynthetic pathway have been found in its genome (Le Bail et al., 2010). In addition, auxin has been shown to have an effect on brown algal development. Chamberlain et al. (1979) showed that the auxin indole-3-acetic acid (IAA), when applied exogenously, significantly reduced growth of primary laterals in *Sargassum muticum*. *Fucus vesiculosus* and *Ectocarpus siliculosus* have both been shown to exhibit auxin-related phenotypic changes – a modified branching pattern (Basu et al., 2002; Le Bail et al., 2010). However, the local effect of auxin or other phytohormones on brown algal phyllotaxis has not yet been explored to date.

In *S. muticum*, while a clear apical cell is present (Yoshida et al., 1983) the shoot apex is similar in organisation to that seen in ferns and spermatophytes: a large central area is surrounded by emerging organs in a spiral pattern (Simons, 1906). Since the brown algae have evolved completely independently from plants (Baldauf, 2003), it is fascinating to see similar spiral leaf patterns emerging in the shoots of *Sargassum* as those seen in that distant kingdom. Here I explore the apical organisation and spiral phyllotaxis observed in *S. muticum*, and begin to investigate its robustness and underlying mechanisms by comparison to those proposed in plants.

2.3. Materials and Methods

2.3.1 Sample collection and processing

The samples were collected in Rottingdean (East Sussex, United Kingdom) between November 2015 and February 2017. After collection, they were transported in seawater to the laboratory and kept at 4^0C. Processing was done shortly after returning back to the laboratory. The specimens were dissected using fine tweezers and used for further experiments. The medium used in the experiments was filter sterilised artificial seawater (ASW, Tropic Marin Sea Salt; Tropic Marin, Germany).

2.3.2. Imaging of the apices for divergence angle measurements

Sargassum apices were dissected using fine tweezers by removing all the leaves from their base, until the central region of the apex was clearly visible. The apices were then cut to a 1 cm length and anchored by insertion into Petri dishes containing 1% agarose melted in ASW and flooded with ASW to cover. Images were taken using a VHX 5000 microscope (Keyence (UK) Ltd, UK). Measurements for the divergence angle were done using the VHX 5000 Keyence software; centres of each organ were used in reference to the centre of the apex.

2.3.3. Histology

The apices were fixed in a fixative containing 2.5% glutaraldehyde and 2% formaldehyde in artificial seawater. They were then dehydrated through 10% ethanol steps and embedded in LR White resin (Agar Scientific, UK). Samples were then cut in 1 µm slices using an ultramicrotome. Sections were placed onto slides and left to dry at room temperature. Sections were then stained with 0.05% Toluidine blue O solution for 5 minutes, washed, covered with a cover slip and imaged under a light microscope.

2.3.4. Cell division pattern quantification

As time-course analysis of division was technically impossible around the apical cell due to its internal position, I was limited to fixed and sectioned material and so needed to make assumptions on division time based on position, the so-called ‘pseudo-time progression’. I hypothesised that the three-sided apical cell divides by sequentially cutting off a daughter cell from each of its three faces in a progressive manner. The pattern described was based on this phenomenon: the daughter cell with least cell divisions (usually just one or none) and closest to the mother apical cell was therefore determined to be the youngest newly formed daughter. From this daughter cell, the second youngest was determined based on the same parameters: least cell divisions (one, two or three) and still close to the mother cell, but at a rotated position. If the daughter cells on two sides of the mother apical cell had the same number of divisions, the age of them was assessed by

looking at the next layer of cells, again based on how many cell divisions are present.

The apical cell resembles an equilateral triangle and because the divisions are predicted to occur at sequential faces of this triangle, the angle is roughly 120°. The central point of the triangle was calculated by finding the crossing point of the three altitude lines. After calculating the centre, lines from there to the interface of the two daughter cells were drawn and the angle was calculated for each of these divisions (Fig. 2.1).

2.3.5. Apex ablation

Sargassum apices were dissected and handled as described above. The following manipulations were performed:

a. The apices were precisely stabbed using a fine needle in the middle of the meristem, where the apical cell is located.
b. *The apices were cut perpendicular to the surface with a double sided razor blade, creating a slice through the meristem and the peripheral area.
c. *A single bud was removed from the apex by making a circular cut around it with a fine needle.

The images of the apices were taken using a VHX 5000 microscope (Keyence (UK) Ltd, UK). The samples were kept in culture under 16^0C, 12:12 hour day night cycle, 60 µmol m-2 s-1. After 20 days, they were dissected again to remove the newly grown leaves and imaged again. Furthermore, the stabbed meristems were fixed, dehydrated, embedded in resin as previously described. The embedded apices were then cut into serial 1 µm sections (every 5 µm throughout the meristem), stained with TBO as above and imaged under Zeiss Axio Imager M2 (Zeiss, Germany).

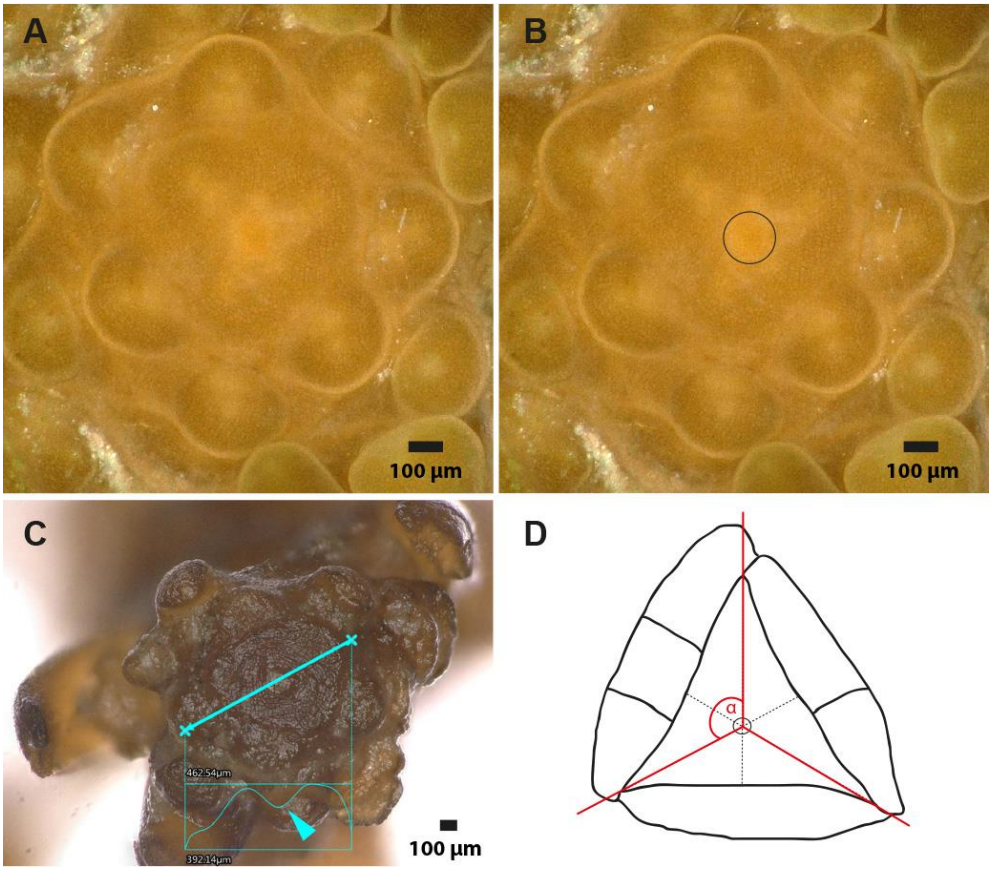

Figure 2.1. Analysis processes for meristem zones and apical cell division angles. A) Raw image of a meristem showing lighter colour in the middle (area where the apical cell is positioned); (B) same image with a black circle around the approximated apical pit area. (C) 3D image of a *Sargassum* apex with a topological line drawn through the middle; blue arrow points and the apical pit. (D) Scheme of a transverse section of an apical cell and daughter cells showing the method of determining the division process: apical cell is seen as an equilateral triangle; dotted lines correspond to the altitude for each triangle side whose crossing point determines the centre. The division angle is measured by drawing 2 lines from the centre through the two interfaces which the daughter cell shares with its neighbouring cells.

2.3.6. Alginate immunolocalisation

The apices, *stem and leaf tissues were fixed, dehydrated and embedded in resin as described above. The sections were placed on Vectabond coated multitest 8-well slides, 2 sections per well (Vector Laboratories, USA).

The samples were incubated in a blocking solution of 5% milk for 2 hours. They were then rinsed with phosphate buffered saline (PBS; 2.7 mM KCl, 6.1 mM Na_2HPO_4, and 3.5 mM KH_2PO_4) and incubated in 60 µl of 1/5 (in 5% milk) monoclonal primary antibody for 1.5 hours. After the incubation, the slides were

washed with PBS 3 times for 5 minutes each, followed by incubation in 60 µl of 1/100 (in 5% milk) IgG-FITC secondary antibody (F1763, Sigma-Aldrich). This was followed with a 5x5 minute wash in PBS, after which the samples were mounted in Citifluor (Agar Scientific, UK), covered with a coverslip, sealed and imaged under a Leica SP8 confocal microscope (Leica Microsystems, Germany). Three antibodies were used: BAM6 (M-rich areas), BAM7 (MG-rich areas) and BAM10 (G-rich areas). The antibodies used were gifts from Prof. Paul Knox (University of Leeds).

2.3.7. Auxin immunolocalisation

The protocol was adapted from Le Bail et al. (2010). The *Sargassum* and *Arabidopsis* apices were dissected and prefixed in 3% of 1-ethyl-3-(3-dimethylaminopropyl)-carbodiimide (EDAC, Sigma-Aldrich, USA) followed by an overnight fixation in FAA (47.5% ethanol, 5%acetic acid, and 10% formaldehyde in ASW). Samples were then dehydrated and embedded in resin as described above. One µm sections were cut using the Leica ultramicrotome and placed on Vectabond coated slides. The slides were placed into PBS for 5 minutes and then incubated in a blocking solution (0.1% [v/v] Tween 20, 1.5% [w/v] Glycine, and 5% [w/v] bovine serum albumin (BSA) in dH_2O) for 45 minutes. The sections were rinsed in a salt rinse solution for 5 minutes, a quick wash with 0.8% (w/v) BSA in PBS and incubated in 60 µl of 1:100 monoclonal anti-IAA antibody (Sigma Aldrich, USA) overnight at 4°C. The slides were vigorously washed three times for 10 minutes with a high salt rinse solution (2.9% [w/v] NaCl, 0.1% [v/v] Tween 20, and 0.1% [w/v] BSA in dH_2O) and then washed for an additional 10 minutes in a salt rinse solution and a rinse with 0.8% (w/v) BSA and then in PBS. 60 µl of 1:100 (v/v) dilution of 1mg mL^{-1} goat anti-mouse IgG antibody Alexa Fluor® 488 (Invitrogen, USA) was added to each well and incubated for 4 h at room temperature. The slides were washed 5 times for 10 minutes in the salt rinse solution followed by a brief was in PBS, mounted in Citifluor (Agar Scientific, UK), covered, sealed and imaged under a Leica SP8 confocal microscope (Leica Microsystems, Germany).

2.3.8. *Atomic force microscopy (AFM)

The apices were dissected using fine tweezers, cut to a length of approximately 3-5 mm, placed onto a glass slide and fixed in place with 1% agarose, making sure not to cover the apex. The glass slides were then positioned under the atomic force microscope. The AFM data were collected using a NanoWizard AFM with a CellHesion (JPK Instruments AG, Germany). The elasticity of the meristematic area was determined by indenting the surface in 100 µm x 100 µm squares with 3 N/m stiffness cantilever and a 10 nm diameter tip (Nanosensors, PPP-CONT, Windsor Scientific Ltd., UK). The indentation depth was around 1.5 µm with a force of 500 nN.

Each force-indentation experiment was treated with a Hertzian indentation model to extrapolate the apparent Young's modulus (E_A) using the JPK Data Processing software (JPK Instruments AG, Germany). The E_A was presented as a stiffness heat map.

2.3.9. Exogenous auxin treatment

The *Sargassum* apices were cut to a length of approximately 1 cm, dissected and anchored by insertion into 250 mL sterile plastic containers containing 1% agarose melted in ASW. They were then flooded with exogenous auxin in ASW - 50µM 1-Naphthaleneacetic acid (NAA) and 2, 4-Dichlorophenoxyacetic acid (2, 4-D). The same amount of DMSO in ASW was used as a control treatment (50µM). The images were taken using a VHX 5000 microscope (Keyence (UK) Ltd, UK). The samples were kept in culture under 16ºC, 12:12 hour day night cycle, 60 µmol m^{-2} s^{-1}. After 20 days, they were dissected again to remove the newly grown leaves and imaged again.

2.4. Results

2.4.1. The arrangement of leaf buds in the *S. muticum* meristem follows the golden angle

The *S. muticum* plant is attached to the substrate (e.g. rock) through a discoid holdfast from which the upper body arises. Its main body is formed of one main primary branch and a number of lateral branches that hold leaves, air vesicles and reproductive structures (Fig. 2.2A). The apex of *S. muticum* has a striking 'phyllotactic' pattern, where subsequent branches are spirally organised with respect to each other (Church, 1920; Peaucelle and Couder, 2016). At the apex, these branches begin as leaf buds (Critchley, 1983a). In order to characterise the spiral pattern more fully, a detailed analysis of *S. muticum* apices collected in the field was performed.

S. muticum apices were qualitatively divided into two zones: the apical pit-region, where pro-meristem cells were produced (Fig. 2.2B, pink), and the peripheral region where new leaf buds formed (Fig. 2.2B, yellow). In primary lateral apices the meristem size (proxied by presented area of the pit-region, Fig. 2.2B, pink) was not correlated with stipe length, which is representative of apex age (n (individuals) = 7, n (branches) = 22, Fig. 2.3). Within the peripheral region, the phyllotactic pattern was spiral and presented an average divergence angle (angle between two sequentially-aged buds) of 137.53 ± 2.08° (Fig. 2.2B, C; n (meristems) = 57). The organisation and phyllotactic pattern observed in the apices of *S. muticum* was highly regular and resembled that seen in complex multicellular plant apices.

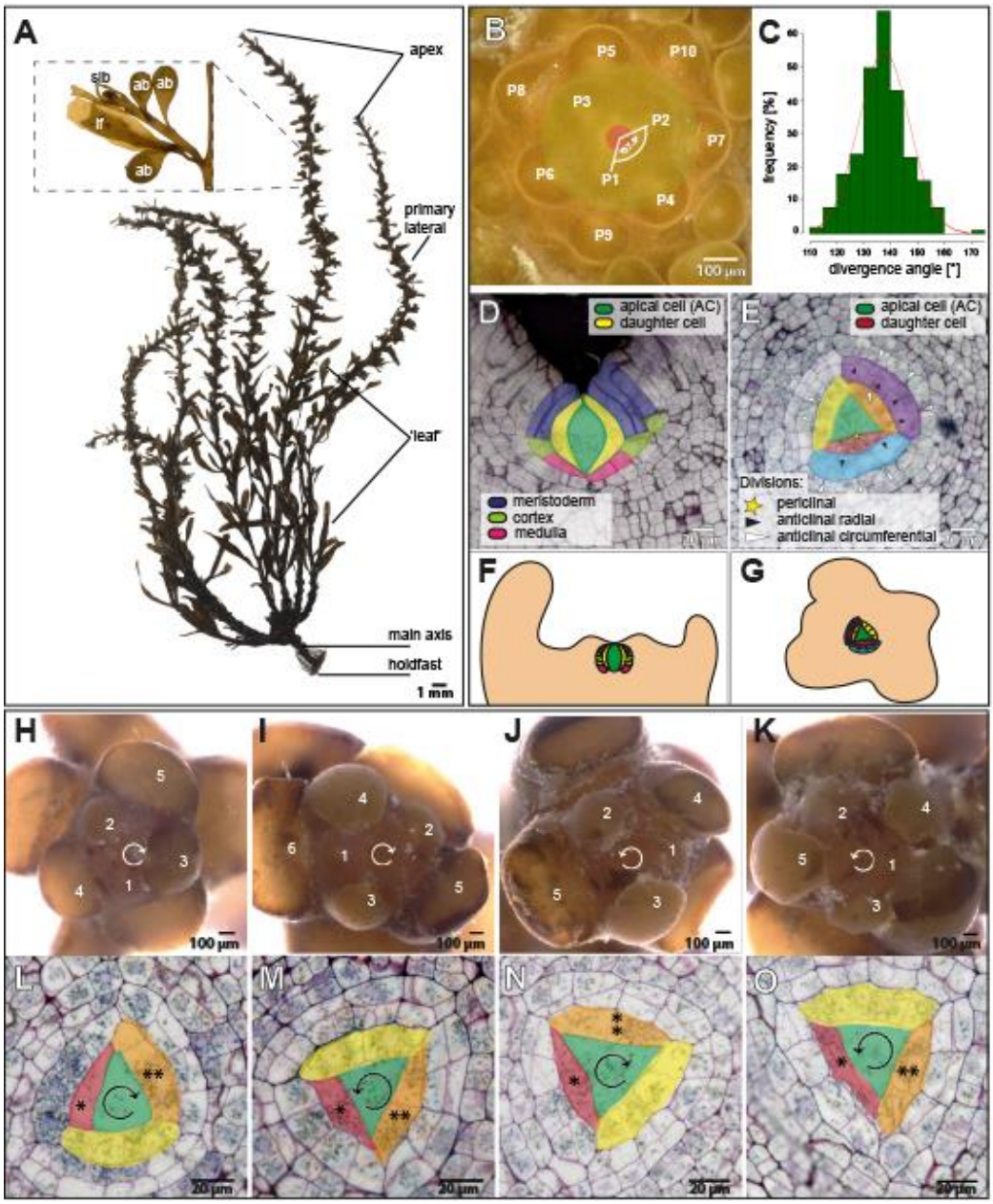

Figure 2.2. The *S. muticum* apex displays distinct patterns which are independent of each other. (A) The morphology of an adult *S. muticum* alga. (B) Newly forming buds numbered by increasing age (P1 -> P10) with a representative divergence angle illustrated between the two consecutive buds. (C) Divergence angles distribution of measured apices (mean=137.53 ± 2.08°; n=260). (D) Division pattern in a longitudinal section of a *Sargassum* apex; AC divides to give rise to three tissues (meristoderm, cortex, and medulla). (E) Apical cell division pattern in a transverse section of a *Sargassum* apex; first periclinal apical cell division (red; yellow star) followed by radial (orange, yellow; white arrowhead) and circumferential (blue; black arrowhead) anticlinal divisions. Schematic representation of the division in the longitudinal direction (F) and the transverse direction (G). (H, I) Clockwise phyllotaxis with a (L) clockwise or (M) counter-clockwise apical cell division orientation. (J, K) Counter-clockwise phyllotaxis with a (N) clockwise or (O) counter-clockwise apical cell division orientation (n=27). *youngest daughter cell, **next-to-youngest daughter cell.

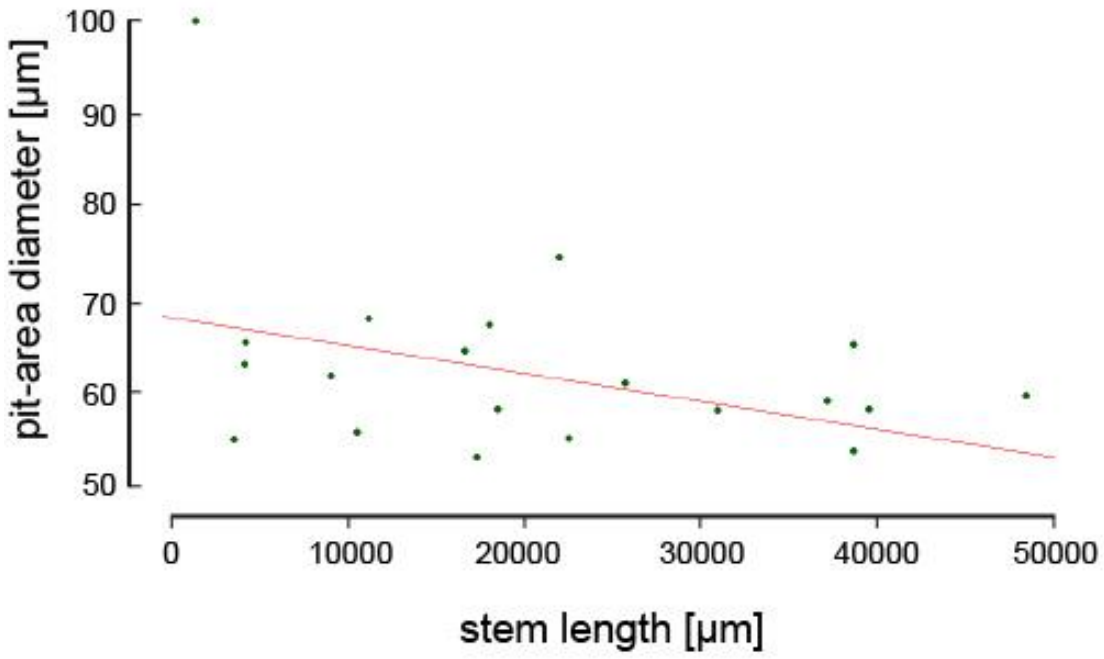

Figure 2.3. The age of the stipe and the meristem area. Scatter plot showing a lack of significant correlation between the length (proxy for age) of an individual stipe with the diameter of its pit-area (proxy for meristem size; apical cell and the promeristem cells around it) (n=22, p-value=0.07, r=-0.39; two-sample t-test).

2.4.2. The *S. muticum* apical cell area suggests a highly organised division pattern

As the literature seemed to indicate that brown algae phyllotaxis might be lineage-dependent, we next examined the division patterns of the *Sargassum* apical cell to see if its pattern exhibited a golden angle, as in moss. In order to investigate the possible patterning of cell divisions in the promeristem, and any connection to the phyllotactic pattern, we examined transverse and longitudinal sections of *S. muticum* apices.

In sections, the apical cell of *S. muticum* presented as bi-convex and lenticular (longitudinally; Fig. 2.2D) and as three-sided (transversely; Fig. 2.2E) consistent with literature (Kaur, 1999; Moss, 1969; Nizamuddin, 1967; Yoshida et al., 1983). Unlike *Fucus* apical cells, which are reported to stimulate their neighbours

to divide but refrain themselves (Moss, 1967), evidence of apical cell division was observed (Fig. 2.2E and Fig. 2.4). In the longitudinal view, divisions appeared to give rise to three tissues – outer layer (meristoderm) and two inner layers (cortex and medulla) (Fig. 2.2D, F and Fig. 2.5).

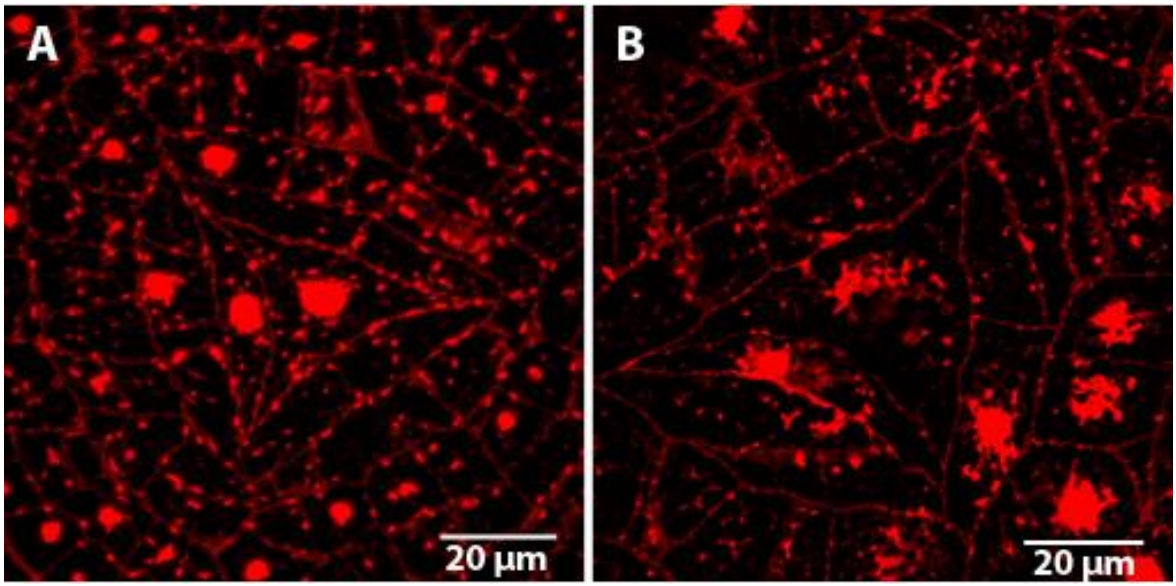

Figure 2.4. Active division of the apical cell. Propidium iodide staining of DNA on transverse sections showing (A) dense signal localized in the nucleus (B) diffuse signal of DNA staining – active division stage.

In the transverse direction, the youngest (apical-cell-proximal) division always appeared to be asymmetric periclinal followed by sequential face divisions from the apical cell producing promeristem daughters at 119° angles to each other (Fig. 2.2E, red). In the first three rounds of division (a division round was defined as a pseudo-time progression that each daughter cell would undergo as it moved away from the apical cell; see Methods), the daughter cell underwent one or more anticlinal radial divisions (Fig. 2.2E, orange/yellow/blue; white arrowhead); the rounds of radial division never produced more than four cells (Fig. 2.2E, blue). The further divisions were anticlinal circumferential and created 8 cells in total (Fig. 2.2E, blue, purple; black arrowhead). After this point it became difficult to discern lineages in histological sections. The pattern described here was highly conserved although occasionally an anticlinal circumferential division was observed before the 4-cell

stage (n=1/30). From these data, it was concluded that the *S. muticum* apical cell divided asymmetrically from sequential faces, producing daughter cells at 120° angles, and that these promeristematic daughter cells further underwent a regimented division pattern.

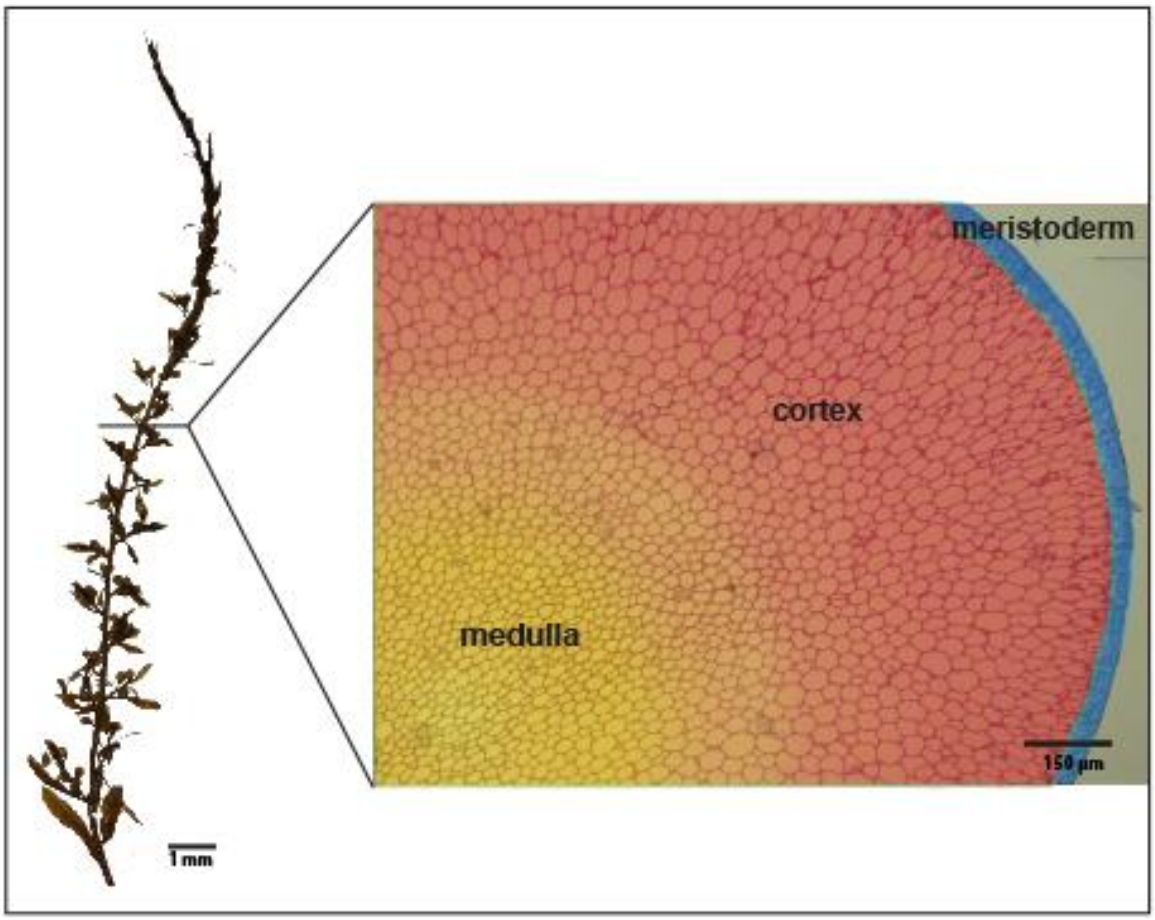

Figure 2.5. Types of tissues found in *S. muticum* as illustrated on a stipe section. Outer layer (meristoderm, blue), middle layer (cortex, red) and inner layer (medulla, yellow).

2.4.3. The phyllotaxis pattern and the apical cell division pattern are not linked

In *Cystophora*, the apical cell division pattern (bifacial divisions) has been correlated with the apical branching pattern (Klemm and Hallam, 1987). The observations in *S. muticum* suggest that the apical cell divides from all three faces

to produce promeristem daughter cells at an approximate 120° angle (α=119.01 ± 6.11°, n=74), while the phyllotactic pattern follows at ~137.5° spiral pattern. In order to examine whether these two patterns in *S. muticum* were linked, the chirality in both the apical and phyllotactic patterns in the same meristems was examined.

The spiral phyllotaxis in *S. muticum* had either a clockwise or a counter-clockwise direction with a ratio of ~1:1 (58/118 clockwise, 60/118 counter-clockwise). In the clockwise and counter-clockwise orientation the older buds were located to the left side of the younger bud forming a right-handed or a left-handed spiral, respectively (Fig. 2.2H, I, J, K). This 1:1 ratio is observed in plants as well (Allard, 1946; Thompson, 1917). With respect to apical cell division patterning, two patterns were observed: moving out from the apical cell, daughter cells were produced to the left or the right yielding both counter- and clockwise patterns in a 1:1 ratio (Fig. 2.2L, M, N, O; 28/56 clockwise, 28/56 counter-clockwise).

In order to examine if a connection in chirality was observed, individuals were imaged under a light microscope and subsequently sectioned to check the orientation of the apical cell division. In either the counter or clockwise phyllotactic groups, the apical cells presented as ~1:1 counter- and clockwise (Fig. 2.2H-O, clockwise phyllotaxis – 8/16 clockwise, 8/16 counter-clockwise apical cell divisions; counter-clockwise phyllotaxis – 7/11 clockwise, 4/11 counter-clockwise apical cell divisions). These data strongly suggest that these two patterning mechanisms are unlinked and may be under separate control. This is highly similar to the patterning mechanisms seen in multicellular plant apices where the phyllotactic pattern and the stem cell niche are separately defined by two hormones; auxin and cytokinin (Chickarmane et al., 2012; Reinhardt et al., 2003a).

2.4.4. Ablation of the apical cell leads to formation of a new apical centre indicating pattern self-organisation

Given the observed similarities to multicellular plant meristems, I next examined whether the apical cell and phyllotaxis could re-establish after ablation of the apical cell. In plants, the stem cell region can re-establish in this way pointing to

a robust self-organising patterning system (Reinhardt et al., 2003b). In *Fucus*, such manipulations led to growth arrest and termination (Moss, 1967).

Apical cell ablations were performed on partially dissected apices either using a thin needle aimed at the centre of the pit-area, *cutting through the meristem (Fig. 2.6A, B, G; white and orange arrowheads) or by removing a single bud (Fig. 2.7A). Apices were grown in culture, and re-dissected after a 3-week recovery period before a second imaging. For the first experiment, four scenarios were observed: in 30% (7/23) of the apices the growth of the central zone had stopped or they were dead (6/7 dead, 1/7 no new meristem formed, but the existing buds continued to grow); in 30% of the samples growth continued from what appeared to be a new pit-region (Fig. 2.6C, D; blue arrowhead, n= 7/23). In these apices, the phyllotactic pattern after recovery exhibited a spiral pattern. In another 20% of apices, the meristems seemed to split in two Fig. 2.6E; n= 5/23) but again appeared to present spiral patterning. In the remaining 20% of the samples, the results were inconclusive as the imaging methods did not always produce sufficient quality data for pit-area positioning. Culturing itself did not alter the pattern of buds (Fig. 2.6F). In the samples where a new pit-area appeared to establish, the wound had moved to the side of the meristem and the new pit-area was roughly centrally positioned (Fig. 2.6C, D).

In the second experiment where the meristem was cut in half using a sharp razor, similar outcomes were observed. 50% of meristems re-established a new centre on one of the halves and continued developing in the spiral manner (Fig 2.6G, H, I; n=7/15). In 25% of the individuals no visible change was observed (n=4/15), and in another 25% no conclusions could be drawn, due to imaging limitations or possible initial accuracy in splitting the meristem in two equal halves (n=4/15).

Isolation of a single bud (Fig. 2.7A) resulted in 25% (Fig. 2.7B, C, black arrowheads; n=4/16) of meristems presenting an enlarged bud. The other 75% (Fig. 2.7D; n=12/16) of the meristems showed no effect upon removal. Performing such a precise surgical experiment proved to be difficult, and although a number of meristems showed a disruption, the interpretation of the results remained inconclusive.

These data suggest that the meristematic region of the *Sargassum* meristem could re-establish itself indicating a self-organising system similar in nature to that in plant meristems. The data also imply that when a new apical cell is established, the spiral phyllotactic pattern can also re-establish.

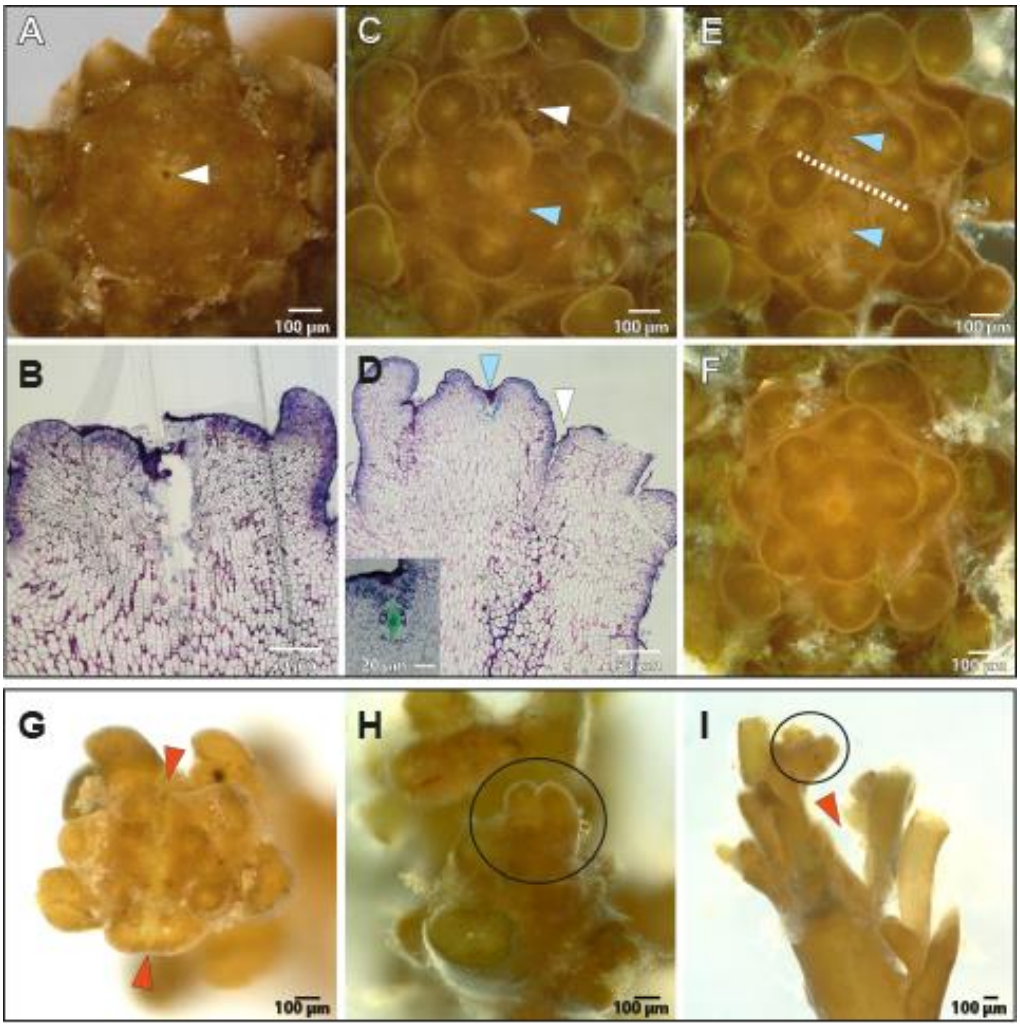

Figure 2.6. Abolishing the apical cell can induce formation of a new central meristem. *Sargassum* meristem stabbed (white arrowhead) in the region of the apical cell in top view (A) and in subsequent longitudinal section (B). (C) Formation of a new central meristem; white arrowhead marks the spot of the stab, blue arrowhead shows the location of the new meristem. (D) Longitudinal section of a newly formed meristem (as in C) showing a new apical cell in the new meristem centre (blue arrowhead) and stabbed area (white arrowhead). Inset: magnified view of the new apical cell. (E) Apex presenting a split meristem; dashed line shows the separation of the two new meristems, centers indicated by blue arrowheads. (F) Control apex, not stabbed. Sample numbers: n=23 stabbed (12 recovered, 7 ceased growth, 4 unclassified). (G) Top view of the meristem with a cut through the middle (orange arrowheads). (H) Newly formed meristem on one of the cut sides in top view and in side view (I). Black circle marks the new spiral phyllotactic arrangement. N=15 (7 recovered, 4 no change, 4 unclassified).

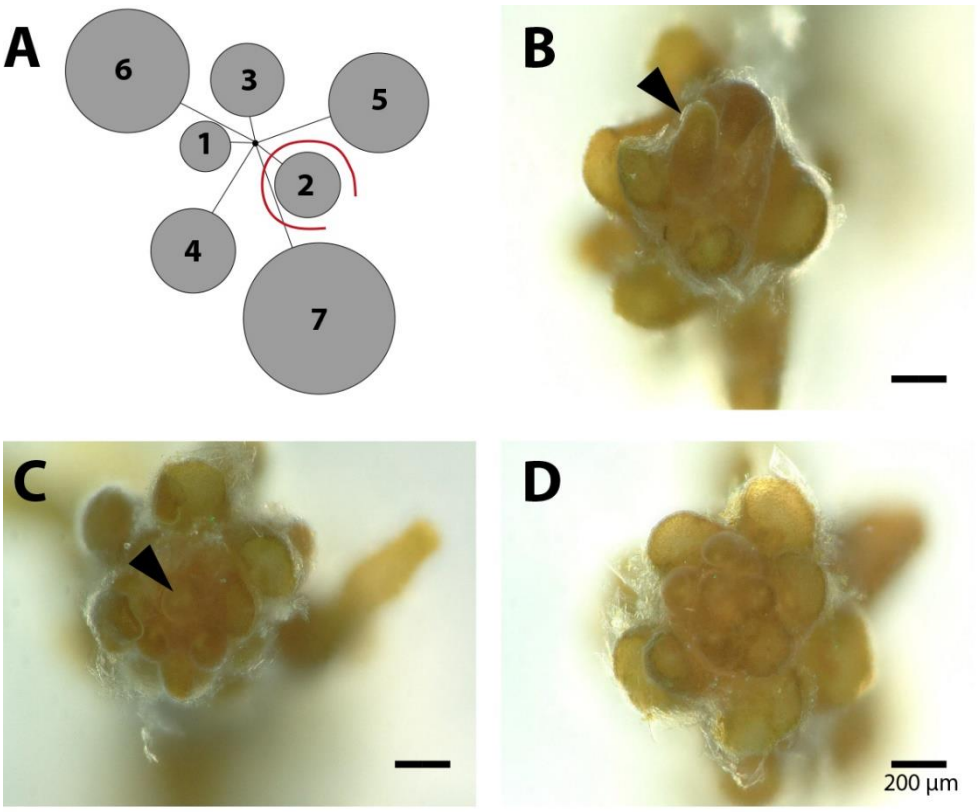

Figure 2.7. Removal of a growing bud can perturb the normal apical growth. (A) Scheme of the surgical approach; one of the newest buds was removed by circular incision. 25% (n=4/16) of apices shows aberrant growth where one of the buds becomes enlarged (B, C); black arrowheads point at those buds. (D) 75% of apices (n=12/16) continue growing normally.

2.4.5. A potential link between auxin and brown algal phyllotaxis is unlikely

In plants, auxin distribution within the peripheral zone dictates the phyllotactic pattern (Reinhardt et al., 2003a). The brown algae *Fucus vesiculosus* and *Ectocarpus siliculosus* have both been shown to exhibit auxin-triggered morphogenetic changes (Basu et al., 2002; Le Bail et al., 2010). Since the phyllotaxis in *S. muticum* is spiral and highly resembles the one observed in higher plants, and given the potential for auxin response in brown algae, I next examined whether auxin could alter, or be correlated with, the phyllotactic pattern.

Applying auxin externally in the artificial seawater cultivation medium in order to see if phyllotaxis could be altered had no effect on growth or the phyllotactic pattern after 20 days in the media containing 50 µM concentration of a natural (1-Naphthaleneacetic acid, NAA) and a synthetic auxin (2,4-Dichlorophenoxyacetic acid, 2,4-D) compared to the control (Fig. 2.8). Due to the aqueous nature of the culture system it was not possible to apply auxin locally, as has been performed in tomato and *Arabidopsis* (Braybrook and Peaucelle, 2013; Reinhardt et al., 2000). These experiments were therefore inconclusive but possibly suggest that external auxin could not alter phyllotaxis in *Sargassum* in these conditions.

In order to determine if auxin showed patterned distribution within the apex, I performed immunolocalisations on sectioned apices using the anti-IAA antibody. The anti-IAA signal was strongest in the meristoderm and mucilage external to the meristoderm with accumulation at apical pits and the bases of buds (Fig. 2.9A, white arrowhead). Internally, there were regions of high signal within the apex in the meristoderm although these did not correlate with bud size or position (Fig. 2.9A, B). Upon close examination, a large amount of signal originated from the mucilage external to the meristoderm (Fig. 2.9C). These data suggest that auxin may be accumulating in the meristoderm and mucilage, although its source is undetermined (see Discussion), and there was little correlation with bud position.

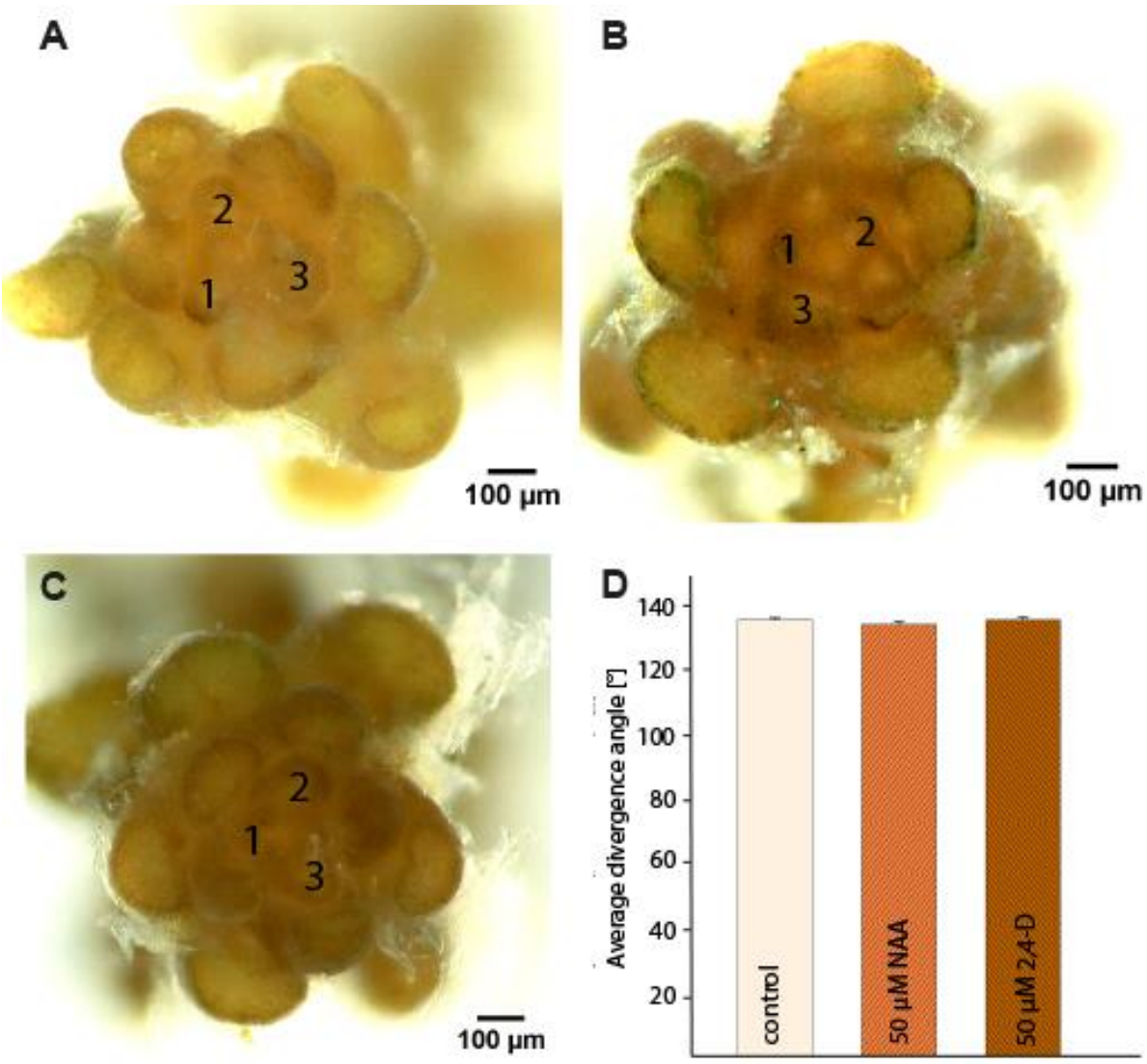

Figure 2.8. The effect of exogenous auxin on *S. muticum* phyllotaxis. When compared to control treatments (A, 50µM DMSO), neither NAA (B) or 2,4-D (C) auxins influenced phyllotactic patterning when supplied to the apices at 50µM in artificial sea water. Divergence angle was quantified for n=20 apices per treatment (D).

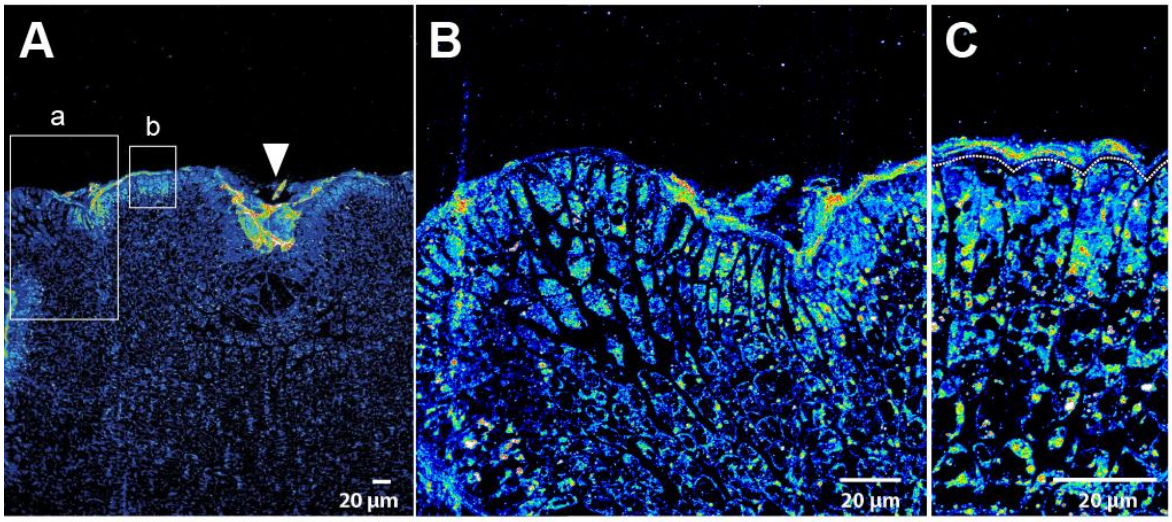

Figure 2.9. Indole 3-acetic acid immunolocalisation signal does not appear to correlate with new bud formation in the *S. muticum* apex. (A) Anti-IAA antibody localising to the buds, surface of the meristoderm and the apical pit (white arrowhead). Higher magnification view of the bud (B) and of the meristoderm cells (C). Dashed line in (C) delineates the meristoderm outer cell wall. n (meristems) =4.

2.4.6. Elongating organs are predicted to have softer walls and the apical cell to have stiffer cell walls

In plants, new organs form in the peripheral zone after auxin maxima lead to wall softening (Braybrook and Peaucelle, 2013). The central zone, containing the meristematic stem cells, exhibits stiffer cell walls than the peripheral zone or new primordia (Milani et al., 2014). In most walled organisms, it is assumed that cell growth is limited by the cell wall and its mechanical properties, in turn linked to its biochemical composition (Braybrook and Jönsson, 2016; Peaucelle et al., 2008). Since *Sargassum* apices were so similar in pattern to the *Arabidopsis* apex, we checked whether they might follow similar mechanical rules. Alginate biochemistry was examined *in muro* using antibodies raised against different biochemical epitopes: the BAM10 antibody preferentially recognises guluronic acid within alginate (Torode et al., 2016), which should be mechanistically rigid through calcium cross-linking (Grant et al., 1973); furthermore, the BAM7 antibody binds to chains of mixed mannuronic and guluronic acid residues (MG-blocks) and the BAM6 antibody preferentially binds to mannuronic acid residues within alginate, which should be mechanically less rigid, as these are unable to form calcium cross-links (Torode et al., 2016).

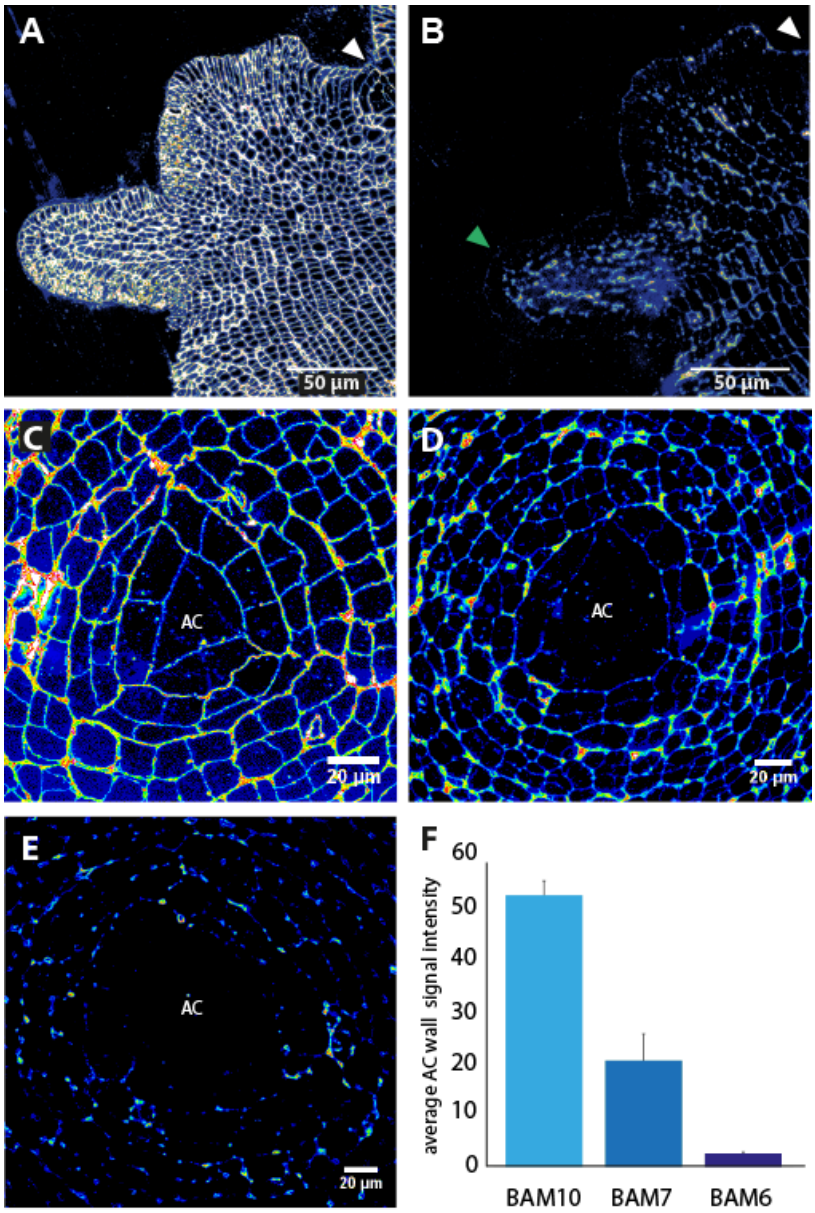

Figure 2.10. Mannuronic and guluronic acid immunolocalisation in *S. muticum* apical cell. The signals do not show apparent correlation in respect to bud outgrowth in the *S. muticum* apex, but show differential localisation in the apical cell region. (A) BAM10 antibody binds to the guluronic acid rich areas in the cell wall with a homogeneous distribution throughout the apex. (B) BAM6 antibody binds to mannuronic acid rich areas in the cell wall, localised at the surface and on cell-cell junctions in the inner tissues and with a slightly higher abundance in a young bud (green arrowhead). (C) BAM10 (G-block alginate) antibody signal is distributed throughout the apical cell and promeristem region in transverse sections. (D) BAM7 (MG-block alginate) antibody signal is present in the apical cell walls and the cell walls of the promeristem (E) BAM6 (M-block alginate) antibody signal is not detected in the apical cell and immediate neighbours. BAM6 localises mainly in the cell junctions around the apical cell. (F) Average fluorescence signal from three sides of the apical cell for three alginate antibodies. White arrowheads mark the pit-area (with an apical cell). AC = apical cell location. n (transverse) = 5, n (longitudinal) = 7.

In longitudinal sections, BAM10 showed a wide distribution of signal across the apex (Fig. 2.10A). BAM6 signal was found at the junctions of cells and on the outer periclinal walls of the meristoderm cells (Fig. 2.10B). There was no obvious pattern of mannuronic/soft alginate associated with young buds, however signal did appear higher in slightly older elongating buds (BAM6; Fig. 2.10B; green arrowhead). I next looked at the apical cell alginate biochemistry using immunolocalisations on transverse sections. The BAM10 signal was present and equally distributed across the apical cell, promeristem cells and the surrounding cells (Fig. 2.10C, F). The BAM7 signal was present to an extent in the cell walls of the apical cell, but not equally distributed. The signal was also found in the promeristem cells (Fig. 2.10D, F). The BAM6 signal was excluded from the apical cell and promeristem cells (Fig. 2.10E, F). BAM6 signal was detected in more mature tissues at the junctions between cells (Fig. 2.10E; BAM11= 51.42±4.66, BAM7= 24.06±8.77, BAM6= 2.52±0.48). Control immunolocalisations are shown in Fig. 2.11.

To determine whether a differential localisation of alginate signals could be observed in the rest of the *S. muticum* plant, immunolocalisations on three different transverse tissue sections were performed of the primary stem close to the meristem area, primary stem close to the holdfast, and leaves. In upper stem and leaves, the BAM6 signal was present in the meristoderm and the medulla, whereas the lower stem exhibited a BAM6 signal mostly in the cortex and to a lesser extent in the other two tissues (Fig. 2.12).

These data suggest that the apical cell, young promeristem cells and the peripheral area in the apex have more guluronic acid residues than mannuronic acid residues, which may lead to stiffer cell walls. Furthermore, a fluorescence signal was examined in the stem from two areas, a young stem (close to the apex) and an older stem close to the holdfast. In the younger stem, mannuronic acid rich areas were found in the outermost and innermost tissues, suggesting softer walls (and potentially more growth). In the older thallus, mannuronic acid rich areas were found in the middle tissue, the cortex. Different localisation of mannuronic rich areas in two distinct areas of the stem could indicate a different growth mode between the two.

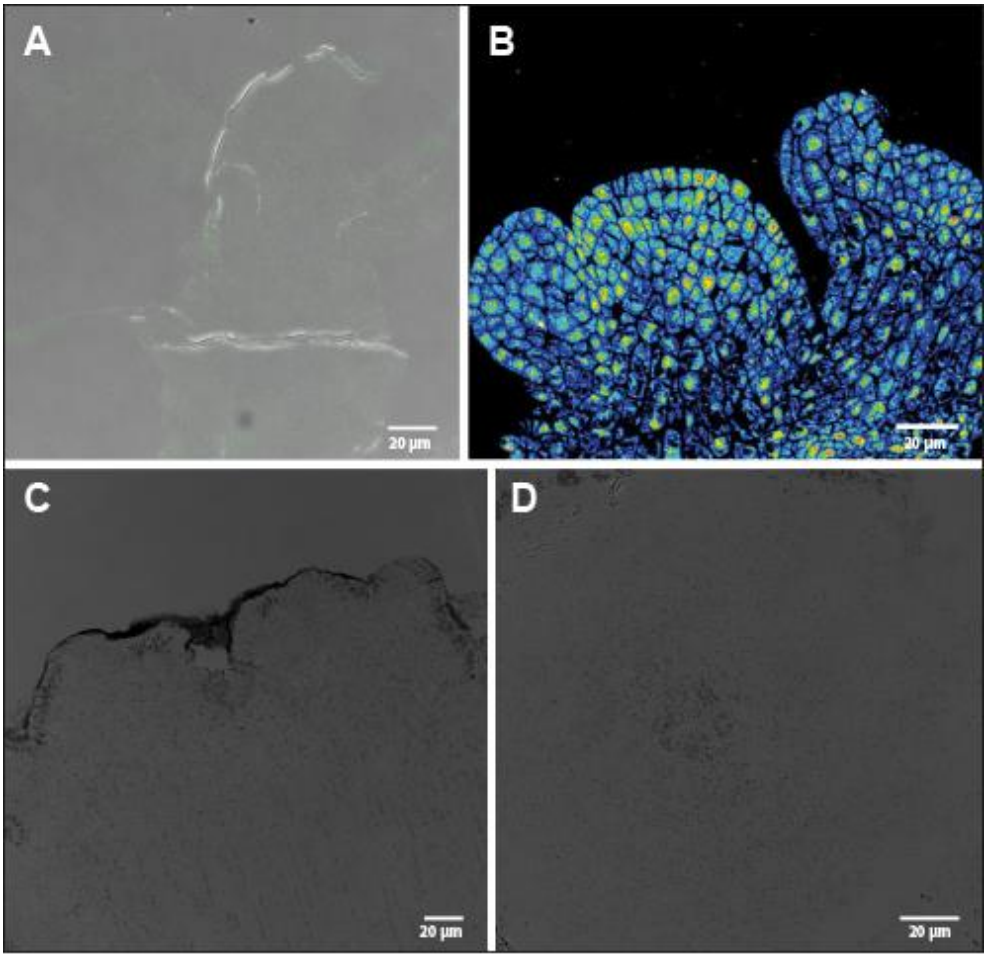

Figure 2.11. Control confocal images for the auxin and alginate immunolocalisations. *Arabidopsis thaliana* longitudinal section with no primary antibody control (A) and anti-IAA (B). (C) No primary antibody controls of *S. muticum* apex sections for alginate immunolocalisation. (C) Longitudinal section and (D) transverse. All controls merged with a brightfield image for visualisation. Scale bar 20 µm.

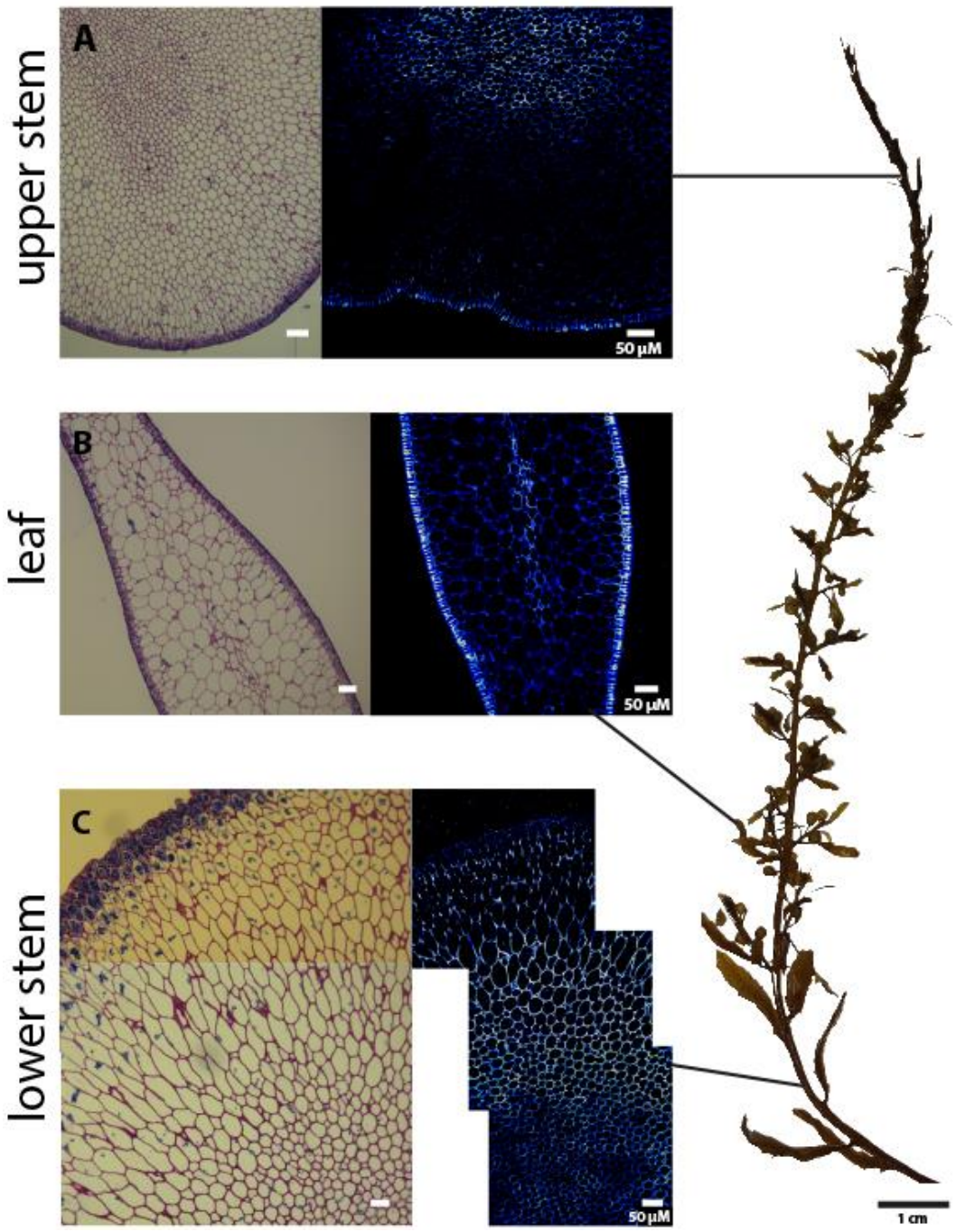

Figure 2.12. Mannuronic acid immunolocalisation (BAM6) in different structures of a *S. muticum* plant. Brightfield (left) and BAM6 antibody immunolocalisation (right) in upper younger parts of the stem (A), leaves (B) and older parts of the stem (C).

2.4.7. Apex wall mechanics does not change depending on the position of growing buds

In plant meristems, new organ formation is correlated with local changes in the wall stiffness. The areas of formed primordia or primordial initials have been shown to have softer cell walls when examined using atomic force microscopy (Peaucelle et al., 2011). In order to examine whether the same pattern could be observed in the *Sargassum* meristem, the same approach was taken.

Apices from three individuals were tested under the atomic force microscope to look for changes in wall stiffness relating to new bud outgrowth. Nine to eleven force maps were created for each apex and grouped according to their position on the meristem (Fig. 2.13). All three maps covered both growing and non-growing regions of the apices. Close examination revealed no differences between the two distinct regions; the newly forming buds did not show a smaller Young's modulus (softer walls) when compared to the meristematic region or the non-growing areas between the buds. This could mean that the pattern of the growing buds might not be corresponding to the local stiffness decrease in the cell walls, in contrast to what is observed in plants.

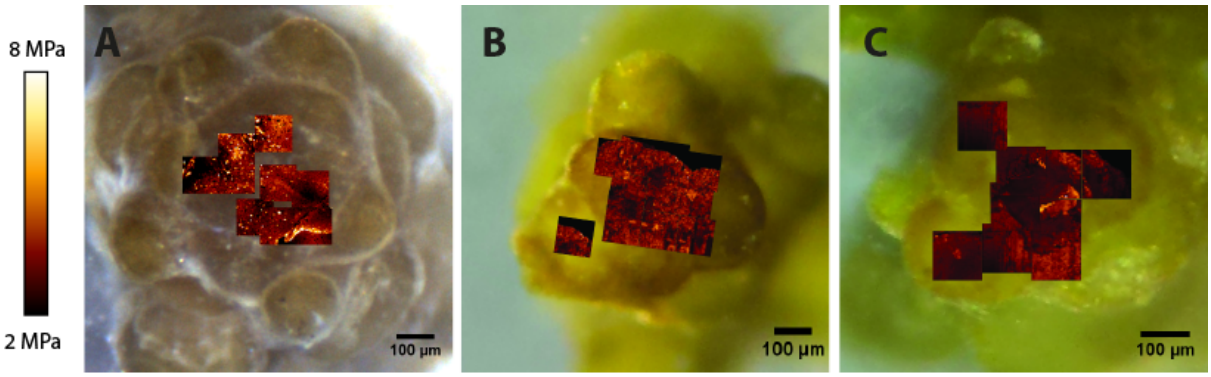

Figure. 2.13. Cell wall mechanics in the *S. muticum* apical meristem. Maps of the apparent Young's modulus (E_A) of the three individual meristems (A, B, C) showing no clear differences in E_A between the growing (buds) and non-growing regions. The maps represent a collage of 9 (A, C) or 11 (B) 100x100 µm force maps.

2.5. Discussion

2.5.1. Phyllotaxis is a phenomenon found in evolutionarily distant photosynthetic lineages

Here I report that the spiral phyllotactic pattern in *S. muticum* follows the Golden Angle (~137.5°) in a pattern almost identical to that found in many multicellular plants. Developmentally, this may not be so surprising since both organisms display indeterminate growth and produce new organs from an apical meristem-like region, and both utilise their shoots and branches for light interception and reproduction. However, it is interesting to see a similar pattern when the building blocks of multicellularity are completely independent: while both organisms have cell walls and cell adhesion, the polysaccharides that make up the wall matrix (pectin and alginate) are distinct. These organisms have evolved multicellularity independently (Baldauf, 2008) and therefore may have different communication strategies (morphogen identity). The data presented here indicate that complex parenchymatous brown algae have a position-dependent patterning mechanism that results in spiral phyllotaxis, similar to that observed in plants.

2.5.2. AC-based patterning does not underlie phyllotactic patterning in *S. muticum*

The apical cell is the centre of the brown algal meristem; its sequential face divisions create a pool of cells that build the body of the adult alga. In the spiral meristem of *S. muticum* the division pattern of the algal apical cell does not relate to phyllotactic patterning. Firstly, the difference in the divergence angles between the two patterns does not support a causative relationship – in apical cell divisions, the angle of the newly produced daughter cell to the previous is 120°, whereas the observed phyllotactic angle centres on the golden angle of 137.5°. In the moss *Atrichum undulatum*, the triangular apical cell exhibits sequential face divisions but these occur at ~137.5°, an angle which is reflected directly in the phyllotactic angle (Gola and Banasiak, 2016). In *Physcomitrella patens*, spiral apical cell divisions lead to spiral leaf arrangement (Harrison et al., 2009). As this correlation in pattern is not

seen in *S. muticum*, apical cell division pattern and phyllotaxis appear to be unrelated. While growth distortion post-apical-cell cannot be discounted, I believe it is unlikely given the highly organised nature of divisions seen in the apex. A second piece of evidence comes from the observation that both patterns could follow either a left- or a right-handed rotation but the two could be disconnected. My experiments suggest that apical cell division pattern and phyllotactic pattern are not correlated. I hypothesise that an apical-cell-independent patterning mechanism exists in *Sargassum*, that position is more instructive than lineage.

2.5.3. Apical robustness in *S. muticum*

When a stem-cell niche or apical cell are destroyed in plants, there are two outcomes reported in the literature for plants: the apical growth can cease, or the apex will develop a new stem-cell centre and restart growth (Cutter, 1965; Reinhardt et al., 2003b; Steeves and Sussex, 1989; Wardlaw, 1949). In examined brown algae, destruction of the apical cell leads to the termination of apical growth (Clayton and Shankly, 1987; Moss, 1967); no re-establishment of patterning has been reported to our knowledge.

In my experiments, *S. muticum* apices exhibited both outcomes upon apical-cell destruction (30% of the apices ceased growing, while another 50% showed continued growth after re-organisation). The continued growth was observed in the second set of experiments where the meristems were split in two halves (in 50% of individuals). Similar to plants, my data showed that the phyllotactic pattern in the *Sargassum* meristem was also re-established (or maintained) upon apical cell destruction or meristem disruption (50% of individuals showed re-establishment of a phyllotactic pattern after splitting the meristems). These data indicate that the *S. muticum* apex is capable of re-organisation after apical cell destruction, in a similar way to that seen in plants. This complexity, and its similarity to those of plants, may represent a more robust system when it comes to development. This further supports a morphogen-based position-dependent patterning mechanism.

2.5.4. Auxin is an unlikely candidate for the phyllotactic morphogen

The potential of auxin as a morphogen has been established in flowering plants (Reinhardt et al., 2003a), and it has been found to have an effect in the development of bryophytes (Bennett et al., 2014; Coudert et al., 2015) and brown algae (Basu et al., 2002; Le Bail et al., 2010; Sun et al., 2004). As such, auxin was a prime candidate for morphogen-like behaviour in the *Sargassum* apex. However, I was unable to detect an effect of exogenous auxin on phyllotactic patterning in *S. muticum*. It is possible that the auxins used (1-Naphthaleneacetic acid and 2,4-Dichlorophenoxyacetic acid) were not effective or that their concentrations require further optimisation. It is also possible that local applications might have been more effective: local applications could alter phyllotaxis in the plants *Lupinus* and *Epilobium* (Snow and Snow, 1937) but when more broadly applied in *Tropaeolum* a lesser effect was seen (Ball, 1944).

In order to gain a more spatial view of possible endogenous auxin, I then switched to IAA-immunolocalisations. My data suggest that there is no particular localisation of auxin to newly growing buds observed in sections of *S. muticum* apices, but a higher signal localized in the meristoderm cells and mucilage attached to the surface of the alga. I cannot completely rule out non-specific antibody reactions to the mucilage; however, the no primary antibody controls were negative (Fig. 2.11) and the cell wall antibodies did not show such signals (Fig. 2.10). Detecting a small and highly dynamic molecule such as auxin using immunolocalisations is limiting; however, using a specific pre-fixation step auxin could be fixed and detected using this approach in plants and brown algae (Avsian-Kretchmer et al., 2002; Le Bail et al., 2010). It is possible that IAA is not the functional auxin in *Sargassum*, although it has been detected by GC/MS in the brown alga *Ectocarpus* (Le Bail et al., 2010). In addition, application of exogenous auxin (50 µM NAA) affected *Ectocarpus* development in various stages. In the young sporophytes, cell shapes (from both cell types, round and elongated) were abnormal, dispositioned and a higher number of branching points could be observed. *Ectocarpus* adult development is quite different than *Sargassum*; while *Ectocarpus* builds its filamentous body from two cell types (round and elongated cells), *Sargassum* builds a more complex body structure through coordinated

branch formation. Different responses (or lack of a response in the *Sargassum* case) to external auxin might be explained by differences in body-building strategies. To explore this hypothesis further, a wider range of different brown algal species should be incorporated in the auxin response studies. The data presented here suggest auxin is an unlikely morphogen for *Sargassum* phyllotaxis, but without a tool such as the molecular reporter constructs in plants it is not possible to be certain.

There is no evidence to date that brown algae have homologues of the auxin transporters found in plants (based on the genome of *Ectocarpus siliculousus*; Le Bail et al., 2010; Yue et al., 2014), although the algae may have completely different transport mechanisms, even diffusion. Classical phyllotactic patterning mechanisms have relied on reaction-diffusion equations in the past (Bernasconi, 1994; Swinton, 2004), and as such it is possible that auxin diffusion may be instructive in brown algae. Another question that has been a topic of discussion is whether the auxin detected is being produced by the alga itself or being provided by auxin-producing associated bacteria on the surface of their thallus (Evans and Trewavas, 1991). Bacteria have been described living in association with brown algae (Hengst et al., 2010; Lachnit et al., 2011), and having an effect on their development (Tapia et al., 2016). A similar process has been recently described in a sister class to brown algae – diatoms (Amin et al., 2015). The recent interest in exploring the algal-bacterial interactions could lead to a better understanding of whether and how the bacteria might be affecting the development in a more ‘advanced’ brown algal species such as *S. muticum*.

2.5.5. Cell wall softening and algal bud outgrowth

The cell walls of brown algae are composed mostly out of matrix polysaccharides called alginates and sulphated fucans and a small amount of cellulose (Deniaud-Bouët et al., 2014). In plants, the role of the cell wall and its relationship to auxin in organ formation has been previously explored (Braybrook and Peaucelle, 2013; Fleming, 1997; Peaucelle et al., 2008; Peaucelle et al., 2011; Reinhardt et al., 1998), but no information of such is available for the brown algae. Given the recent evidence for a role of pectin in organ emergence, and the predominant nature of alginate in the algal cell wall it seems plausible that alginate

may be involved in bud formation. Alginate is formed of two residues, mannuronic and guluronic acid, the latter being able to cross-link with Ca^{2+} ions (Grant et al., 1973), similarly to pectin in plants, and thus change its mechanical properties (Mancini et al., 1999).

New techniques have been recently developed to look into the brown algal cell wall biochemistry by using immunolocalisations targeted towards specific epitopes in alginate chains (Torode et al., 2016). Our data suggest that the guluronic acid rich areas are more abundant throughout the apex of *S. muticum*, but there was no clear distinction between growing and non-growing parts. The mannuronic acid (BAM6) signal tended to be higher in rapidly growing older buds without obviously marking young buds. These observations differ from the ones seen in *A. thaliana* meristems where pectin biochemical changes did mark new organ sites (Peaucelle et al., 2011). In slightly older, elongating buds, a stronger signal from BAM6 was detected, indicating a possible role for alginate biochemistry in elongation but not initiation of buds.

In transverse sections, I observed that the guluronic acid signal (BAM10) was high, whereas that for mannuronic acid (BAM6) was barely detected. The mixed mannuronic and guluronic acid residue (BAM7) signal was present in the cell walls of the apical cell, but to a lesser extent than BAM10. Even though conclusions can be made based on the spatial information obtained from immunolocalisation (where an epitope is found in the tissue), comparing the signal fluorescence intensities among different antibodies is not always accurate if the exact epitopes are unknown. Antibodies can bind to their respective epitopes with different affinities. Conclusions about a single antibody binding to different samples are possible, as long as the experimental processes are consistent. In the case of monoclonal antibodies in my experiments, the binding sites have not been completely characterized, which makes the comparison of fluorescence signals hard to interpret.

Based on the localisation data only, I could suggest that the area around the apical cell and the apical cell itself has the potential to make stiffer walls. This is similar to the situation observed in plants, where the stem cells have been shown to be stiffer than the surrounding peripheral cells (Milani et al., 2014). Taken together, it seems that the apical cell in *Sargassum* may behave mechanically similar to the

stem-cell niche in spermatophyte plants and that softer alginate may be present in rapidly elongating new buds. However, it does not appear that new bud positions display biochemical markers of softer alginate and as such it is possible that alginate biochemistry is not related to bud positioning in *Sargassum*, only in outgrowth.

My observations of differential mannuronic acid distribution in the *S. muticum* organs and the hypothesis that those residues create a softer cell wall, could indicate a differential mode of growth in different parts of the alga. Higher signal in the meristoderm and medulla in growing stem and leaves suggests that these two types of tissues could be important in the growth of these structures. Conversely, the lack of signal in these tissues in the lower stem and a higher signal in the cortex cell walls suggests the growth mostly results from these areas. Due to issues with the secondary antibody in this experiment, it was not possible to perform immunolocalisation using the other two antibodies, BAM7 and BAM10. Initially an anti-rat IgM was used as the secondary antibody. This antibody showed strong binding towards BAM6, but did not result in any signal from the other primary antibodies. After finding the solution of the fluorescence issue, a new secondary IgG antibody was used for all subsequent immunolocalisation experiments.

Performing these immunolocalisations again in the future, with the more amenable secondary antibody, would be a step forward into understanding better the potential mechanical contributions of alginate to the growth of different structures in *S. muticum*.

2.5.6. Possible mechanisms of phyllotaxis in *S. muticum*

In the *Sargassum* apex, a new leaf will develop its own apical cell, and further cells along the meristoderm between this and the primary apical cell will follow suit, each giving rise to another organ on each branch (Critchley, 1983a). It has been suggested that all meristodermal cells in *Fucus* have a meristematic ability which could indicate that any cell from this cell layer could ‘switch on’ and become an apical cell and start producing its own bud (Moss, 1967). This is not dissimilar to the specification seen in ferns for the production of new leaves from the epidermis (Bierhorst, 1977; Mueller, 1982). Based on the robust, self-organising nature of the *Sargassum* apex and the lack of correlation between the apical cell division pattern

and that of new buds, it seems likely that a positional mechanism is in place for phyllotactic patterning in *Sargassum*, possibly a morphogen.

The secondary specification of further apical cells between the leaf and main apical cell also hints at a position-dependent specification of meristodermal conversion into apical cells. It has been observed that the apical cell can divide to potentially create a daughter apical cell which then continues to create a new branch (Kaur, 1999). In my experiments, I never observed an equal division of the apical cell that could explain the previously described situation. This is similar to the case in *Cystophora* where division to produce a second apical cell was rarely observed (Klemm and Hallam, 1987). If this hypothesis is assumed to be true, and that I simply missed such special divisions, based on the observed patterns of longitudinal division, it seems unlikely that this could produce a golden-angled spiral and would more likely produce a 120° spiral.

The absence of cell wall biochemical marks associated with alginate softening correlated to new bud positions indicates that the physical events of initial bud outgrowth may be different than that in plants. However, it might be that alginate does not represent the main component regulating wall mechanics, as pectin has been shown to be. Two other major wall components, cellulose and sulphated fucans might have an influence (explored in Chapters 3 and 4). This absence of alginate correlation with bud outgrowth is further supported by the atomic force microscopy data, which did not reveal any differences between the growing buds and the non-growing regions of the apex. However, there are some challenges when performing experiments such as nano-indentation in this species. The apex of the alga is covered in mucilage, which can interfere with the execution of the experiment since it tends to adhere to the cantilevers and tips during force scanning. Furthermore, only the elastic changes were measured in this experiment (elastic coefficient, Young's modulus). The mechanical properties of plant walls exhibit time-dependent behaviour representative of viscoelastic materials. Viscoelastic properties were not tested for in these apices; since these properties might show a difference based on positioning, experiments measuring this in the future would be helpful to make deeper conclusions.

This does not rule out a physically-based positioning system for the brown algal apex; physical buckling may give rise to phyllotactic patterns. If the underlying cortex tissue is growing at a faster rate to the meristoderm physical buckling may result through compression of the outer tissue (Dumais, 2007). This possibility is worthy of further investigation. Furthermore, it has been shown in *Epilobium* that by an operation of a decussate meristem, it is possible to convert it into one or two meristems with spiral phyllotaxis (Snow and Snow, 1935). As the authors suggest, it is possible that the development of a phyllotaxis system can be explained on the basis of the theory that each leaf arises in the first available space and less on the physiological properties of the apex itself.

The similarity between the *Sargassum* apex and that of complex multicellular plant meristems is striking: the presence of a golden-angled phyllotactic spiral; the robust reorganisation after meristem ablation; the presence of equal clockwise and counter-clockwise patterns; the apparent independence of phyllotactic patterning to meristem divisions. However, there are many obvious differences as well: there is not currently strong evidence for auxin as a patterning morphogen; it was also not possible to detect softening of the algal cell walls coincident with new bud outgrowth. While the experiments presented here make a case for the *Sargassum* apex as being more plant-like in its patterning and organisation principals, there are many new questions. Is there a re-specification of a meristodermal cell into a new apical cell, and how is this regulated? If auxin is an unlikely morphogen, what might be the identity of the algal functional analogue (if it exists at all)? If auxin can in fact be instructive, is it produced by the algae or by associated bacteria (implying a more communal evolution of patterning in the brown algae)? How universal are morphogenetic strategies within brown algal lineage due to their high variability in shapes? The answers to many of these questions undoubtedly require advances in molecular techniques and genetics within the brown algae or specific groups within. These techniques are beginning to be developed in *Ectocarpus* and hopefully can be translated into other interesting algae. Another hurdle is the inability to culture many brown algae for their full life cycle *in vitro*, thus limiting when questions might be asked (seasonally). Currently methods exist for *Ectocarpus* and *Dictyota* (Bogaert et al., 2016; Charrier et al., 2008).

Chapter 3. Exploring growth and wall properties in *Fucus serratus* embryo development

A part of this chapter was done as a collaborative effort with Dr Anna Gogleva (Schornack Group, SLCU). All the methods and analyses performed by the collaborator are marked with a sign Δ.

3.1. Summary

Fucus embryogenesis represents a highly interesting developmental system. The fertilised zygote is initially spherical after which it is transformed into a highly polarized cell, exhibiting asymmetric distribution of cytoplasmic and cell wall components. This polar distribution results in an asymmetrical cell division giving rise to two distinct cell types: thallus and rhizoid. The growth at the early stages is localised to the rhizoid only (tip growth), with the thallus cell undergoing divisions and starting to elongate only later in development. In Chapter 3, I describe the *F. serratus* embryo development from a single celled stage to the maturing 2 week old alga. The results suggest that exocytosis mechanisms during early rhizoid tip growth act similarly to plant systems, with a higher rate of vesicle deposition on the tip sides. Due to a significant role of cell walls in brown algal growth, I examined the wall mechanical and biochemical properties during this process. The change in wall mechanics corresponds to growing and non-growing regions (rhizoid vs. thallus), whereas the wall biochemistry mildly indicates involvement. In addition, this chapter begins to explore the molecular basis of embryogenesis through RNA sequencing, focusing on a family of genes involved in alginate biosynthesis. The results suggest different expression patterns of individual genes, possibly relating to different alginate modifications during *Fucus* embryo morphogenesis.

3.2. Introduction

In the last few decades, fucoid zygotes have served as a system to explore the processes related to cell polarisation as well as asymmetrical cell divisions (Goodner and Quatrano, 1993; Brownlee, Bouget and Corellou, 2001 and references therein). The ease with which these zygotes can be obtained and manipulated *in vitro* has established them as model systems for these types of studies. Unfertilized fucoid eggs, after being released into the surrounding seawater, are a natural protoplast: apolar and lacking a cell wall (Callow et al., 1978). Shortly after fertilisation, a cell wall is secreted around the zygote (Bothwell et al., 2008; Quatrano et al., 1985) and by 4h after fertilisation (AF) turgor pressure begins to build (Allen et al., 1972). Zygotes then undergo asymmetric growth (germination) after which an initial asymmetric division takes place (Fowler and Quatrano, 1997; Kropf, 1997). This germination is preceded by a polar distribution of cytoplasmic and cell wall material which results in the formation and fixation of the polar axis (Kropf and Quatrano, 1987; Quatrano and Shaw, 1997; Alessa and Kropf, 1999) and an increase in internal pressure to 0.7 to 0.8 MPa, which is needed for outgrowth to occur (Kropf, 1992).

After germination an initial asymmetric cell division produces two cells with distinct morphologies and fates: a rhizoid and a thallus cell. The rhizoid cell generates the holdfast (attachment disc) and the stipe (‘stem’) of the mature plant, whereas the thallus cell develops into the algal body (Bouget et al., 1998; Quatrano, 1978). The rhizoid cell elongates rapidly by tip growth, dividing transversely to the growth axis. The rhizoid represents the only site of active growth in the embryo at this stage. On the other side, the thallus cell undergoes a series of divisions transverse to each other in the first couple of days of development. Eventually, the divisions give rise to an elongated thallus (Bouget et al., 1998; Kropf et al., 1999). Concurrently with thallus elongation, the apical part of the thallus starts producing apical hairs. The apical hair formation is an important step during embryo development because at the apical hair base the meristematic apical cell is produced. Inhibiting the production of these hairs prevents thallus development (Galun and Torrey, 1969). Soon after apical cell appearance, the tip growing rhizoid

produces a holdfast, a structure that allows the embryo to attach firmly to the substrate.

In the past, fucoid zygotes have served as models for exploring cell wall biosynthesis and understanding the main components of cell walls in developing fucoid zygotes. Cellulose and alginates constitute the first deposited polysaccharides (equal amounts in the first 30 minutes; Quatrano and Stevens, 1976). The alginate proportions in embryo walls have been found to be 69% G blocks, 27% M blocks, and 4% MG blocks (Larsen, 1981 via Kropf, 1992). Recently, arabinogalactan proteins (AGPs) have been demonstrated to be present in the cell wall along with alginates and cellulose. AGPs have been shown to have an effect on zygotic development (delay in cell elongation; Herve *et al.*, 2016) as well as potentially being involved in mannuronic acid epimerisation (Torode et al., 2016). Sulphated fucans, as the third major component, can only be detected after 4 hours AF. The composition at this time is around 60% alginate, 20% cellulose and 20% fucans. As development progresses, the ratios between these three components remain unchanged, although overall more polysaccharides are found during rhizoid elongation (Quatrano and Stevens, 1976).

During polar axis fixation, the sulphated fucan (F2) localisation is correlated with the future rhizoid pole (Quatrano and Shaw, 1997). Although the F2 fucan localises to the rhizoid during axis fixation, it seems not to be essential for germination and cell division (Crayton et al., 1974). Met-embryos are embryos in which F2 is not sulphated and secreted into the zygote wall due to lack of sulphate in the medium. Even without sulphate, the zygotes can still germinate and divide normally. However, the process of germination is somewhat slower and the zygotes cannot adhere to the substrate very well (Crayton et al., 1974), indicating the role of sulphated fucans in adhesion, rather than polarisation.

Genetic and molecular approaches have not been developed for fucoid algae, due to a relatively long life cycle and difficulties in closing their life cycles *in vitro*. Molecular tools have however started to be developed in brown algal research, e.g. RNA interference (Farnham et al., 2013), *in situ* hybridisation (Bouget et al., 1995a; Bouget et al., 1995b), heterologous expression of genes (Fischl et al., 2016), UV mutagenesis, NGS-based mapping and positional cloning (Billoud *et al.*, 2015

and references therein). A little is known about protein and RNA synthesis during early stages of fucoid development. Most zygotic mRNAs are inherited maternally via the egg cell, but activation of the zygotic transcription and translation are necessary to complete the first cell cycle (germination and cell division). The first cell cycle completion depends on RNA synthesis during the first 5 h after fertilisation, whereas protein synthesis is needed for the first 12 h (Kropf et al., 1989a; Quatrano, 1968). However, the specific mRNAs and proteins that must be translated in order for the first cell cycle to occur still remain unknown, let alone those required for further morphogenesis.

In fucoid zygotes, studies have demonstrated the importance of polar cell wall deposition for growth axis fixation (Kropf et al., 1988) as well as determining cell fates (Berger et al., 1994). In addition, cell wall assembly during early zygote/embryo development has been studied in detail (Quatrano and Stevens, 1976). Although an amount of work has been done in the past to explore the wall characteristics during cell polarisation and germination, recent cell wall related studies have been limited and mostly oriented toward early zygotic/embryonic development (Torode et al., 2015; Torode et al., 2016). The development of young fucoid embryos is very interesting from a mechanical perspective since it exhibits both diffuse (thallus) and tip (rhizoid) growth in the first 10 days of development. In order to understand how the cell wall relates to growth of fucoid embryos, in this Chapter a novel approach was undertaken to explore wall properties: a combination of atomic force microscopy and immunohistochemistry. This study represents the first attempt to link the mechanical properties with developmental patterns and the underlying biochemical properties of fucoid cell walls during development. Furthermore, a molecular approach was taken to explore how cell wall related genes might be regulated during *F. serratus* embryogenesis.

3.3. Materials and methods

3.3.1. Sample collection and processing

The samples were collected in Rottingdean (East Sussex, United Kingdom) during winter months between November 2015 and May 2017. After collection, they were transported in seawater to the laboratory and kept at 4^0C. The fertile adult samples were rinsed with tap water and processed as follows: each receptacle was first identified as a male or female by checking for antheridia or oogonia, respectively. The receptacles were then separated, wrapped into damp tissue paper and aluminium foil (darkness) and kept at 4^0C for further use up to 2 weeks.

3.3.2. Fertilisation

The female receptacles were taken out of the 4^0C, washed, cut into small segments, placed into beakers with filter sterilised artificial seawater (ASW, Tropic Marin Sea Salt; Tropic Marin, Germany) and left to release the eggs for approximately 1 hour. The tissue was then removed and the egg mixture was filtered through a 100 µm mesh to eliminate oogonia and leftover pieces of adult tissue. The male receptacles were then taken out of the 4^0C, washed, cut into small segments and added to the egg mixture. After 15 minutes, the male segments were removed and the egg/sperm mixture was filtered through a 40 µm mesh to remove the sperm. The fertilised eggs were then placed in droplets of ASW on either:

1. Superfrost Ultra Plus slides (Thermo Scientific, USA) or
2. Multitest 8-well slides (Vector Laboratories, USA)

and placed in the incubator. After allowing them to settle for 6 hours, the eggs were flooded with ASW to completely cover the slides and cultured under a unilateral light overnight followed by 12:12 hour day night cycle, 16^0C, 60 µmol m^{-2} s^{-1}.

3.3.3. Light microscopy and measuring length/growth rate

To measure their growth in time, the embryos were cultured under the previously mentioned conditions and imaged using a VHX 5000 microscope

(Keyence (UK) Ltd, UK) for a certain number of consecutive days, depending on the experiment. The images were then processed using ImageJ software where the length of the embryos was measured (drawing the line in the middle of the embryo body from the tip of the rhizoid until the top of the thallus). The growth rate was determined via difference between sequential daily lengths over 15 days.

3.3.4. Quantifying cell divisions

To investigate the division pattern in the *Fucus* embryos, the embryos were cultured on slides and one slide was taken daily for further confocal imaging during 10 consecutive days. The embryos were first stained with Calcofluor White (18909, Sigma-Aldrich, USA) for 5 minutes, rinsed thoroughly with ASW and imaged under a Leica SP8 confocal microscope (Leica Microsystems, Germany). The confocal images were then processed using MorphoGrapX software (Barbier de Reuille et al., 2015, www.MorphoGraphX.org) to extract the information about the individual cells.

The z-stack output from the confocal microscope was loaded into the MorphoGraphX software. The images were first blurred by averaging, after which a global shape of the object was created. Following this, the surface was extracted from this shape as a mesh formed of triangles which were then subdivided and smoothed. This confocal fluorescence signal was then projected onto the mesh after which individual cells were seeded and segmented. Surface areas of each of the cells were analysed and surface area heat maps were created for individual embryos.

3.3.5. Fluorescence recovery after photobleaching (FRAP)

Fluorescence recovery after photobleaching (FRAP) method represents a real-time visualisation of dynamics (exocytosis and endocytosis) of fluorescently labelled vesicles to/from the cell membrane. In this thesis, FRAP experiment was used to detect the main deposition place of vesicles containing cell wall related components (alginates, sulphated fucans). To perform the FRAP experiments, embryos were fertilised and grown on glass slides for 2 days after which they were taken for further processing. The slides were covered with FM1-43 dye for 30

minutes in a 1000-fold dilution in ASW from the stock solution. Slides were rinsed for 5-6 times with artificial seawater after which they were covered with a coverslip and imaged under the Leica SP8 confocal microscope (Leica Microsystems), exciting using a 476 nm line of argon laser with emission collection at 520-600 nm. An initial image was obtained with the aforementioned settings after which the photobleaching started (using the 405, 442 and 488 nm lasers at 100% power) and continued for 10 seconds. The regions of interest (ROI) were chosen before photobleaching; they were localised to the tip and the sides of each rhizoid (Fig. 3.4). The recovery was followed by imaging every 1.2 s for 40 consecutive frames. Quantifications of FRAP were performed using ImageJ software. Circles were drawn inside the photobleached areas; the average fluorescence intensity was measured for each frame starting with the pre-photobleached image onwards.

To check for potential diffusion of dye from the sides of the photobleached areas, the same approach was taken as above, with only one bigger area at the tip chosen as the ROI instead of two. The same principle was taken to analyse the recovery and potential diffusion of the fluorescence signal.

3.3.6. Atomic force microscopy (AFM)

Embryos were fertilised, cultured and grown as described above on glass slides and used when reaching the stage of interest: 24hAF, 72hAF or 10dAF. They were covered with a droplet of water and placed under the atomic force microscope. The AFM data were collected using a NanoWizard AFM with a CellHesion (JPK Instruments AG, Germany). Since no previous data were available for these experiments, an initial test was done to determine the proper indentation force and conditions. The measurement of wall properties was done by either suppressing the turgor pressure by placing the embryos in a hypertonic solution of ASW with 0.6M mannitol 30 minutes before imaging and keeping them in the same solution while imaging, or placing them just in ASW before and during imaging. The following cantilevers were used: 0.5 N/m stiffness cantilever and a 10 nm diameter tip (Nanosensors, PPP-CONT, Windsor Scientific Ltd., UK). A range of setpoints (50, 150, 250, 350 nN) and a range of relative setpoints (50, 150, 250, 350 nN) was used for this test. The condition chosen to proceed with was 150nN setpoint and 150nN

relative setpoint. After testing the optimal force, the elasticity of all samples was determined by indenting with the tip over the whole embryo in 100 µm x 100 µm squares with the indentation depth of between 1 and 3 µm.

Each force-indentation experiment was treated with a Hertzian indentation model to extrapolate the apparent Young's modulus (E_A) using the JPK Data Processing software (JPK Instruments AG, Germany). The E_A was presented as a stiffness heat map. The E_A of interest was measured by picking points in a line along the middle of the embryo, from the tip of the rhizoid to the top of the thallus, using a MatLab-based script.

3.3.7. Alginate and sulphated fucan immunolocalisation

Embryos were fertilised and cultured as above on multitest 8-well slides (Vector Laboratories, USA) and taken when reaching the stage of interest (24 hours and 72 hours). They were fixed overnight in ASW containing 2% formaldehyde and 2.5% glutaraldehyde and washed 3 times for 15 minutes with ASW, followed by a rinse in phosphate buffered saline (PBS; 2.7 mM KCl, 6.1 mM Na_2HPO_4, and 3.5 mM KH_2PO_4).

The samples were incubated in a blocking solution of 5% milk for 2 hours. They were then rinsed with phosphate buffered saline (PBS; 2.7 mM KCl, 6.1 mM Na_2HPO_4, and 3.5 mM KH_2PO_4) and incubated in the 60 µl of 1/5 (in 5% milk) monoclonal primary antibody for 1.5 hours. After the incubation, the slides were washed with PBS 3 times for 5 minutes each, followed by the incubation in the 60 µl of 1/100 (in 5% milk) IgG-FITC secondary antibody (F1763, Sigma-Aldrich). This followed with a 5x5 minute wash in PBS, after which the samples were mounted in Citifluor (Agar Scientific, UK), covered with a coverslip, sealed and imaged under a Leica SP8 confocal microscope (Leica Microsystems, Germany). Three antibodies were used against alginate (BAM6, BAM7 and BAM10) and two against sulphated fucans (BAM3 and BAM4).

Quantification of signal was performed in ImageJ. The fluorescence profile was created by drawing a line from the tip of the rhizoid to the top of the thallus. Line

thickness matched the thickness of the thallus. Average fluorescence along the line was presented.

3.3.8. Making an Alcohol Insoluble Residue (AIR)

Embryo samples were taken 24, 72 hours and 10 days after fertilisation, placed in a microcentrifuge tube and placed in 70% ethanol at -20ºC until further use. The samples were ground using a tissue lyser (Tissue Lyser II, Qiagen, Germany), washed in 70% ethanol, 100% ethanol and followed by two acetone washes. The final alcohol insoluble residues (AIRs) were dried overnight at 40ºC.

3.3.9. Cell wall extraction

The AIRs were extracted sequentially with 2% (w/v) $CaCl_2$, 3% (w/v) Na_2CO_3 and 4M KOH. The initial weight of AIR used for extractions was 1.6 mg mL^{-1} (sample 10_NF) or 0.8 mg mL^{-1} (samples: 10_1, 72, 24). Each step involved rocking the AIR in 2mL of solution for 1 hour followed by a centrifugation and collection of the supernatant. KOH extracts were neutralised with glacial acetic acid before proceeding to the enzyme linked immunosorbent assay (ELISA).

3.3.10. Enzyme-linked immunosorbent assay (ELISA)

ELISAs were performed based on a previously described protocol (Torode et al., 2015), in 96-well microtitre plates (Maxisorb, NUNC). The plates were coated with 100 µL per well of antigen in PBS overnight at 4°C. The plates were then washed out using tap water and incubated in 200 µL of blocking solution (5% milk powder in PBS). After 2 hours at room temperature, plates were rinsed in tap water and incubated in 100 µL of primary antibody (1/25 dilution in PBS). Plates were incubated at room temperature for 1 hour, washed with tap water, and incubated with 1/100 dilution of rabbit anti-rat IgG secondary antibody (whole molecule, coupled to horseradish peroxidase (HRP), Sigma-Aldrich, USA) for 1 hour. Plates were then washed in tap water followed by the addition of 150 µL per well of HRP substrate (0.1 M sodium acetate buffer, pH 6.0, 1% tetramethyl benzidine, 0.006% (v/v) H_2O_2) to detect the antibody binding. The reaction was allowed to develop for 5 min and stopped by the addition of 30 µL of 2.5 M H_2SO_4. The plates were then

imaged using a microplate reader (SpectraMax i3x Multi-Mode, Molecular Devices, USA).

3.3.11. RNA extraction and cDNA synthesis

Total RNA of *F. serratus* embryo samples was extracted using the PureLink Plant RNA Reagent (Thermo Fisher Scientific, USA) following the manufacturer's instructions for all experiments. The integrity of RNA samples was checked by Agilent 2100 Bioanalyzer (Agilent Technologies, USA) and the quantity was assessed using NanoDrop 1000 spectrophotometer (Thermo Fisher Scientific, USA) and Qubit 2.0 Fluorometer with RNA High Sensitivity assay (Thermo Fisher Scientific, USA). First strand cDNA synthesis was performed using *F. serratus* RNA, an oligo dT(18) primer and Invitrogen Superscript II reverse transcriptase (Thermo Fisher Scientific, USA) as per manufacturers recommendations.

3.3.12. Designing primers for potential mannuronan C-5 epimerases in *Fucus*

The gene sequences coding for *Ectocarpus siliculosus* mannuronan C-5 epimerases (MC5E) were found using the UniProt online database. These sequences were then used to search for sequences with similarities in the *F. vesiculosus* transcriptome (Martins et al., 2013) using the NCBI tBLASTn algorithm in SRA archive. BLASTn was then used to validate the detected sequences in the general NCBI nucleotide database. All the sequences were highly similar to other brown algal MC5Es. All the sequences were aligned using MultAlin (Corpet, 1988) to check for conserved nucleotide regions. Forward and reverse primers were designed for each of the sequences, to amplify 200-400 bp of coding regions (depending on the sequence length) of MC5E genes in *F. serratus* to check for their expression in embryo tissues. After the initial test, new set of primers were designed for each epimerase (from the same gene sequences as above) to amplify a smaller region of around 100bp (adjusted for future qPCR amplifications, which require smaller fragments, Appendix 5.). All PCR reactions were performed in a GStorm thermal cycler (UK) using Taq-based amplification protocol (RedTaq, Sigma Aldrich). The PCR products were visualised on a 1% agarose gel, purified using

QIAquick PCR purification kit (Qiagen, UK) and sequenced via Sanger Sequencing Service (Source Bioscience, UK).

3.3.13. RNA-sequencing library preparation

Total RNA of 3 biological replicates from 7, 24, 72 hours and 10 days after fertilisation was extracted using the PureLink Plant RNA Reagent (Thermo Fisher Scientific, USA). cDNA library was generated using TruSeq LT DNA Sample Prep Kit (Illumina, USA) according to the manufacturer's instructions with the following modifications: the beads used were home-made SeraPure beads (Rohland and Reich, 2012) instead of AMPure XP beads. The library sequencing was performed on a NextSeq 500 using paired-end sequencing (2x76 cycles) with NextSeq 500/550 High Output v2 kit (Illumina, USA).

3.3.14. *De novo* transcriptome assemblyΔ

To reconstruct *F. serratus* transcriptome samples were pooled together from all 4 time points (7h, 24h, 72h and 10dAF). Initial read quality assessment was done with FastQC (Babraham Bioinformatics, www.bioinformatics.babraham.ac.uk/ projects/fastqc/). Adaptors were removed using CutAdapt (Martin, 2011). Reads were further subjected to quality control using Trimmomatic (minimum read length = 60). The quality parameters for the library were assessed using FastQC. The resulting filtered reads were subjected to *de novo* assembly with Trinity (trinity v2.4.0) on a high-RAM server with minimal k-mer coverage = 2 and k-mer length = 25. *In silico* read normalization was used due to the large number of input reads, in order to improve assembly efficiency and to reduce run times (Haas et al., 2014).

3.3.15. De novo assembly statistics and integrity assessmentΔ

General statistics of the assembly were determined using the 'TrinityStats.pl' script provided with Trinity release and independently using Transrate (http://hibberdlab.com/transrate/) and Detonate (http://deweylab.biostat.wisc.edu/ detonate/) tools. Assembly completeness was estimated using the eukaryotic set of BUSCO profiles (v1) (Simão et al., 2015). BUSCO analysis was performed for the full transcriptome assembly and for the reduced assembly, obtained after retaining

only the longest isoform per trinity gene. Overall expression support per assembled transcript was performed after transcript abundance estimation. Trinity genes with TPM ≥ 1 in at least 3 samples were considered further.

3.3.16. Protein prediction and annotationΔ

Open reading frames were predicted using TransDecoder software (https://transdecoder.github.io; Haas et al., 2014). At the first step open reading frames longer than 100 amino acids were extracted. The top 500 longest ORFs were used for training a Markov model for coding sequences, candidate coding regions were identified based on log-likelihood score.

3.3.17. Annotation of genes of interest

A BLAST database was built with local sequences of predicted proteins which was used to find sequence similarities with known *E. siliculosus* mannuronan C5 epimerases (obtained from OrcAE and UniProt). The candidate genes were chosen based on high matching characteristics between the transcriptome proteins and known *E. siliculosus* proteins. Three parameters were chosen to describe a high match: percentage of identity (portion of the known sequence that aligns to the transcriptome proteins; >50), alignment length (>100) and e-value ($<10^{-40}$).

3.3.18. Expression analysisΔ

Initial reads after quality control were aligned back to the resulting *F. serratus de novo* transcriptome assembly. Alignment-based transcript quantification was done using RSEM (version: RSEM-1.2.25, (http://deweylab.github.io/RSEM; Li and Dewey, 2011). Quantification was performed on 'trinity gene' level. For within-sample normalisation TPMs were calculated. Between-sample normalisation was done using trimmed means approach (TMM; Robinson and Oshlack, 2010). TMM-normalised TPMs were reported.

3.3.19. Statistics

All samples were tested for normality with Shapiro-Wilk normality test and for equal variance using Brown-Forsythe equal variance test. Significance tests were performed according to their distribution: two sample t-test to compare two samples with normal distribution, Mann-Whitney Rank Sum test for comparing two non-normal distributed samples, ANOVA or ANOVA on Ranks for more than 2 samples for normal and non normal distribution, respectively.

3.4. Results

3.4.1. *F. serratus* embryo exhibits two phases of growth: fast vs. slow

A significant amount of research has been done investigating fucoid embryo development. However, different studies present different timings in this process (e.g. apical hair formation: *Fucus vesiculosus* – 7 days; Galun and Torrey, 1969; *Fucus spiralis* - 3-4 weeks; Bouget, Berger and Brownlee, 1998). In order to study the role of cell walls in this *F. serratus* embryo model, I performed an analysis of embryo growth for this species.

After fertilisation, the zygotes underwent the first asymmetrical cell division, which gave rise to two distinct cell types, as previously observed (Fig. 3.1A day1; Bouget, Berger and Brownlee, 1998). The first asymmetrical division was followed by further divisions in both cell types. Only the rhizoid cell actively elongated at this stage (Fig. 3.1A 1-4; green). The overall embryo growth, proxied by length, was fast in the first day with a high growth rate and an average length increase of 93.7 ± 6.51 µm/day (Fig. 3.1B, C; green, n=3x50). The further embryo length increase in time had slight variations from day 2 until day 10 (62-80 µm/day, after day 10 it decreased to 47 ± 18.53 µm/day). The growth was faster between day 6 and 7 reaching 96 ± 9.18 µm/day. In conclusion, two different modes of growth could be distinguished: fast rhizoid growth (Fig 3.1. green shading) and slower rhizoid growth and thallus expansion (Fig. 3.1. yellow, blue). The timing of the developmental steps resembled

the previously reported fucoid growth (*Fucus vesiculosus* – 7 days) from Galun and Torrey (1969).

In addition to overall embryo length, the series of cell divisions that happened as embryogenesis progressed were also examined; studies in the literature have focused on the first few divisions only (Bouget et al., 1998; Henderson et al., 1998; Kropf et al., 1999). After fertilisation, the embryos were taken at different developmental stages (hours/days after fertilisation, h/d AF), stained with a cell-wall dye Calcofluor White, imaged under a confocal microscope and analysed using a segmentation software MorphoGraphX (Barbier de Reuille *et al.*, 2015; Fig. 3.2A). In the active rhizoid growth phase (1dAF - 3dAF), there were new cells forming by transverse division of the initial rhizoid cell (Fig. 3.2B, white arrowheads).

Quantitative proof that only the rhizoid cell was growing came from the segmentation analysis of individual cells in early embryogenesis: at 24h AF the initial asymmetric division had already taken place producing a single celled rhizoid. Once the rhizoid divided, the summed surface area of the daughter cells was larger than the initial single rhizoid cell indicating growth (Fig. 3.2B). During this time, the thallus cell divided as well, but did not change in the surface area (Fig. 3.2B; divisions not shown, only the sum of their surface area as a single thallus cell). Divisions originating from the thallus cell were happening fast; 8 cells by day 2, around 20 cells by day 3. Since it was not possible to visualise the whole embryo thallus by confocal microscopy due to laser penetration issues, but rather just one side, the conclusions of the actual cell number were approximate. However, changes in the surface areas in the individual cells could be observed as embryogenesis progressed. From the initial thallus cell, the surface area of the daughter cells decreased fast in the beginning and then came to a plateau around day 5. These data suggest that in the early stages of development only cleavage divisions of the initial thallus cell were taking place, with no cell expansion. After day 5, cell expansion was observed (Fig. 3.2C; day 5 – day 10 = constant surface areas of 242 ± 22 μm^2). This corresponds to the stage of development where the apical hairs and apical meristematic cell start forming, allowing the whole thallus to elongate and expand (Galun and Torrey, 1969).

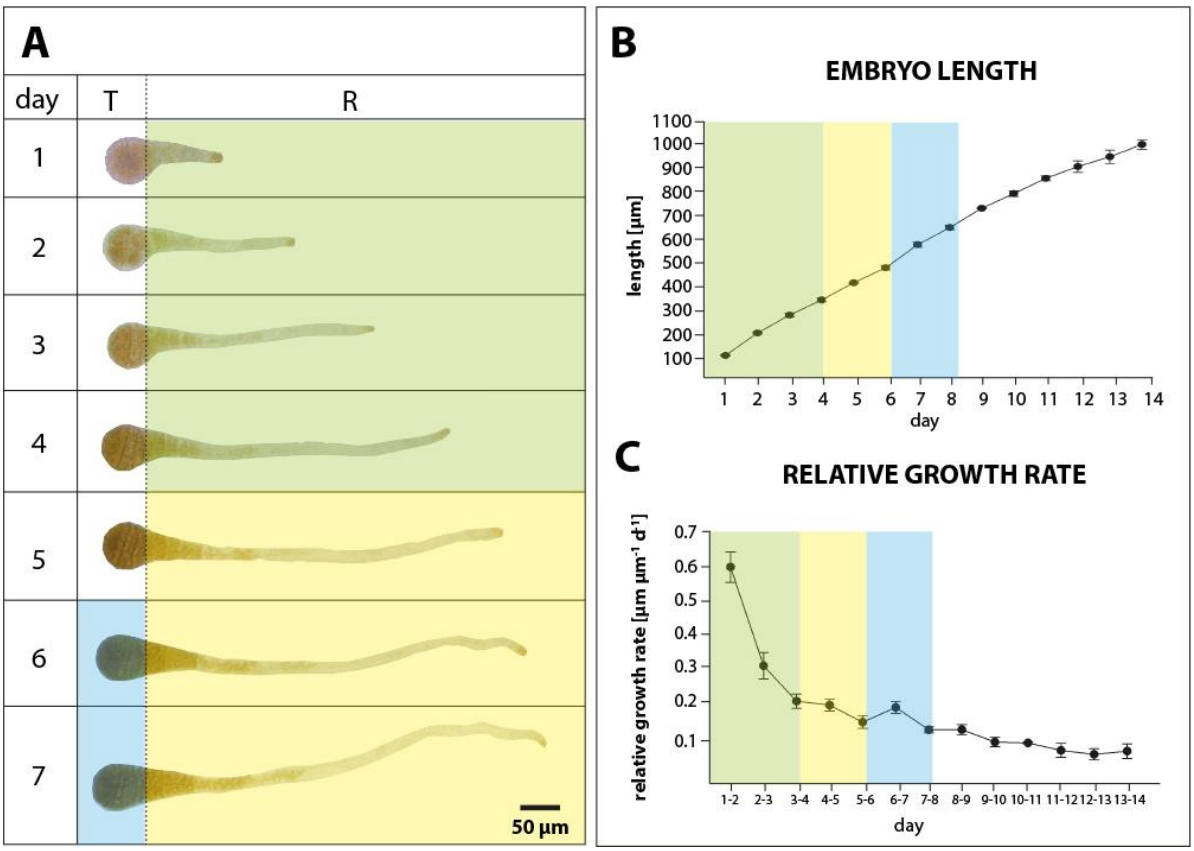

Figure 3.1. ***F. serratus*** **embryo development.** (A) Representative images of F. serratus embryo in the first 7 days of development. T - thallus cell (and derivatives), R - rhizoid cell (and derivatives). (B) Embryo length increase and change in growth rate (C) during the first 15 days of development. Different stages are marked with different colours: green – rhizoid elongation; fast growth rate, yellow – rhizoid slower elongation + blue – thallus elongation; slower growth rate n=3x50.

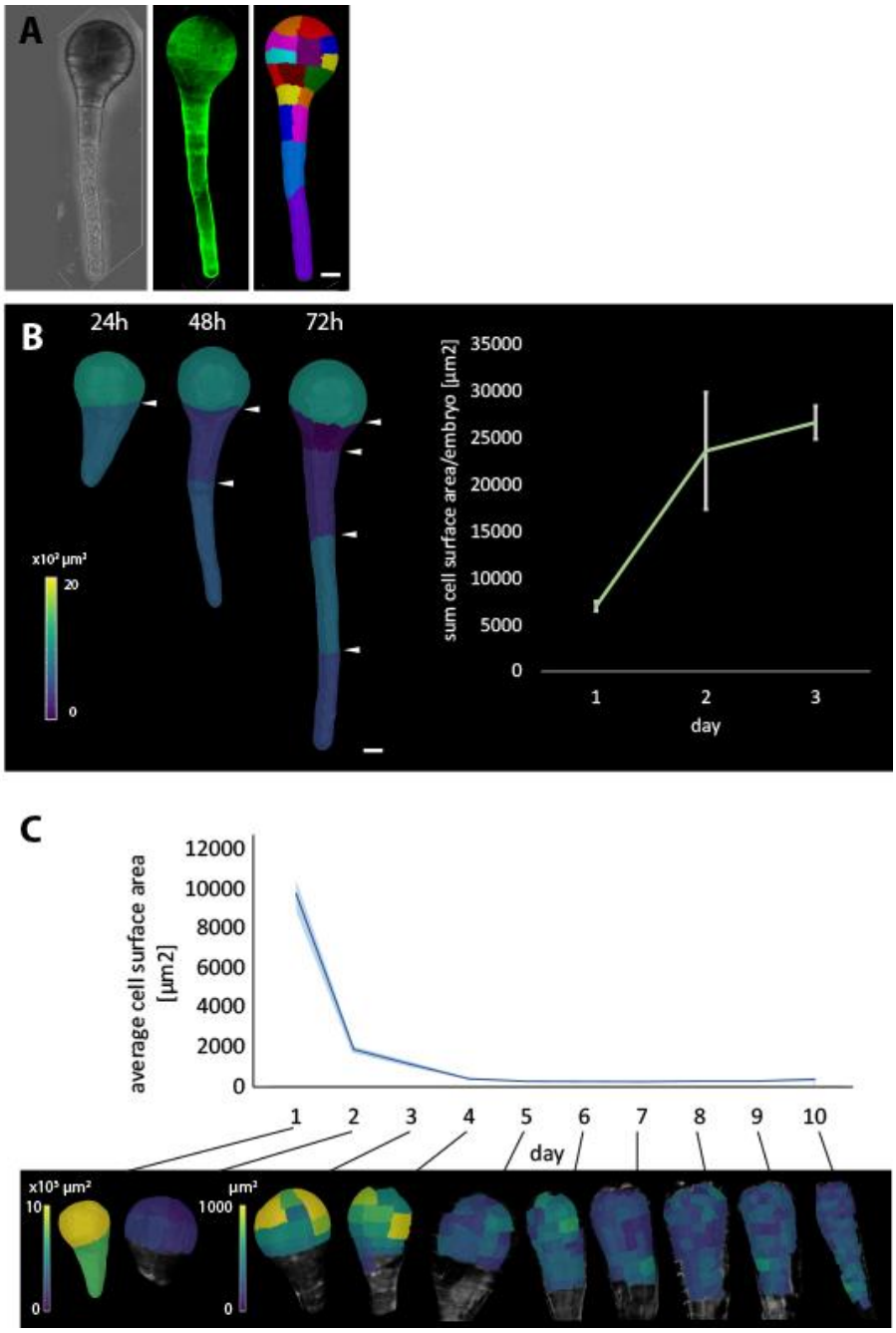

Figure 3.2. Cell division analysis in the growing *F. serratus* embryo. (A) Process of cellular segmentation in MorphoGraphX. Differential Interference Contrast (DIC) image of *F. serratus* 59h old embryo. Embryo is stained with Calcofluor White wall stain, 500nm sections are taken through the embryo and merged into a z-stack. The cellular segmentation algorithm detects cellular surface and segments the cells based on the fluorescence signal of the stain (B) Surface area heat maps of rhizoid cells in the first 3 days; transverse rhizoid divisions (white arrowheads). The sum of the cell surface areas is increasing over time showing active growth of the rhizoid. (C) The graph represents average surface area of a single cell in a given time point; representative heat maps of cell surface areas are depicted below the graph. Original cell undergoes cleavage divisions without surface area change. At day 5 to day 10 the cell surface area becomes close to constant suggesting diffuse growth; cell division and enlargement. Scale bar=20 µm.

4.4.2. Rhizoid cell elongation - tip growth or diffuse growth?

The *Fucus* rhizoid is thought to grow via tip growth. There have been many studies conducted in fucoid embryos to investigate the key components for tip growth known from other systems, such as polarisation of actin, calcium and vesicle trafficking (Alessa and Kropf, 1999; Belanger and Quatrano, 2000; Berger and Brownlee, 1993; Brownlee and Wood, 1986; Kropf and Quatrano, 1987). However, precise vesicular trafficking and the site of exocytosis has not been determined yet. Therefore, to understand more deeply how vesicular transport is organised in the *F. serratus* embryos, the dynamics of exocytosis was investigated.

Zygotes were initially stained with Calcofluor White to stain the cell walls at 24 hours. To investigate the progression of growth, the stain was removed and the embryos were imaged every 24 hours for the next 2 consecutive days (Fig. 3.3). At day 1, the whole embryo was stained (Fig. 3.3A, D). At day 2, the stain was no longer present in the medium and so the only fluorescence could come from the previously stained walls. The decrease in fluorescence was mostly present at the rhizoid tip area in both days following the staining (Fig. 3.3B, C, E, F; white arrowheads).

In addition, a fluorescence recovery after photobleaching (FRAP) experiment was performed in order to determine the exact positioning of vesicular exocytosis. The rhizoids were stained with a styryl membrane dye FM1-43 (Fig. 3.4A), after which photobleaching was performed at three sites, from which two were later analysed (e.g. Fig. 3.4B; white asterisks). The recovery was followed for the next 50 seconds (Fig. 3.4C). The fluorescence recovery happened slower at the tip (20.7±2.6s) than on the sides of the rhizoid (12.2±1.8s) (Fig. 3.4D, E, n=16, p-value=0.0251), suggesting a higher exocytosis rate at the side of the rhizoid just below the tip.

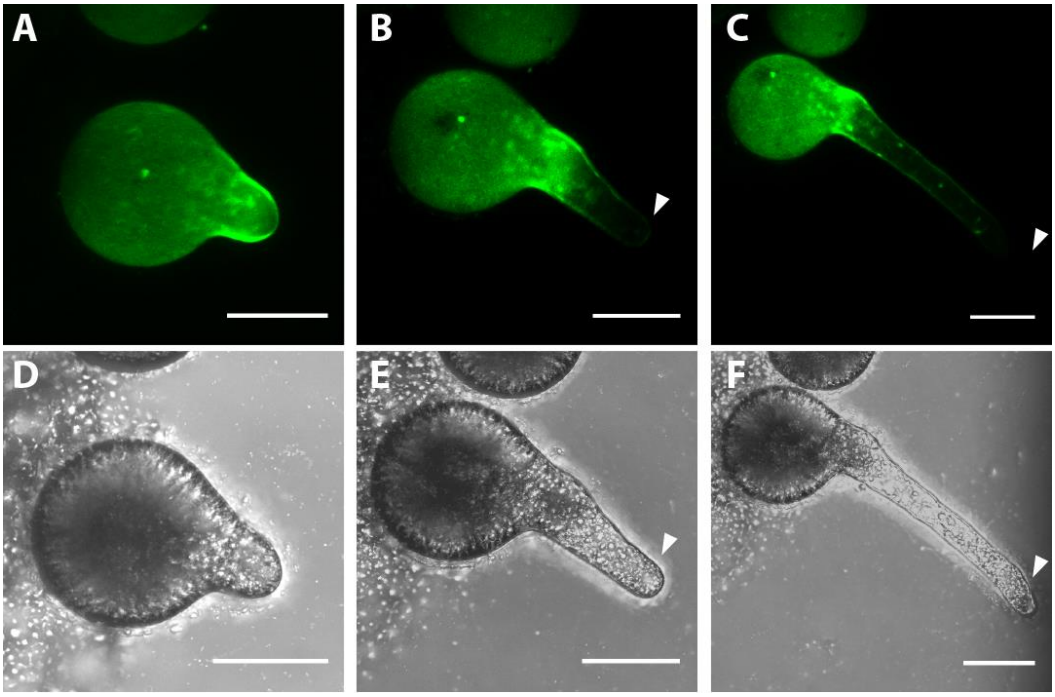

Figure 3.3. Tip growth in *F. serratus* embryo. Calcofluor White staining of the embryo cell wall at (A) 24h after fertilisation (AF) after which the stain was removed from the medium. Embryos were imaged (B) 48 and (C) 72h AF. Images represent an embryo with the retained stain and the new part of the unstained wall at the tip (white arrowhead). (D, E, F) Brightfield images of the three stages. Scale bar 50 µm.

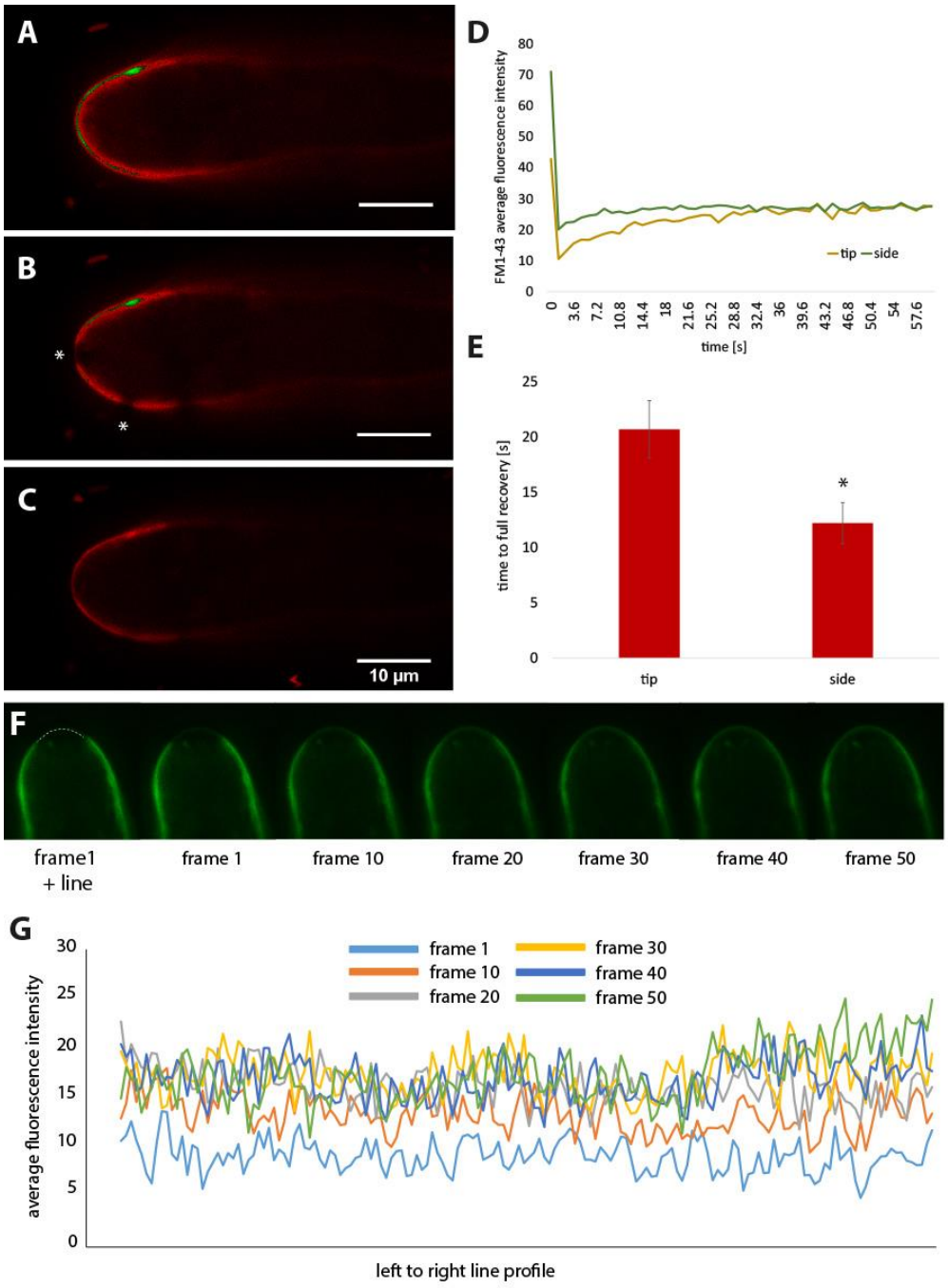

Figure 3.4. FRAP analysis of exocytosis in the rhizoid tip. (A) Image of the rhizoid before photobleaching, (B) after photobleaching (asterisk marks areas analysed) and (C) after 50s of recovery. (D) Example of fluorescence intensity in time for a single representative rhizoid; first point marks before photobleaching, second point marks after photobleaching, after which the recovery is measured in tip and side (E) Graph representing the difference between the time needed to reach the highest recovery (Mann-Whitney test; p=0.0251, n=16) (F) Lateral vesicle diffusion test; time course of rhizoid tip stained with a membrane dye FM1-43. The apical area (white rectangle) was laser photobleached (frame 1) after which the recovery of the signal was observed. Each frame corresponds to the time of around 1s. (G) Line graphs represent the signal recovery after photobleaching; each line corresponds to a profile of fluorescence from left to right inside the white rectangle.

Some of the fluorescence recovery might have happened due to unbleached membrane diffusing from the sides of the FRAP area into the photobleached area. If this was happening, it might lead to the wrong conclusion about the vesicular deposition after photobleaching; the recovery might have been due to purely passive diffusion, rather than an active exocytosis process. To test this, a large area was photobleached at the rhizoid tip and the recovery was observed at the centre and edges of the area; if the edges recovered more quickly it would indicate membrane diffusion contributions. The fluorescence recovered equally on the border of the FRAP area (where diffusion would begin) in comparison with the central area (Fig. 3.4F, G). This indicated that diffusion was unlikely to be a major factor in FRAP measurements, but rather the recovery was due to active exocytosis events.

3.4.3. Wall mechanics in the embryo vary depending on active growth processes

Due to the clear differences between the two initial cells and their fates (rhizoid tip-growth and divisions vs. thallus cell divisions only followed by diffuse growth), fucoid embryos were chosen to explore cell wall mechanics during these two contrasting growth types. In this study, atomic force microscopy (AFM) was used to investigate the wall mechanical properties of growing embryos.

An initial optimisation was performed to obtain the best parameters for the indentation method. A variety of indentation forces were used in two conditions, artificial seawater and artificial seawater with 0.6M mannitol to avoid the effects of potential turgor pressure within the cell (Appendix 2.). The forces used ranged from 50 to 350 nN. The indentations obtained varied depending on the force used and no difference was seen when performing the experiments in mannitol, suggesting the turgor pressure was not affecting the microscopy method or the plasmolysis level was not reached with this concentration. The force chosen for further experiments was 150 nN in seawater; the indentation depth in these was around 1-2 µM, which corresponds to the average thickness of the fucoid cell wall (Novotny and Forman, 1975).

The spatial profile revealed that for all samples examined, a layer of extracellular mucilage surrounded the whole rhizoid (Fig. 3.5).

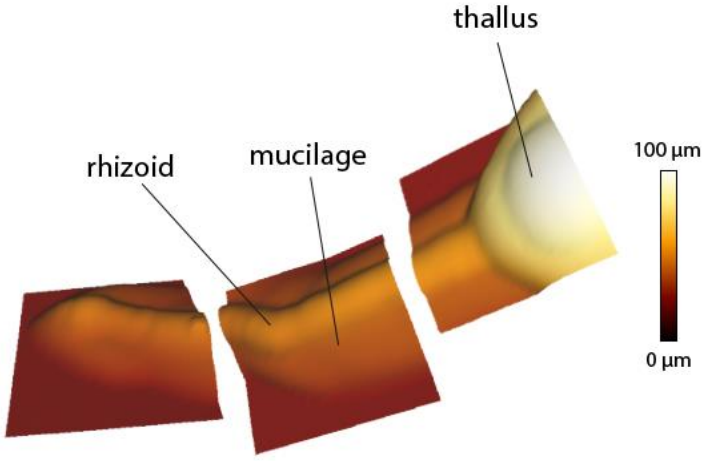

Figure 3.5. 3D representation of the embryo and surrounding area topology using atomic force microscopy (AFM). Figure shows three height maps (100x100 µm) covering the full length of a 72h old *F. serratus* embryo. Three parts are distinguished: embryo thallus, rhizoid and the adhesive mucilage.

Furthermore, the mechanical properties of the *F. serratus* embryos displayed a gradient in the longitudinal direction along the rhizoid, for 3 chosen developmental stages (24h, 72h and 10dAF). The gradient started at the tip which was the softest and continued toward the thallus, which had the highest apparent Young's modulus (Fig. 3.6A, B, and C). The rhizoid apparent Young's modulus also changed in developmental time. The lowest value was observed in the 24h, followed by the 72h, with the highest value in 10 day old embryos (Fig. 3.6D; lower graph, E_A(24h)= 1.47±0.58 MPa, E_A(72h)=5.84±1.09, E_A(10h)=6.4±1.1, n= 3 (24h), 7 (72h), 7 (10d)). The holdfast, which started occurring during 9-10d AF, was also examined; the apparent Young's Modulus was around 4.5 MPa (Fig. 3.7, n=3). The thallus region was always more rigid than the rhizoid but its pattern during development behaved somewhat differently. The lowest Young's Modulus was observed again at the 24h after fertilisation (Fig. 3.6D; 54±7.03 MPa, n=3). However, the value observed at 72h AF was higher (Fig. 3.6D; 266±158.76 MPa, n=7) than the one observed in the later developmental stage, 10 days AF (Fig. 3.6D; 95±19.83 MPa, n=7).

In order to investigate more fully the rhizoid rigidity gradient at the rhizoid tip, a finer-scale analysis was conducted. A measurement was taken every 50 µm to

investigate whether there were any significant changes at the very tip, compared to the upper part of the rhizoid. These data were useful given the observations of tip growth earlier. In three examined stages, no significant stiffness variations were seen in the 200 µm range (100 µm for 24h AF) extending away from the rhizoid tip in each individual time point (Fig. 3.8). These data imply that the rigidification of the rhizoid happens at least 200 µm from the tip during growth.

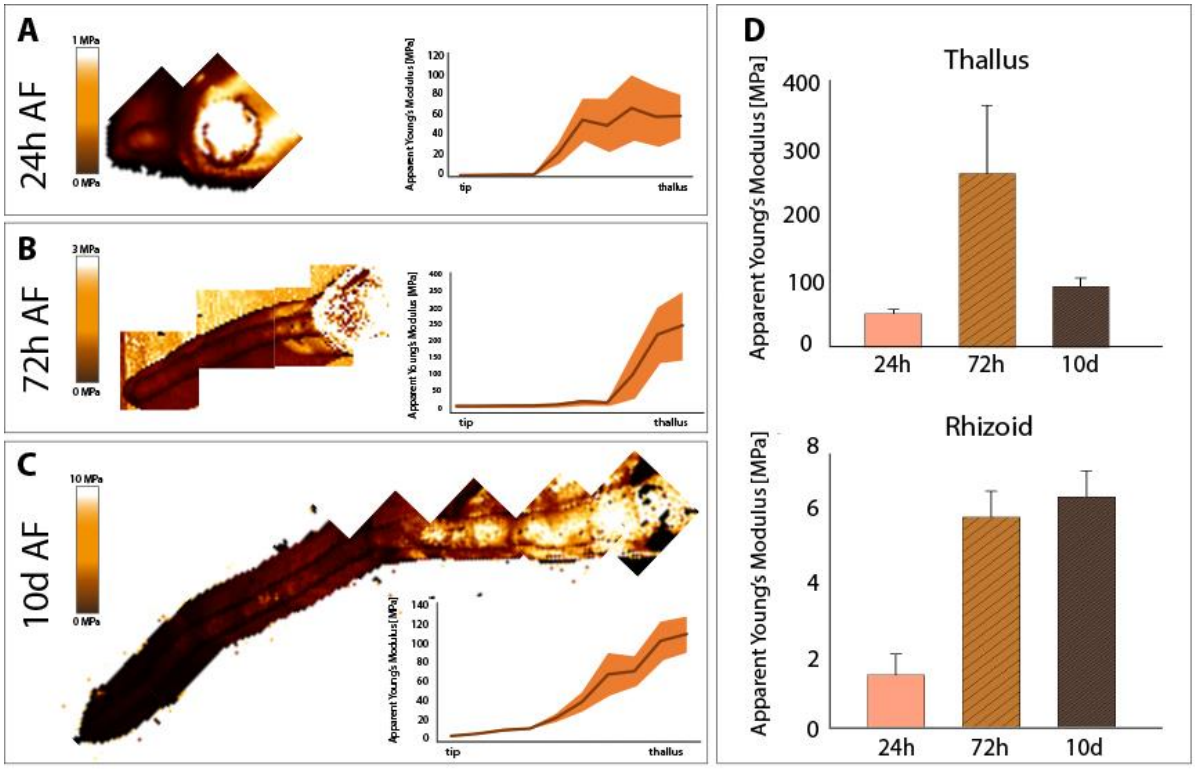

Figure 3.6. Cell wall mechanics in the *F. serratus* embryo. Representative maps of the apparent Young's modulus (E_A) with the profile graphs of a 24h (A), 72h (B) and 10 day (C) old embryo, showing increase in the E_A from rhizoid to the thallus (n=3 (24h), 7(72h), 7(10d)). (D) Graphs representing the differences between the E_A in tip growing rhizoid and thallus in three developmental stages (error bars: standard error).

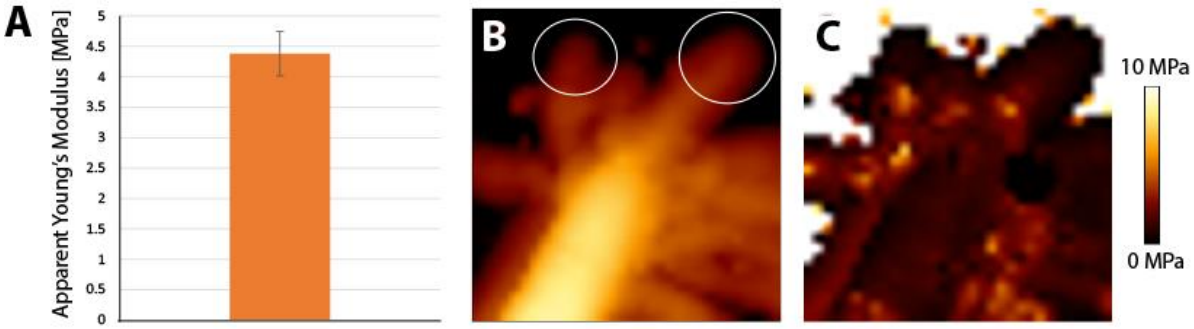

Figure 3.7. Apparent Young's modulus EA of the embryo holdfast. (A) Graph representing the E_A of the holdfast area (white circles). Maps are showing the height (B) and stiffness (C) of the 10 day old embryo holdfast (error bars: standard error, n=3).

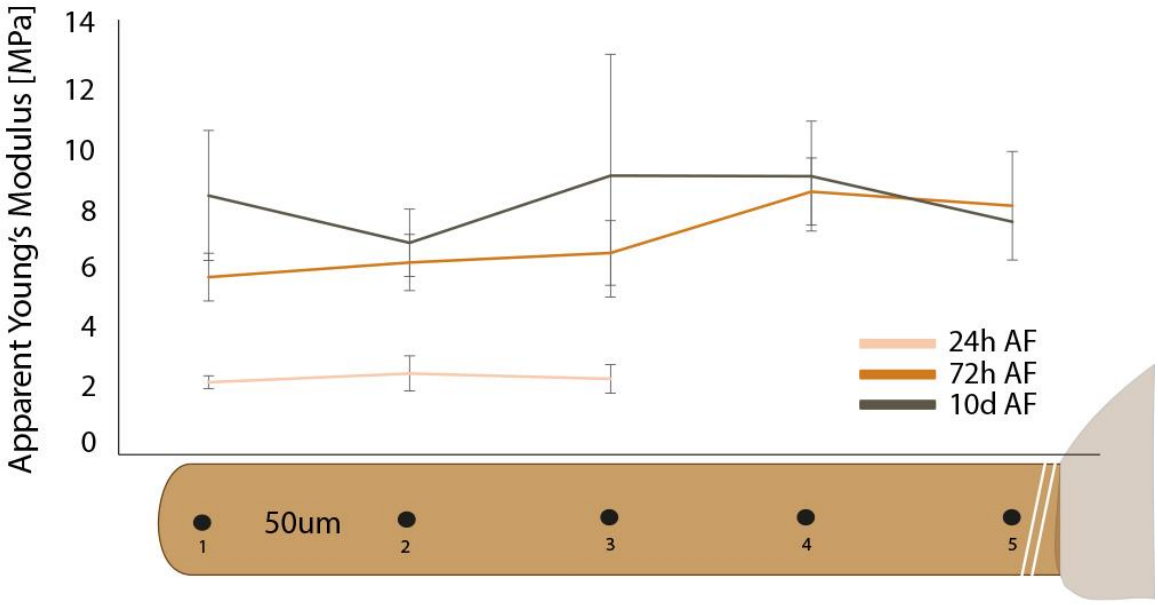

Figure 3.8. Profile of apparent Young's modulus (EA) along the *F. serratus* rhizoid. Three line graphs represent three developmental stages; 24h AF (beige), 72h AF (orange) and 10 days AF (brown). Each measurement is around 50 µm apart (error bars: standard error; (n=3 (24h), 7(72h), 7(10d)).

3.4.4. Spatial distribution of wall components in the *F. serratus* embryos

The fucoid zygote has been utilized in previous research to explore how the wall components change during early development (Quatrano and Stevens, 1976; Quatrano et al., 1985). Since wall components might have a role in mechanical

properties of the brown algal wall, their localisation was investigated in this study during early embryogenesis, for comparison with the obtained AFM data. *F. serratus* zygotes were grown in artificial seawater for 24h or 72h AF after which they were fixed and whole-mount *in muro* detection of alginate and sulphated fucan epitopes was performed.

Surface labelling of 24h and 72h AF embryos (Fig. 3.9) showed that all five epitopes were detectable in the growing rhizoid tip. The BAM10 (G-rich areas) antibody also labelled the thallus body. Its epitope could be detected very strongly in the thallus at the later developmental stage, 72h AF. BAM7 (MG-rich areas) labelled the majority of the embryo, especially the collar where the thallus body meets the rhizoid and the rhizoid tip. Similarly to BAM10, the signal was stronger in the 72h old embryo. BAM6 (M-rich areas) did not label the embryo strongly; it was detected only at the rhizoid tip in both developmental stages, albeit with low fluorescence intensity. At 24h AF, the BAM3 (potentially sulphated fucan) antibody showed reaction at the rhizoid tip region, although more broad than what was observed for the alginate antibodies. In addition, it was detected in the collar and thallus region. At 72h AF, the epitope was detected in the areas derived from the initial rhizoid cell. BAM4 (highly sulphated fucan) antibody showed a polarised binding at the rhizoid tip at 24h AF and a more broad deposition in the rhizoid at 72h AF (Fig. 3.9, blue).

In summary, the distribution of specific antibodies against alginate and sulphated fucans showed distinct patterns. The MG-rich and G-rich areas were mostly present in the non-growing thallus. The highly sulphated fucan epitope was localised to the rhizoid, correlating with this actively growing structure.

3.4.5 Epitope detection in cell wall extracts of developing *Fucus* embryo

In order to explore a broader range of epitopes that might be found in the developing embryos, the cell walls were extracted and $CaCl_2$ (alginate-independent), Na_2CO_3 (alginate-associated) and KOH (alkaline soluble) fractions were assayed via enzyme linked immunosorbent assay (ELISA). This experiment was performed as a preliminary study with a wider range of antibodies involving only

a single replicate for three different samples: 24h, 72h and 10 day old embryos (Fig. 3.10).

The data revealed a variable epitope detection depending on the fraction and the antibody used. The $CaCl_2$ fraction resulted in only a few epitopes detected, whereas the other two fractions had an abundant signal from most of the antibodies. Six alginate antibodies were used. BAM10 (G-rich) and BAM7 (MG-rich) antibodies were detected in all three developmental stages. BAM8 and 9 (MG-rich) were detected only in the Na_2CO_3 fraction in the 10dAF sample. Similarly, BAM6 (M-rich) antibody was detected only in 10dAF sample as well. BAM11 (G) antibody was very mildly detected in the 10dAF sample in the Na_2CO_3 fraction. Sulphated fucan epitopes were found in all three fractions. BAM1 (non-sulphated epitope) was detected in all three fractions; similarly expressed in all three developmental stages, besides the Na_2CO_3 fraction where the 10dAF sample had the most abundant detection. BAM 2, 3 (potentially sulphated epitope) and 4 (sulphated epitope) were mostly detected in the oldest time point, 10dAF. LM23 antibody binds to a pectic xylogalacturonan/xylan epitope in plants, but has also been found to bind to algal preparations (Torode et al., 2015). This antibody served as a positive control and its binding was detected in all three samples in both Na_2CO_3 and KOH fraction.

Overall the data presents a wide recognition of the antibodies in the three developmental stages tested. Sulphated fucan epitopes were more abundant in the older stages whereas several alginate epitopes (MG-rich and G-rich) showed to be common in the 72 hour old embryos.

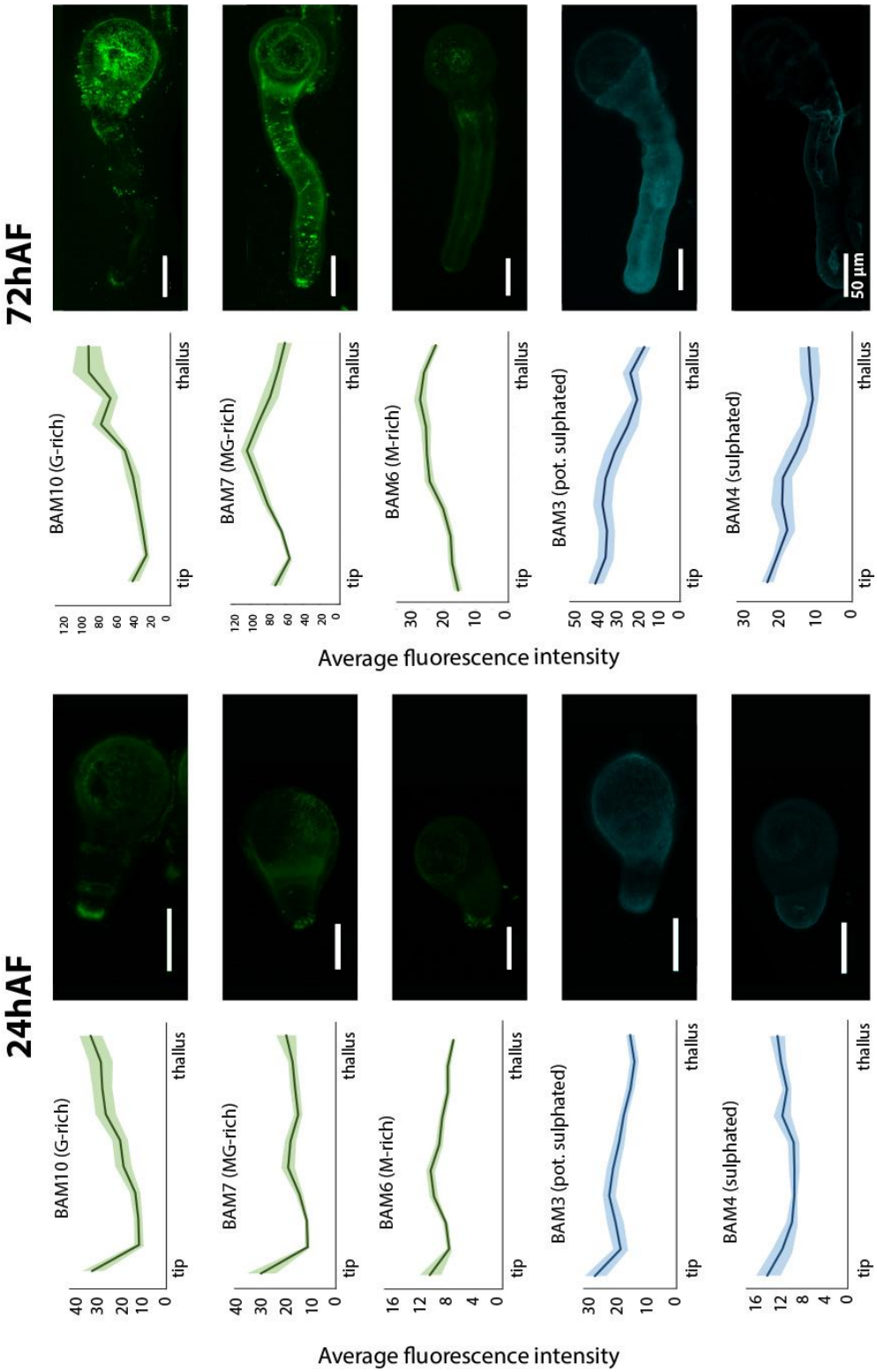

Figure 3.9. Indirect immunofluorescence labelling of wall polysaccharides *in F. serratus* embryo. The embryos were fixed and labelled 24h and 72h after fertilisation. The green fluorescence shows the detection of BAM6, BAM7 and BAM10 alginate epitopes; the blue fluorescence shows the detection of BAM3 and BAM4 sulphated fucan epitopes. n (24h BAM10) =11, n (24h BAM7) =11, n (24h BAM6) =11, n (24h BAM3) =7, n (24h BAM4) =10, n (72h BAM10) =9, n (72h BAM7) =12, n (72h BAM6) =21, n (72h BAM3) =8, n (72h BAM4) =7.

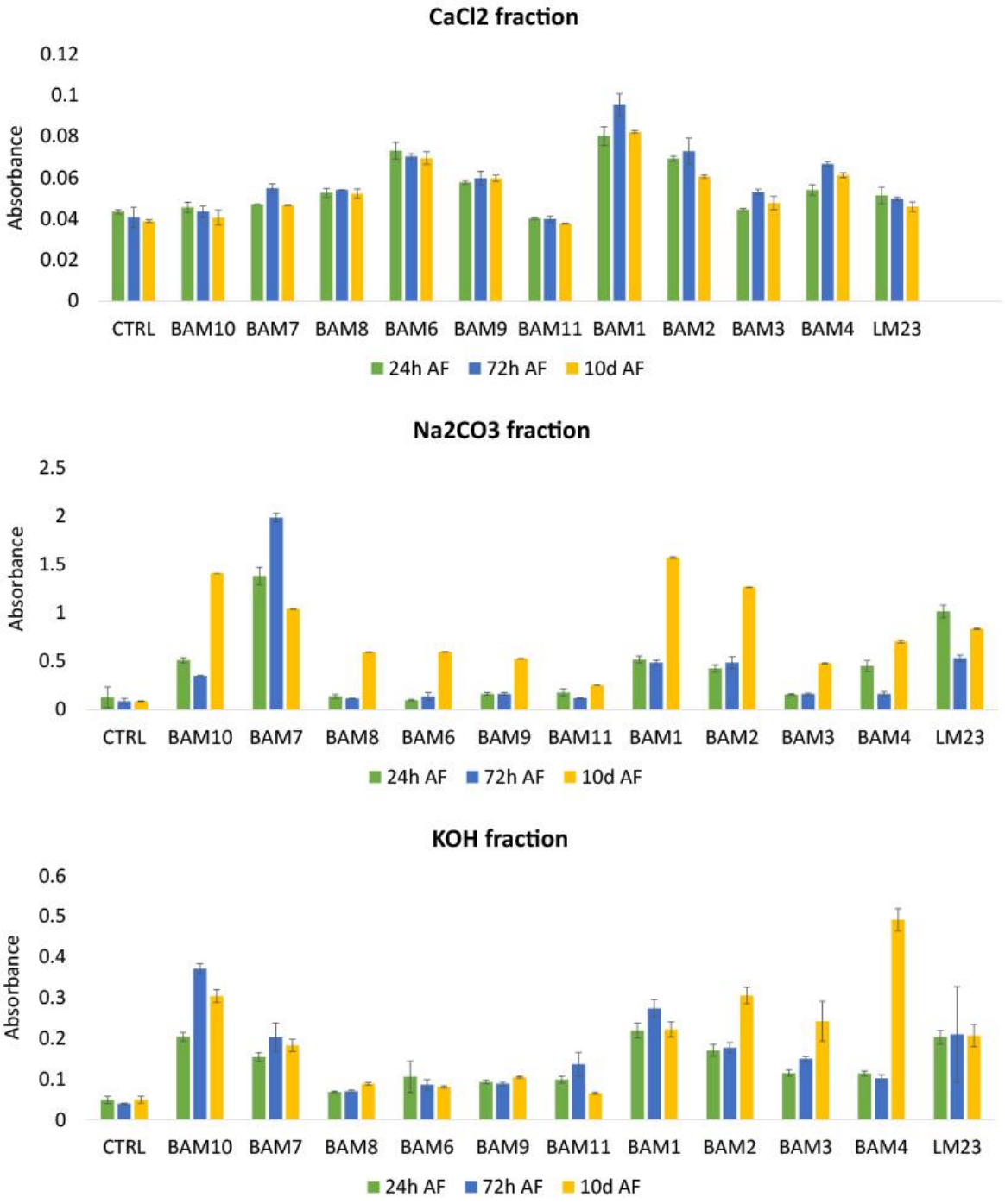

Figure 3.10. ELISA analysis of alginate and sulphated fucan epitope levels in three fractions of *F. serratus* embryo wall extracts. Graphs represent absorbance of alginate (BAM6-BAM11), sulphated fucans (BAM1-BAM4), plant pectin/xylan (LM23) epitopes and control of three fractions in the process of alcohol insoluble residue (AIR) extraction. Error bars: standard error between 3 technical replicates.

3.4.6. Detecting and investigating genes encoding the mannuronan C-5 epimerases

The mechanical properties of an alginate gel correlate with the proportion of GG-blocks in the alginate structure (Draget et al., 1994). This correlation is due to the ability of GG-block regions to form “egg-box” junctions with calcium in the cell wall (Grant et al., 1973). The alginate chain is initially produced as mannuronic acid (M) after which a subsequent epimerization of the M residues into G residues occurs; this process is catalysed by putative mannuronan C5-epimerases (MC5Es; section 1.3.1.2. in Introduction). Since these enzymes have a potential role in changing mechanical properties of walls through their activity, possible gene candidates were identified. In addition, their expression was examined during progressing developmental stages.

The initial step involved finding known epimerase protein sequences in the annotated *Ectocarpus siliculosus* genome via UniProt online database (http:// www.uniprot.org/). Each of these protein sequences was aligned using Basic Local Alignment Search Tool (BLAST, default parameters; https://blast.ncbi. nlm.nih.gov/ Blast.cgi) against a known EST database of *F. vesiculosus* (adult male and female tissues; Martins, Mota and Pearson, 2013) where 7 reads aligning to the original proteins could be identified (Appendix 3.). Using the sequences identified, forward and reverse primers were designed for each (Table 3.1). Polymerase chain reaction (PCR) was performed on cDNA made from two *F. serratus* embryo developmental stages to test the primers. All the reactions resulted in amplicons between 220 and 460 bp, depending on the primer pair (Fig. 3.11). The PCR products were then sequenced (Appendix 4.). Three pairs out of the seven nucleotide sequences aligned to each other with a high percentage, indicating they both amplified the same gene (Appendix 4.; orange, green and blue).

Primer ID	F 5'-3'	R 5'-3'
MC5E_241546	GGTCGTTCTTACATCAGCGCCG	GCATCGCTTGGAGGCGATAATCC
MC5E_244229	GGTTGTCTTGCACGAGGTTG	CGAACATGCACTTCGTAATGGG
MC5E_253007	CGTGAAGGTGTTGTCGTG	CGAAGTCTACGACAACGTTAATC
MC5E_253453	CCGGATTACAGCAACGGCAGC	CGACGTTGTCGTGGACCTCG
MC5E_28278	CGACCAAGATGAGAGCGATGG	GGATGGAAACGTTGTTGCATCG
MC5E_32281	GTGAAGGTGTTGTCGTGG	CGTTAATCATGGTATCATCGCG
MC5E_56536	CCGCGCCCATGGAGGTG	CGTTAAGCCCGTTGTCGTCGTCG

Table 3.1. Primer sequences used to amplify the regions of genes potentially encoding for mannuronan C-5 epimerases (MC5Es). The sequences were designed based on the *F. vesiculosus* transcriptome data reads (Martins et al., 2013) after performing BLAST against *E. siliculosus* MC5Es. F-forward primer, R-reverse primer.

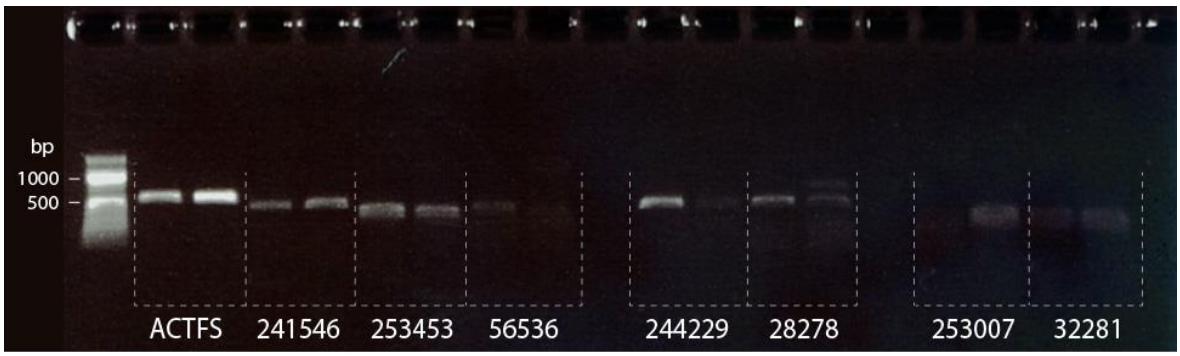

Figure 3.11. MC5E gene products from *F. serratus*. Agarose gel showing 15 µl of PCR products: ladder, actin control (primers from Farnham *et al.*, 2013), MC5E_241546, MC5E_253453, MC5E_56536, MC5E_244229, MC5E_28278, MC5E_253007, MC5E_32281. Two band for each primer set represent two *F. serratus* embryo samples, 1h AF and 14 days AF.

To confirm that the potential translated MC5E proteins of the obtained nucleotide sequences have similarities with the *Ectocarpus* proteins, a protein BLAST was executed. Firstly, the nucleotide sequences obtained from PCR were processed through the ExPASy online translation tool to determine the potential translated proteins. All of the combinations underwent a protein BLAST against all available databases to check for the best hits. Six out of seven potential translated proteins aligned highly with a mannuronan C5 epimerase originating from *Ectocarpus*. A preliminary quantification of the detected four unique epimerase genes was performed next using semi-quantitative RT-PCR. Two replicates of three

different time points (24hAF, 72hAF and 10dAF) were examined; cDNA from each of the embryo samples was amplified using 4 primer sets for the 4 epimerases, together with two housekeeping genes characterised for *Ectocarpus siliculosus* (Le Bail et al., 2008a), elongation factor alpha (ELα) and alpha tubulin (TUB; Fig. 3.12). The data suggest that the epimerase genes are expressed relatively constantly, apart from MC5E_32281, which might be expressed more highly early on in development than at the later stages.

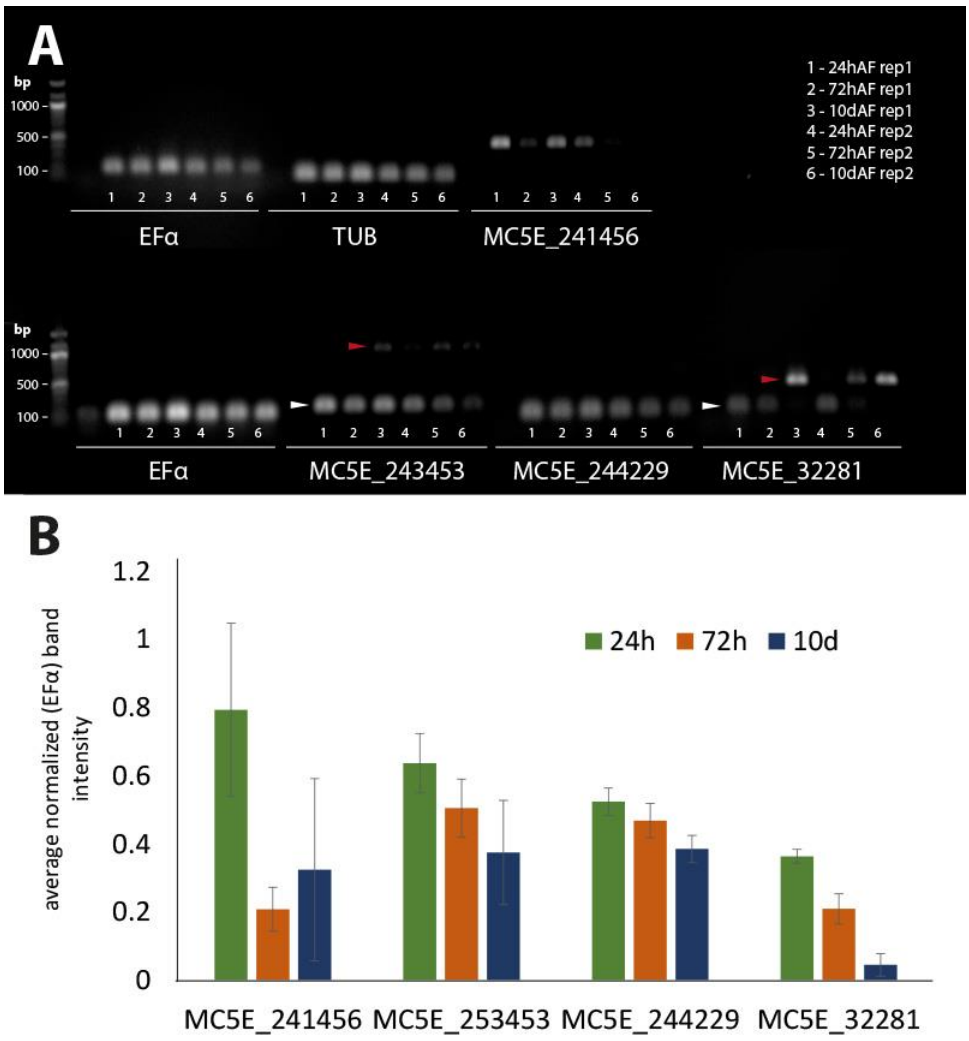

Figure 3.12. Semi-quantitative RT-PCR of potential epimerase genes in *F. serratus* embryos. (A) PCR amplicons for each of the epimerases (MC5E_x) and housekeeping genes (EFα and TUB); first row was analysed after 36 cycles, second row after 40 cycles in the thermal cycler. Red arrowheads represent contamination via potential gDNA contamination or unspecific cDNA amplification, white arrowheads represent the desired epimerase amplicons. (B) Graphic representation of the average fluorescence for 4 epimerase genes normalised by the elongation factor alpha (EFα) housekeeping gene. Error bars represent the standard error between the two replicates.

3.4.7. Mannuronan C5 epimerase genes in the *F. serratus* transcriptome

In a developmental system such as a fucoid embryo with very distinct growth patterns, it is interesting to explore how embryogenesis is regulated on a molecular level. To start addressing this question, an RNA sequencing experiment was performed. Poly (A) + RNA was extracted from 4 distinct developmental stages: 7hAF (round zygote, no fixed polar cue), 24hAF (germination and first division already took place), 72hAF (elongation of the rhizoid with thallus cell sequential division) and 10dAF (thallus elongation, rhizoid growth stops and holdfast starts forming). After library preparation and sequencing, $^{\Delta}$*de novo* transcriptome assembly, $^{\Delta}$protein prediction and $^{\Delta}$transcript expression analysis was performed. These were carried out by Dr Anna Gogleva (Schornack Group, Sainsbury Laboratory, University of Cambridge).

In the scope of this thesis and due to time constraints, only a small portion of RNA-seq data was used. After protein prediction, a BLAST database was created to look for sequence similarities with known mannuronan C5 epimerases originating from *E. siliculosus*. Twenty two genes were identified as potential MC5E genes in the *F. serratus* transcriptome, which had high similarity with different *E. siliculosus* MC5E sequences (Appendix 6. And 7.). Transcript expression levels for 22 candidate genes were examined for all 4 developmental stages in three independent biological replicates. The preliminary data (no full statistical differential expression has yet been performed) suggest all 22 genes are expressed in at least one of the developmental stages (high or low expression level; Appendix 8.). Although a full differential analysis was not performed due to time limitation, the resulting data could be split into different patterns, depending on the expression trends. Eight genes seemed to be expressed at quite low levels and constantly throughout development (Appendix 9.; the sequences of three candidate genes from this list matched the sequences from the above mentioned MC5E genes: 32281, 241456, 253453). A further 11 genes were found to exhibit high expression values early in development; 6 specific for 7hAF (Fig. 3.13A), 4 specific for 24hAF (Fig. 3.13B) and 1 expressed higher in both of the time points (Fig. 3.13D; the sequence of this candidate gene matches the sequence of MC5E_244229). Two genes had a varying expression with higher values either at 7 and 72hAF (Fig. 3.13C) or at 24 and 72hAF (Fig.

3.13E). One gene was expressed at later stages, 72h and 10d AF (Fig. 3.13F). The preliminary data here show that the candidate MC5E genes in the *F. serratus* transcriptome are expressed during embryogenesis, and, depending on the epimerase, different expression trends can be observed.

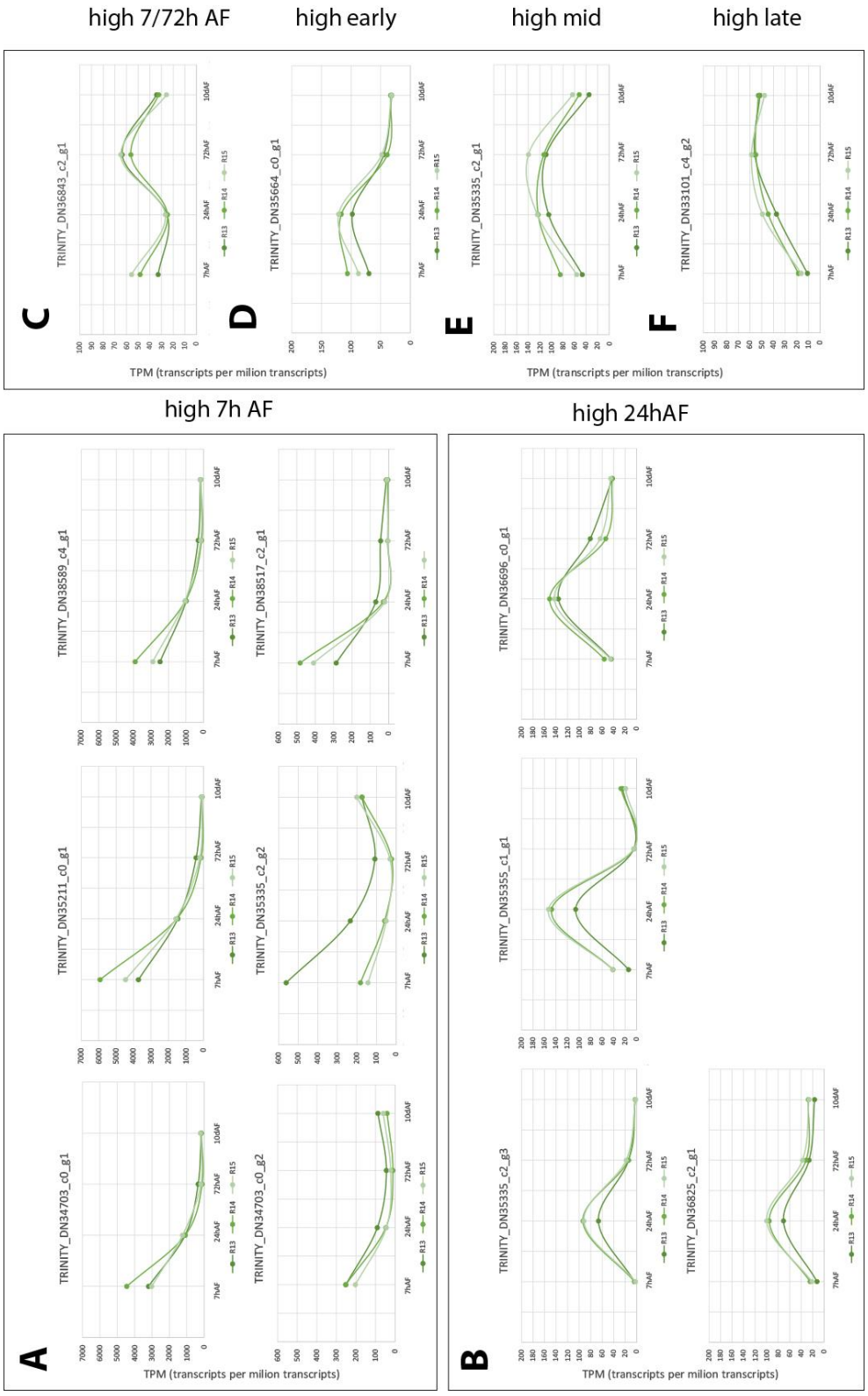

Figure 3.13. Transcript expression values of mannuronan C5 epimerase candidate genes during embryo development. Each of the graphs represent a single mannuronan C5 epimerase transcript expression levels in 4 developmental time points of 3 individual biological replicates. The graphs can be separated based on the trend of epimerase expression (A) early expression at 7hAF, (B) early expression at 24hAF, high expression at 7hAF and 72h AF (C), 7hAF and 24hAF (D) or late expression at 72hAF and 10dAF (E). The sequence of the gene candidate in (E) matches the MC5E_244229 found in *F. serratus* above.

3.5. Discussion

3.5.1. *Fucus* embryogenesis – an interesting developmental pattern

During embryogenesis, fucoid embryos have to coordinate a series of important developmental steps in order ultimately to create their adult body plan. Starting with polar axis formation and the first asymmetrical cell division, the direction of growth is already set. Manipulating these two events can heavily influence the growth of young embryos (Bisgrove et al., 2003; Farnham et al., 2013; Peters and Kropf, 2010). An initial asymmetrical cell division gives rise to two distinct cell types: rhizoid and thallus cell. This work demonstrates that the initial embryo growth occurs solely in the rhizoid, where active cell elongation accompanied by cell division takes place. During this time the thallus only undergoes cleavage divisions that partition the original surface area and thus do not contribute to overall embryo length. Thallus cell expansion begins to occur around 6d AF. This switch corresponds to the appearance of apical hairs, which are a crucial step for the development of meristematic area and further body development (Galun and Torrey, 1969). Following this at around 10dAF, the embryo develops a protuberance from the rhizoid to attach itself firmly to the substrate – a holdfast. These data are in line with previous reports on early fucoid development (Bouget et al., 1998; Galun and Torrey, 1969). However, the timing of these steps does not seem to be similar across different fucoid species. In *F. distichus*, the appearance of apical hairs was reported to happen only 3-4 weeks after fertilisation (Bouget et al., 1998), whereas in *F. vesiculosus* this happens sooner, around day 6 (Galun and Torrey, 1969), similarly to our observations.

After fertilisation, a fucoid alga develops a polar axis after which it undergoes germination. This germination represents the initiation of tip growth, a mode of growth observed in a variety of systems such as pollen tubes, root hairs, fern protonemata, moss chloronemata and caulonemata, fungal and oomycete hyphae (Carol and Dolan, 2002; Krichevsky et al., 2007; Menand et al., 2007; Parton et al., 2000; Riquelme, 2013). Our data showed that the rhizoid growth (proxied by average embryo growth) varied depending on its developmental stage, starting with 90 µm/day, decreasing to 60-80 µm/day from day 2-5 and then another increase at day 6-7 with 90 µm/day. This increase could be coming from the initiation of the thallus growth; since the rhizoid was still elongating and the thallus started its elongation, the result could be an increase in length. After day 7 the growth was reduced gradually to 40 µm/day at day 11 when it became relatively constant. Previous reports showed a rhizoid extension rate of 1 to 5 µm/h (Kropf, 1992), which is similar to these observations. As the rhizoid is the only actively growing structure in the first 5-6 days of development, the whole body length (and embryo growth rate) could be used as a proxy to determine the average rhizoid elongation. Although an hourly dynamics time lapse was not done in this study, if it is assumed that the elongation was constant (the embryos grew the same amount during the day and night), the data in this study would show the elongation rates from 2.5 - 3.75 µm/h in the first 5 days of development.

3.5.2. Tip growth or not-so-tip growth?

Tip growth in the *F. serratus* rhizoid was suggested by Calcofluor White wall staining, where the walls were stained at 24 hours after fertilisation, rinsed and embryos were left to develop another 24 and 48 hours before imaging. The data (Fig. 3.3) show that the stain fluorescence is lower in the newly grown areas (rhizoid) indicating a deposition of wall material. However, provided with this information, it is hard to conclude if the lower amounts of staining come only from vesicle secretion into the wall (exocytosis) or a reverse process of recycling of vesicles via endocytosis. In fucoid zygotes, there is evidence that the vesicles are located in the tip region during germination and following tip growth (Belanger and Quatrano, 2000). However, the direct location of their deposition to the cell wall remains unclear.

When exposed to laser photobleaching, the regions of interest have decreased fluorescence, which is regained via exocytotic processes in the cell. The data here show that recovery after photobleaching occurs in the *Fucus* rhizoid. This indicates that active exocytosis is taking place. Moreover, the data suggest that this recovery happens faster at the sides of the apical cell (12.2±1.8s) than the apical tip itself (20.7±2.6s). This is similar to what is observed in pollen tubes where the active exocytosis is taking place just below the apex; the vesicles fuse with the plasma membrane in a region 3–10 µm away from the apex (Zonia and Munnik, 2008).

How tip growth exactly occurs has been a long standing question in all tip-growing systems. Vesicle trafficking is important because the cell would not be able to expand without additional deposition of membrane and wall material at the site of active growth (tip). In pollen tubes, the vesicles travel along actin-myosin cytoskeleton (Geitmann and Emons, 2000; Vidali et al., 2001). Lily pollen tubes have actin filaments organised parallel to the tube until the subapical area where they have been shown to organise in a fine actin fringe (Lovy-Wheeler et al., 2005). The delivery of vesicles has been found to correspond to this subapical actin fringe. This region is thought to be the region of the highest exocytosis (Bove et al., 2008; Zonia and Munnik, 2008). A cone-shaped vesicle aggregation is observed at the pollen tube tip that corresponds to the vesicles that have been taken up by the cell via endocytosis (retrograde trafficking) at the tip (Bove et al., 2008). This creates a trafficking process referred to as an ‘inverse fountain’ (Bove et al., 2008).

Although still not completely known, this study suggests that the fucoid rhizoid tip growth might be similar to the one observed in pollen tubes, where faster exocytosis is happening on the sides, rather than the tip. A pulse chase experiment would be useful to determine in more detail the exact spatiotemporal dynamics of endocytosis and exocytosis in the rhizoids. Similarly to plants, it is known that actin is driving the localised vesicular trafficking in fucoid rhizoids (Hable et al., 2008). In addition, an ‘actin patch’ has been found to form in a spherical zygote that predicts the site of new rhizoid formation (Alessa and Kropf, 1999; Pu et al., 2000). After germination, this patch transforms into a ring which remains expressed during the growth of the rhizoid. This structure has been hypothesized to distinguish the growing and non-growing parts of the cell or to restrict certain components to the

growing rhizoid tip, such as calcium (Alessa and Kropf, 1999; Pu et al., 2000). Although not tested in this study, the deposition profile (higher on sides) might be spatially correlated to the previously observed actin ring. This might indicate that the possible relationship between the actin ring and secretion exists. A combination of actin imaging (as preformed in Alessa and Kropf, 1999) and FRAP experiments would elucidate this hypothesis.

3.5.3. Mechanical properties of the *Fucus* embryo

The local confinement of the growth process to the rhizoid during early *Fucus* embryogenesis suggests a differential distribution of mechanical properties in these embryos. For the first time, a mechanical approach was used to understand the potential mechanical contributions to the observed growth patterns. The experiments using AFM revealed that this might be the case. The cellular stiffness of the growing rhizoid was lower in comparison to the thallus region for all three developmental regions tested (24h, 72h and 10 days after fertilisation) correlating very well with areas of faster growth.

During the first days of embryogenesis, the initial thallus cell undergoes cleavage divisions and only after the appearance of the apical cell around day 6-7 it starts elongating, indicating both cell division and expansion are taking place. The decrease in apparent stiffness observed at day 10 seemed to correlate with the developmental stage that the embryo was undergoing. Each of the cells are undergoing cellular expansion at this stage, which requires loosening of the cell wall in order to accommodate the new larger cell.

The rhizoid cell had a different pattern during development that correlated with the embryo growth stage. The lowest apparent Young's modulus was observed at 24h AF, followed by 72h, with the highest at 10 days after fertilisation. During embryogenesis, embryos for the first few days exhibit the highest rates of growth which ultimately slows down and produces an adhering structure holdfast. These data support that pattern, where the fastest growth correlates with the softest rhizoid (24hAF) and the slower growth correlates with the stiffest rhizoid (10d AF).

In pollen tubes the spatial profile of the growing tip shows that the apex is significantly softer than the shank (cylindrical region of the cell). This gradient is observed within the first 20 µm of the tip (Chebli et al., 2012; Geitmann and Parre, 2004; Zerzour et al., 2009). The data here did not show such a clear increase in cellular stiffness as it moved away from the tip region. At 24h AF, the cellular stiffness of the rhizoid was constant throughout the 80-100 µm along the whole rhizoid. At 72 AF there seemed to be a change in stiffness moving away from the tip, however, this was not a significant change and not as prominent as the one observed in angiosperm pollen tubes. One explanation is that the stiffness change could not be observed due to limitations of the method: due to the rhizoid curvature, it was difficult to obtain valid data on the apparent Young's modulus close to the very tip. In force maps obtained from AFM the rhizoid always appeared softer (darker colour on the heat maps). However, this artefact most probably came from the difficulty of the machine to properly indent a curved area, hence resulting in false detection of reduced stiffness. Another indication of this phenomenon is apparent when observing the edges of the whole rhizoid; the line between the rhizoid and the mucilage/glass always seemed to be darker (appearing softer). On the other hand, it might be that the *Fucus* rhizoid does not behave similarly to what is observed in plants, and there is something else besides pure mechanical drive of the wall that controls the polarised elongation. One possibility might be the differential thickness of the wall; it is known to exist in brown algal tip-growing systems such as *Sphacelaria* (Katsaros et al., 2006) and *Pelvetia* (Bisgrove and Kropf, 2001), a close relative to *Fucus*. At 10 days after fertilisation the growth is almost stopped and no change in stiffness along the rhizoid is detected. This might indicate that elongation indeed is no longer happening.

In summary, there is a trend in the *Fucus* embryo showing the gradient of stiffness along the growth axis. This stiffness difference correlates with the fast growing rhizoid and the non-growing/slow-growing thallus. The rhizoid tip does not show a significant stiffness decrease relative to the shank region above it. This is dissimilar to that observed in plants, where the apex of the tip-growing pollen tube is significantly softer than the shank. Reasons for this are still not completely clear, but it is suggested that the AFM method was unable to detect a change at the very

tip due to geometrical limitations, or there might be another geometrical (or a different) mechanism of polarised growth involved.

3.5.4. A relationship between mechanical properties and wall biochemistry

Tip growth is a very specific mode of growth with a relatively fast (varies from species to species) directional elongation. This means that the tip wall has to be able to withstand the turgor pressure from the inside of the cell, but at the same time, be able to allow this fast growth to occur by loosening. The loosening might be controlled by modifying wall components in a specific way: alginate, sulphated fucans or cellulose. Due to its possible mechanical implications in algal growth, as well as correlating its potential function with the function of its analogue in plants (pectin, detailed in Chapter 1), alginate was chosen to be investigated as the main candidate. The three epitopes tested with three available antibodies BAM6, BAM7 and BAM11 had different patterns of distribution during embryo development. The M-rich epitope was present throughout the embryos at both 24h AF and 72h AF. The MG rich epitopes were present in two areas, specifically the rhizoid tip and the collar zone, with some signal in the rest of the rhizoid as well as the thallus. The spatial distribution of BAM10 (G-rich epitope) in the thallus indicated there might be a correlation between the wall mechanical properties and alginate distribution (G-blocks can crosslink with calcium ions); the thallus cell was much stiffer than the entire rhizoid in both 24h and 72h AF. However, the high signal at the rhizoid tip for both MG-rich and G-rich epitope does not link directly into this hypothesis. This might indicate that, even though the BAM10 binds to a G-rich area that could crosslink with calcium, the change in alginate structure necessary for visual correlation with the mechanical properties, is not covered by the currently available antibodies, or that the signal at tip originates from outside the cell during the process of mucilage excretion.

To examine a possible correlation with another wall component *in muro* immunolabelling of the sulphated fucan components was investigated next. From a set of fucoidan antibodies available (Torode et al., 2015), two of the antibodies with a detectable signal were chosen, BAM3 and BAM4. Both sulphated fucan epitopes were detected along the rhizoid part of the embryo. The data in this study follow the

same distribution patterns as previous reports. In round zygotes which are developing a polar axis, alginate and cellulose are uniformly distributed in growing rhizoids, whereas a sulphated fucan named F2 localises to the growing tip (Novotny and Forman, 1975). More recently, the same set of antibodies was used to look at the early *Fucus* embryogenesis and showed that both of the used antibodies were localising to the rhizoid pole of the zygote (Torode et al., 2016). However, progressing in development, the signal for both BAM3 and BAM4 spread all over the germinated zygotes, whereas in our study, although present in the thallus, it was mostly detected in the rhizoid. Even though sulphated fucans polarise to the rhizoid pole during early polar axis fixation, it does not suggest that they have a direct role in wall properties during cell loosening and following local germination. In previous reports, they have been linked to zygote adhesion (Crayton et al., 1974), although they have also been suggested to strengthen the tip-growing rhizoid during elongation (Bisgrove and Kropf, 2001). The data here show some correlation with the mechanical properties, however it is difficult to conclude whether this provides a causal relationship at this time.

In the *Fucus* zygote, cellulose might be acting as a strengthening component; its low signal detected during germination corresponds to the growth initiation (Novotny and Forman, 1974). In the scope of this project, due to the time limitations, cellulose was not looked at. However, to elucidate its potential involvement in the mechanical properties during embryo growth, this is a next-step future direction.

3.5.5. Molecular aspects of cell wall related embryo morphogenesis

The alginate biosynthesis pathway has not yet been fully described in the brown algal lineage. However, a few genes homologous to bacterial genes involved in this pathway have been identified (Michel et al., 2010). One of the interesting steps in alginate biosynthesis, with a potential effect on mechanical properties, represents epimerisation of a mannuronic acid residue into a guluronic acid residue via MC5Es. Because of the alginate structure and biological function in cell walls (provides flexibility and strength to the algal body), alginate might be thought of as an analogue to pectin. This would then suggest that the MC5Es might have the same role as pectin methylesterases (PMEs), modelling the pectin (or in this case

alginate) into the right conformation to cross-link with calcium and rigidify the wall (details of this process are described in Chapter 1). To date, a number of bacterial genes encoding MC5Es have been discovered and the exact function of some of these enzymes (patterns of epimerisation) has been investigated (Ertesvåg, 2015; Hartmann et al., 2002a). In the brown alga *Ectocarpus*, a family of 31 genes encoding these enzymes has been found (Fischl et al., 2016; Michel et al., 2010), and one of these enzymes has been heterologously expressed in *E. coli* to determine its function (Fischl et al., 2016). It could be assumed that a group of these enzymes is used by the alga to produce variations of alginate structure, which could have implications in regulating mechanical or physiological properties during development. In *F. serratus*, genes that could be encoding for these enzymes or other cell wall related enzymes have not been fully explored and their expression during embryogenesis has not been looked at.

One approach taken here was to detect the potential genes related to the *Ectocarpus* MC5Es through already available datasets for *Fucus* species. Thirty one protein sequences found in *Ectocarpus* were BLASTed against the *F. vesiculosus* RNA-seq dataset (Martins et al., 2013). Seven nucleotide sequences were discovered that aligned with high similarity; 6 of these represented only 3 different reads since they aligned perfectly with the other sequence (in Appendix 4. highlighted in colour). Matching of these reads to each other does not come as a surprise, taking into account that a transcriptome database was used; this would provide information about sequence fragments shorter than the full gene sequences (depending on the sequencing protocol). The following step involved detecting expression of these genes in the studied system, *F. serratus*. All 7 sequences were found in the cDNA originating from embryos at two developmental stages, 1h AF and 14d AF. These samples served solely as a control for the sequence detection and were not used afterwards in testing the expression levels. Semi-quantitative RT-PCR has suggested that the 4 potential epimerases are expressed during the embryo development (Fig. 3.12). The results indicate that one of the epimerases MC5E_32281 seems to be expressed at a higher level in the early stages after which the expression decreases. However, the variation between the two samples tested was quite significant, so all the conclusions made with these data, although

suggestive, need to be supported better with more replicates as well as confirmed using a more accurate method, such as quantitative PCR (qPCR).

A more sophisticated approach was then taken for in depth analysis of all the transcripts through RNA sequencing. The transcriptome resulting from this study is to our knowledge the first one to explore gene expression during embryogenesis in a fucoid alga. Although still ongoing, some aspects of it have been addressed as a part of this thesis, where the idea was initiated. The preliminary results suggest that at least 21 epimerase genes are expressed during embryogenesis, with patterns of expression observed for each of these genes that indicate potentially different roles during embryo development. The four MC5E genes identified through a database search (section 3.4.6.) corresponded to four different Trinity genes from the transcriptome analysis. Three of the genes were found to be in the group of Trinity genes unlikely to have a differential expression pattern during embryogenesis (Appendix 9.). A small discrepancy was observed: one of the genes in this group (MC5E_32281) did show a downward trend of expression when RT-PCR was performed. However, as mentioned above, the variation between the two samples was quite significant, so a more accurate method should be used in the future to test this. Furthermore, one of the MC5E (MC5E_244229) genes corresponded to a Trinity gene that presented a slightly higher expression pattern at 24h and 72h AF. However, this was not observed in the semi quantitative RT-PCR. This is likely due to the very slight changes in expression during chosen time points which would have been missed in an RT-PCR experiment, but detected using a more sensitive approach such as RNA-sequencing.

Moving forward, the next steps involve: detailed analysis of differential epimerase gene expression, validation of candidate genes via qPCR, as well as widening the search by looking at different gene families involved in cell wall biosynthesis or remodelling. These include arabinogalactan proteins found in brown algal cell walls, with a potential role in guluronate modelling (Torode *et al.*, 2016), and sulfatases and sulfotransferases involved in sulphated fucan biosynthesis and degradation (Michel *et al.*, 2010). Transcriptome analysis originating from this study will serve as a great source for future exploration of different bases of embryogenetic control in fucoid brown algal systems.

Chapter 4. Exploring the effects of cell wall modification on development in a *Fucus serratus* embryo

4.1. Summary

Early stages of embryogenesis are marked by the elongation of the rhizoid which exhibits tip growth. The growth here is focused to the dome-shaped apex where secretory vesicles are being incorporated into plasma membrane and the cell wall, depositing new material. The polar behaviour of the system is governed by F-actin filaments and polar distribution of ions (e.g. Ca^{2+}), whose role has been confirmed using pharmacological treatments. Chapter 4 explores the role of cell walls in growth by investigating the changes in rhizoid wall properties when subjected to cytoskeleton depolymerising drugs, a reduced influx of calcium ions (reduction of external calcium) and disruption of alginate. All of the treatments reduced rhizoid elongation ultimately resulting in shorter rhizoids. The results suggest actin and microtubules are both involved in deposition during tip growth since a significant reduction of cell wall epitopes was observed when embryos were treated with cytoskeleton depolymerising agents. Furthermore, a significant increase in rhizoid cellular stiffness was observed, indicating the interplay between cytoskeleton-linked deposition and wall mechanics is important for rhizoid elongation. In addition, tip swelling and branching was observed when cytoskeleton was disrupted, indicating its role in controlling tip shape integrity. Removing alginate from the wall and depleting calcium from the medium had different effects on wall properties. Alginate removal did not result in stiffness change, suggesting the alginate involvement in elongation, but not mechanical properties during growth. Depletion of calcium resulted in a thicker layer of mucilage around the rhizoid (associated with sulphated fucans), accompanied by an increase in cellular stiffness, indicating the ion imbalance might have an effect on embryo adhesion.

4.2. Introduction

The fucoid zygotes have served as a useful system to explore the mechanisms of cell polarity and early development. The fertilisation occurs independently of mother tissue with a high number of resulting individuals which are initially apolar and only afterwards develop a polar axis. Some of the most relevant and important aspects of these mechanisms relate to the cell cytoskeleton, cell wall remodelling and the role of calcium ions and ion fluxes. These factors, and their interplay, are the main driving force in the process of fucoid zygote polarisation.

This interplay between wall deposition, ion fluxes, and the cytoskeleton begins as early as fertilisation. It has been shown that at the sperm entry site of the egg, a polar cell wall deposition takes place in the first 5 minutes of fertilisation (Bothwell et al., 2008). Localized cortical $[Ca^{2+}]_{cyt}$ elevations occur (Bothwell et al., 2008; Roberts et al., 1994). This creates a gradient of Ca^{2+} along the rhizoid-thallus axis, with the highest concentration of Ca^{2+} at the future rhizoid tip (Brownlee and Pulsford, 1988; Brownlee and Wood, 1986; Kropf and Quatrano, 1987) The actin network has also been found to localize in the cortex of the cell at the location of sperm entry (Hable and Kropf, 2005). The localisation of both calcium and actin can be modified. The polarisation of a fucoid zygote responds to post-fertilisation external cues, which then determine the polar axis. It has been observed that the aforementioned calcium gradient and actin network move to the new site of future rhizoid pole, if affected by these external cues, such as light (Alessa and Kropf, 1999; Brawley and Robinson, 1985; Hable and Kropf, 2005; Hable et al., 2003; Kropf et al., 1989b). These two processes are essential for normal zygote polarisation, as has been proven by blocking their function with pharmacological treatments. Cytochalasin D and latrunculin B have been shown to prevent polarisation by interfering with the actin cytoskeleton in zygotes of *Pelvetia* and *Fucus* (Brawley and Robinson, 1985; Nelson and Jaffe, 1973; Quatrano, 1973). It has also been shown that the actin network is localised in growing rhizoid tips (Kropf et al., 1989b) and that disrupting actin polymerisation results in growth cessation in the *Pelvetia compressa* rhizoid (Hable and Kropf, 2005). On the other hand, the other cytoskeletal component, microtubules, do not seem to play an essential role during the zygote polarisation process. Zygotes incubated continuously in microtubule-

depolymerizing drugs photopolarized and germinated normally, under conditions where microtubules could not be detected by immunofluorescence (Brawley and Quatrano, 1979; Kropf et al., 1990). However, an aberrant phenotype following cell division could be observed, a dispositioned first cell plate. The disruption of cell division was seen when pharmacologically blocking microtubule polymerisation (nocodazole) or by using RNA interference to knock down a tubulin gene (Farnham et al., 2013).

There is another key player that has a role in normal polarisation and zygote development during the first hours of development – the cell wall. After the cell wall is deposited around the fertilised zygotes, three major components can be detected: alginate, cellulose and two different fucoidans named F1 and F3 (Quatrano et al., 1985). There is also a third type of fucoidan, F2, which only starts appearing around 8 hours after fertilisation, in specialised Golgi-derived vesicles where it is sulphated (Quatrano and Shaw, 1997). Upon establishing the polar axis, these F2-vesicles travel to the future rhizoid pole where they are deposited into the cell wall. The F2-fucoidan is incorporated in the cell wall while the zygote is still spherical and can be detected using an acidic solution of toluidine blue stain (Quatrano and Shaw, 1997; Shaw and Quatrano, 1996). Treatments with actin disrupting agents result in the inability of the F2-fucoidan to be incorporated into the cell wall, suggesting that polarising actin serves as a ‘highway’ for the trafficking of these vesicles (Brawley and Robinson, 1985; Quatrano et al., 1985). Another line of evidence about the importance of cell wall in zygote polarisation comes from enzymatic treatments which removed the cell wall from 6-h-old *Fucus* zygotes. The resulting protoplast was found not to develop as long as the cell wall was absent (Kloareg and Quatrano, 1987a).

An important role for actin in tip growth has been demonstrated in different tip-growing systems across the evolutionary tree (plant root hairs: Carol and Dolan, 2002; Miller et al., 1999; pollen tubes: Gibbon et al., 1999; Vidali et al., 2001; fungal hyphae: Heath et al., 2003; Ketelaar et al., 2012; Taheri-Talesh et al., 2008; and other algae: Karyophyllis et al., 2000). Tip growth does not rely solely on actin, but on calcium ion fluxes and localisation as well (Jackson and Heath, 1989; Jackson

and Heath, 1993; Malhóai and Trewavasb, 1935; Pierson et al., 1994; Pierson et al., 1996; Steinhorst and Kudla, 2013).

Considerable effort has been devoted to investigating mechanisms behind the fucoid zygote polarisation and the subsequent first cell division, separating the thallus and rhizoid. However, moving forward in development to the later stages of embryogenesis, there is less information about how cytoskeleton, calcium and cell wall remodelling affect development in brown algae. The change of cell shape in plants is based on turgor-driven expansion and the addition of new material into the cell wall. This makes the cell wall a crucial player in the process of growth. Here I investigate the effect of cytoskeleton disruption on *F. serratus* embryo rhizoid elongation and its potential link to the cell wall properties. In addition, hypothesizing that alginate would behave similarly to pectin in plants (see Chapter 1), I looked into what effect modifying exogenous calcium or alginate structure would have on cell wall stiffness and biochemistry.

4.3. Materials and methods

4.3.1. Sample collection, fertilisation and culturing

See Chapter 3: sections 3.3.1. ‘Sample collection and processing’ and 3.3.2. ‘Fertilisation’.

4.3.2. Applying treatments

24 h after fertilisation, the seawater medium was replaced with a treatment of interest and the embryos were kept in the solution for 48 hours unless otherwise stated. The 72 hour old embryos were used for further analysis.

Pharmacological manipulation of cell wall deposition/composition

Chemical screen

To test the effect of actin, microtubule and cellulose disrupting chemicals on embryo development, an initial phenotype screen was performed using various

pharmacological agents with a range of concentrations. All chemicals were diluted to the appropriate concentration from stock solutions as follows: isoxaben 2mM in dimethyl sulfoxide (DMSO); brefeldin A (10mM); dichlobenil (200mM); latrunculin B 1mM; oryzalin 5mM, nocodazole 17mM in DMSO. The DMSO in ASW was used as control treatment (one control for all experiments – concentration of DMSO used was the same as the highest concentration of the pharmacological agent).

The embryos underwent the processing as above and the phenotypes were observed and imaged under a VHX 5000 microscope (Keyence (UK) Ltd) 48 hours after fertilisation/ 24 hours after treatment application. The appropriate treatments and concentrations were chosen for further investigation based on the significant reduction in embryo length while maintaining high embryo viability.

Altering cell wall via actin and microtubule disruption

After determining the suitable conditions, embryo development was investigated more closely through a 5 day time course where the length of the embryo was measured every 24 hours. The images were taken under a VHX 5000 microscope (Keyence (UK) Ltd, UK).

Altering growth and alginate crosslinking via calcium

To test the effect of calcium on embryo development, three experiments were performed:

EGTA treatment

To test the effect of calcium removal through Ca^{2+} chelation, 24 hours after fertilisation the embryos were moved into ASW containing 4 different EGTA concentrations; 100 µM, 1 mM and 10 mM. 48h after fertilisation they were imaged and the final length was measured.

Calcium removal

24 hours after fertilisation, the embryos were put into artificial seawater (450 mM NaCl, 10 mM KCl, 9 mM $CaCl_2$, 30 mM $MgCl_2$, 16 mM $MgSO_4$) or seawater

where no calcium was provided, either in its ionic form Ca^{2+} or as $CaCl_2$. The embryos were imaged 48 hours after fertilisation for length measurement.

Calcium depletion

After 24 hours in ASW, the embryos were moved into solutions with decreased amount of calcium in the form of $CaCl_2$ in the following concentrations: 9 mM (control), 6 mM, 3 mM and 1 mM. The embryos were imaged 72 hours after fertilisation and their length was measured.

Altering cell wall composition with alginate lyase

To test the effect of altering alginate composition in the cell wall, an enzyme degrading M-blocks of alginate (alginate lyase) was used. The embryos were kept in ASW for the first 24 hours, after which the medium was replaced by ASW mixed with different concentrations of alginate lyase; 0.5 U mL^{-1}, 2 U mL^{-1}, and 5 U mL^{-1}. Embryos were incubated on 16°C.

The length of embryos was measured 3 days after fertilisation for all concentrations after which the most suitable concentration was chosen for further experiments. The chosen concentration was used in determining the length in time, cell wall biochemistry and cell wall mechanics.

4.3.3. Quantifying cell divisions

To investigate the early division pattern in the *Fucus* embryos, the embryos were cultured on slides and taken 24h after fertilisation (looking at the effect of microtubule disrupting agents on first cell division).

4.3.4. Immunohistochemistry

Embryos were fertilised and cultured as above on multitest 8-well slides (Vector Laboratories, USA), taken at 72h AF (control or treated), fixed overnight (2% formaldehyde and 2.5% glutaraldehyde in ASW). Fixation followed by 3x15 minute wash with ASW, and a rinse in phosphate buffered saline (PBS; 2.7 mM KCl, 6.1 mM Na_2HPO_4, and 3.5 mM KH_2PO_4). The following protocol and quantification is

detailed in Chapter 3; section 3.3.7. ‘Alginate and sulphated fucan immunolocalisation’. The quantification was done for the rhizoid tip only.

4.3.5. Atomic force microscopy

Embryos were fertilised, cultured and grown in artificial seawater or a treatment solution for 72h after which they were used for experimentation. The following protocol is described in Chapter 3; 3.3.6. ‘Atomic force microscopy’, with the following modification: the elasticity of all samples was determined by indenting with the tip over the rhizoid tip in 100 µm x 100 µm squares.

4.3.6. Statistics

All samples were tested for normality with Shapiro-Wilk normality test and for equal variance using Brown-Forsythe equal variance test. Significance tests were performed according to their distribution: two sample t-test to compare two samples with normal distribution, Mann-Whitney Rank Sum test for comparing two non-normal distributed samples, ANOVA or ANOVA on Ranks for more than 2 samples for normal and non normal distribution, respectively.

4.4. Results

4.4.1. Inhibiting actin and microtubule polymerisation leads to reduced growth rate and change in morphology in *F. serratus* embryos

It has previously been shown that the actin cytoskeleton is important in axis fixation in fucoid embryos and its inhibition results in blocked tip growth (Hable and Kropf, 2005; Hable et al., 2003). However, microtubule disruption via chemical agents was not found to have an effect during this process (Brawley and Quatrano, 1979; Kropf et al., 1990). Reduced embryo growth was seen only after the microtubule disruption resulted in the misalignment of the first cell division, indicating the positioning of that division is important in future embryonic development (Bisgrove and Kropf, 1998).

An initial screen was performed to determine the optimal conditions where the pharmacological agent treatment was effectively reducing (but not abolishing) the final embryo length whilst not affecting their viability (Fig. 4.1). This procedure was designed to isolate growth defects from other affected processes due to embryo death. The embryos were grown in artificial seawater for 24 hours, after which they were moved into subsequent treatments. They were kept in treatment for 5 days and imaged on the second and fifth day. Six pharmacological agents were chosen, which were known to have an effect on disrupting cellular trafficking, actin and microtubule cytoskeleton or cellulose synthesis.

Cell wall material is deposited through the action of vesicle trafficking. Brefeldin A acts as a protein inhibitor between the endoplasmic reticulum and the Golgi apparatus hence blocking the normal vesicular transport (Klausner et al., 1992). In this experiment, Brefeldin A treatment showed a significant effect by decreasing embryo growth at concentrations of 1 and 10 µM 2 days after fertilisation (p-value<0.001, n=50, Fig. 4.1A). However, both of these treatments were fatal to the embryos in the later days of exposure (Fig. 4.1A). Dichlobenil and isoxaben both affect cellulose synthesis by blocking the glucose incorporation in the cellulose chain (Cox, 1997; Heim et al., 1990). In this experiment, embryos grown in dichlobenil showed a reduced length 2 days after fertilisation in 100 nM and 10 µM (Fig. 4.1B), but the viability of those embryos was very low 5 days after fertilisation. Isoxaben treatment at concentrations of 100 nM and 1µM did not show a significant effect on the embryo growth (Fig. 4.1C).

Latrunculin B prevents actin filament re-polymerisation by binding to actin monomers (Morton et al., 2000). It had a strong effect on reducing *F. serratus* embryo growth even at concentrations as low as 1nM. The embryos were viable after treatment with 1nM and 10nM, but treating them with higher concentrations severely reduced viability (Fig. 4.1D). The disruption of the other cell cytoskeletal component, microtubules, was performed using two agents: nocodazole and oryzalin. They both bind to tubulin and prevent its polymerisation (Davidse, 1986; Strachan and Hess, 1983). The results here show that they both had an effect on embryo length – embryos were significantly shorter under all the examined concentrations of nocodazole (10 nM to 10 µM), whereas oryzalin had a similar

effect when the concentration reached 100 nM (Fig. 4.1E, F). Based on this screen, treatments were selected that were satisfying both of the set criteria: effect on embryo length and maintained viability of the embryos for at least 5 days after fertilisation (4 days in treatment). Those were as follows: 10 nM latrunculin B, 100 nM nocodazole and 100 nM oryzalin.

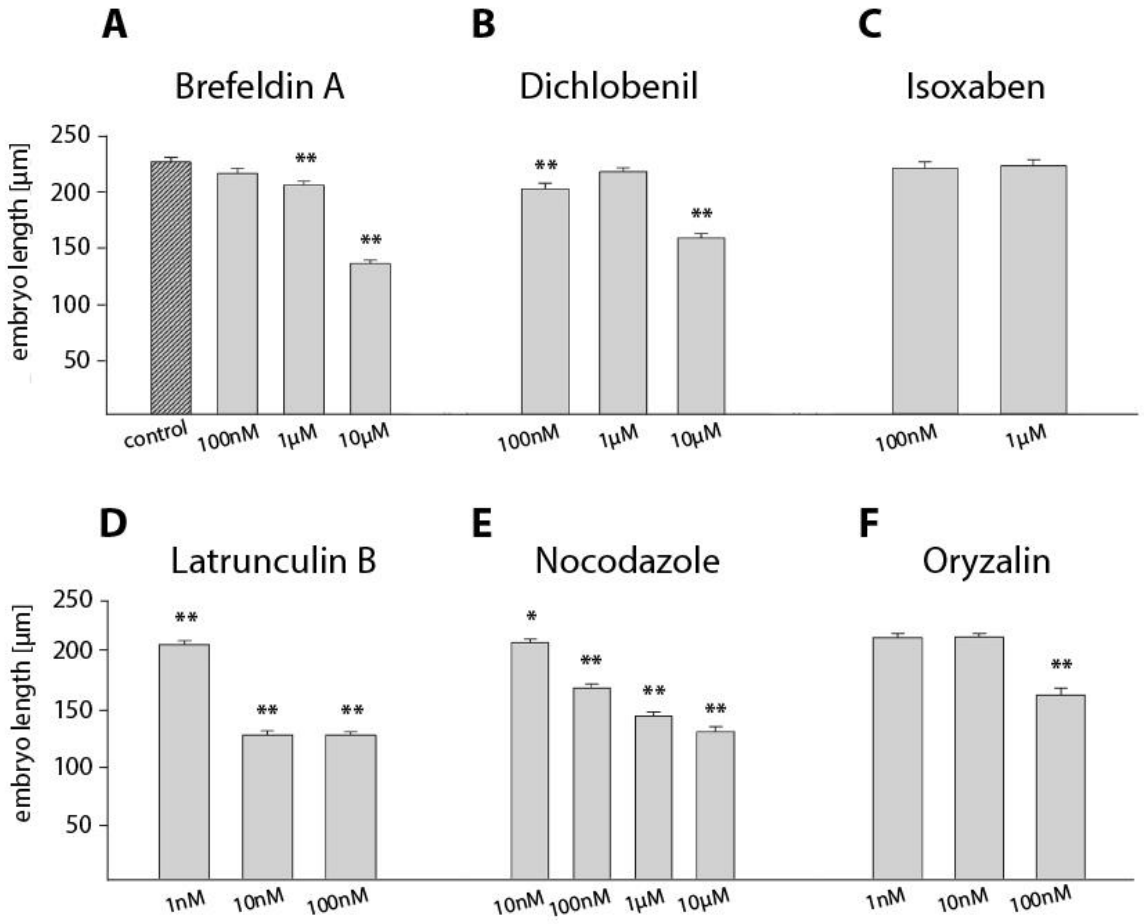

Figure 4.1. Screen for effective treatments and concentrations of pharmacological agents on embryo length and rhizoid elongation 2 days after fertilisation. (A) Brefeldin A (disrupts vesicular trafficking) treatment showed a significant effect in embryo length reduction when treated with a concentration of 1µM and higher (p-value<0.001) (B) Dichlobenil (inhibits cellulose synthesis) shows a significant effect for concentrations of 100nM and 10 µM (p-value<0.001). (C) Isoxaben (inhibits cellulose biosynthesis) does not have a significant effect under two given concentrations. (D) Latrunculin B (inhibits actin polymerisation) has a strong effect in a variety of concentrations starting from 1nM (p-value<0.001). (E) Nocodazole (inhibits microtubule polymerisation) shows a significant effect in length reduction from a concentration of 10nM up (p-values: 10nM (0.004), other (<0.001)) and (F) Oryzalin (inhibits microtubule polymerisation) has a significant effect on embryo length at 100nM concentration (p=-value<0.001), n=50/treatment.

To check in detail how cytoskeleton inhibition affected the dynamics of growing embryos rather than just initial rhizoid formation (as previously described in the literature), growth was tracked during the consecutive 5 day period after fertilisation. In artificial seawater, *F. serratus* embryos grew approximately 80-110 µm/day in the first 5 days (Fig. 4.2A; embryo length: 131 ±0.92 µm on day 1, 514±5.74 µm on day 5) with a decreasing relative growth rate starting from 0.46±0.008 on day 1-2 to 0.145±0.013 on day 4-5 (Fig. 4.2B). When in cytoskeleton disrupting treatments, they grew less with a smaller average relative growth rate per day (Fig. 4.2A, B; LatB 0.089±0.01, nocodazole 0.286±0.01, oryzalin 0.319±0.009 on day 1-2, LatB 0.08±0.014, nocodazole 0.08±0.018, oryzalin 0.12±0.016 on day 4-5, p-value (individual treatment against control) <0.001, n=100/treatment). At these concentrations, the latrunculin B treatment showed the largest effect, with a low constant relative growth rate of around 0.1, while nocodazole and oryzalin had the same trend as control, but lower – rate decreased from 0.3 to just over 0.1. Looking at 72h AF, which was the period of the fast rhizoid elongation (described in Chapter 3), it could be seen that embryo length was significantly lower ($p<0.001$) in all three treatments, on average 164 µm for latrunculin B, 205 µm for nocodazole and 238 µm for oryzalin. Embryos in the control treatment grew normally reaching the final length of 340 µm on day 3 (Fig. 4.2C).

4.4.1.1. Effect of cytoskeleton disruption on rhizoid morphology

Cytoskeleton disruption led to an interesting set of phenotypes. After exposing them to latrunculin B, nocodazole and oryzalin at 24h AF, the embryos changed their morphology which was observed 24 hours after (48h AF). The observed rhizoid phenotypes were divided into 4 groups: normal rhizoid (rhizoid elongation is ongoing; Fig. 4.3B, blue), wide rhizoid (the rhizoid was shorter and wider, especially at the tip; Fig. 4.3B, orange), split rhizoid (the rhizoid was split in two; Fig. 4.3B, grey) and branched (the rhizoid started to branch identically to holdfast formation process; Fig. 4.3B, yellow). The control did not present any aberrant phenotypes, whereas all three treatments showed a fraction of each of the 4 phenotypes to a different extent. When actin was disrupted via latrunculin B, 60% of the embryos had a normal looking rhizoid (shorter, but normal), 20% had a wider and thicker rhizoid and another 16% had a rhizoid that split in two. The remaining 4% presented

a branching phenotype. In the microtubule disrupting treatments, the wide and split rhizoids were mostly not present (5% combined), but the majority of embryos showed either normal rhizoid (nocodazole 90%, oryzalin 58%) or a branched one (nocodazole 9%, oryzalin 38%) (Fig. 4.3A).

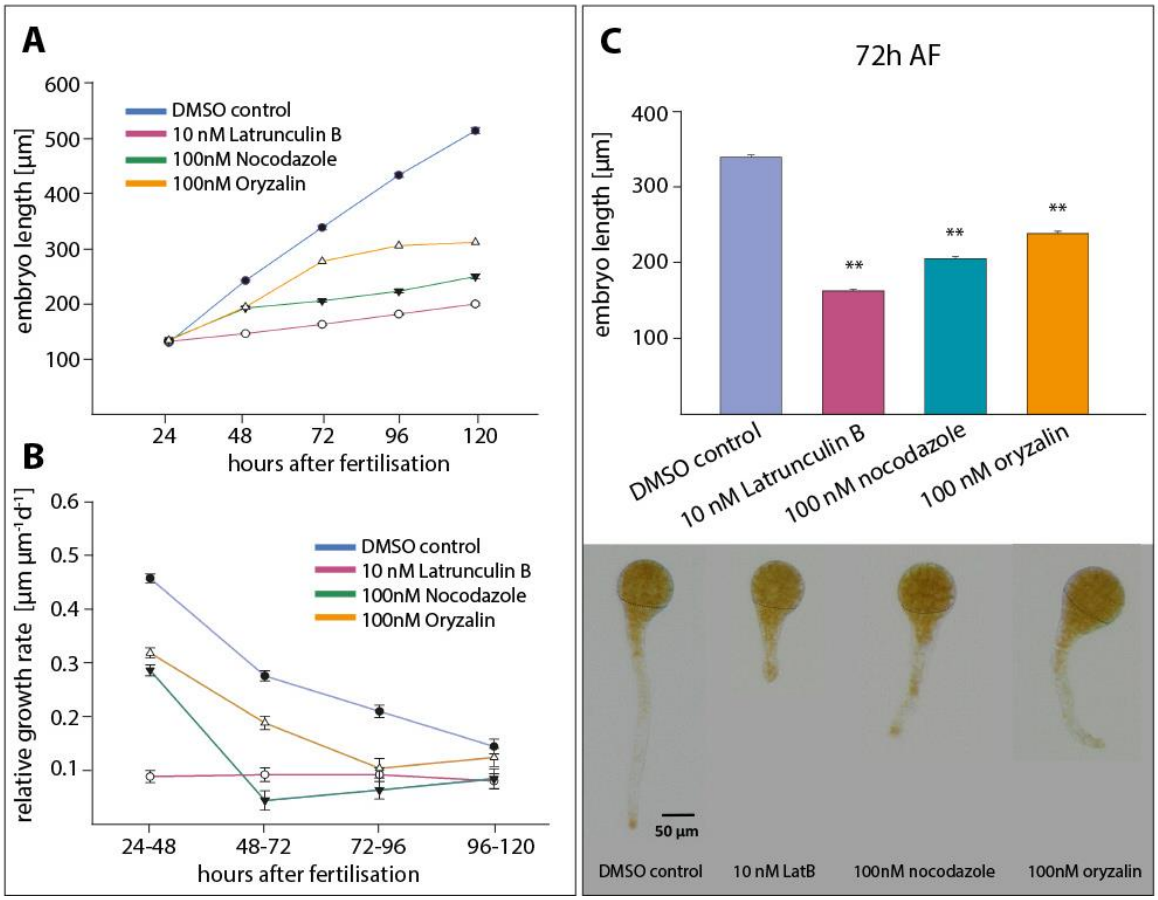

Figure 4.2. Growth of *F. serratus* embryo during cytoskeleton disruption. (A) Increase in embryo length and the growth rate (B) over a course of 5 days when treated with actin (latrunculin B) and microtubule (nocodazole, oryzalin) disrupting agents. (C) All treatments result in significantly shorter embryos 72h after fertilisation (AF) (n=100/treatment, ANOVA on ranks; p-value for all treatments compared to control <0.001).

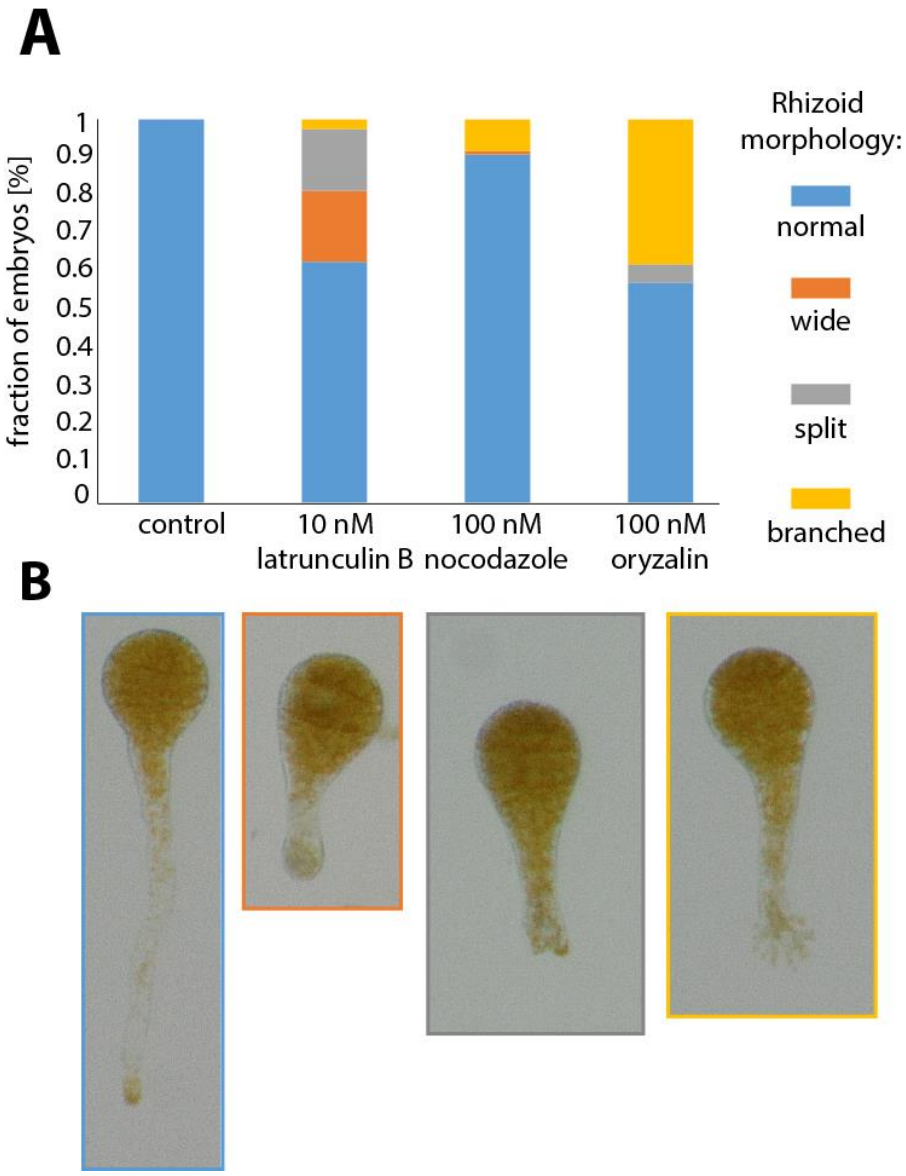

Figure 4.3. *F. serratus* embryo phenotypes observed when treated with cytoskeleton disrupting agents. (A, B blue) In control treatment embryos elongate normally (rarely an aberrant phenotype is observed). Wider rhizoids (A, B orange) and split rhizoids (A, B grey) are a result of mainly actin disruption, but also present when the microtubule skeleton is affected (D). The branched rhizoid (potential holdfast formation, B yellow) is mainly present in embryos treated with microtubule disrupting agents, specifically oryzalin. n (control)= 93 , n (latrunculin B)= 109, n (nocodazole)= 109, n (oryzalin) = 82; numbers represent a cumulative result of 3 independent biological replicates.

4.4.1.2. Microtubule disruption affects initial cell division

It is known that the microtubules are important in the formation of cell plates in plants and algae (Bisgrove et al., 2003; Peters and Kropf, 2010) and that inhibiting the genes related to them affects the cell division position (Farnham et al., 2013). In order to confirm these data and explore them further, 8 hours after fertilisation the embryos were moved to a medium containing 100 nM nocodazole, 100 nM oryzalin or ASW + DMSO (control). The effects on the formation of the first cell division were observed after 24h (Fig. 4.4A). Since the zygotes require actin to polarize their axis and they would not be able to form a rhizoid if put into a medium with actin depolymerizing agent (Quatrano, 1973), this experiment was not conducted using latrunculin B treatment. Similar to the data available from the literature, the zygotes treated with microtubule depolymerizing agents had aberrant first cell division planes. The control treatment had 7% of aberrant cells while nocodazole and oryzalin had 40% and 30%, respectively. A significantly higher number of undivided zygotes was observed as well (control 10%, nocodazole 40%, and oryzalin 20%) (Fig. 4.4B). When the first cell division was formed, the average angle between the axis elongation and that division in the control treatment was around 90°. However, in the aberrant embryos, for both treatments, this angle was reduced, being on average around 50° (Fig. 4.4C).

As for previous observations in fucoid zygotes (Farnham et al., 2013; Hable and Kropf, 2005), these results show that by disrupting the actin or microtubule cytoskeleton in young embryos, their growth is reduced significantly. These results also suggest that cytoskeleton disruption affects the morphology of the rhizoids. This might suggest that the cytoskeleton is not important solely in the rhizoid tip growth, but also in the cell shape control and might influence potential cell fate decision making.

4.4.2. Slower growth of embryos correlates with the increase of the rhizoid cell wall stiffness when cytoskeleton is disrupted

It has been shown that the cytoskeleton serves as the delivery route to deposit vesicles into the tip of the tip-growing structures (Ketelaar and Emons, 2001;

Miller et al., 1999). In plants, tip growth has been associated with changes in the cell wall biochemistry; pectin distribution is correlated with the occurrence of growth and

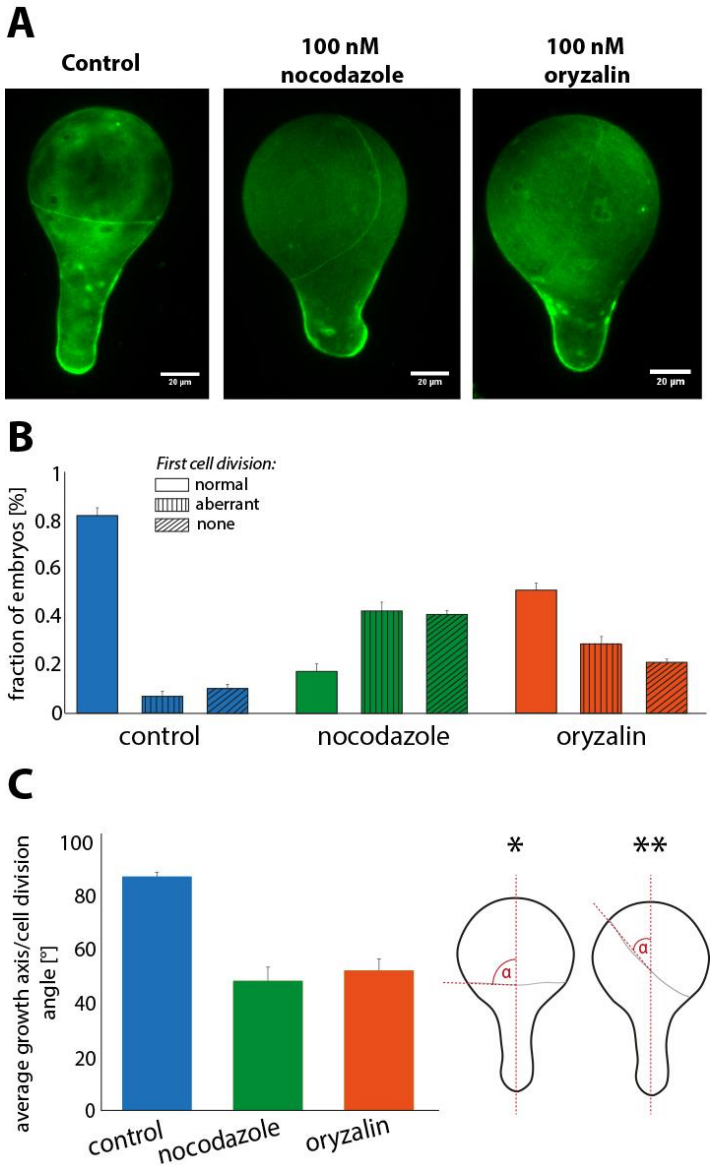

Figure 4.4. Effects of early microtubule disruption on first cell division positioning. (A) Calcofluor White staining of 24h old *F. serratus* embryo cell walls and first cell division in control treatment and when treated with nocodazole or oryzalin 8h after fertilisation. (B) Graph showing distribution of division types (control, aberrant or no division) in control and microtubule disrupting treatments. (C) Graph representing average angles of the axis of growth and the first cell division position. First cell division of embryos in control treatment is close to perpendicular to the growth axis; nocodazole and oryzalin treated embryos have on average smaller angle between the cell division 50º. *angle calculation for a normal embryo, ** angle calculation for an aberrant embryo. n(control)= 9, n(nocodazole)= 10, n(oryzalin)= 11.

elongation (Chebli et al., 2012). In order to explore whether the cytoskeleton-related embryo length reduction could be linked to the changes in wall stiffness, the cell wall mechanics of the *Fucus* embryos were tested using atomic force microscopy. Since the rhizoid is actively growing 72 hours after fertilisation, the imaging and analysis was done for this structure specifically at this time.

Atomic force microscopy (AFM) was used to examine the elasticity of the embryo rhizoid using an AFM cantilever mounted with a 10nm diameter tip. I created 100 x 100 μm^2 elasticity maps for each of the rhizoids investigated. A Hertzian model was used to fit the indentation data, which enabled determination of the apparent Young's modulus (E_A).

The results here show that the E_A in all treatments was higher than in the control (Fig. 4.5). The embryos treated with latrunculin B showed the highest effect of wall stiffness increase with an average of 8.9 ± 0.69 MPa. Likewise, nocodazole and oryzalin treated embryos had significantly stiffer rhizoids with an average Young's modulus of 6.55 ± 0.82 MPa (nocodazole) and 6.61 ± 0.53 MPa (oryzalin). Control E_A was 4.2 ± 0.28 MPa. Stiffer wall, a higher E_A, are correlated with the shorter rhizoids observed in the growth analysis for all of the pharmacological treatments.

4.4.3. Cytoskeleton disruption in *F. serratus* embryos results in decrease in specific alginate and sulphated fucan epitopes in the rhizoid

As described in the introduction to this dissertation (Chapter 1), cell wall mechanics in plants relates to the underlying biochemistry (Chebli et al., 2012; Peaucelle et al., 2011). In order to determine whether the biochemistry in the brown algal cell walls relates to the observed changes in stiffness, I performed immunolocalisation on 72 hour old embryos using antibodies raised against specific epitopes of alginate (BAM6, BAM7 and BAM10) and sulphated fucans (BAM3, BAM4) (Torode et al., 2015; Torode et al., 2016). The alginate epitopes vary based on their ability to cross-link with calcium ions which should make the cell walls stiffer (higher E_A): BAM6 binds to an epitope rich in mannuronic acid (M-blocks, softer material), BAM7 binds to a mix of mannuronic and guluronic acid (MG-blocks) and BAM10 binds to a guluronic acid rich epitope (G-blocks, mechanically stiffer

material). BAM4 and BAM3 antibody bind to sulphated fucan/fucoidan preparations (Torode et al., 2015); BAM4 binds to a sulphate-containing epitope in cell wall fucoidan, whereas BAM3 binds to an epitope that might contain sulphated groups, but its structure is less clear (Torode et al., 2015).

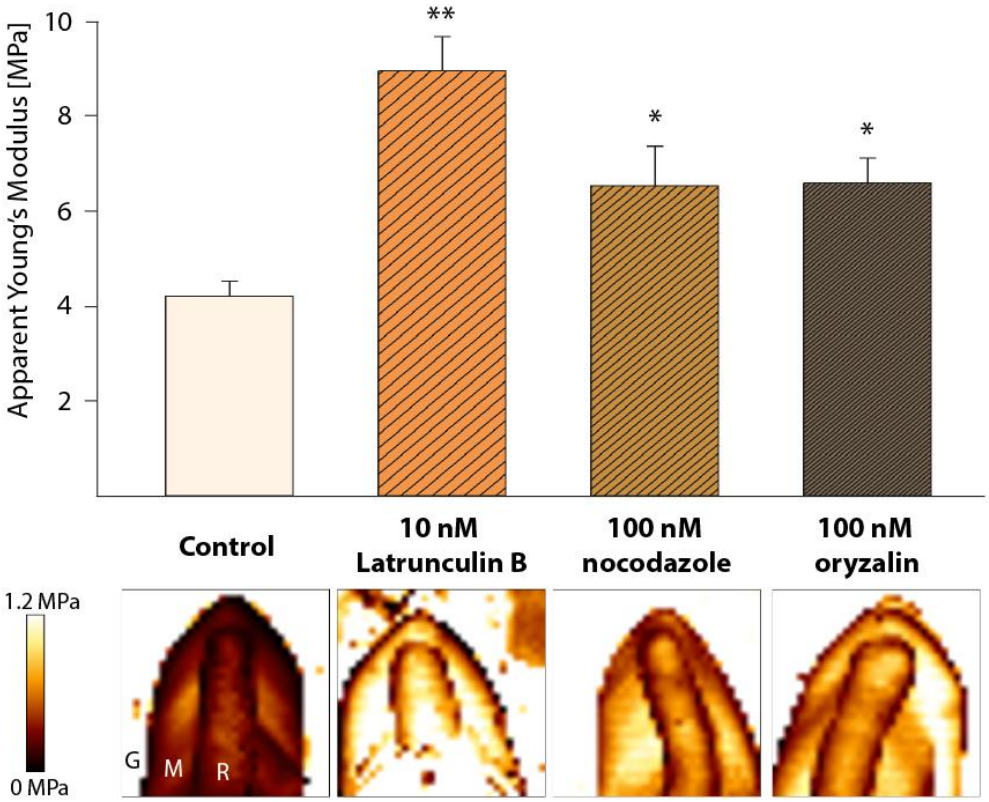

Figure 4.5. Cytoskeleton disruption affects the cell wall's apparent Young's modulus. Apparent Young's modulus values of 72h AF embryos treated with latrunculin B, nocodazole and oryzalin with representative heat maps of the measured rhizoid tip area. Heat maps are a 64x64 pixel square covering a 100x100µm area (n= 27(control), 28 (latrunculin B), 30 (nocodazole), 31(oryzalin)). ANOVA on ranks; p-values: LatB<0.001, nocodazole=0.003, oryzalin=0.037.G – glass, M – mucilage, R – rhizoid.

In this experiment, the latrunculin B treatment showed the most significant change in cell wall biochemistry; BAM10 (Fig. 4.6A) as well as BAM7 (Fig. 4.6B) showed a decreased fluorescence signal suggesting less of the G-rich and MG-rich epitopes present in the alginate. A significantly reduced fluorescence signal was observed for BAM10 (Fig. 4.6A) in the nocodazole treatment and for BAM7 in the

oryzalin treatment (Fig. 4.6B). The M-rich epitopes (BAM6; Fig. 4.6C), although present in low amounts, did not show a significant decrease or increase when the embryos were treated with the cytoskeleton disrupting agents. The sulphated epitope detected by the BAM4 antibody was also not affected by these treatments (Fig. 4.6E), with the only difference observed was in the latrunculin B treatment, suggesting a reduced amount of BAM3 binding epitope (Fig. 4.6D).

In conclusion, these data suggest that there is less G-rich and MG-rich alginate present in the treated embryo rhizoids that have the highest disruption of actin. In addition, when actin cytoskeleton integrity is affected, the presence of a fucoidan epitope is decreased as well. Actin is known to be involved in vesicle trafficking and it is also known that the cell wall material is being deposited via its filaments. The alginate is produced as a chain of mannuronic acid residues, which are then enzymatically converted into their epimerised state – guluronic acid (Haug and Larsen, 1969). The reduction in these epitopes could suggest that mainly actin, but also microtubules, have a role in the delivery of enzymes and cell wall polysaccharides.

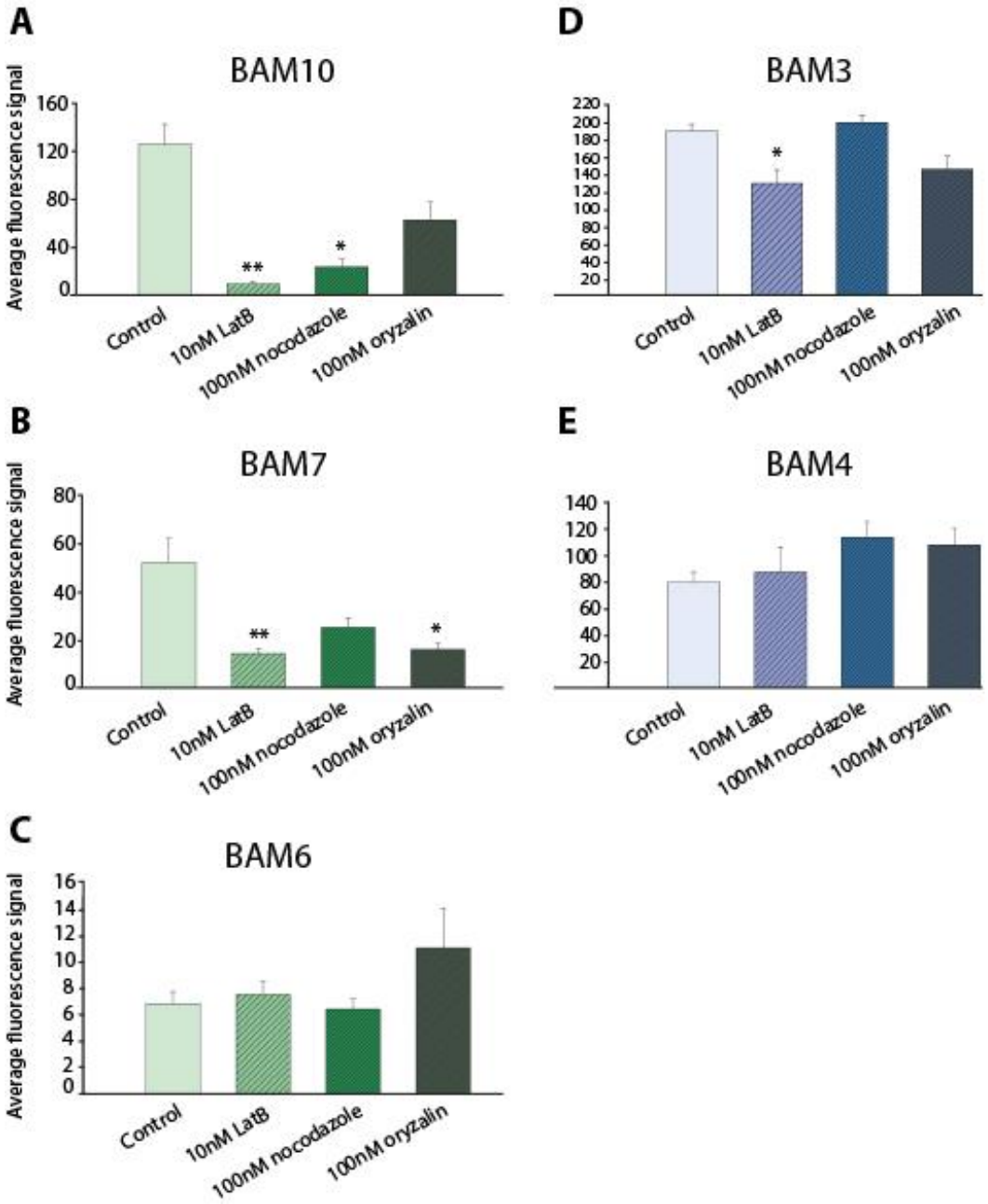

Figure 4.6. Average signal fluorescence for 3 alginate and 2 sulphated fucans epitopes in the rhizoid tip of 72 hour old *F. serratus* embryo cell wall after cytoskeleton disruption treatments. (A) Guluronate-rich epitope (BAM10) shows a significant decrease in fluorescence signal in latrunculin B and nocodazole treatment (n= 12 ctrl, 21 LatB, 9 noco, 13 ory. ANOVA on ranks; p-values: LatB <0.001, Nocodazole=0.008) while the mixed mannuronate and guluronate epitope (BAM7) signal (B) decreases significantly in latrunculin B and oryzalin treatment (n= 8 ctrl, 16 LatB, 12 noco, 12 ory. ANOVA on ranks; p-values: LatB<0.001, oryzalin=0.004). (C) Mannuronate-rich epitope (BAM6) is not significantly affected (n= 12 ctrl, 16 LatB, 9 noco, 15 ory) as well as the epitopes for sulphated fucans (BAM3 and 4; D, E, n (BAM3) = 28 ctrl, 25 LatB, 9 noco, 23 ory; n (BAM4) = 21 ctrl, 15 LatB, 18 noco, 19 ory), with the only exception of latrunculin B treatment immunolabelled with BAM3 antibody (ANOVA on ranks; p-value= LatB 0.013).

4.4.4. Enzymatic degradation of alginate in the growing embryo cell wall results in shorter rhizoids and decrease in mannuronic acid rich epitopes

The majority of algal cell wall is composed of polysaccharides alginate and sulphated fucans. Alginate lyase can degrade alginate by ß-elimination of glycosidic bonds and produce unsaturated oligosaccharides with double bonds at the non-reducing end (Zhu and Yin, 2015). Types of alginate lyases are distinguished depending on their cleaving site; e.g. ones with preference towards poly-M or towards poly-G linkages (Lundqvist et al., 2012; Thomas et al., 2013). Given the hypothesis that the biochemistry of the cell wall could relate to its mechanics, I tested what effect the degradation of alginate had on embryo growth, mechanics and overall biochemistry. For this purpose I used a commercially available poly-M lyase (Sigma Aldrich, USA).

I used two different concentrations to test its effect on embryo growth. Twenty four hours after incubation in ASW, 0.5 units (U) mL^{-1} and 2U mL^{-1} of alginate lyase were added to the medium. The initial 24 hours without the treatment was done to allow the embryos to polarise, form rhizoids and start growing. The results here showed that when treated with 0.5 U mL^{-1} no significant difference was noticed. However, applying 2U mL^{-1} of alginate lyase resulted in highly significant reduction in embryo length when observed 48 hours after fertilisation (24h after treatment application, control 244.12 ± 2.77 µm, treatment 166.507 ± 2.08 µm, n=150, p-value< 0.001; Fig. 4.7A).

Furthermore, to test whether there are any differences in the mechanics of the cell walls when treated with alginate lyase, the embryos were tested using AFM (see Materials and Methods for details). The results show there were no significant differences in the apparent Young's Modulus between the two treatments. The control treatment had an apparent Young's Modulus of 3.6 ± 0.12 MPa (n=48) and the alginate lyase treatment (2U mL^{-1}) was slightly higher, 4.6 ± 0.61 MPa (n=38, p-value= 0.416; Fig. 4.7B).

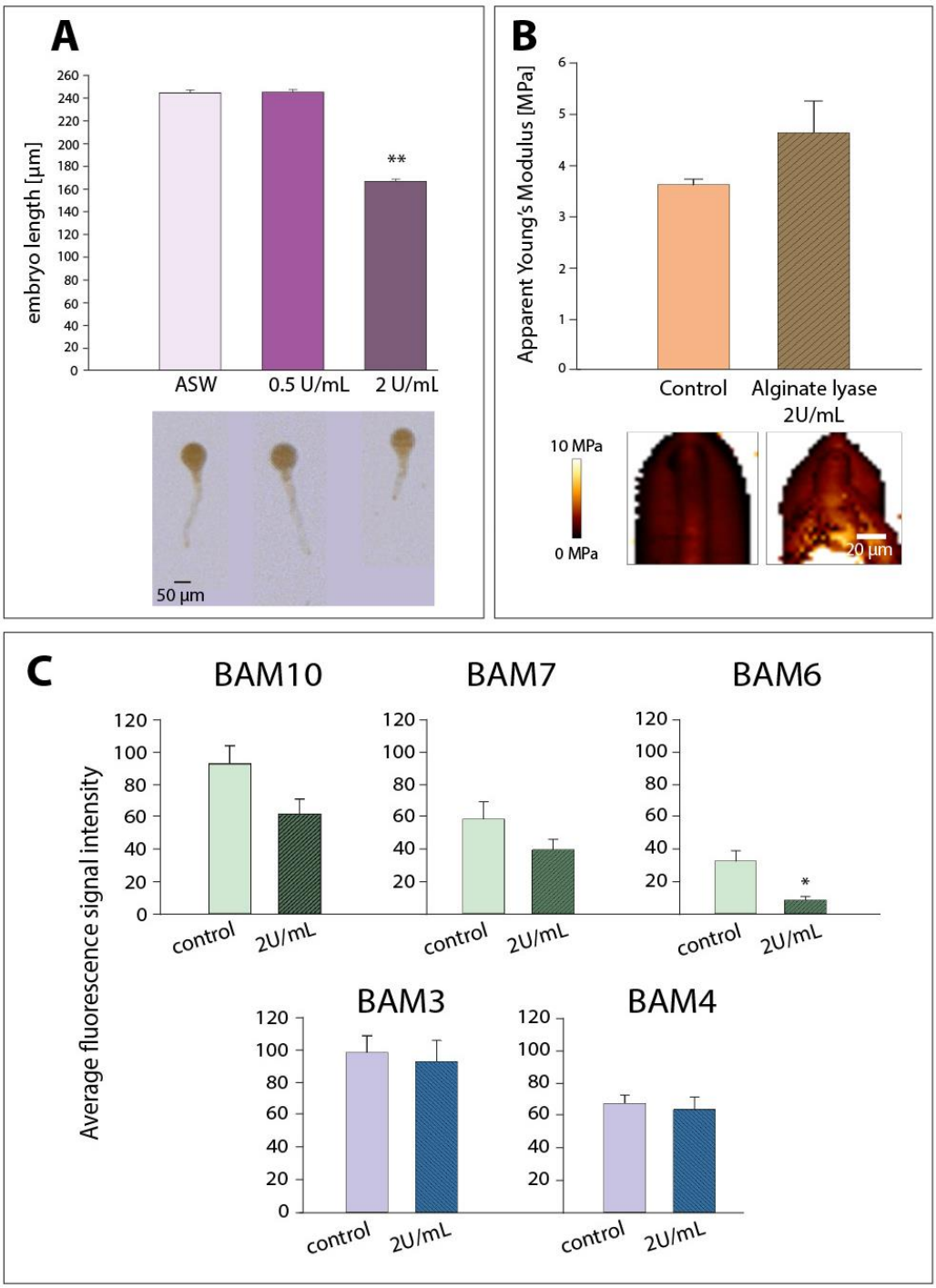

Figure 4.7. Effect of M-alginate lyase treatment on *F. serratus* embryo growth, cell wall stiffness and biochemistry. (A) Embryo length 48h after fertilisation and treatment with alginate lyase; significantly reduced embryo length is seen when applying 2 U mL^{-1} of enzyme (n= 150, ANOVA on ranks; p-value<0.001) (B) Apparent Young's modulus of the control and treated embryos with corresponding stiffness heat maps (64x64, 100x100µm); there is not a significant change in rhizoid stiffness between the two conditions (n= 48 control, 38 treated embryos, Mann-Whitney test; p-value=0.416). (C) Alginate lyase treatment significantly reduces the fluorescence signal of mannuronate-rich epitope in the rhizoid tip (BAM6; n= 18 control, 8 treatment, Mann-Whitney test; p-value=0.004).

In addition, I performed an immunolocalisation experiment to determine the underlying changes in biochemistry that might have been affected due to the enzymatic activity of alginate lyase. The BAM6 antibody showed a significantly reduced fluorescence signal in the treatment in comparison to the control which suggests that M-block rich epitope was less present. The other alginate and sulphated fucan related antibodies did not show any significant difference between the two treatments (Fig. 4.7C).

These data suggest that using the poly-M alginate lyase reduced the amount of M-rich epitopes. Taking into account that the enzyme used had a preference towards degrading the mannuronic acid linkages within the alginate chain, this result is expected. However, although affecting the embryo growth, alginate lyase treatment did not affect the rhizoid cell wall mechanics. This could suggest that in particular the M-block alginate does not contribute to the mechanics of the *F. serratus* embryo cell wall.

4.4.5. *F. serratus* embryos have shorter rhizoids and stiffer cell walls when depleted of a calcium source in the seawater medium

Gel properties of alginate have been known to change in the presence of calcium ions; because of their conformation, guluronic acid residues have the potential to crosslink with Ca^{2+} and create 'egg-box' linkages which results in a stiffer gel material (Grant et al., 1973). Calcium is known to be important in *Fucus* embryo polarisation as well as tip growth in pollen tubes and other tip growing structures (Jackson and Heath, 1989; Jackson and Heath, 1993; Kropf and Quatrano, 1987; Malhóai and Trewavasb, 1935; Roberts et al., 1994; Steinhorst and Kudla, 2013). In order to understand how and if exogenous calcium has an effect on the cell wall properties, I tested the effect of calcium removal, chelation or depletion on the *F. serratus* embryos.

Removing the source of calcium from the seawater medium resulted in embryo growth reduction and death 72 hours after fertilisation (48 hours after calcium removal), both in the form of $CaCl_2$ or just the calcium ions (Ca^{2+}) (Fig. 4.8A). EGTA (ethylene glycol-bis(β-aminoethyl ether)-N,N,N',N'-tetraacetic acid) is a known chelator of calcium ions and has been used before to reduce the amount

of calcium ions in the seawater medium (Love et al., 1997; Robinson, 1996). To test its effect on the growing embryos, I applied 3 concentrations of EGTA (100 µM, 1 mM, and 10 mM) in the seawater medium 24 hours after zygote fertilisation and looked at the effects 24 hours after. There were no significant differences in any of the treatments in comparison to control (Fig. 4.8B). These results suggest that removing the calcium completely is too detrimental for the *Fucus* embryos and chelating calcium, at these concentrations, does not show a significant effect. Even though the chosen concentrations of EGTA matched the ones used in the previous research, it might be that in this study they were too low to show an effect.

To create a more gradual experiment to test the effect of calcium depletion on embryo growth and cell wall properties, I prepared a series of 4 seawater mediums with reduced concentrations of calcium in the form of $CaCl_2$; 9mM (control), 6mM, 3mM, 1mM. The embryos were grown in control seawater (see Materials and Methods for details on seawater composition) for 24 hours after which they were moved into the prepared treatments.

The results show that the 72 hour old embryo length significantly decreased in treatments of 3mM and 1mM $CaCl_2$ (Fig. 4.9A; control 298.13 ± 3.15, 3mM treatment 266.05 ± 4.03, 1mM treatment 264.09 ± 4.47, p-value<0.001). Having observed a change in phenotypes, I continued to do further testing to explore the effects of lower amounts of calcium ions on cell wall properties. The atomic force microscopy was performed on 72 hours old embryo rhizoids and the results show a significant increase in apparent Young's modulus in the calcium depleted treatment (1mM) in comparison to the control (Fig. 4.9B). Interestingly, the AFM data revealed an intriguing morphology of the rhizoid and accompanying mucilage in the 1mM $CaCl_2$ treatment. Looking at the rhizoid height maps obtained by the AFM indentation data, the control treatment clearly showed the separation between the rhizoid (higher; Fig. 4.10A, B, orange arrowheads) and the mucilage around it. This separation was lost when looking at the height maps of the treated embryo rhizoids, where the transverse height profile appeared continuous (Fig. 4.10A, C). This observation was consistent in all samples and only in this particular experiment. Furthermore, the cell wall immunolocalisations were performed to test the effect of calcium reduction on cell wall biochemistry. The data showed an increase in a

sulphated fucan epitope bound with BAM4 antibody. There was no significant change in any other epitope between the two tested treatments (Fig. 4.9C).

In conclusion, these results show that calcium depletion leads to slower growth and increased stiffness in the embryo rhizoid. Similarly to cytoskeleton disruption results, these data suggest a correlative relationship between the rhizoid length and increase in stiffness.

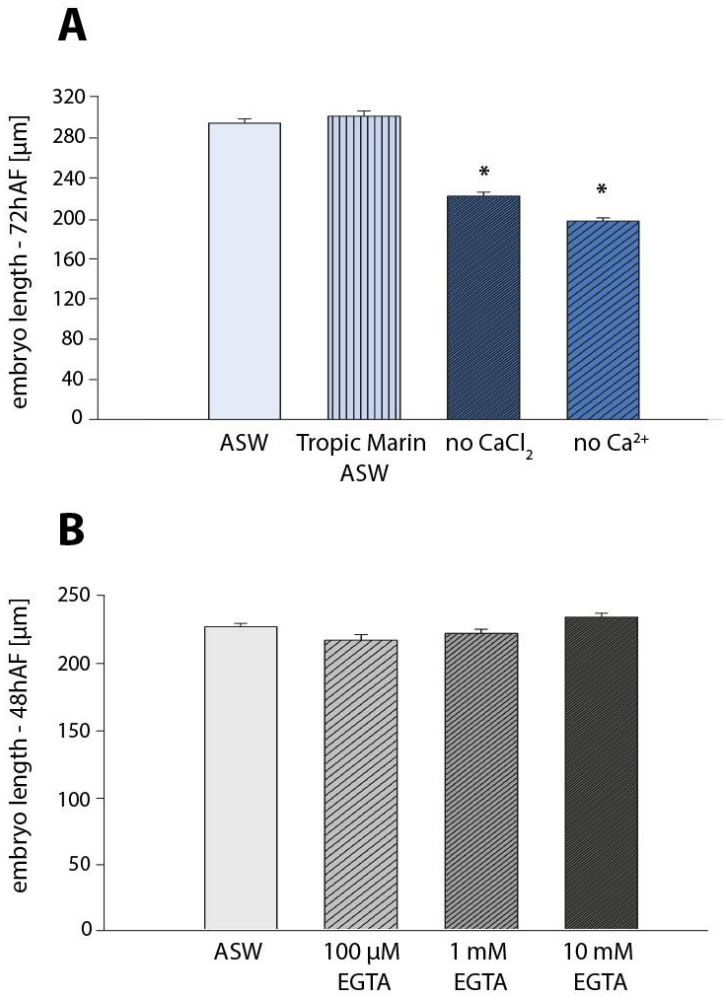

Figure 4.8. The effect on calcium removal and chelation on the embryo length 48 and 72 hours after fertilisation. (A) Final embryo length 72 hours after fertilisation in home-made artificial seawater (ASW), commercially available artificial seawater (Tropic Marin), without the source of calcium in the form of $CaCl_2$ or Ca^{2+}. There is a significant effect on embryo growth in both calcium treatments (ANOVA on ranks; p-value<0.001). n (treatment)=50. (B) Chelation of Ca^{2+} ions with EGTA did not significantly (ANOVA on ranks) affect the length of 2 day old *F. serratus* embryos. n (treatment)=30.

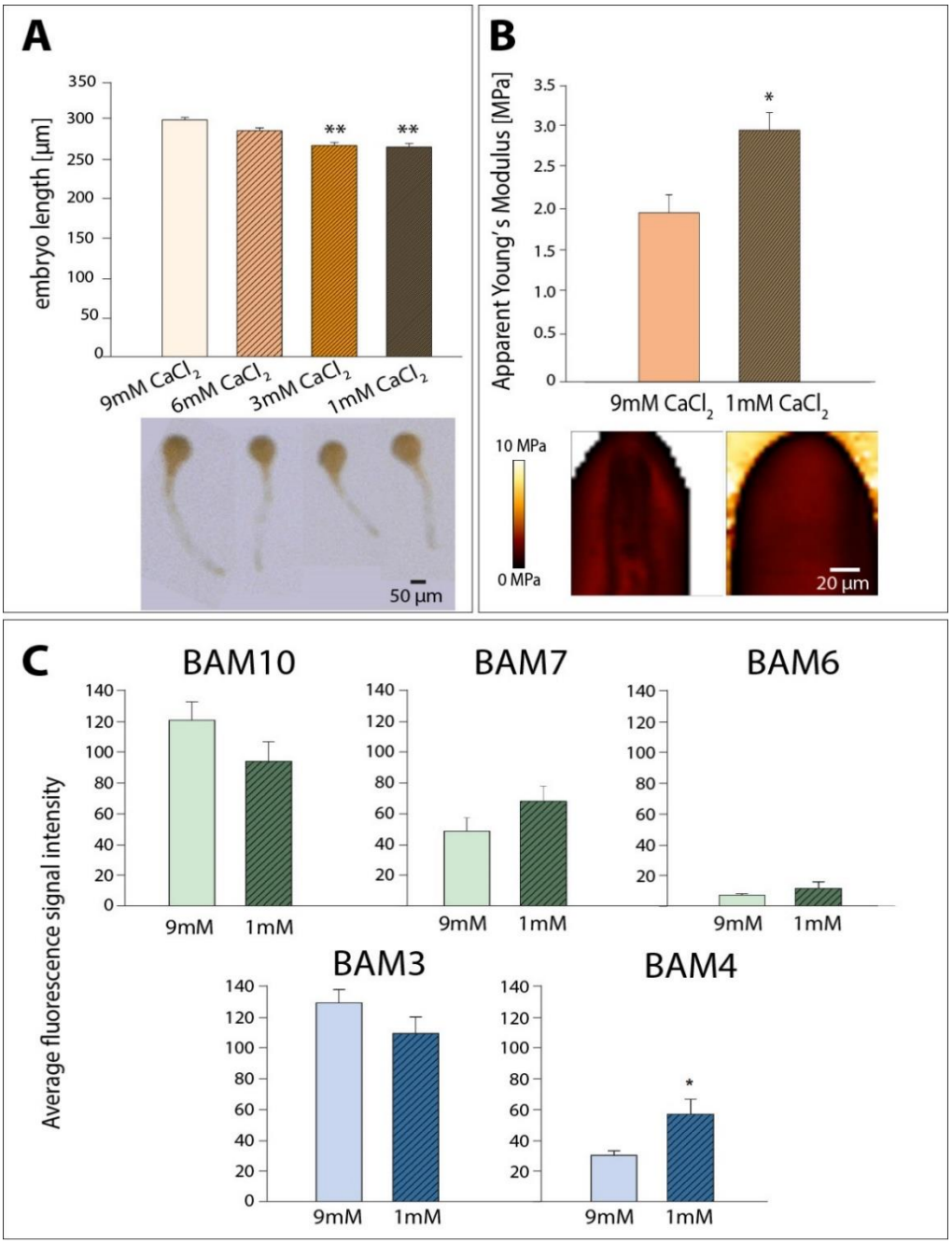

Figure 4.9. Effect of calcium chloride depletion on *F. serratus* embryo growth, cell wall stiffness and biochemistry. (A) Final length of 72h old embryos in treatments with reduced source of calcium ($CaCl_2$); under 3mM a significant decrease in length is observed. n(treatment)=50 (25x2 replicates, ANOVA on ranks; $p<0.001$) (B) A significant increase (Mann-Whitney test; $p=0.002$) in apparent Young's Modulus is observed in treatment with reduced amount of calcium in the medium and an increased amount of mucilage covering the embryo rhizoid. n(control)=22, n(treatment)=24. (C) Alginate (green bars) and sulphated fucans (blue bars) epitopes fluorescence signal is not significantly different between the two treatments with the exception of BAM4 antibody (sulphated fucan, Mann-Whitney test; p-value=0.02). n (control BAM10)=25, n(1mM BAM10)= 16, n (control BAM7)=19, n(1mM BAM7)= 13, n (control BAM6)=15, n(1mM BAM6)= 16, n (control BAM3)=25, n(1mM BAM3)= 26, n (control BAM4)=25, n(1mM BAM4)= 14.

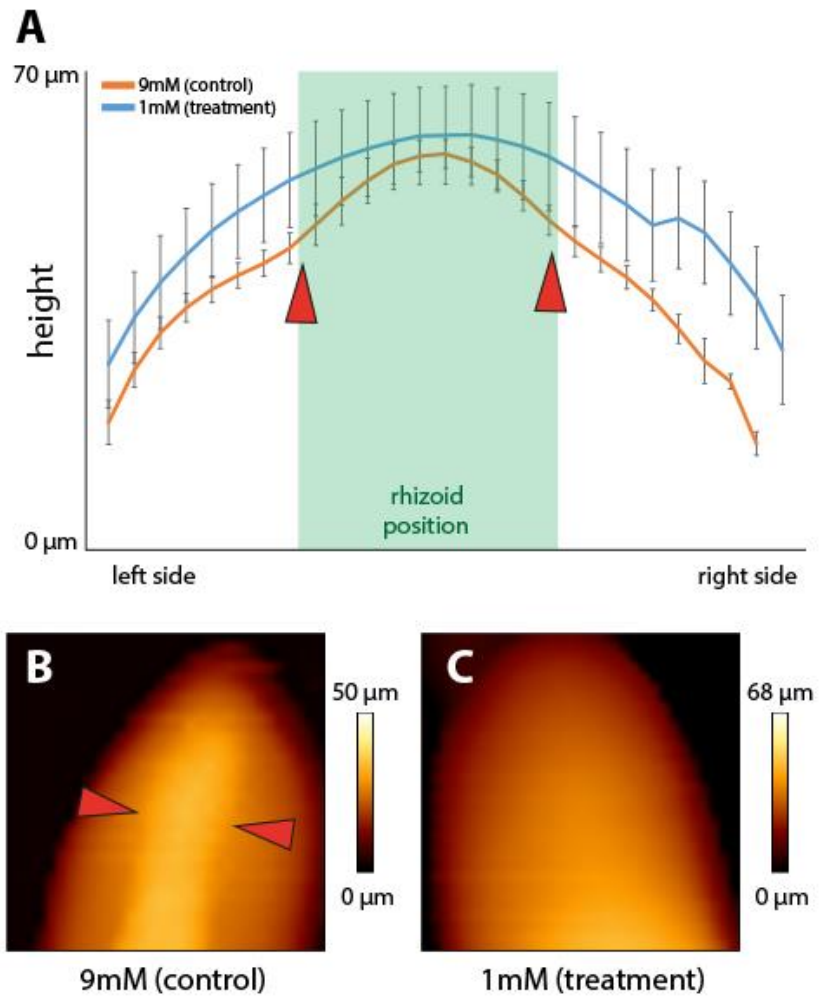

.

Figure 4.10. Modification of mucilage appearance outside the *F. serratus* rhizoid in reduced calcium treatment. (A) Graph representing height lines from one side to the other side of the embryo rhizoid and the accompanying mucilage. In control treatment (B, orange line) overall height is lower and there is a clear distinction between the mucilage and the rhizoid (red arrowheads) whereas in 1mM treatment (C, blue line) this distinction is not seen.

4.5. Discussion

4.5.1. Actin is a driver of *Fucus* rhizoid elongation and can influence tip morphology

Actin filaments have long been hypothesized to transport vesicles to the elongating rhizoid tip since actin inhibitors disrupt transport of vesicles and arrest tip growth (Hable et al., 2003; Quatrano, 1973). In the experiments, I have observed a slower, almost abolished growth of the embryo rhizoid when treated with latrunculin B. The lack of complete growth cessation might be due to the low concentrations of latrunculin B used where some actin filaments might still have been polymerising and active.

An interesting rhizoid phenotype was observed upon latrunculin B treatment - tip swelling and widening. This phenomena has been reported in other tip growing structures. After application of cytochalasin, another actin inhibitor, on fungal hyphae, swelling of the apex was observed, as well as changes in the cell wall ultrastructure in *Neurospora crassa* (Allen et al., 1980), *Gibertella persicaria* (Grove and Sweigard, 1980) and *Uromyces appendiculatus* (Tucker et al., 1986). The swelling of hyphae was linked to the potential role of actin as a reinforcement to the cell wall during tip elongation (Gupta and Heath, 1997; Heath et al., 2003; Jackson and Heath, 1990). In pollen tubes, similar phenomena were observed; after application of cytochalasin or latrunculin B, the apical part of the growing tip started swelling (Geitmann et al., 2000; Gu et al., 2005; Ketelaar et al., 2003).

In their review, Geitmann and Emons (2000) present 4 hypotheses about the role of actin arrays in the tip growth in plants and fungi. The first one relates to the work in fungi in which the arrangement of actin arrays has been proposed to have a stress bearing function together with the cell wall. By investigating the effect of actin caps in cell bursting, together with the pharmacological approach, they concluded that actin and cell wall might work together to determine the stability of the tip-growing apex (Gupta and Heath, 1997; Heath et al., 2003; Jackson and Heath, 1990). Another hypothesis comes from the postulation of Harold et al. (1995) that the apical actin configuration drives the cell elongation, similarly to pseudopods

in animal cells. The most likely hypothesis, based on the authors, would be the 'spatial and temporal vesicle fusion' which represents actin as a pathway to delivering the vesicles to the exact place of exocytosis, the apical tip. The fourth hypothesis is also not excluded from the potential real scenario and it talks about the actin mesh as a filter – as it goes closer to the tip, it becomes finer and does not allow the bigger organelles to penetrate, but rather just the smaller ones such as vesicles.

In fucoid embryos, actin was found to localise in the elongating rhizoid (Kropf et al., 1989b). Alessa and Kropf (1999) used fluorescent phalloidin injection to visualise the actin within the fucoid zygote; fluorescent conjugates with phalloidin are used as F-actin stains. The results showed that F-actin organizes into cortical patches localised at the rhizoid pole which, after germination, transform into a ring-like structure that is located in the sub-apical zone of the elongating tip. The function of these rings is not yet completely understood, but it has been hypothesized that they are involved in tip reinforcement of the rhizoid (Alessa and Kropf, 1999). In pollen tubes, actin bundles in the shank of the tube transport organelles and vesicles to the subapical region where exocytosis takes place. This subapical region has shorter and thinner actin cables that gather into a dynamic structure referred to as an actin band (Cheung and Wu, 2008). The F-actin 'ring' might have a similar role in fucoid systems as it does in pollen tubes. This hypothesis is supported by the FRAP data here, which suggests that the exocytosis is probably happening at the sides of the rhizoid rather than the very tip (Chapter 3). Furthermore, in *Fucus*, vesicles have been found to localise in the area of the germinating rhizoid when probed with the vital stain FM4-64 (Belanger and Quatrano, 2000). These data, together with swelling tip observations found here, suggest that the same mechanism might be involved in fucoid tips. Due to disruption of the actin filaments, the targeted pathway of normal vesicle transport has been abolished, leading to their wider distribution and wider rhizoids, suggesting the third hypothesis from Geitmann and Emons (2000) might be true in this case.

In addition, I have observed another phenotype in the latrunculin B treated embryos, the split of the rhizoid. This is the first such observation in fucoid system to our knowledge when treated with an actin depolymerising agent. A similar

phenotype was observed when treated with an auxin transport inhibitor NPA, probably through altering the accurate auxin localisation (Basu et al., 2002). A similar phenotype has been observed in fugal hyphae, where, besides the wider tip diameter, tip branching/split was visible (Ketelaar et al., 2012). It is still unknown how this phenomenon occurs, but it could relate back to the observations of the wider tip. If the third hypothesis from Geitmann and Emons (2000) were true for this system, one could expect the wider distribution of vesicles along the rhizoid (not just the tip). This would lead to the wider distribution of cell wall components such as F2 fucoidans, whose localisation is known to be important in the rhizoid pole polarisation (Quatrano and Shaw, 1997). The wider deposition of these fucans along the wall would result in creating enough 'signal' to create multiple branching points. Widening the rhizoid would allow greater space for potentially more individual tips to form. A high definition time lapse experiment elucidating the connection between the widening area and the number of branches forming might give more information about this process.

4.5.2. Intact microtubules are required for normal rhizoid elongation and development

In fucoid zygotes microtubules have been shown to be important in the formation of cell plates (Bisgrove et al., 2003; Peters and Kropf, 2010). Their disruption via pharmacological agents or knock-down of tubulin genes has a severe effect on positioning of the first asymmetrical cell division, resulting in aberrant morphologies (Farnham et al., 2013). However, microtubules have not been shown to be involved in the zygote germination or rhizoid growth (Brawley and Quatrano, 1979; Kropf et al., 1990). Likewise, the role of microtubules in pollen tube growth remains debatable. Recent evidence suggests their role in sustaining tip growth through controlling actin-independent exocytosis and endocytosis happening at the tip (Idilli et al., 2013). When subjected to oryzalin and nocodazole, the rhizoid of the *Fucus* embryo showed slow growth compared to that observed in control treatment. These data suggest a role in the rhizoid elongation process. Besides centrosomal microtubules which are present in zygotes, a cortical array has also been visualized when *Fucus* embryos were microinjected with fluorescently labelled tubulin (Correlou et al., 2005). These cortical microtubules are randomly positioned around

the cell in the polarising zygote, but then preferentially localize to the rhizoid pole and become denser when zygotes germinate. They seem not to be connected to the centrosomes. The role of these cortical microtubules is unknown, but my observations suggest that they might have a role in rhizoid tip morphology and elongation, as has been speculated (Bisgrove, 2007).

Another role for microtubules is in cell plate positioning during cytokinesis. My results show that the cell plate in both microtubule disrupting treatments is misplaced and positioned on average at 50 degrees, or not present at all. These observations are in line with the previous reports done in fucoid zygotes (Bisgrove et al., 2003; Farnham et al., 2013; Kropf et al., 1990).

Microtubules are also known to be important in regulating the stability of apical growth in root hairs and treatments with either microtubule stabilising agents or depolymerising agents may result in multiple growth points (Bibikova et al., 1999). These multiple growing points have been observed in other reports as well, such as in caulonemal and protonemal cells of mosses and a marine coenocyte *Bryopsis plumosa* when subjected to colchicine or oryzalin (Mizukami and Wada, 1983; Schmiedel and Schnepf, 1980; Schwuchow et al., 1990). It is suggested that due to the similar effects across different lineages, microtubules might have a common feature, that of maintaining growth to a single point. After the first asymmetrical cell division in fucoid brown algae, two cell types are created – a rhizoid and a thallus cell. The latter give rise to the main body of the algae, while the former creates the stipe and the holdfast. The holdfast is formed early in development; in my experiments this occurred around day 10. It is a crucial developmental feature that anchors the whole algae to the substrate. My observations suggest that due to the effect of the microtubule disrupting agents, this transition from the rhizoid to the holdfast is happening faster than normal. It might be that the formation of holdfast is intrinsically regulated by microtubule depolymerisation in that area, allowing multiple branches to form.

4.5.3. The rhizoid cell wall stiffness changes upon cytoskeleton disruption, and is generally correlated with decreased growth

In walled cells, the cell wall must yield to allow for cell elongation. Based on this one might predict that slower growing cells might have a less yielding wall. After treating the *Fucus* embryos with either actin or microtubule disrupting agents that reduced elongation, a significant increase in the apparent Young's Modulus was observed in the rhizoid cell walls. The only experimental data that observed a similar phenomenon relates to pollen tubes: Zerzour, Kroeger and Geitmann (2009) found that the cytochalasin D-induced apical swelling showed a significantly higher stiffness than the normal growing apex. After removal of the agent, the growth continued. The authors reported that the initiation of this growth was preceded by a local reduction in stiffness at the location of the following outgrowth, suggesting a relationship between cell wall mechanics and outgrowth.

The change in stiffness could be caused by different processes: it can either relate to changes in cell wall properties (biochemistry), wall thickness, changes in turgor pressure, geometry or a combination of these. In my experiment there was a change of shape in a fraction of the embryos (wider swollen rhizoid tips), so this change in stiffness might relate to the change in geometry. However, the AFM analysis was done on randomly chosen embryos (some of which did not present the swollen tip), so the geometry parameter might not be the reason for the stiffness increase. In addition, turgor pressure was thought to be constant since the medium was fresh with a constant osmolarity. From this, I suggest that the change in the cell wall stiffness comes directly from the changes in the cell wall biochemistry and/or wall thickness. In fungal hyphae, it has been suggested that the cytoskeleton acts as a direct mechanical reinforcement to the cell wall (Jackson and Heath, 1990). They have experimentally proven that the actin cap on the tip of the growing hypha serves as an additional prevention mechanism from cellular bursting. Here the actin cap, when disrupted, loses its ability to reinforce the apex, meaning the apex gets softer and more likely to burst. However, this hypothesis contradicts my observations, where, upon disrupting actin, I observe an increase in stiffness.

In brown algae, cellulose deposition was found to correlate with the direction of actin filaments (Karyophyllis et al., 2000; Katsaros et al., 2006), with the absence of cortical microtubules. On the contrary, correlation between microtubules and cellulose microfibril orientation has been observed in *Arabidopsis* epidermal cells (Paredez, 2006) as well as in most other cases, but not without exceptions (Himmelspach et al., 2003). Despite actin being suggested as the main driver of cellulose deposition due to lack of cortical microtubules, a relatively recent discovery has shown that microtubules are present in the fucoid zygote (Correlou et al., 2005). The discovery of these cortical microtubules and the observation of their reorientation parallel to the growth axis, suggests that they might play a role in cell wall formation after all.

A pharmacological study in *Pelvetia* showed interesting results on cell wall deposition in germinating zygotes. When treating the germinating embryos with latrunculin B, the zygotes stopped germinating and developed stronger walls, as suggested based on a lysis assay. Furthermore, birefringent walls started developing in the apex, suggesting cellulose deposition. This process was not present in the control treatments. Ultrastructural investigation also showed that the cell walls of the treated rhizoids had a 2-3 fold increase in thickness in comparison to the controls (Bisgrove and Kropf, 2001). Their findings were similar to my observations – the embryos treated with latrunculin B developed significantly stiffer (stronger) cell walls. This inhibition of elongation could probably be attributed to the disruption of the secretory pathway. However, as in *Pelvetia* zygotes, it might be the case that the cellulose deposition is continued in the latrunculin B treatment which would result in a stiffer cell wall. However, the data from Bisgrove and Kropf (2001) also show that the disruption of microtubules with oryzalin does not show a significant effect on the rhizoid cell wall strength with no data presented on the wall ultrastructure. My observations show a significant increase in cellular stiffness, suggesting microtubules are as well contributing to the change in wall mechanics. Possibly due to less difference in apparent Young's modulus than latrunculin B treatment, this could have been missed in their lysis assay, which would be less sensitive than a nano-indentation method.

There are a few conclusions that can be drawn from this: firstly, the data presented here together with the previous observations suggest that cellulose is being deposited in the absence of actin filaments. The hypothesis that suggests that actin is connected to cellulose deposition in brown algae might not be completely accurate, or at least not accurate for all the species within. These data suggest the microtubules might have a role in cellulose deposition, or there is an alternative way which remains undetermined. Secondly, when disrupting the microtubules an increase in cellular stiffness was observed. This observation again raises the question whether microtubules have a role in cellulose deposition. In these experiments, I used a very low concentration of oryzalin and nocodazole to prevent death of the embryo. This, as a result, might mean that some of the microtubules were able to polymerize and still could deposit cellulose into the cell wall. However, it is difficult to make firm conclusions based on these data and more research would be required in order to elucidate this in detail.

The increase in cellular stiffness due to cytoskeleton disruption in a phenomenon that has not been extensively explored in the past to our knowledge, in brown algal cell walls nor other tip growing structures. The research here represents an initial effort to understand the interplay between mechanics and cytoskeleton on a cellular level.

4.5.4. Detectable alginate and sulphated fucan biochemistry upon cytoskeleton disruption do not correlate with change in wall mechanics

The change in cellular stiffness is known to be linked to cell wall biochemistry modification in plants. Pectin can be de-esterified via an enzymatic reaction and this process can result in the formation of cross-links with positively charged calcium ions and change the mechanical properties of the wall and therefore the cell/tissue growth (Braybrook and Peaucelle, 2013; Chebli et al., 2012; Peaucelle et al., 2011; Zerzour et al., 2009).

Algal cell walls are both similar to and different from those of plants. The pectin analogue in brown algae – alginate, can act mechanically similarly to what is observed in pectin gels. With 4 guluronic acid residues in two alginate chains (2x2) a crosslinking event can occur with a calcium ion and form an ‘egg-box’ junction

(Grant et al., 1973). Therefore, alginate gels with higher G content can form stronger gels (Draget et al., 1994). Bisgrove and Kropf (2001) have also suggested that sulphated compounds play a role in strengthening the apical wall of the elongating rhizoid. Hypothesizing that these cell wall components might control the wall mechanics in brown algae, I investigated whether the observed changes in mechanics correlated with the change in relevant alginate and sulphated fucan epitopes.

In this study 5 antibodies were used: 3 directed towards alginate and 2 towards sulphated fucans. Alginate chain is produced in the form of mannuronic acid residues (mechanically softer gel), which can be then converted to their epimerised state – guluronic acid (mechanically stiffer gel), via activity of a group of enzymes called mannuronan—C5 epimerases. A family of 31 of these genes has been found in *Ectocarpus* genome from which one has been found to have a functional enzymatic activity to date (Cock et al., 2010; Fischl et al., 2016). BAM6, BAM7 and BAM antibodies bind to M-rich, MG-rich and G rich epitopes, respectively. BAM3 and BAM4 antibodies have been raised against two sulphated fucan epitopes and bind to a highly sulphated and a less sulphated fucan chain (Torode et al., 2015; Torode et al., 2016).

My data suggest that, upon cytoskeletal disruption, the majority of these epitopes seem to be less present. As discussed in Chapter 2, it is difficult to make comparative conclusions between multiple antibodies, unless a specific binding region is known. In the case of monoclonal antibodies used in this study, their exact binding sites are still not completely revealed. However, comparisons of a single antibody in different environment (treatments) can still be made. When treated with latrunculin B, both BAM7 and BAM10 showed a significantly lower fluorescence in comparison to control. The BAM6 did not show such an effect. Its fluorescence was very low in the control as well and the insignificance of the results obtained could be due to the inability to detect such low concentrations of the epitope. It could be that this epitope is not present at the tip of the rhizoid.

Alginate is deposited to the cell wall by cytoplasmic vesicles fusing with the plasma membrane (Quatrano and Stevens, 1976). These vesicles are assumed to be targeted to the particular areas via the actin network which serves as a “guidance

highway" (Hable and Kropf, 1998). The proof for this comes from pharmacological treatments where, upon treatment with cytochalasin B and D, vesicles are not transported to the cortex, but remain in the perinuclear region of *F. distichus* zygotes (Brawley and Quatrano, 1979). The inability to transport the vesicles to the cell wall in the region of interest (our case, the rhizoid tip) correlates with the data collected from this study. BAM7, BAM10 and BAM3 all show reduction in fluorescence, indicating less MG- and G-rich areas of alginate as well as a sulphated fucan. However, the results could not be correlated with the observed change in increased rhizoid cellular stiffness. Several conclusions can be made from this: firstly, the epitopes detected by the antibodies might not be linked to the stretches of alginate which can be linked with wall mechanics, such as already calcium cross-linked alginate. Secondly, alginate and sulphated fucans might not be the main contributors to the wall mechanics, but another component might be taking over. Cellulose could be a potential player, as described above.

4.5.5. Exogenous calcium depletion decreases elongation and affects the wall mechanics

The formation of a polar axis in the fucoid embryos has been associated with the appearance of an electrical current that flows inwards at the site where the future rhizoid will form (Nuccitelli, 1978). Calcium is a part of this inward driving current and this process creates a gradient inside the zygote (Robinson and Jaffe, 1975). This gradient is then thought to be responsible for stimulating the F-actin assembly which is also necessary for germination to happen. Another important aspect of calcium is linked to the cell wall and the mechanical properties of alginate component. In the presence of calcium, guluronic acid within alginate can crosslink with the ions and make the walls stiffer (Draget et al., 1994; Grant et al., 1973), potentially reducing the elasticity and the ability of the wall to expand.

In order to study the role of Ca^{2+} in rhizoid growth, I investigated the effects of reducing Ca^{2+} uptake by decreasing the amount of extracellular Ca^{2+}. Lower amount of calcium in the medium would result in less influx and potentially less amount of calcium that could be targeted to the cell wall. A similar approach was taken in previous studies to investigate the localisation of calcium in the polarising

and germinating fucoid zygotes by using chlorotetracycline. They have proven that these calcium reducing treatments do affect the overall calcium influx from the surrounding medium (Kropf and Quatrano, 1987).

My results from the growth analysis show that external Ca^{2+} is important for tip growth which is in line with previous studies showing a reduction in elongation when reducing the amount of calcium in the medium to 1mM (Kropf and Quatrano, 1987). When depleted from the external calcium source, the embryos showed a significantly higher apparent Young's modulus than the control indicating a potential increase in calcium-guluronic acid crosslinking. This contradicts the hypothesis that with the reduced amount of calcium, less crosslinking would take place. Firstly, a lower amount of extracellular calcium would result in less calcium uptake and lower amounts that could potentially end up in the cell wall. This would prevent the crosslinking to occur and the walls would not get stiffer. Secondly, it might be expected that the calcium store in the cell wall would be taken into the cytosol for other calcium driven processes such as different signalling pathways, but also tip growth. Intracellular calcium is suggested to be involved in vesicle fusion with the membrane at the apical tip, but also in regulating microfilaments that direct vesicles to the tip (Brawley and Robinson, 1985; Picton and Steer, 1982). However, in this case an increase in stiffness is still observed. Although the possibility that the calcium stays within the cell wall and still creates cross-linkages with alginate might be true, there might be another mechanism involved. As discussed above, other components might be involved in regulating mechanics of the wall. A possible candidate is cellulose microfibrils. As an embryo grows, new layers are deposited at a certain speed. However, when the growth is slower, with the cellulose being continuously deposited, this could affect the final mechanics observed in the cell wall. The third major component of the cell wall are the sulphated fucans, and they might have a role in wall strengthening as has been suggested (Bisgrove and Kropf, 2001), although their role needs to still be elucidated. The immunolocalisation data showed that the abundance of none of the alginate epitopes were affected by the reduction of extracellular calcium ions. However, an increase in a sulphated fucan epitope (BAM4) was observed. In *Ectocarpus subulatus*, change in salinity affects the BAM4 sulphated epitope (Torode et al., 2015) suggesting that BAM4 might be

involved in the osmotic regulation. Due to the loss of ions from the medium due to $CaCl_2$ removal, BAM4 might adjust to the changes due to osmotic change.

Another interesting phenomenon was observed when imaging the embryo rhizoid in the low amounts of extracellular calcium – an increased amount of external mucilage. Following fertilisation, fucoid embryos deposit a sticky polyphenolic and acidic carbohydrate adhesive which keeps them immobilised and allows them to adhere to the substrate (Hable and Kropf, 1998). These data suggest that lower amounts of calcium in the medium results in a wider distribution of the mucilage which completely covers the embryo rhizoid. It has been suggested that sulphated fucan F2 is important in the zygote adhesion to the substrate during the early development in fucoid zygotes. In the absence of extracellular SO_4^{2-} (zygotes were grown in a medium in which sulphate was replaced by methionine; met-embryos), embryos were not able to adhere to the substrate suggesting that a sulphated F2 was required for adhesion (Crayton et al., 1974). The increased fluorescence of the BAM4 antibody might also be linked to an increased amount of mucilage produced, since the signal was present throughout the rhizoid, not just localised to the sides or the tip (as seen in alginate immunolocalisations). The increase of this particular epitope could also be connected to the observed change in stiffness. Two possibilities can be explored: that a sulphated fucan has a direct role in mechanical properties of the wall or that the increase in stiffness occurred due to increased amount of mucilage produced associated with the increased BAM4 signal.

4.5.6. Enzymatic removal of mannuronic acids does not show an effect on cell wall properties

Alginate lyases are a family of enzymes which catalyse the degradation of alginate by a β-elimination mechanism, targeting the glycosidic 1-4 O linkage between monomers. Although all lyases have the same action, they can have different preferences for the glycosidic bond connecting M and G monomers. Depending on the cleaving specificity, they break down different parts of the alginate chain. M-lyases cleave M-MM motifs (Lundqvist et al., 2012), whereas G-lyases cleave the G-GG motifs (Thomas et al., 2013). Alginate lyase has been extensively used as a component in an enzymatic cocktail to obtain protoplasts from brown

algae (Boyen et al., 1990; Ducreux and Kloareg, 1988; Kloareg and Quatrano, 1987a; Kloareg and Quatrano, 1987b; Rusig et al., 1994; Sawabe et al., 1993). I have used a commercially available M-lyase on growing embryos to try to degrade a part of the alginate within the wall to check for potential effects on growth and cell wall properties. An initial concentration screen was performed to detect an ideal concentration which would have an effect on growth without effecting the viability. The results show that using 2U mL^{-1} of alginate lyase has a significant effect on embryo rhizoid elongation, decreasing it.

Immunolocalisation data show that there was a significant fluorescence decrease in an alginate antibody – BAM6. This antibody binds to a mannuronic acid rich epitope and its fluorescence decrease is in line with the action of the lyase used, which cleaves M-MM motifs. However, degrading alginate did not have an effect on the rhizoid mechanics, the wall stiffness resembled the one observed in the control. The effect of an exogenous alginate lyase is not known when applied to living embryos since the only studies performed were the ones that were looking to obtain their protoplasts. In these cases, higher concentrations were used (~6U mL^{-1}; Kloareg and Quatrano, 1987b). One hypothesis why the growth was reduced and mechanics was not changed could be due to the growth cessation because there was less wall material (no M-blocked alginate or just fragmented alginate chain) which would prevent further tip expansion. Another hypothesis might suggest that, although the embryos appeared alive, this lyase had a detrimental effect on the embryos. Furthermore, the absence of M-blocked alginate could suggest that there is less of it to be epimerised into G-blocked alginate which could then form egg-box crosslinks with calcium ions. In addition, the immunolocalisation data obtained when disrupting cytoskeleton show that mannuronic rich areas were not affected, while stiffness increased. There are two sets of experimental data presented here that lead to reduction in embryo length, but have a different effect on wall properties: a stiffness increase with no BAM6 epitope change and a no change in stiffness with a reduction in BAM6 epitope. These data suggest that M-blocked alginate might play a role in rhizoid elongation, but seems not to be involved in regulating the mechanics of the cell wall.

However, finer methods would need to be developed to investigate this in more detail, such as modulating alginate in a specific manner; e.g. using mannuronan C5 epimerises which, depending on each enzyme, have very specific cleavage sites. The epimerises that localise in the tip region could be overexpressed and their effect on wall properties could be investigated. Currently there is experimental proof of several functional bacterial and one brown algal epimerases (Fischl et al., 2016; Hartmann et al., 2002a; Hartmann et al., 2002b; Høidal et al., 1999). To date, no alginate lyases have been found in brown algal genomes (Cock et al., 2010; Michel et al., 2010; Ye et al., 2015) and it is suggested that brown algae might have evolved novel mechanisms in alginate modification or their epimerises might have a dual action, acting both as an epimerase and a lyase, similarly to bacterial AlgE7 (Ertesvåg et al., 1999). However, specific molecular tools need to be developed for brown algae before these questions could be answered.

4.5.7. Possible role of cell wall properties in growth

This chapter represents the first efforts to try to elucidate the involvement of wall properties during embryo growth and development. It suggests that the cell cytoskeleton has a direct influence in controlling cellular stiffness. The direct inhibition of the cytoskeleton led to decreased growth and increased cellular stiffness of the actively growing rhizoid. This process might be possibly driven via reducing the targeted deposition of vesicles (alginate and sulphated fucans) to the active sites of growth (tip), which would decrease the amount of wall material needed for normal elongation. The accompanying increase in stiffness could be linked to the continuous deposition of cellulose, which does not require vesicular transport but is deposited directly to the cell wall via cellulose synthases (Peng and Jaffe, 1976). Splicing the mannuronic acid residues from the wall affects the rhizoid elongation, but not the stiffness, which suggests that the mannuronic acid might be involved in the elongation, but does not influence mechanical properties of walls alone. Furthermore, reduction of calcium in the medium (and its following reduced influx) resulted in slower growth and additional excretion of mucilage adhesive around the rhizoid. Reduced growth might come as a consequence of reduced calcium concentration at the tip, which is shown to be important for tip growth. The cellular stiffness was found to be significantly higher in the treated embryos. The

increased stiffness without an effect on amounts of alginate epitopes can suggest that the detectable alginate might not be directly linked in mechanical changes. This treatment resulted in increased production of extracellular mucilage and an increase in sulphated fucan epitope suggestion a connection between the two. The increase in stiffness could also be a consequence of a thicker layer of mucilage around the wall. A sulphated fucan might also be directly involved in the mechanical properties, however, this was not observed when stiffness increased during cytoskeleton disruption.

Alginate, as an algal analogue to plant pectin, does not seem to be involved in wall mechanical properties as is observed in plants. However, the very specific epitope binding of three antibodies used here might not be appropriate; probing alginate parts, which could be directly linked to changes in mechanical properties (such as already calcium cross-linked alginate), could give us a better understanding. Sulphated fucans have been shown to be linked to the extracellular adhesive, however, no clear role of their direct link with mechanical changes was evident. Exploring the cellulose component could elucidate whether it is involved in modifying mechanical properties, as the third major component of the brown algal cell wall.

Chapter 5. General discussion

The main questions in developmental biology relate to the mechanisms underlying cell differentiation, patterning and ultimately morphogenesis on an organism level. These questions have been addressed many times in the past in multicellular organisms, mostly focusing on either animal or plant systems. Brown algae are another, independently evolved, group of multicellular organisms worthy of study (Charrier et al., 2012). Their evolutionary distance from walled organisms such as land plants opens an interesting discussion about shared origins or convergent features, which these two groups developed to counter similar physical constraints on morphogenesis. The plant and brown algal systems developed a cell wall, which restricted the ways they could build their bodies and resulted in many position-dependent developmental cues relying on intercellular communication. The presence of a cell wall also restricts the physical mechanisms by which morphogenesis can occur – cell walls must yield to allow growth. The insights on cell wall behaviour during brown algal development in this thesis are discussed below and the future directions, questions and suggestions are addressed.

5.1. The universal role for cell walls – what can we conclude so far?

Cell wall and turgor-driven body expansion represents the key physical mechanism for morphogenesis in walled organisms. This thesis reflects on this basic structural fact by addressing questions about the cell wall's role during brown algal morphogenesis. How does one start to address such a fundamental question within a large group of organisms such as brown algae? Brown algae are an extremely diverse group when it comes to their morphologies and modes of building their bodies. In this thesis, the focus was given to two different morphogenetic processes in brown algal development, quite different from each other, hoping to gain insight on developmental rules and patterns involved in their shape formation. These two processes are apical patterning in *S. muticum* and embryo development

in *F. serratus*. Major conclusions obtained from these two systems are discussed below.

The central aim behind this thesis was to understand some of the roles of cell wall in brown algal development, with a hypothesis that its properties have to be changed in order for growth to occur. Firstly, this would involve wall loosening, which would be proxied by a decrease in stiffness. Secondly, any decrease in stiffness would be connected to biochemical changes within the wall itself. The main candidate chosen for investigation was alginate. The reasoning behind this lies in two previous scientific discoveries: the mechanical role of its analogue in plants – pectin (Chebli et al., 2012; Peaucelle et al., 2011), and a correlation between the flexibility of brown algal tissues with alginate composition (Draget et al., 1994).

When examining the wall properties during *F. serratus* embryo growth, there seemed to be a correlation between growth and wall stiffness: the growing rhizoid had softer walls and the non-growing thallus had stiffer walls. The alginate antibodies available in this study (BAM6, 7 and 10) indicated a specific patterning of alginate that could be correlated with part of the observed mechanical properties; BAM10 antibody (G-rich, potentially stiffer) could be found in the stiffer region of the embryo, the thallus. In the apex of *S. muticum* the outgrowth of new buds did not seem to be correlated with local changes in mechanics or linked to specific alginate modifications in the cell walls. How do these observations relate to the initial hypothesis? The results presented in this thesis, on one hand, suggest that wall mechanical properties correlate with active growth (embryo). On the other hand, the apical growth with bud outgrowth does not support this hypothesis.

Why these two growth processes might not share the same mechanisms remains debatable. One must be aware that the two developmental processes observed are quite different from each other developmentally. The *Fucus* embryo represents a system that starts off as a single cell and, through distinct growth mechanisms, develops its shape. Here we can distinguish two types of growth – diffuse (cell division and cell enlargement; thallus) and tip growth (polar elongation of a single cell; rhizoid). On the other hand, *S. muticum* apex represents a more complex system. There is an apical cell that has a meristematic role; the constant divisions here result in multiple cells placed within different tissues. An interesting

feature here, besides the spiral branching pattern, is the appearance of each of the forming and growing branches. My observations indicate that the formation of each of these buds is controlled by an apical cell, which serves as a local 'meristem' to produce each branch. This could suggest that perhaps the inability to detect the local softening of the cell wall is not due to different mechanisms of cell wall-accompanied growth between the apex and embryo, but rather a different mode of growth. While in the fucoid embryo there is a clear enlargement of individual cells, it is likely that the branch growth relies on cell division produced by the meristematic apical cell from each branch, and not cell enlargement.

5.2. Apex patterning in brown algae

The mechanism behind apical branching pattern in *S. muticum* seems to be quite distinct from what can be observed in plant systems; auxin transport and accumulation, as well as cell wall properties, do not seem to be correlating with the new branch outgrowth. Since every newly forming branch has its own meristematic apical cell (Critchley, 1983b), exploring how this cell forms in a spatio-temporal manner would be the first step towards understanding the pattern formation in the spiral phyllotaxis of *Sargassum*. The indication of *Sargassum* apex as a self-organising structure (ablation of the central apical cell and re-initiation of spiral pattern and growth; Chapter 2) suggests that its morphogenetic complexity is indeed intriguing. The ability to self-organise might suggest that a fine spatial control of growth processes in *Sargassum* apex is taking place and local cues are regulating it. Although there is no indication of auxin being responsible for pattern formation in my results, its possible role in pattern formation cannot be ruled out completely. In plants, auxin accumulation in the newly forming bud has an effect on the cell walls of multiple cells by modifying their properties (Braybrook and Peaucelle, 2013). Since *Sargassum* buds each have only one cell that might be controlling the outgrowth, the auxin (or a different phytohormone) effect might be very local, accumulating solely in that one cell or a small number of cells around it. If present, the phytohormone might not act in the same way observed in plants; it might be responsible for positioning the new meristematic bud apical cell, but not changing

the wall properties of the affected cells. Having a positional cue (through phytohormone accumulation) without wall modification would fit into current observations, where no change in stiffness of biochemistry could be correlated with the new outgrowth.

To test this hypothesis, serial sections through each of the bud apical cells would need to be done, followed by immunolocalisation using anti-IAA antibodies used in this study. It might be that auxin is not playing the role of a positional cue; this opens up a variety of possibilities about the identity of a potential 'cue' compound. Recently, a technique that can measure the spatio-temporal distribution of biomolecules in plant tissues and sectioned material has started to be used in many areas of plant research (Boughton et al., 2016), mass spectrometry imaging. Potentially this method could be applied here, to determine whether spatial distribution of any of the detected metabolites correspond to the spatial pattern of new branch formation. Besides being produced inside the organism, auxin might be coming to the alga externally, through a symbiotic relationship with bacteria. This relationship has been already investigated in diatoms, a sister clade to brown algae (Amin et al., 2015). It would be interesting to explore this possibility in a brown macroalga such as *S. muticum.* The potential interactions could be explored via transcriptomic and targeted metabolite analyses in both the host (*Sargassum*) and bacteria, when cultured axenically and co-cultured.

Since no mechanical changes are observed in the apex that correlate with new branch outgrowth, it is likely that cell divisions are responsible for forming the branch, and little or no cell expansion is happening. A detailed temporal map of divisions occurring in the apical region will give indications if this is the case.

Not all 'complex' brown algae have the same branching pattern. In most cases they exhibit dichotomous branching patterns (e.g. *Fucus sp.*; Moss, 1967). However, the apices of these branches have apical cells themselves, similarly to *Sargassum*. To explore the mechanism of branching, other species could be used to address several questions. In cases where the apical cell is thought not to divide asymmetrically to create another daughter apical cell (e.g. *Fucus sp*.; similar to observations here), the hypothesis of positional information through a phytohormone accumulation could be tested. In addition, another system with a

spiral phyllotaxis could be used in combination with *S. muticum* to investigate their similarities in development. An ideal candidate would be *Cystoseira sp*., which, similarly to *Sargassum* exhibits a spiral branching pattern (Church, 1920).

In plant systems, the studies on phyllotactic pattern have produced an immense amount of data on the mechanisms controlling this process. Modelling and experimental approaches incorporating complex interactions between wall mechanics, meristem size, phytohormone transport and gene regulation (reviewed in Braybrook and Kuhlemeier, 2010) have managed to explain all of the phyllotactic patterns observed in plants. Although there are still a lot of questions and uncertainties regarding the phyllotactic processes in brown algae, they most likely have a different approach to building their bodies. However, there is a lot to learn from the vast knowledge available from plant systems, and applying similar strategies to answering morphogenesis questions in brown algae (e.g. computational modelling of growth, gene expression analysis) might be a good first step into understanding the basis of creating complex morphogenetic features.

Patterns formed in nature are not a random trait, but rather an optimised process, with origins embedded in mathematical laws. The most interesting examples of pattern formation are related to the Fibonacci series and the golden ratio of 1.618. The golden ratio be found everywhere in nature and space, from humans (face features, body and limb ratios and finger bones), animals (spiral shells of molluscs such as *Nautilus*), DNA molecule, stellar constellations, plant and algal leaf organisation. The presence of a golden ratio in the meristem of *S. muticum* is very intriguing, but far from being rare. Although the mechanisms of its spiral branch formation remains to be explored, the existence of this type of pattern in the brown lineage as well, suggests a fundamental role of spirals in all of nature.

5.3. Mechanisms of cell growth

There are two quite distinct modes of growth observed in algae and plants: diffuse growth and tip growth. Diffuse growth refers to the expansion of cells over the whole cell surface, which could be isotropic (same in all directions) or anisotropic

(different in different directions). In tip growth, however, the cellular expansion is located in the apex of the elongated cell (Kropf et al., 1998). The process of growth occurs by local insertion of plasma membrane and wall material at the apical growth site (Steer and Steer, 1989). Tip growth represents a valuable system to explore how the wall regulates polar elongation on a single cell level.

In brown algae, tip growth is present in several species: in the filamentous algal bodies such as that found in *Ectocarpus* (Le Bail et al., 2008b), but also in rhizoids of fucoid embryos (explored here). The incorporation of new wall material at the tip, which drives growth, happens through the process of exocytosis. FRAP experiments can be performed to track the dynamics of exocytosis and have been applied in plant systems for this purpose (Bove et al., 2008; Zonia and Munnik, 2008). The results here are indicative that the exocytosis is happening faster at the sides of the rhizoid, rather than the tip itself, similarly to what has been observed in plant pollen tubes (Zonia and Munnik, 2008). Although in need of further optimisation and more detailed temporal dynamics experiments, it is suggested that tip growth in these two very divergent systems might have convergently developed the same mechanism of membrane and wall deposition. Future experiments aimed at understanding the interplay between exocytosis and endocytosis would have to include FRAP experiments in cases where the vesicle deposition is defective due to delivering machinery (e.g. actin filaments; as a continuation of the experiments performed in Chapter 4 of this thesis). In addition, live actin staining with a combined FM4-64 and FM1-43 pulse chase might indicate the spatial correlation of these two events.

The wall in tip growing systems such as pollen tubes has been shown to have a stiffness gradient with the softest part at the very tip (Chebli et al., 2012; Geitmann and Parre, 2004; Zerzour et al., 2009). These studies suggest that the change in stiffness might be related to the underlying chemistry that is observed. However, the stiffness gradient can also be explained purely on a geometrical basis (Vogler et al., 2013). As the surface of the pollen tube is being indented, the angle of tilt between the indentation direction and the surface is gradually increasing, since the tip has a shape of a hemisphere. The lower values that are observed at the pollen tube tip can be expected, since the force measured comes only from the direction of

indentation, which is modified in this case, due to an increased tilt angle. The data here failed to detect these very fine changes in mechanical properties along the rhizoid cell, suggesting that either there is a different mechanism of controlling polar elongations than pure regulation of wall properties or that these changes were missed due to caution taken during analysis (the measurements at the very apex were avoided during analysis due to the geometry issue discussed above).

Interestingly, wall mechanics and biochemistry could be modified when disrupting the major driver of tip growth, the cytoskeleton. The change in the mechanical properties when cytoskeleton is disrupted suggests the direct role of wall components in this process. Available alginate and sulphated fucan epitopes did not seem to be correlated with these changes, however, potential candidates have been suggested (cellulose microfibrils; see Chapter 4). A particular case when higher stiffness was not observed with slower growth was alginate disruption. The lack of stiffness increase does suggest that alginate acts as an important component in wall integrity and its destruction leads to overall destruction of wall compactness.

As mentioned above, mechanical modifications are most likely linked to the changes within the wall itself. Investigating wall thickness and cellulose (as the next candidate) using transmission electron microscopy represents the next step into revealing the mechanical contribution of brown algal cell walls during tip growth. Since actin and microtubules have been found to be guiding the vesicles and cellulose during wall deposition (Baskin, 2005; Katsaros et al., 2002), investigating their orientation whilst disturbed could provide useful information on how the deposition can be linked to observed phenotypes (Chapter 4).

As previously mentioned, two types of cellular growth are found in brown algae: tip and diffuse growth. Whilst a polar deposition of material drives tip growth, mechanisms controlling diffuse growth rely more on overall wall changes in a cell (Kropf et al., 1998). To gain a more accurate picture of how cellular growth occurs in brown algal species, both types of growth would have to be considered. Exhibiting both types of growth, a fucoid embryo thallus (after day 7, when elongation starts happening) could be a good system to explore these processes.

5.4. Application of new tools and methods to explore brown algal development

5.4.1. Exploring wall properties in brown algae

This thesis represents the first investigation of brown algal embryogenesis combining cell wall mechanics and biochemistry, and the second to explore the possibilities of using atomic force microscopy as a tool in brown algal research (Tesson and Charrier, 2014). The characterisation of mechanical properties is important when trying to address the questions of cell growth and enlargement in a walled organism since the wall must deform to allow growth. The data presented here support the importance of cell walls and their mechanical properties in morphogenesis; the cell walls are softer where active growth is taking place (Chapter 3). This thesis has shown that atomic force microscopy is efficient and can be used in brown algal research, on a single cell level or tissue level (embryo rhizoid tip cell and shoot apex). Although the approach has many advantages (ability to image in water and ability of embryos to adhere to the substrate) of this method, some difficulties do occur. The naturally produced mucilage on the outside of the cells/tissues can come in the way of imaging, by adhering to the cantilever and modifying the resulting measurements. An adequate preparation (thorough rinsing) and methodology (determining right indentation forces) should be enough to overcome this issue. In addition, the mechanical behaviour of cell walls is not purely elastic, but rather shows characteristics of a viscoelastic material. In order to fully understand the mechanical properties of brown algal cell walls, viscoelastic behaviour needs to be taken into account in the future as well.

The advances of detecting spatial distribution of wall components, alginate and sulphated fucans (Torode et al., 2015; Torode et al., 2016), has allowed understanding of the relationship between wall mechanics and the potential accompanying biochemical modifications. A portion of the data presented in this thesis is suggestive of that relationship; an alginate epitope rich in guluronic acid is present in stiffer areas, whereas a sulphated fucan is present in the softer areas. Taking into account the biological role in adhesion of the latter component (Crayton et al., 1974), it is difficult to conclude that its spatial distribution contributes to wall

properties, instead of just a role in embryo adhesion to the substrate. The underlying biochemical changes that might be affecting the mechanical properties of the wall need to be examined in detail, possibly by characterising the exact epitopes of already existing antibodies or developing new ones in addition. Furthermore, mass spectrometry is a powerful method for identification and structural information on compounds present in complex mixtures such as cell walls (Bauer, 2012; Pettolino et al., 2012). It is known that the cell wall determines cell fates in fucoid zygotes (Berger et al., 1994); physical dissection of rhizoid and thallus cells and the corresponding walls would allow us to distinguish their differential composition as well.

5.4.2. Molecular mechanisms of wall modification linked to morphogenesis

Potential analogues to plant/bacterial genes involved in biosynthetic pathways of alginate, sulphated fucans and cellulose have been explored in *Ectocarpus siliculosus,* currently the only brown alga with a sequenced genome (Cock et al., 2010; Michel et al., 2010). The major molecular focus in my project was given to exploring the characterisation and expression of mannuronan C5 epimerase genes in several developmental stages (7h AF, 24h AF, 72h AF and 10d AF) during *F. serratus* embryogenesis. The preliminary results suggest that several epimerase genes are actively expressed and their expression levels vary during embryogenesis, suggesting there might be different epimerisation patterns needed during different embryo life stages. One of the limitations in exploring the diversity of these genes in *F. serratus* relates to the selection strategy: all of the candidate genes for MC5Es in *F. serratus* have been selected based on the *Ectocarpus* MC5E sequence homology, which is a quite distant evolutionary clade (different orders). Nevertheless, the preliminary data presented in this thesis as well as ongoing work provide the first step to the molecular basis of embryogenesis in a fucoid alga.

A more in depth approach needs to be taken to investigate the molecular mechanisms underlying growth in brown algae. Sequencing of the transcriptome in this study in *F. serratus* serves as a good basis to explore distinct molecular mechanisms in more depth. The short-term future steps for this involve examining the transcriptome into more detail and validating all the preliminary cell wall-related

gene expression analysis presented in this thesis. In addition, to be able to conclude where these genes are expressed (rhizoid or thallus) and what their role might be, an *in situ* hybridization assay would be of great importance. *In situ* hybridization experiments have been shown to be possible in *Fucus* systems (Bouget et al., 1995b). Pinpointing the location of transcription in growing fucoid embryos could provide even more details about control of cell expansion in these different growth regimes (since there are two different modes of growth during embryogenesis; tip vs. diffuse). Furthermore, the possibility of gene knock-down or knock-out via RNA interference (Farnham et al., 2013) or CRISPR-Cas9 genome editing in the future, could serve as an additional method to investigate how certain aspects of embryogenesis are controlled. Looking at the transcriptional level provides a lot of information about the amount of each specific gene transcript in a cell or a tissue. However, many post-transcriptional changes can occur before the mRNA is transcribed into a functional protein. These changes need to be taken into consideration when discussing data originating from a transcriptomics experiments. Although a transcriptomic approach is powerful on its own, performing a proteomic analysis in combination would be of high importance for these studies as well.

Transferring the knowledge into other brown algal models is of high importance due to several disadvantages of fucoid embryos, such as reproductive seasonality and inability to close the life cycle *in vitro*. *Ectocarpus siliculosus* has been shown to serve as a good model in brown algal research since its general biology has been well investigated and its genome has been sequenced and annotated (Charrier et al., 2008; Cock et al., 2010). *Ectocarpus* has been already used to explore different aspects of brown algal biology and several mutant lines have been established and analysed (Charrier et al., 2008; Coelho et al., 2011; Le Bail et al., 2010; Le Bail et al., 2011; Peters et al., 2008). Investigating mutants (and transformants in the future, once the stable transformation protocols are developed) that have developmental defects, could provide a further great understanding about the role of cell walls in morphogenesis.

Recently, another brown algal model has arisen, *Dictyota dichotoma* (Bogaert, 2015). *D. dichotoma*, unlike *Ectocarpus*, has a multi-layered body and its embryogenesis, although distinct, resembles fucoid systems. Several publications

have shown that *Dictyota* could be a great system when exploring several aspects of brown algal development, at this stage mostly related to early polarisation processes (Bogaert et al., 2016; Bogaert et al., 2017a; Bogaert et al., 2017b). Interestingly, several aspects of *Dictyota* development are similar to fucoid development, such as rhizoid outgrowth at the dark side of the cell and sulphated fucan accumulation at the future rhizoid spot (TBO staining). Since both this study and the study in *Dictyota* have performed an early embryogenesis transcriptomics approach (Bogaert et al., 2017b), a comparative analysis of cellular mechanisms in the early developmental stages would be quite interesting to explore. One of the aspects could involve exploring the common patterns during first asymmetrical cell division and the rhizoid growth.

An interesting question in developmental biology relates to exploring how similar developmental patterns are during early development (embryogenesis) between different species of a particular group. A stage in development which reflects the highest conservation in development is called a phylotypic stage. A recent study in plants and previous studies in animals have shown that embryos appear different in very early stages and late stages of development, with high similarities during mid-embryogenesis (Domazet-Lošo and Tautz, 2010; Kalinka et al., 2010; Quint et al., 2012). This pattern is known as the embryonic “hourglass”. No phylotypic stage has yet been explored in algal systems. With the transcriptomic information originating from this study (a developmental time series of the *Fucus* embryo), it would be intriguing to explore the possibility of phylotypic stage in a group of brown algae.

5.5. Fundamental research leading to industry applications

The interest in brown algae has increased in recent years due to their industrial potential; as a source for food and feed industry, as well as the source of ‘high end’ products such as pharmaceuticals. Some of their bioactivities have been mentioned in the introduction of this thesis (Chapter 1). A significant amount of industrially targeted compounds are found in cell walls (alginate, sulphated fucans,

cellulose and phlorotannins). Regardless of a high number of compounds with potential interest for industry, the limitations to obtaining them are quite high. Macroalgal cultivation is not yet so advanced to support the market demand due to their slow growth, but also necessary knowledge behind their development. The key to revolutionising brown algae as a source for industrial use, requires coming back to step one - research. A great effort has been made recently to establish a consortia of both research-related and industry-related groups, in order to create a knowledge-transferring bridge between them (Charrier et al., 2017). One of the goals of this initiative is to help answer questions on brown algal fertilisation, development and growth. The outcomes of this research could then be translated into better, more productive and cost-effective large scale brown algal production.

The aspect that is somewhat more related to the research presented here, is focused on extracting components of cell walls for industry. Possibly the most interesting components derived from brown algal cell walls are sulphated fucans and phlorotannins. These compounds have been found to have very specific medicinal use in fighting bacterial and viral infections (e.g. food-borne pathogenic bacteria and HIV virus), inflammations as well as a potential chemopreventive effect in treating cancer (Artan et al., 2008; Kong et al., 2009; Nagayama et al., 2002). Finding more algal species with new or a higher production of already existing compounds that can be used in medicine is of high value and importance. Furthermore, developing molecular tools to modulate the production (e.g. increase expression) of such molecules is another approach worth exploring in the future.

5.6. Conclusion

This thesis explored the potential mechanisms behind brown algal development in two systems, *Sargassum muticum* and *Fucus serratus*. The striking similarity in apical patterning between the *S. muticum* apex and a plant apex led to exploring the potential common or different mechanisms in this process (Chapter 2). As the cell walls are responsible for controlling the growth in walled organisms, their role was explored in more detail during *F. serratus* embryogenesis (Chapter 3) using atomic force microscopy, immunolocalisation and transcriptome sequencing.

Tip elongation and the changes in cell wall properties in fucoid embryos were further explored by manipulating the known players responsible for driving this type of growth (Chapter 4).

The recent interest to study brown algae has allowed the rebirth of the field that had become neglected. Brown algae are a group of diverse organisms that have an enormous potential for novel applications, both for industrial uses, as well as scientific discoveries. A deeper exploration of different biological aspects in this interesting group (development, population genetics and ecology) in the future, will allow better understanding of how the processes they have acquired during evolution relate to other groups on the evolutionary tree of life.

Bibliography

Alessa, L. and Kropf, D. L. (1999). F-actin marks the rhizoid pole in living *Pelvetia compressa* zygotes. *Development* **126**, 201–209.

Allard, H. A. (1946). Clockwise and counterclockwise spirality in the phyllotaxy of tobacco. *J. Agric. Res.* **73**, 237–242.

Allen, R. D., Jacobsen, L., Joaquin, J. and Jaffe, L. F. (1972). Ionic concentrations in developing *Pelvetia* eggs. *Dev. Biol.* **27**, 538–545.

Allen, E. D., Aiuto, R. and Sussman, A. S. (1980). Effects of cytochalasins on Neurospora crassa I. Growth and ultrastructure. *Protoplasma* **102**, 63–75.

Amin, S. A., Hmelo, L. R., Van Tol, H. M., Durham, B. P., Carlson, L. T., Heal, K. R., Morales, R. L., Berthiaume, C. T., Parker, M. S., Djunaedi, B., et al. (2015). Interaction and signalling between a cosmopolitan phytoplankton and associated bacteria. *Nature* **522**, 98–101.

Aquino, R., Landeira-Fernandez, A. M., Valente, A. P., Andrade, L. R. and Mourão, P. A. S. (2005). Occurrence of sulfated galactans in marine angiosperms: evolutionary implications. *Glycobiology* **15**, 11–20.

Arenas, F., Viejo, R. M. and Fernández, C. (2002). Density-dependent regulation in an invasive seaweed: Responses at plant and modular levels. *J. Ecol.* **90**, 820–829.

Artan, M., Li, Y., Karadeniz, F., Lee, S. H., Kim, M. M. and Kim, S. K. (2008). Anti-HIV-1 activity of phloroglucinol derivative, 6,6′-bieckol, from *Ecklonia cava*. *Bioorganic Med. Chem.* **16**, 7921–7926.

Avsian-Kretchmer, O., Cheng, J. C., Chen, L., Moctezuma, E. and R, S. Z. (2002). Indole acetic acid distribution coincides with vascular differentiation pattern during *Arabidopsis* leaf ontogeny. *Plant Physiol.* **130**, 199–209.

Baldauf, S. L. (2003). The deep roots of eukaryotes. *Science.* **300**, 1703–1706.

Baldauf, S. L. (2008). An overview of the phylogeny and diversity of eukaryotes. *J. Syst. Evol.* **46**, 263–273.

Ball, E. (1944). The effects of synthetic growth substances on the shoot apex of *Tropaeolum majus* L. *Am. J. Bot.* **31**, 316–327.

Barbier de Reuille, P., Routier-Kierzkowska, A., Kierzkowski, D., Bassel, G. W., Schüpbach, T., Tauriello, G., Bajpai, N., Strauss, S., Weber, A., Kiss, A., et al. (2015). MorphoGraphX: A platform for quantifying morphogenesis in 4D. *Elife* **4**, DOI: 10.7554/eLife.05864.

Baskin, T. I. (2005). Anisotropic expansion of the plant cell wall. *Annu. Rev. Cell Dev. Biol.* **21**, 203–222.

Basu, S., Sun, H., Brian, L., Quatrano, R. L. and Muday, G. K. (2002). Early embryo development in *Fucus distichus* is auxin sensitive. *Plant Physiol.* **130**, 292–302.

Bauer, S. (2012). Mass spectrometry for characterizing plant cell wall polysaccharides. *Front. Plant Sci.* **3**, DOI: 10.3389/fpls.2012.00045.

Belanger, K. D. and Quatrano, R. S. (2000). Membrane recycling occurs during asymmetric tip growth and cell plate formation in *Fucus distichus* zygotes. *Protoplasma* **212**, 24–37.

Bennett, T. A., Liu, M. M., Aoyama, T., Bierfreund, N. M., Braun, M., Coudert, Y., Dennis, R. J., O 'Connor, D., Wang, X. Y., White, C. D., et al. (2014). Plasma membrane-targeted PIN proteins drive shoot development in a moss. *Curr. Biol.* **24**, 2776–2785.

Berger, F. and Brownlee, C. (1993). Ratio confocal imaging of free cytoplasmic calcium gradients in polarising and polarised *Fucus* zygotes. *Zygote* **1**, 9–15.

Berger, F., Taylor, A. and Brownlee, C. (1994). Cell fate determination by the cell-wall in early *Fucus* development. *Science.* **263**, 1421–1423.

Bernasconi, G. P. (1994). Reaction-diffusion model for phyllotaxis. *Phys. D* **70**, 90–99.

Bibikova, T. N., Blancaflor, E. B. and Gilroy, S. (1999). Microtubules regulate tip growth and orientation in root hairs of *Arabidopsis thaliana*. *Plant J.* **17**, 657–665.

Bierhorst, D. W. (1977). On the stem apex, leaf initiation and early leaf ontogeny in filicalean ferns. *Am. J. Bot.* **64**, 125–152.

Billoud, B., Jouanno, Ã., Nehr, Z., Carton, B., Rolland, Ã., Chenivesse, S. and Charrier, B. (2015). Localization of causal locus in the genome of the brown macroalga *Ectocarpus*: NGS-based mapping and positional cloning approaches. *Front. Plant Sci.* **6**, 1–12.

Bisgrove, S. R. (2007). Cytoskeleton and early development in fucoid algae. *J. Integr. Plant Biol.* **49**, 1192–1198.

Bisgrove, S. R. and Kropf, D. L. (1998). Alignment of centrosomal and growth axes is a late event during polarization of *Pelvetia compressa* zygotes. *Dev. Biol.* **194**, 246–56.

Bisgrove, S. R. and Kropf, D. L. (2001). Cell wall deposition during morphogenesis in fucoid algae. *Planta* **212**, 648–658.

Bisgrove, S. R., Henderson, D. C. and Kropf, D. L. (2003). Asymmetric division in fucoid zygotes is positioned by telophase nuclei. *Plant Cell* **15**, 854–862.

Black, W. A. P. (1954). The seasonal variation in the combined L-fucose content of the common British Laminariaceae and Fucaceae. *J. Sci. Food Agric.* **5**, 445–

448.

Bogaert, K. A. (2015). Cell polarisation and asymmetric cell division using *Dictyota dichotoma* as a new experimental model.

Bogaert, K., Beeckman, T. and De Clerck, O. (2016). Abiotic regulation of growth and fertility in the sporophyte of *Dictyota dichotoma* (Hudson) J.V. Lamouroux (Dictyotales, Phaeophyceae). *J. Appl. Phycol.* DOI 10.1007/s10811-016-0801-z

Bogaert, K. A., Beeckman, T. and De Clerck, O. (2017a). Egg activation-triggered shape change in the *Dictyota dichotoma* (Phaeophyceae) zygote is actin–myosin and secretion dependent. *Ann. Bot.* **120**, 529–538.

Bogaert, K. A., Beeckman, T. and De Clerck, O. (2017b). Two-step cell polarization in algal zygotes. *Nat. Plants* **3**,.

Boisson-Vidal, C., Haroun, F., Ellouali, M., Blondin, C., Fischer, A. M., de Agostini, A. and Jozefonvicz, J. (1995). Biological activities of polysaccharides from marine algae. *Drugs Future* **20**, 1237–1249.

Bothwell, J. H. F., Kisielewska, J., Genner, M. J., McAinsh, M. R. and Brownlee, C. (2008). Ca2+ signals coordinate zygotic polarization and cell cycle progression in the brown alga *Fucus serratus*. *Development* **135**, 2173–81.

Bouget, F. Y., Gerttula, S. and Quatrano, R. S. (1995a). Spatial redistribution of poly(A)+ RNA during polarization of the *Fucus* zygote is dependent upon microfilaments. *Dev. Biol.* **171**, 258–261.

Bouget, F.-Y., Gerttula, S., Kloareg, B. and Quatranop, R. S. (1995b). A new, nonradioactive whole-mount in situ hybridization protocol for *Fucus* (Phaeophyta) embryos. *J. Phycol.* **31**, 1027–1030.

Bouget, F. Y., Berger, F. and Brownlee, C. (1998). Position dependent control of cell fate in the *Fucus* embryo: role of intercellular communication. *Development* **125**, 1999–2008.

Boughton, B. A., Thinagaran, D., Sarabia, D., Bacic, A. and Roessner, U. (2016). Mass spectrometry imaging for plant biology: a review. *Phytochem. Rev.* **15**, 445–488.

Bove, J., Vaillancourt, B., Kroeger, J., Hepler, P. K., Wiseman, P. W. and Geitmann, A. (2008). Magnitude and direction of vesicle dynamics in growing pollen tubes using spatiotemporal image correlation spectroscopy and fluorescence recovery after photobleaching. *Plant Physiol.* **147**, 1646–1658.

Boyen, C., Kloareg, B., Polnefuller, M. and Gibor, A. (1990). Preparation of alginate lyases from marine mollusks for protoplast isolation in brown-algae. *Phycologia* **29**, 173–181.

Brawley, S. H. and Quatrano, R. S. (1979). Effects of microtubule inhibitors on pronuclear migration and embryogenesis in *Fucus distichus* (Phaeophyta). *J.*

Phycol. **15**, 266–272.

Brawley, S. H. and Robinson, K. R. (1985). Cytochalasin treatment disrupts the endogenous currents associated with cell polarization in fucoid zygotes: Studies of the role of F-actin in embryogenesis. *J. Cell Biol.* **100**, 1173–1184.

Braybrook, S. A. and Jönsson, H. (2016). Shifting foundations: The mechanical cell wall and development. *Curr. Opin. Plant Biol.* **29**, 115–120.

Braybrook, S. A. and Kuhlemeier, C. (2010). How a plant builds leaves. *Plant Cell* **22**, 1006–1018.

Braybrook, S. A. and Peaucelle, A. (2013). Mechano-chemical aspects of organ formation in *Arabidopsis thaliana*: the relationship between auxin and pectin. *PLoS One* **8**, e57813.

Brown Jr., R. M. (1996). The biosythesis of cellulose. *J. Macromol. Sci. Part A* **A33**, 1345–1373.

Brownlee, C. and Pulsford, A. L. (1988). Visualization of the cytoplasmic Ca2+ gradient in *Fucus serratus* rhizoids: correlation with cell ultrastructure and polarity. *J. Cell Sci.* **91**, 249–256.

Brownlee, C. and Wood, J. W. (1986). A gradient of cytoplasmic free calcium a in growing rhizoid cells of *Fucus serratus*. *Nature* **320**, 624–626.

Brownlee, C., Bouget, F.-Y. and Corellou, F. (2001). Choosing sides: establishment of polarity in zygotes of fucoid algae. *Semin. Cell Dev. Biol.* **12**, 345–351.

Callow, M. E., Evans, L. V, P, B. G. and Callow, J. A. (1978). Fertilisation in brown algae I. SEM and other observations on *Fucus serratus*. *J. Cell Biol.* **32**, 45–54.

Carol, R. J. and Dolan, L. (2002). Building a hair: tip growth in *Arabidopsis thaliana* root hairs. *Philos. Trans. R. Soc. B* **357**, 815–821.

Chamberlain, A. H. L., Gorham, J., Kane, D. F. and Lewey, S. A. (1979). Laboratory growth studies on *Sargassum muticum* (Yendo) Fensholt: II. Apical dominance. *Bot. Mar.* **22**, 11–20.

Charrier, B., Coelho, S. M., Le Bail, A., Tonon, T., Michel, G., Potin, P., Kloareg, B., Boyen, C., Peters, A. F. and Cock, J. M. (2008). Development and physiology of the brown alga *Ectocarpus siliculosus*: two centuries of research. *New Phytol.* **177**, 319–32.

Charrier, B., Le Bail, A. and De Reviers, B. (2012). Plant Proteus: Brown algal morphological plasticity and underlying developmental mechanisms. *Trends Plant Sci.* **17**, 468–477.

Charrier, B., Abreu, M. H., Araujo, R., Bruhn, A., Coates, J. C., De Clerck, O., Katsaros, C., Robaina, R. R. and Wichard, T. (2017). Furthering knowledge of seaweed growth and development to facilitate sustainable aquaculture. *New*

Phytol. **216**, 967–975.

Chebli, Y., Kaneda, M., Zerzour, R. and Geitmann, A. (2012). The cell wall of the Arabidopsis pollen tube - spatial distribution, recycling, and network formation of polysaccharides. *Plant Physiol.* **160**, 1940–1955.

Cheung, A. Y. and Wu, H. (2008). Structural and signaling networks for the polar cell growth machinery in pollen tubes. *Annu. Rev. Plant Biol.* **59**, 547–572.

Chickarmane, V. S., Gordon, S. P., Tarr, P. T., Heisler, M. G. and Meyerowitz, E. M. (2012). Cytokinin signaling as a positional cue for patterning the apical–basal axis of the growing *Arabidopsis* shoot meristem. *Proc. Natl. Acad. Sci.* **109**, 4002–4007.

Church, A. H. (1920). *On the interpretation of phenomena of phyllotaxis*. London: Humphrey Milford and Oxford University Press.

Clayton, M. N. and Shankly, C. M. (1987). The apical meristem of *Splachnidium rugosum* (Phaeophyta). *J. Phycol.* **23**, 296–307.

Clayton, M. N., Hallam, N. D., Luff, S. E. and Diggins, T. (1985). Cytology of the apex, thallus development and reproductive structures of *Hormosira banksii* (Fucales, Phaeophyta). *Phycologia* **24**, 181–190.

Cock, J. M., Sterck, L., Rouzé, P., Scornet, D., Allen, A. E., Amoutzias, G., Anthouard, V., Artiguenave, F., Aury, J. M., Badger, J. H., et al. (2010). The *Ectocarpus* genome and the independent evolution of multicellularity in brown algae. *Nature* **465**, 617–621.

Coelho, S. M., Godfroy, O., Arun, A., Le Corguille, G., Peters, A. F. and Cock, J. M. (2011). OUROBOROS is a master regulator of the gametophyte to sporophyte life cycle transition in the brown alga *Ectocarpus*. *Proc. Natl. Acad. Sci.* **108**, 11518–11523.

Corpet, F. (1988). Multiple sequence alignment with hierarchical clustering. *Nucleic Acids Res.* **16**, 10881–10890.

Correlou, F., Coelho, S. M., Bouget, F. Y. and Brownlee, C. (2005). Spatial re-organisation of cortical microtubules in vivo during polarisation and asymmetric division of zygotes. *J. Cell Sci.* **118**, 2723–2734.

Cosgrove, D. J. (2005). Growth of the plant cell wall. *Nat. Rev. Mol. Cell Biol.* **6**, 850–861.

Cosgrove, D. J. (2016). Plant cell wall extensibility: connecting plant cell growth with cell wall structure, mechanics, and the action of wall-modifying enzymes. *J. Exp. Bot.* **67**, 463–476.

Cosgrove, D. J. and Jarvis, M. C. (2012). Comparative structure and biomechanics of plant primary and secondary cell walls. *Front. Plant Sci.* **3**, 1–7.

Coudert, Y., Palubicki, W., Ljung, K., Novak, O., Leyser, O. and Harrison, J. C.

(2015). Three ancient hormonal cues co-ordinate shoot branching in a moss. *Elife* **4**, e06808.

Cox, C. (1997). Dichlobenil. *J. Pestic. Reform* **17**, 14–20.

Craigie, J. S., Morris, E. R., Rees, D. A. and Thom, D. (1984). Alginate block structure in Phaeophyceae from Nova Scotia: Variation with species, environment and tissue type. *Carbohydr. Polym.* **4**, 237–252.

Crayton, M. A., Wilson, E. and Quatrano, R. S. (1974). Sulfation of fucoidan in *Fucus* embryos II. Separation from initiation of polar growth. *Dev. Biol.* **39**, 164–167.

Critchley, A. T. (1983a). Experimental observations on variability of leaf and air vesicle shape of *Sargassum muticum. J. Mar. Biol. Assoc. UK* **63**, 825–831.

Critchley, A. T. (1983b). *Sargassum muticum*: a morphological description of european material. *J. Mar. Biol. Assoc. United Kingdom* **63**, 813–824.

Cronshaw, J., Myers, A. and Preston, R. D. (1958). Chemical and physical investigation of the cell walls of some marine algae. *Biochim. Biophys. Acta* **27**, 89–103.

Cutter, E. G. (1965). Recent experimental studies of the shoot apex and shoot morphogenesis. *Bot. Rev.* **31**, 7–113.

Cutter, E. G. and Voeller, B. R. (1948). Changes in leaf arrangement in individual fern apices. *Bot. J. Linn. Soc.* **56**, 225–238.

Davidse, L. C. (1986). Benzimidazole fungicides: mechanism of action and biological impact. *Annu. Rev. Phytopathol.* **24**, 43–65.

de Reviers, B. and Rousseau, F. (1999). Towards a new classification of the brown algae. In *Progress in Phycological Research*, pp. 107–201.

de Reviers, B., Rousseau, F. and Draisma, S. G. A. (2007). Classification of the Phaeophyceae from past to present and current challenges. In *Unravelling the algae: the past, present, and future of algal systematics*, pp. 267–284.

Delmer, D. P. and Amor, Y. (1995). Cellulose biosynthesis. *Plant Cell* **7**, 987–1000.

Demes, K. W., Graham, M. H. and Suskiewicz, T. S. (2009). Phenotypic plasticity reconciles incongruous molecular and morphological taxonomies: the giant kelp, *Macrocystis* (Laminariales, Phaeophyceae), is a monospecific genus. *J. Phycol.* **45**, 1266–1269.

Deniaud-Bouët, E., Kervarec, N., Michel, G., Tonon, T., Kloareg, B. and Hervé, C. (2014). Chemical and enzymatic fractionation of cell walls from Fucales: Insights into the structure of the extracellular matrix of brown algae. *Ann. Bot.* **114**, 1203–1216.

Domazet-Lošo, T. and Tautz, D. (2010). A phylogenetically based transcriptome

age index mirrors ontogenetic divergence patterns. *Nature* **468**, 815–819.

Donati, I., Holtan, S., Mørch, Y. A., Borgogna, M., Dentini, M. and Skjåk-Bræk, G. (2005). New hypothesis on the role of alternating sequences in calcium-alginate gels. *Biomacromolecules* **6**, 1031–1040.

Draget, K. I. and Taylor, C. (2011). Chemical, physical and biological properties of alginates and their biomedical implications. *Food Hydrocoll.* **25**, 251–256.

Draget, K. I., Skjåk Bræk, G. and Smidsrød, O. (1994). Alginic acid gels: the effect of alginate chemical composition and molecular weight. *Carbohydr. Polym.* **25**, 31–38.

Draget, K., Smidsrød, O. and Skjåk-Bræk, G. (2005). Alginates from algae. In *Pollysaccharides and Plyamides in the Food Industry. Properties, Production, and Patents.*, pp. 1–30.

Ducreux, G. and Kloareg, B. (1988). Plant regeneration from protoplasts of *Sphacelaria* (Phaeophyceae). *Planta* **174**, 25–29.

Dumais, J. (2007). Can mechanics control pattern formation in plants? *Curr. Opin. Plant Biol.* **10**, 58–62.

Engelen, A. H., Åberg, P., Olsen, J. L., Stam, W. T. and Breeman, A. M. (2005). Effects of wave exposure and depth on biomass, density and fertility of the fucoid seaweed *Sargassum polyceratium* (Phaeophyta, Sargassaceae). *Eur. J. Phycol.* **40**, 149–158.

Enquist-Newman, M., Faust, A. M. E., Bravo, D. D., Santos, C. N. S., Raisner, R. M., Hanel, A., Sarvabhowman, P., Le, C., Regitsky, D. D., Cooper, S. R., et al. (2013). Efficient ethanol production from brown macroalgae sugars by a synthetic yeast platform. *Nature* **505**, 239–243.

Ertesvåg, H. (2015). Alginate-modifying enzymes: biological roles and biotechnological uses. *Front. Microbiol.* **6**, DOI: 10.3389/fmicb.2015.00523.

Ertesvåg, H. and Valla, S. (1998). Biosynthesis and applications of alginates. *Polym. Degrad. Stab.* **59**, 85–91.

Ertesvåg, H., Høidal, H. K., Hals, I. K., Rian, A., Doseth, B. and Valla, S. (1995). A family of modular type mannuronan C-5-epimerase genes controls alginate structure in *Azotobacter vinelandii*. *Mol. Microbiol.* **16**, 719–731.

Ertesvåg, H., Hoidal, H. K., Schjerven, H., Iren, B., Svanem, G. and Valla, S. (1999). Mannuronan C-5-epimerases and their application for in vitro and in vivo design of new alginates useful in biotechnology. *Metab. Eng.* **1**, 262–269.

Evans, L. V and Trewavas, A. J. (1991). Is algal development controlled by plant growth substances? *J. Phycol.* **27**, 322–326.

Fagerberg, W. R. and Dawes, C. J. (1976). Studies on Sargassum. I. A light microscopic examination of the wound regeneration process in mature stipes

of *S. filipendula*. *Am. J. Bot.* **63**, 110–119.

Falace, A. and Bressan, G. (2006). Seasonal variations of *Cystoseira barbata* (Stackhouse) C. Agardh frond architecture. *Hydrobiologia* **555**, 193–206.

Farnham, G., Strittmatter, M., Coelho, S., Cock, J. M. and Brownlee, C. (2013). Gene silencing in *Fucus* embryos: Developmental consequences of RNAi-mediated cytoskeletal disruption. *J. Phycol.* **49**, 819–829.

Feng, T., Shao, S., Pang, J., Li, J. and Li, X. (2015). De novo transcriptome analysis of the gametophyte of *Undaria pinnatifida* (Phaeophyceae). *J. Appl. Phycol.* **27**, 1011–1019.

Fernandes, A. N., Chen, X., Scotchford, C., Walker, J., Wells, D. M., Roberts, C. J. and Everitt, N. M. (2012). Mechanical properties of epidermal cells of whole living roots of *Arabidopsis thaliana*: An atomic force microscopy study. *Phys. Rev. E* **85**, DOI: 10.1103/PhysRevE.85.021916.

Fischl, R., Bertelsen, K., Gaillard, F., Coelho, S., Michel, G., Klinger, M., Boyen, C., Czjzek, M. and Hervé, C. (2016). The cell-wall active mannuronan C5-epimerases in the model brown alga *Ectocarpus*: From gene context to recombinant protein. *Glycobiology* **26**, 973–983.

Fleming, A. J. (1997). Induction of leaf primordia by the cell wall protein expansin. *Science (80-.).* **276**, 1415–1418.

Fowler, J. E. and Quatrano, R. S. (1997). Plant cell morphogenesis: plasma membrane interactions with the cytoskeleton and cell wall. *Annu. Rev. Cell. Dev. Biol.* **13**, 697–743.

Franklin, M. J., Chitnis, C. E., Gacesa, P., Sonesson, A., White, D. C. and Ohman, D. E. (1994). *Pseudomonas aeruginosa* AlgG is a polymer level alginate C5-mannuronan epimerase. *J. Bacteriol.* **176**, 1821–1830.

Fritsch, F. E. (1945). Observations on the anatomical structure of the Fucales. *New Phytol.* **44**, 1–16.

Fulcher, R. G. and McCully, M. E. (1969). Histological studies on the genus *Fucus*. IV. Regeneration and adventive embryony. *Can. J. Bot.* **70**, 1643–1649.

Galun, E. and Torrey, J. G. (1969). Initiation and suppression of apical hairs of *Fucus* embryos. *Dev. Biol.* **19**, 447–459.

Geitmann, A. and Emons, A. M. C. (2000). The cytoskeleton in plant and fungal cell tip growth. *J. Microsc.* **198**, 218–245.

Geitmann, A. and Parre, E. (2004). The local cytomechanical properties of growing pollen tubes correspond to the axial distribution of structural cellular elements. *Sex. Plant Reprod.* **17**, 9–16.

Geitmann, A., Snowman, B. N., Emons, A. M. and Franklin-Tong, V. E. (2000). Alterations in the actin cytoskeleton of pollen tubes are induced by the self-

incompatibility reaction in *Papaver rhoeas*. *Plant Cell* **12**, 1239–1251.

Gibbon, B. C., Kovar, D. R. and Staiger, C. J. (1999). Latrunculin B has different effects on pollen germination and tube growth. *Plant Cell* **11**, 2349–2363.

Gola, E. M. and Banasiak, A. (2016). Diversity of phyllotaxis in land plants in reference to the shoot apical meristem structure. *Acta Soc. Bot. Pol.* **85**, 3529. DOI:10.5586/asbp.3529.

Golub, S. J. and Wetmore, R. H. (1948). Studies of development in the vegetative shoot of *Equisetum arvense* L. I. The shoot apex. *Am. J. Bot.* **35**, 755–767.

Gómez-Díaz, D. and Navaza, J. M. (2003). Rheology of aqueous solutions of food additives. *J. Food Eng.* **56**, 387–392.

Goodner, B. and Quatrano, R. S. (1993). *Fucus* embryogenesis - a model to study the establishment of polarity. *Plant Cell* **5**, 1471–1481.

Grant, G. T., Mon, E. R., Rees, D. A., Smith, P. J. C. and Thom, D. (1973). Biological interactions between polysaccharides and divalent cations: the egg-box model. *FEBS Lett.* **32**, 195–198.

Grove, S. N. and Sweigard, J. A. (1980). Cytochalasin A inhibits spore germination and hyphal tip growth in *Gilbertella persicaria*. *Experimantal Mix.* **4**, 239–250.

Gu, Y., Fu, Y., Dowd, P., Li, S., Vernoud, V., Gilroy, S. and Yang, Z. (2005). A Rho family GTPase controls actin dynamics and tip growth via two counteracting downstream pathways in pollen tubes. *J. Cell Biol.* **169**, 127–138.

Guiry, M. D. and Guiry, G. M. (2017). http://www.algaebase.org. *AlgaeBase. World-wide Electron. Publ. Natl. Univ. Ireland, Galw.*

Gupta, G. D. and Heath, I. B. (1997). Actin disruption by latrunculin B causes turgor-related changes in tip growth of *Saprolegnia ferax* hyphae. *Fungal Genet. Biol.* **21**, 64–75.

Haas, B. J., Papanicolaou, A., Yassour, M., Grabherr, M., Philip, D., Bowden, J., Couger, M. B., Eccles, D., Li, B., Macmanes, M. D., et al. (2014). Reference generation and analysis with Trinity. *Nat. Protoc.* **8**, 1–43.

Hable, W. E. and Kropf, D. L. (1998). Roles of secretion and the cytoskeleton in cell adhesion and polarity establishment in *Pelvetia compressa* zygotes. *Dev. Biol.* **198**, 45–56.

Hable, W. E. and Kropf, D. L. (2005). The Arp2/3 complex nucleates actin arrays during zygote polarity establishment and growth. *Cell Motil. Cytoskeleton* **61**, 9–20.

Hable, W. E., Miller, N. R. and Kropf, D. L. (2003). Polarity establishment requires dynamic actin in fucoid zygotes. *Protoplasma* **221**, 193–204.

Hable, W. E., Reddy, S. and Julien, L. (2008). The Rac1 inhibitor, NSC23766,

depolarizes adhesive secretion, endomembrane cycling, and tip growth in the fucoid alga, *Silvetia compressa*. *Planta* **227**, 991–1000.

Harold, F. M., Harold, R. L. and Money, N. P. (1995). What forces drive cell wall expansion. *Can. J. Bot.* **73**, 379–383.

Harrison, C. J., Roeder, A. H. K., Meyerowitz, E. M. and Langdale, J. A. (2009). Local cues and asymmetric cell divisions underpin body plan transitions in the moss *Physcomitrella patens*. *Curr. Biol.* **19**, 461–471.

Hartmann, M., Holm, O. B., Johansen, G. A. B., Skjåk-Bræk, G. and Stokke, B. T. (2002a). Mode of action of recombinant *Azotobacter vinelandii* mannuronan C-5 epimerases AlgE2 and AlgE4. *Biopolymers* **63**, 77–88.

Hartmann, M., Duun, A. S., Markussen, S., Grasdalen, H., Valla, S. and Skjåk-Bræk, G. (2002b). Time-resolved 1H and 13C NMR spectroscopy for detailed analyses of the *Azotobacter vinelandii* mannuronan C-5 epimerase reaction. *Biochim. Biophys. Acta* **1570**, 104–112.

Haug, A. and Larsen, B. (1969). Biosynthesis of alginate. Epimerisation of D-mannuronic to L-guluronic acid residues in the polymer chain. *Biochim. Biophys. Acta* **192**, 557–559.

Haug, A., Larsen, B. and Smidsrød, O. (1966). A study of the constitution of alginic acid by partial acid hydrolysis. *Acta Chem. Scand.* **20**, 183–190.

Haug, A., Larsen, B. and Smidsrød, O. (1967). Studies on the sequence of uronic acid residues in alginic acid. *Acta Chem. Scand.* **21**, 691–704.

Haug, A., Larsen, B. and Smidsrød, O. (1974). Uronic acid sequence in alginate from different sources. *Carbohydr. Res.* **32**, 217–225.

Heath, I. B. (1974). A unified hypothesis for the role of membrane bound enzyme complexes and microtubules in plant cell wall synthesis. *J. Theor. Biol.* **48**, 445–449.

Heath, I. B., Bonham, M., Akram, A. and Gupta, G. D. (2003). The interrelationships of actin and hyphal tip growth in the ascomycete *Geotrichum candidum*. *Fungal Genet. Biol.* **38**, 85–97.

Heim, D. R., Skomp, J. R., Tschabold, E. E. and Larrinua, I. M. (1990). Isoxaben inhibits the synthesis of acid insoluble cell wall materials in *Arabidopsis thaliana*. *Plant Physiol.* **93**, 695–700.

Henderson, D. C., Bisgrove, S. R., Hable, W. E., Alessa, L. and Kropf, D. L. (1998). Division patterns in the thallus of *Pelvetia compressa* embryos and the effects of gravity. *Protoplasma* **203**, 112–117.

Hengst, M. B., Andrade, S., González, B. and Correa, J. A. (2010). Changes in epiphytic bacterial communities of intertidal seaweeds modulated by host, temporality, and copper enrichment. *Microb. Ecol.* **60**, 282–290.

Henry, B. E. and Van Alstyne, K. L. (2004). Effects of UV radiation on growth and phlorotannins in *Fucus gardneri* (Phaephyceae) juveniles and embryos. *J. Phycol.* **40**, 527–533.

Hervé, C., Siméon, A., Jam, M., Cassin, A., Johnson, K. L., Salmeán, A. A., Willats, W. G. T., Doblin, M. S., Bacic, A. and Kloareg, B. (2016). Arabinogalactan proteins have deep roots in eukaryotes: Identification of genes and epitopes in brown algae and their role in *Fucus serratus* embryo development. *New Phytol.* **209**, 1428–1441.

Himmelspach, R., Williamson, R. E. and Wasteneys, G. O. (2003). Cellulose microfibril alignment recovers from DCB-induced disruption despite microtubule disorganization. *Plant J.* **36**, 565–575.

Hirst, E. and Rees, D. A. (1965). The structure of alginic acid. Part V. Isolation and unambiguous characterisation of some hydrolysis products of the methylated polysaccharide. *J. Chem. Soc.* 1182–1187.

Høidal, H. K., Ertesvåg, H., Skjåk-Bræk, G., Stokke, B. T. and Valla, S. (1999). The recombinant *Azotobacter vinelandii* mannuronan C-5-epimerase AlgE4 epimerizes alginate by a nonrandom attack mechanism. *J. Biol. Chem.* **274**, 12316–12322.

Idilli, A. I., Morandini, P., Onelli, E., Rodighiero, S., Caccianiga, M. and Moscatelli, A. (2013). Microtubule depolymerization affects endocytosis and exocytosis in the tip and influences endosome movement in tobacco pollen tubes. *Mol. Plant* **6**, 1109–1130.

Inoue, A., Satoh, A., Morishita, M., Tokunaga, Y., Miyakawa, T., Tanokura, M. and Ojima, T. (2016). Functional heterologous expression and characterization of mannuronan C5-epimerase from the brown alga *Saccharina japonica*. *Algal Res.* **16**, 282–291.

Jackson, S. L. and Heath, I. B. (1989). Effects of exogenous calcium ions on tip growth, intracellular Ca2+ concentration, and actin arrays in hyphae of the fungus *Saprolegnia ferax*. *Exp. Mycol.* **13**, 1–12.

Jackson, S. L. and Heath, I. B. (1990). Evidence that actin reinforces the extensible hyphal apex of the oomycete *Saprolegnia ferax*. *Protoplasma* **157**, 144–153.

Jackson, S. L. and Heath, I. B. (1993). Roles of calcium ions in hyphal tip growth. *Microbiol. Rev.* **57**, 367–382.

Jönsson, H., Heisler, M. G., Shapiro, B. E., Meyerowitz, E. M. and Mjolsness, E. (2006). An auxin-driven polarized transport model for phyllotaxis. *Proc. Natl. Acad. Sci.* **103**, 1633–1638.

Kalinka, A. T., Varga, K. M., Gerrard, D. T., Preibisch, S., Corcoran, D. L., Jarrells, J., Ohler, U., Bergman, C. M. and Tomancak, P. (2010). Gene expression divergence recapitulates the developmental hourglass model. *Nature* **468**, 811–816.

Karyophyllis, D., Katsaros, C. and Galatis, B. (2000a). F-actin involvement in apical cell morphogenesis of *Sphacelaria rigidula* (Phaeophyceae): mutual alignment between cortical actin filaments and cellulose microfibrils. *Eur. J. Phycol.* **35**, 195–203.

Karyophyllis, D., Katsaros, C., Dimitriadis, I. and Galatis, B. (2000b). F-actin organization during the cell cycle of *Sphacelaria rigidula* (Phaeophyceae). *Eur. J. Phycol.* **35**, 25–33.

Katsaros, C. I. (1995). Apical cells of brown algae with particular reference to Sphacelariales, Dictyotales and Fucales. *Phycol. Res.* **43**, 43–59.

Katsaros, C. and Galatis, B. (1988). Thallus development in *Dictyopteris membranacea* (Phaeophyta, dictyotales). *Br. Phycol. J.* **23**, 71–88.

Katsaros, C. I., Karyophyllis, D. A. and Galatis, B. D. (2002). Cortical F-actin underlies cellulose microfibril patterning in brown algal cells. *Phycologia* **41**, 178–183.

Katsaros, C., Karyophyllis, D. and Galatis, B. (2006). Cytoskeleton and morphogenesis in brown algae. *Ann. Bot.* **97**, 679–693.

Kaur, I. (1999). Apical meristem of *Sargassum vulgare* C. Agardh (Phaeophyta, Fucales). *Algae* **14**, 37–42.

Kaur, I. and Vijayaraghavan, M. R. (1992). Physode distribution and genesis in *Sargassum vulgare* C. Agardh and *Sargassum johnstonii* Setchell & Gardner. *Aquat. Bot.* **42**, 375–384.

Ketelaar, T. and Emons, A. M. C. (2001). The cytoskeleton in plant cell growth : lessons from root hairs. *New Phytol.* **152**, 409–418.

Ketelaar, T., de Ruijter, N. C. and Emons, A. M. C. (2003). Unstable F-actin specifies the area and microtubule direction of cell expansion in *Arabidopsis* root hairs. *Plant Cell* **15**, 285–292.

Ketelaar, T., Meijer, H. J. G., Spiekerman, M., Weide, R. and Govers, F. (2012). Effects of latrunculin B on the actin cytoskeleton and hyphal growth in *Phytophthora infestans*. *Fungal Genet. Biol.* **49**, 1014–1022.

Kim, A. R., Shin, T. S., Lee, M. S., Park, J. Y., Park, K. E., Yoon, N. Y., Kim, J. S., Choi, J. S., Jang, B., Byun, D. S., et al. (2009). Isolation and identification of phlorotannins from *Ecklonia stolonifera* with antioxidant and anti-inflammatory properties. *J. Agric. Food Chem.* **57**, 3483–3489.

Klausner, R. D., Donaldson, J. G. and Lippincott-Schwartz, J. (1992). Brefeldin A: Insights into the control of membrane traffic and organelle structure. *J. Cell Biol.* **116**, 1071–1080.

Klemm, M. F. and Hallam, N. D. (1987). Branching pattern anf growth in *Cystophora* (Fucales, Phaeophyta). *Phycologia* **26**, 252–261.

Kloareg, B. and Quatrano, R. S. (1987a). Enzymatic removal of the cell walls from zygotes of *Fucus distichus* (L.) Powell (Phaeophyta). *Hydrobiologia* **151/152**, 123–129.

Kloareg, B. and Quatrano, R. S. (1987b). Isolation of protoplasts from zygotes of *Fucus distichus* (L.) Powell (Phaeophyta). *Plant Sci.* **50**, 189–194.

Kloareg, B. and Quatrano, R. S. (1988). Structure of the cell walls of marine algae and ecophysiological functions of the matrix polysaccharides. *Oceanogr. Mar. Biol. Annu. Rev.* **26**, 259–315.

Knox, J. P. (2008). Revealing the structural and functional diversity of plant cell walls. *Curr. Opin. Plant Biol.* **11**, 308–313.

Kong, C. S., Kim, J. A., Yoon, N. Y. and Kim, S. K. (2009). Induction of apoptosis by phloroglucinol derivative from *Ecklonia cava* in MCF-7 human breast cancer cells. *Food Chem. Toxicol.* **47**, 1653–1658.

Kovalenko, I., Zdyrko, B., Magasinski, A., Hertzberg, B., Milicev, Z., Burtovyy, R., Luzinov, I. and Yushin, G. (2011). A major constituent of brown algae for use in high-capacity Li-ion batteries. *Science.* **334**, 75–79.

Krichevsky, A., Kozlovsky, S. V, Tian, G. W., Chen, M. H., Zaltsman, A. and Citovsky, V. (2007). How pollen tubes grow. *Dev. Biol.* **303**, 405–420.

Kropf, D. L. (1992). Establishment and expression of cellular polarity in fucoid zygotes. *Microbiol. Rev.* **56**, 316–339.

Kropf, D. L. (1997). lnduction of polarity in fucoid zygotes. *Plant Cell* **9**, 1011–1020.

Kropf, D. L. and Quatrano, R. S. (1987). Localization of membrane-associated calcium during development of fucoid algae using chlorotetracycline. *Planta* **171**, 158–170.

Kropf, D. L., Kloareg, B. and Quatrano, R. S. (1988). Cell wall is required for fixation of the embryonic axis in *Fucus* zygotes. *Science .* **239**, 187–190.

Kropf, D. L., Hopkins, R. and Quatrano, R. S. (1989a). Protein synthesis and morphogenesis are not tightly linked during embryogenesis in *Fucus*. *Dev. Biol.* **134**, 452–461.

Kropf, D. L., Berger, S. K. and Quatrano, R. S. (1989b). Actin localization during *Fucus* embryogenesis. *Plant Cell* **1**, 191–200.

Kropf, D. L., Maddock, A. and Gard, D. L. (1990). Microtubule distribution and function in early *Pelvetia* development. *J. Cell Sci.* **97**, 545–552.

Kropf, D. L., Bisgrove, S. R. and Hable, W. E. (1998). Cytoskeletal control of polar growth in plant cells. *Curr. Opin. Cell Biol.* **10**, 117–122.

Kropf, D. L., Bisgrove, S. R. and Hable, W. E. (1999). Establishing a growth axis in fucoid algae. *Trends Plant Sci.* **4**, 490–494.

Lachnit, T., Meske, D., Wahl, M., Harder, T. and Schmitz (2011). Epibacterial community patterns on marine macroalgae are host-specific but temporally variable. *Environ. Microbiol.* **13**, 655–665.

Le Bail, A., Dittami, S. M., de Franco, P. O., Rousvoal, S., Cock, M. J., Tonon, T. and Charrier, B. (2008a). Normalisation genes for expression analyses in the brown alga model *Ectocarpus siliculosus*. *BMC Mol. Biol.* **9**, DOI: 10.1186/1471-2199-9-75.

Le Bail, A., Billoud, B., Maisonneuve, C., Peters, A. F., Cock, J. M. and Charrier, B. (2008b). Early development pattern of the brown alga *Ectocarpus siliculosus* (Ectocarpales, Phaeophyceae) sporophyte. *J. Phycol.* **44**, 1269–1281.

Le Bail, A., Billoud, B., Kowalczyk, N., Kowalczyk, M., Gicquel, M., Le Panse, S., Stewart, S., Scornet, D., Cock, J. M., Ljung, K., et al. (2010). Auxin metabolism and function in the multicellular brown alga *Ectocarpus siliculosus*. *Plant Physiol.* **153**, 128–44.

Le Bail, A., Billoud, B., Le Panse, S., Chenivesse, S. and Charrier, B. (2011). ETOILE regulates developmental patterning in the filamentous brown alga *Ectocarpus siliculosus*. *Plant Cell* **23**, 1666–1678.

Leblanc, C., Schaal, G., Cosse, A., Destombe, C., Valero, M., Riera, P. and Potin, P. (2011). Trophic and biotic interactions in *Laminaria digitata* beds: Which factors could influence the persistence of marine kelp forests in northern brittany? *Cah. Biol. Mar.* **52**, 415–427.

Li, B. and Dewey, C. N. (2011). RSEM: accurate transcript quantification from RNA-Seq data with or without a reference genome. *BMC Bioinformatics* **12**, www.biomedcentral.com/1471-2105/12/323.

Lockhart, J. A. (1965). An analysis of irreversible plant cell elongation. *J. Theor. Biol.* **8**, 264–275.

Love, J., Brownlee, C. and Trewavas, A. J. (1997). Ca2+ and calmodulin dynamics during photopolarization in *Fucus serrafus* zygotes. *Plant Physiol.* **115**, 249–261.

Lovy-Wheeler, A., Wilsen, K. L., Baskin, T. I. and Hepler, P. K. (2005). Enhanced fixation reveals the apical cortical fringe of actin filaments as a consistent feature of the pollen tube. *Planta* **221**, 95–104.

Lundqvist, L. C. E., Jam, M., Barbeyron, T., Czjzek, M. and Sandström, C. (2012). Substrate specificity of the recombinant alginate lyase from the marine bacteria *Pseudomonas alginovora*. *Carbohydr. Res.* **352**, 44–50.

Mabeau, S. and Kloareg, B. (1987). Isolation and analysis of the cell walls of brown algae : *Fucus spiralis, F. ceranoides, F. vesiculosus, F. serratus, Bifurcaria bifurcata* and *Laminaria digitata*. *J. Exp. Bot.* **38**, 1573–1580.

Malhóai, R. and Trewavasb, A. J. (1935). Localized apical increases of cytosolic free calcium control pollen tube orientation. *Plant Cell* **8**, 1935–1949.

Mancini, M., Moresi, M. and Rancini, R. (1999). Mechanical properties of alginate gels: empirical characterisation. *J. Food Eng.* **39**, 369–378.

Mann, K. H. (1973). Seaweeds: their productivity and strategy for growth. *Science.* **182**, 975–981.

Martin, M. (2011). Cutadapt removes adapter sequences from high-throughput sequencing reads. *EMBnet* **17**, 10–12.

Martins, M. J. F., Mota, C. F. and Pearson, G. A. (2013). Sex-biased gene expression in the brown alga *Fucus vesiculosus*. *BMC Genomics* **14**, 294–308.

Matsubara, K., Hori, K., Matsuura, Y. and Miyazawa, K. (2000). Purification and characterization of a fibrinolytic enzyme and identification of fibrinogen clotting enzyme in a marine green alga, *Codium divaricatum*. *Comp. Biochem. Physiol. - B* **125**, 137–143.

McCully, M. E. (1968). Histological studies on the genus Fucus II. Histology of the reproductive tissues. *Protoplasma* **66**, 205–230.

Menand, B., Calder, G. and Dolan, L. (2007). Both chloronemal and caulonemal cells expand by tip growth in the moss *Physcomitrella patens*. *J. Exp. Bot.* **58**, 1843–1849.

Meyerowitz, E. M. (1997). Genetic control of cell division patterns in developing plants. *Cell* **88**, 299–308.

Michel, G., Tonon, T., Scornet, D., Cock, J. M. and Kloareg, B. (2010). The cell wall polysaccharide metabolism of the brown alga *Ectocarpus siliculosus*. Insights into the evolution of extracellular matrix polysaccharides in Eukaryotes. *New Phytol.* **188**, 82–97.

Milani, P., Braybrook, S. A. and Boudaoud, A. (2013). Shrinking the hammer: Micromechanical approaches to morphogenesis. *J. Exp. Bot.* **64**, 4651–4662.

Milani, P., Mirabet, V., Cellier, C., Rozier, F., Hamant, O., Das, P. and Boudaoud, A. (2014). Matching patterns of gene expression to mechanical stiffness at cell resolution through quantitative tandem epifluorescence and nanoindentation. *Plant Physiol.* **165**, 1399–1408.

Miller, D. D., De Ruijter, N. C. A., Bisseling, T. and Emons, A. M. C. (1999). The role of actin in root hair morphogenesis: Studies with lipochito-oligosaccharide as a growth stimulator and cytochalasin as an actin perturbing drug. *Plant J.* **17**, 141–154.

Mizukami, M. and Wada, S. (1983). Morphological anomalies induced by antimicrotubule agents in *Bryopsis plumosa*. *Protoplasma* **114**, 151–162.

Mørch, Ý. A., Holtan, S., Donati, I., Strand, B. L. and Skjåk-Bræk, G. (2008). Mechanical properties of C-5 epimerized alginates. *Biomacromolecules* **9**, 2360–2368.

Morton, W. M., Ayscough, K. R. and Mclaughlin, P. J. (2000). Latrunculin alters the actin-monomer subunit interface to prevent polymerization. *Nat. Cell Biol.* **2**, 376–378.

Moss, B. (1950). Studies in the genus *Fucus*: II. The anatomical structure and chemical composition of receptacles of *Fucus vesiculosus* from three contrasting habitats. *Ann. Bot.* **14**, 395–410.

Moss, B. (1965). Apical dominance in *Fucus vesiculosus*. *New Phytol.* **3**, 387–392.

Moss, B. (1967). The apical meristem of *Fucus*. *New Phytol.* **66**, 67–74.

Moss, B. (1969). Apical meristems and growth control in *Himanthalia elongata* (S. F. Gray). *New Phytol.* **68**, 387–397.

Mourão, P. A. S. and Bastos, I. G. (1987). Highly acidic glycans from sea cucumbers. *Eur. J. Biochem.* **166**, 639–645.

Mueller, R. J. (1982). Shoot morphology of the climbing fern *Lygodium* (Schizaeaceae): general organography, leaf initiation, and branching. *Bot. Gaz.* **143**, 319–330.

Mueller, S. C. and Brown, R. M. (1980). Evidence for an intramembrane component microfibril-synthesizing complex in higher plants. *J. Cell Biol.* **84**, 315–326.

Mulloy, B., Ribeiro, A. C., Alves, A. P., Vieira, R. P. and Mourão, P. A. S. (1994). Sulfated fucans from echinoderms have a regular tetrasaccharide repeating unit defined by specific patterns of sulfation at the 0-2 and 0-4 positions. *J. Biol. Chem.* **269**, 22113–22123.

Nagayama, K., Iwamura, Y., Shibata, T., Hirayama, I. and Nakamura, T. (2002). Bactericidal activity of phlorotannins from the brown alga *Ecklonia kurome*. *J. Antimicrob. Chemother.* **50**, 889–893.

Nägeli, C. (1845a). Wachtumsgeschiehte von *Delesseria hypoglossum*. *Zeitschrit. Wiss. Bot* **2**, 121–137.

Nägeli, C. (1845b). Wachtumsgesehichte der Laub- und Lebermoose. *Zeitschrit. Wiss. Bot* **2**, 138–210.

Nelson, D. R. and Jaffe, L. F. (1973). Cells without cytoplasmic movements respond to cythochalasin. *Dev. Biol.* **30**, 206–208.

Nizamuddin, M. (1967). Morphology and anatomy of *Phyllospora*, *Scytothalia* and *Seirococcus* (Fucales). *Bot. Mar.* 81–105.

Novotny, A. M. and Forman, M. (1974). The relationship between changes in cell wall of and the establishment of polarity in *Fucus* embryos. *Dev. Biol.* **40**, 162–173.

Novotny, A. M. and Forman, M. (1975). The composition and development of cell

walls of *Fucus* embryos. *Planta* **122**, 67–78.

Nuccitelli, R. (1978). Ooplasmic segregation and secretion in the *Pelvetia* egg is accompanied by a membrane-generated electrical current. *Dev. Biol.* **62**, 13–33.

Nyvall, P., Corre, E., Boisset, C., Barbeyron, T., Rousvoal, S., Scornet, D., Kloareg, B. and Boyen, C. (2003). Characterization of mannuronan C-5-epimerase genes from the brown alga *Laminaria digitata*. *Plant Physiol.* **133**, 726–735.

Okada, Y., Ishimaru, A., Suzuki, R. and Okuyama, T. (2004). A new phloroglucinol derivative from the brown alga *Eisenia bicyclis*: potential for the effective treatment of diabetic complications. *J. Nat. Prod.* **67**, 103–105.

Paredez, A. R. (2006). Visualization of cellulose synthase demonstrates functional association with microtubules. *Science.* 1491–1495.

Parton, R. M., Dyer, A. F., Read, N. D. and Trewavas, A. J. (2000). Apical structure of actively growing fern rhizoids examined by DIC and confocal microscopy. *Ann. Bot.* **85**, 233–245.

Peaucelle, A. and Couder, Y. (2016). Fibonacci spirals in a brown alga [*Sargassum muticum* (Yendo) Fensholt] and in a land plant [*Arabidopsis thaliana* (L.) Heynh.]: a case of morphogenetic convergence. *Acta Soc. Bot. Pol.* **85**, 3526. DOI:10.5586/asbp.3526.

Peaucelle, A., Louvet, R., Johansen, J. N., Höfte, H., Laufs, P., Pelloux, J. and Mouille, G. (2008). *Arabidopsis* phyllotaxis is controlled by the methyl-esterification status of cell-wall pectins. *Curr. Biol.* **18**, 1943–1948.

Peaucelle, A., Braybrook, S. A., Le Guillou, L., Bron, E., Kuhlemeier, C. and Höfte, H. (2011). Pectin-induced changes in cell wall mechanics underlie organ initiation in *Arabidopsis*. *Curr. Biol.* **21**, 1720–1726.

Peng, H. B. and Jaffe, L. F. (1976). Cell-wall formation in *Pelvetia* embryos. A freeze-fracture study. *Planta* **133**, 57–71.

Percival, E. G. V and Ross, A. G. (1950). Fucoidin. Part I . The isolation and purification od fucoidin from brown seaweeds. *J. Chem. Soc.* 717–720.

Pereira, M. G., Benevides, N. M. B., Melo, M. R. S., Valente, A. P., Melo, F. R. and Mourão, P. A. S. (2005). Structure and anticoagulant activity of a sulfated galactan from the red alga, *Gelidium crinale*. Is there a specific structural requirement for the anticoagulant action? *Carbohydr. Res.* **340**, 2015–2023.

Pereira, T. R., Engelen, A. H., Pearson, G., Serrão, E., Destombe, C. and Valero, M. (2011). Temperature effects on gametophyte development of L. ochroleuca and S. polyschides, kelps with contrasting life histories. *Cah. Biol. Mar.* **52**, 395–403.

Peters, N. T. and Kropf, D. L. (2010). Asymmetric microtubule arrays organize the

endoplasmic reticulum during polarity establishment in the brown alga *Silvetia compressa*. *Cytoskeleton* **67**, 102–111.

Peters, A. F., Scornet, D., Ratin, M., Charrier, B., Monnier, A., Merrien, Y., Corre, E., Coelho, S. M. and Cock, J. M. (2008). Life-cycle-generation-specific developmental processes are modified in the immediate upright mutant of the brown alga *Ectocarpus siliculosus*. *Development* **135**, 1503–1512.

Pettolino, F. A., Walsh, C., Fincher, G. B. and Bacic, A. (2012). Determining the polysaccharide composition of plant cell walls. *Nat. Protoc.* **7**, 1590–1607.

Picton, J. M. and Steer, M. W. (1982). A model for the mechanism of tip extension in pollen tubes. *J. Theor. Biol.* **98**, 15–20.

Pierson, E. S., Miller, D. D., Callaham, D. A., Shipley, A. M., Rivers, B. A., Cresti, M. and Hepler, P. K. (1994). Pollen tube growth is coupled to the extracellular calcium ion flux and the intracellular calcium gradient: effect of BAPTA-type buffers and hypertonic media. *Plant Cell* **6**, 1815–1828.

Pierson, E. S., Miller, D. D., Callaham, D. A., van Aken, J., Hackett, G. and Hepler, P. K. (1996). Tip-localized calcium entry fluctuates during pollen tube growth. *Dev. Biol.* **174**, 160–173.

Podkorytova, A. V, Vafina, L. H., Kovaleva, E. A. and Mikhailov, V. I. (2007). Production of algal gels from the brown alga, *Laminaria japonica* Aresch., and their biotechnological applications. *J. Appl. Phycol.* **19**, 827–830.

Popper, Z. A., Michel, G., Herve, C., Domozych, D. S., Willats, W. G., Tuohy, M. G., Kloareg, B. and Stengel, D. B. (2011). Evolution and diversity of plant cell walls: from algae to flowering plants. *Annu. Rev. Plant Biol.* **62**, 567–590.

Pu, R., Wozniak, M. and Robinson, K. R. (2000). Cortical actin filaments form rapidly during photopolarization and are required for the development of calcium gradients in *Pelvetia* compressa zygotes. *Dev. Biol.* **222**, 440–449.

Purves, C. B. (1954). Chain structure. In *Cellulose and cellulose derivatives: Part I*, p. 539.

Quatrano, R. S. (1968). Rhizoid formation in *Fucus* zygotes: dependence on protein and ribonucleic acid syntheses. *Science.* **162**, 468–470.

Quatrano, S. (1973). Separation of processes associated with differentiation of two-celled *Fucus* embryos. *Dev. Biol.* **30**, 209–213.

Quatrano, R. S. (1978). Development of cell polarity. *Annu. Rev. Plant Physiol.* **20**, 487–510.

Quatrano, R. S. and Crayton, M. A. (1973). Sulfation of fucoidan in *Fucus* embryos. I. Possible role in localization. *Dev. Biol.* **30**, 29–41.

Quatrano, R. and Shaw, S. (1997). Role of the cell wall in the determination of cell polarity and the plane of cell division in embryos. *Trends Plant Sci.* **2**, 15–21.

Quatrano, R. S. and Stevens, P. T. (1976). Cell wall assembly in *Fucus* zygotes I. Characterization of the polysaccharide components. *Plant Physiol.* **62**, 518–525.

Quatrano, R. S., Griffing, L. R., Huber-Walchli, V. and Doubet, R. S. (1985). Cytological and biochemical requirements for the establishment of a polar cell. *J. Cell Sci.* **2**, 129–141.

Quint, M., Drost, H. G., Gabel, A., Ullrich, K. K., Bönn, M. and Grosse, I. (2012). A transcriptomic hourglass in plant embryogenesis. *Nature* **490**, 98–101.

Ragan, M. A. (1976). Physodes and the phenolic compounds of brown algae , composition and significance of physodes in vivo. *Bot. Mar.* **14**, 145–154.

Rehm, B. H. A. and Valla, S. (1997). Bacterial alginates: biosynthesis and applications. *Appl. Microbiol. Biotechnol.* **48**, 281–288.

Reinhardt, D., Wittwer, F., Mandel, T. and Kuhlemeier, C. (1998). Localized upregulation of a new expansin gene predicts the site of leaf formation in the tomato meristem. *Plant Cell* **10**, 1427–1437.

Reinhardt, D., Mandel, T. and Kuhlmeier, C. (2000). Auxin regulates the initiation and radial position of plant lateral organs. *Plant Cell* **12**, 507–518.

Reinhardt, D., Pesce, E. R., Stieger, P., Mandel, T., Baltensperger, K., Bennett, M., Traas, J., Friml, J. and Kuhlemeier, C. (2003a). Regulation of phyllotaxis by polar auxin transport. *Nature* **426**, 255–260.

Reinhardt, D., Frenz, M., Mandel, T. and Kuhlmeier, C. (2003b). Microsurgical and laser ablation analysis of interactions between the zones and layers of the tomato shoot apical meristem. *Development* **130**, 4073–4083.

Renzaglia, K. S., Du¡, R. J., Nickrent, D. L. and Garbary, D. J. (2000). Vegetative and reproductive innovations of early land plants: implications for a uni ed phylogeny. *Philos. Trans. R. Soc. B* 769–793.

Reyes-Prieto, A., Weber, A. P. M. and Bhattacharya, D. (2007). The origin and establishment of the plastid in algae and plants. *Annu. Rev. Genet.* **41**, 147–168.

Riquelme, M. (2013). Tip growth in filamentous fungi: a road trip to the apex. *Annu. Rev. Microbiol.* **67**, 587–609.

Roberts, S. K., Gillot, I. and Brownlee, C. (1994). Cytoplasmic calcium and Fucus egg activation. *Development* **120**, 155–163.

Robinson, K. R. (1996). Calcium and the photopolarization of *Pelvetia* zygotes. *Planta* **198**, 378–384.

Robinson, K. R. and Jaffe, L. F. (1975). Polarising fucoid eggs drive a calcium curent through themselves. *Science.* **187**, 70–72.

Robinson, M. D. and Oshlack, A. (2010). A scaling normalization method for differential expression analysis of RNA-seq data. *Genome Biol.* **11**, http://genomebiology.com/2010/11/3/R25.

Rohland, N. and Reich, D. (2012). Cost-effective, high-throughput DNA sequencing libraries for multiplexed target capture. *Genome Res.* **22**, 939–946.

Rusig, A. M., Leguyader, H. and Ducreux, G. (1994). Dedifferentiation and microtubule reorganization in the apical cell protoplast of *Sphacelaria* (Phaeophyceae). *Protoplasma* **179**, 83–94.

Saga, N., Uchida, T. and Sakai, Y. (1978). Clone *Laminaria* from single isolated cell. *Bull. Japanese Soc. Sci. Fish.* **44**, 87.

Sampathkumar, A., Yan, A., Krupinski, P. and Meyerowitz, E. M. (2014). Physical forces regulate plant development and morphogenesis. *Curr. Biol.* **24**, 475–483.

Sawabe, T., Ezura, Y. and Kimura, T. (1993). Application of an alginate lyase from Alteromonas sp. for isolation of protoplasts from a brown algae Laminaria japonica. *Nippon Suisan Gakkaishi* **59**, 705–709.

Scheres, B. (2001). Plant cell identity. The role of position and lineage. *Plant Physiol.* **125**, 112–114.

Schmiedel, G. and Schnepf, E. (1980). Polarity and growth of caulonema tip cells of the moss *Funaria hygrometri*ca. *Planta* **197147**, 405–413.

Schoenwaelder, M. E. (2002). The occurrence and cellular significance of physodes in brown algae. *Phycologia* **41**, 125–139.

Schüepp, O. (1926). Meristeme. In *Handbuch der Pflanzenanatomie*, p. Berlin: Gebrüder Borntraeger.

Schwuchow, J., Sack, F. D. and Hartmann, E. (1990). Microtubule distribution in gravitropic protonemata of the moss *Ceratodon*. *Protoplasma* **159**, 60–69.

Shaw, S. L. and Quatrano, R. S. (1996). The role of targeted secretion in the establishment of cell polarity and the orientation of the division plane in *Fucus* zygotes. *Development* **122**, 2623–2630.

Shibata, T., Fujimoto, K., Nagayama, K., Yamaguchi, K. and Nakamura, T. (2002). Inhibitory activity of brown algal phlorotannins against hyaluronidase. *Int. J. Food Sci. Technol.* **37**, 703–709.

Silberfeld, T., Leigh, J. W., Verbruggen, H., Cruaud, C., de Reviers, B. and Rousseau, F. (2010). A multi-locus time-calibrated phylogeny of the brown algae (Heterokonta, Ochrophyta, Phaeophyceae): Investigating the evolutionary nature of the “brown algal crown radiation.” *Mol. Phylogenet. Evol.* **56**, 659–674.

Simão, F. A., Waterhouse, R. M., Ioannidis, P., Kriventseva, E. V and Zdobnov,

E. M. (2015). BUSCO: Assessing genome assembly and annotation completeness with single-copy orthologs. *Bioinformatics* **31**, 3210–3212.

Simons, E. B. (1906). A morphological study of *Sargassum filipendula*. *Bot. Gazzette* **41**, 161–182.

Smidsrød, O., Haug, A. and Bjørn, L. (1972). Properties of ply(1,4-hexuronates) in the gel state I. Evaluation of a method for the determination of stiffness. *Acta Chem. Scand.* **26**, 71–78.

Snow, M. and Snow, R. (1935). Experiments on phyllotaxis. III. diagonal splits through decussate apices. *Philos. Trans. R. Soc. B Biol. Sci.* **225**, 63–94.

Snow, M. and Snow, R. (1937). Auxin and leaf formation. *New Phytol.* **36**, 1–18.

Steer, M. W. and Steer, J. M. (1989). Pollen tube tip growth. *New Phytol.* **111**, 323–358.

Steeves, T. and Sussex, I. (1989). *Patterns in plant development*. UK: Cambridge University Press.

Steinhorst, L. and Kudla, J. (2013). Calcium - a central regulator of pollen germination and tube growth. *Biochim. Biophys. Acta - Mol. Cell Res.* **1833**, 1573–1581.

Steneck, R. S., Graham, M. H., Bourque, B. J., Corbett, D., Erlandson, J. M., Estes, J. A. and Tegner, M. J. (2002). Kelp forest ecosystems: biodiversity, stability, resilience and future. *Mar. Sci. Fac. Scholarsh.**65**, http://digitalcommons.library.umaine.edu/sms_facpub/65*

Strachan, S. D. and Hess, F. D. (1983). The biochemical mechanism of action of the dinitroaniline herbicide oryzalin. *Pestic. Biochem. Physiol.* **20**, 141–150.

Sun, H., Basu, S., Brady, S. R., Luciano, R. L. and Muday, G. K. (2004). Interactions between auxin transport and the actin cytoskeleton in developmental polarity of *Fucus distichus* embryos in response to light and gravity. *Plant Physiol.* **135**, 266–78.

Svanem, B. I., Skjåk-Braek, G., Ertesvåg, H. and Valla, S. (1999). Cloning and expression of three new *Azotobacter vinelandi*i genes closely related to a previously described gene family encoding mannuronan C-5-epimerases. *J. Bacteriol.* **181**, 68–77.

Swinton, J. (2004). Watching the daisies grow: Turing and Fibonacci phyllotaxis. In *Alan Turing: life and legacy of a great thinker* (ed. Teuscher, C.), pp. 477–498. Berlin, Heidelberg: Springer Berlin Heidelberg.

Taheri-Talesh, N., Horio, T., Araujo-Bazan, L., Dou, X., Espeso, E. A., Penalva, M. A., Osmani, S. A. and Oakley, B. R. (2008). The tip growth apparatus of *Aspergillus nidulans*. *Mol. Biol. Cell* **19**, 1429–1449.

Tamura, H., Mine, I. and Okuda, K. (1996). Cellulose-synthesizing terminal

complexes and microfibril structure in the brown alga *Sphacelaria rigidula* (Sphacelariales, Phaeophyceae). *Phycol. Res.* **44**, 63–68.

Tapia, J. E., González, B., Goulitquer, S., Potin, P. and Correa, J. A. (2016). Microbiota influences morphology and reproduction of the brown alga *Ectocarpus sp*. *Front. Microbiol.* **7**,DOI:10.3389/fmicb.2016.00197.

Targett, N. M. and Arnold, T. M. (1998). Predicting the effects of brown algal phlorotannins on marine herbivores in tropical and temperate oceans. *J. Phycol.* **34**, 195–205.

Targett, N. M., Coen, L. D., Boettcher, A. A. and Tanner, C. E. (1992). Biogeographic comparisons of marine algal polyphenolics: evidence against a latitudinal trend. *Oecologia* **89**, 464–470.

Tesson, B. and Charrier, B. (2014). Brown algal morphogenesis: atomic force microscopy as a tool to study the role of mechanical forces. *Front. Plant Sci.* **5**, 471.

Thomas, F., Lundqvist, L. C. E., Jam, M., Jeudy, A., Barbeyron, T., Sandstrom, C., Michel, G. and Czjzek, M. (2013). Comparative characterization of two marine alginate lyases from *Zobellia galactanivorans* reveals distinct modes of action and exquisite adaptation to their natural substrate. *J. Biol. Chem.* **288**, 23021–23037.

Thompson, D. W. (1917). *On growth and form*. UK: Cambridge University Press.

Torode, T. A., Marcus, S. E., Jam, M., Tonon, T., Blackburn, R. S., Herve, C. and Knox, J. P. (2015). Monoclonal antibodies directed to fucoidan preparations from brown algae. *PLoS One* **10**, e0118366.

Torode, T. A., Siméon, A., Marcus, S. E., Jam, M., Le Moigne, M. A., Duffieux, D., Knox, J. P. and Hervé, C. (2016). Dynamics of cell wall assembly during early embryogenesis in the brown alga *Fucus*. *J. Exp. Bot.,*DOI: 10.1093/jxb/erw369

Tucker, B. E., Hoch, H. C. and Staples, R. C. (1986). The involvement of F-actin in *Uromyces* cell differentiation: The effects of cytochalasin E and phalloidin. *Protoplasma* **135**, 88–101.

Uehara, T., Takeshita, M. and Maeda, M. (1992). Studies on anticoagulant-active arabinan sulfates from the green alga, *Codium latum*. *Carbohydr. Res.* **235**, 309–311.

Van Alstyne, K. L. (1989). Adventitious branching as a herbivore-induced defense in the intertidal brown alga *Fucus distichus*. *Mar. Ecol. Prog. Ser.* **56**, 169–176.

Vidali, L., Mckenna, S. T. and Hepler, P. K. (2001). Actin polymerization is essential for pollen tube growth. *Mol. Biol. Cell* **12**, 2534–2545.

Vogler, H., Draeger, C., Weber, A., Felekis, D., Eichenberger, C., Routier-Kierzkowska, A. L., Boisson-Dernier, A., Ringli, C., Nelson, B. J., Smith, R.

S., et al. (2013). The pollen tube: a soft shell with a hard core. *Plant J.* **73**, 617–627.

Vreeland, V. and Laetsch, W. M. (1989). Identification of associating carbohydrate sequences with labelled oligosaccharides. *Planta* **177**, 423–434.

Wang, T., Jónsdóttir, R., Liu, H., Gu, L., Kristinsson, H. G., Raghavan, S. and Ólafsdóttir, G. (2012). Antioxidant capacities of phlorotannins extracted from the brown algae *Fucus vesiculosus*. *J. Agric. Food Chem.* **60**, 5874–5883.

Wardlaw, C. W. (1949). Phyllotaxis and organogenesis in ferns. *Nature* 167–169.

Wargacki, A. J., Leonard, E., Win, M. N., Regitsky, D. D., Santos, C. N. S., Kim, P. B., Cooper, S. R., Raisner, R. M., Herman, A., Sivitz, A. B., et al. (2012). An engineered microbial platform for direct biofuel production from brown macroalgae. *Science.* **335**, 308–313.

Wei, N., Quarterman, J. and Jin, Y. S. (2013). Marine macroalgae: An untapped resource for producing fuels and chemicals. *Trends Biotechnol.* **31**, 70–77.

Ye, N., Zhang, X., Miao, M., Fan, X., Zheng, Y., Xu, D., Wang, J., Zhou, L., Wang, D., Gao, Y., et al. (2015). *Saccharina* genomes provide novel insight into kelp biology. *Nat. Commun.* **6**, 6986.

Yoon, H. S., Hackett, J. D., Ciniglia, C., Pinto, G. and Bhattacharya, D. (2004). A molecular timeline for the origin of photosynthetic eukaryotes. *Mol. Biol. Evol.* **21**, 809–818.

Yoshida, T., Majima, T. and Marui, M. (1983). Apical organization of some genera of Fucales (Phaeophyta) from Japan. *J. Fac. Sci. Hokkaido Univ.* **13**, 49–56.

Yue, J., Hu, X. and Huang, J. (2014). Origin of plant auxin biosynthesis. *Trends Plant Sci.* **19**, 764–770.

Zerzour, R., Kroeger, J. and Geitmann, A. (2009). Polar growth in pollen tubes is associated with spatially confined dynamic changes in cell mechanical properties. *Dev. Biol.* **334**, 437–446.

Zhao, D., Zhuo, R. X. and Cheng, S. X. (2012). Alginate modified nanostructured calcium carbonate with enhanced delivery efficiency for gene and drug delivery. *Mol. Biosyst.* **8**, 753–759.

Zhu, B. and Yin, H. (2015). Alginate lyase: Review of major sources and classification, properties, structure-function analysis and applications. *Bioengineered* **6**, 125–131.

Zonia, L. and Munnik, T. (2008). Vesicle trafficking dynamics and visualization of zones of exocytosis and endocytosis in tobacco pollen tubes. *J. Exp. Bot.* **59**, 861–873.

Appendices

Appendix 1. List of available antibodies against brown algal sulphated fucans and alginate. BAM1-4 target sulphated fucan epitopes, BAM6-11 target alginate epitopes.

	Antibody	Epitope
Sulphated fucan	BAM1	non-sulphated epitope that is present on a sulphated glycan
	BAM2	specific to sulphated fucan/fucoidan preparations, with no clear epitope
	BAM3	specific to sulphated fucan/fucoidan preparations, with no clear epitope
	BAM4	sulphated epitope
Alginate	BAM6	M-rich epitope
	BAM7	MG-rich epitope
	BAM8	MG-rich epitope
	BAM9	MG-rich epitope
	BAM10	G-rich epitope
	BAM11	epitope of 7 G residues

Appendix 2. Effect of different indentation settings on the embryo rhizoid stiffness. Apparent Young's modulus maps (100 x 100 µm) of embryo rhizoids in artificial seawater (A) and artificial seawater with mannitol (B) under different indentation forces. The lack of one image in A originates from the data corruption that was detected post imaging. RSP – relative setpoint, SP – setpoint.

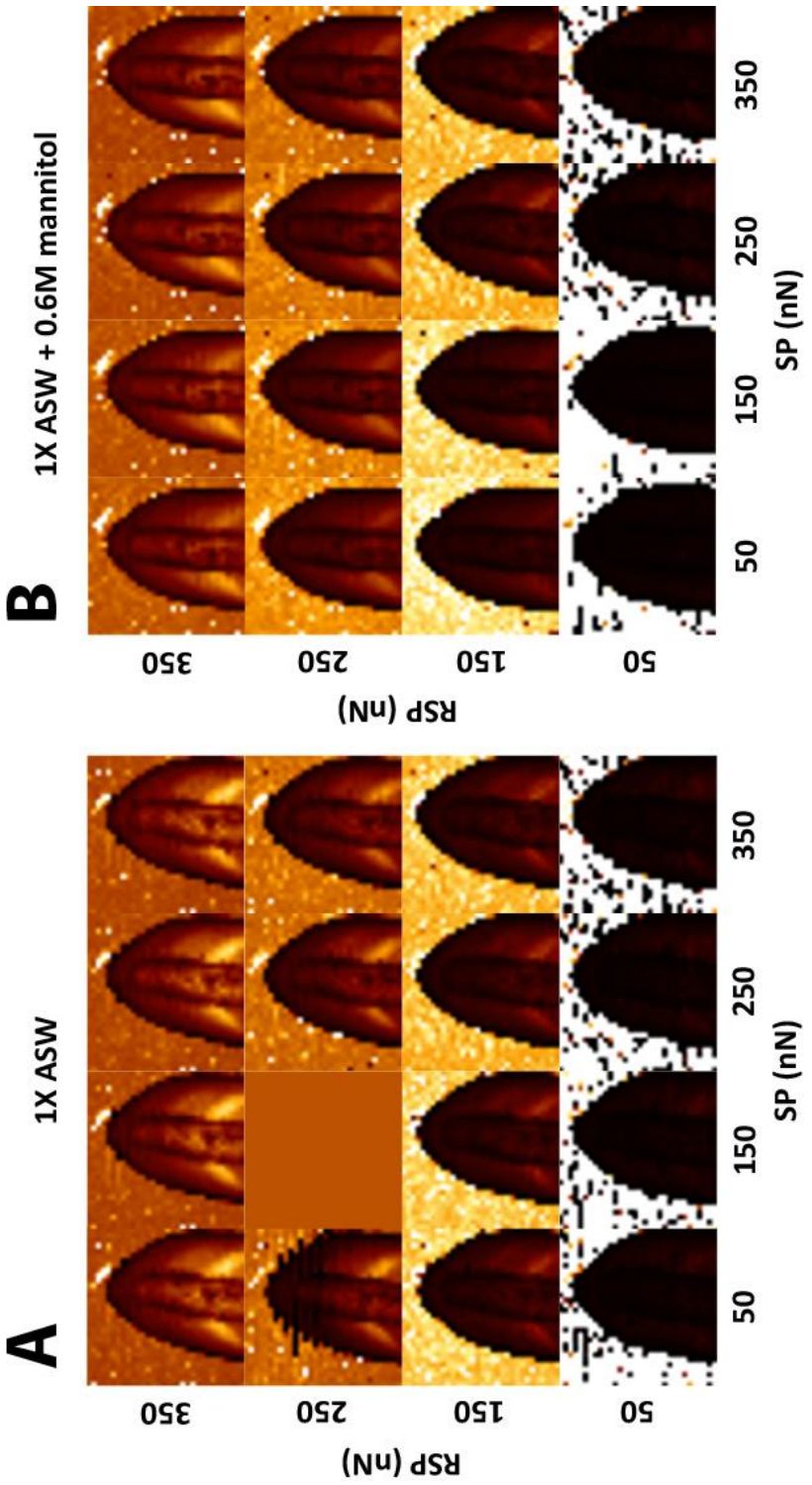

Appendix 3. BLAST analysis of the *Ectocarpus siliculosus* mannuronan C-5 epimerases (MC5Es) against the *F. vesiculosus* transcriptome data. The protein sequences from a family of MC5Es in *E. siliculosus* were aligned with BLAST against a known database of *F. vesiculosus* transcriptome (Martins et al., 2013). The BLAST resulted in obtaining 7 different corresponding reads (column 2; 4 unique reads depicted in different colours).

E. siliculosus **epimerase ID**	***F. vesiculosus*** **transcriptome read ID**
MEP7	SRR575725.241546.2 MS_VSBGE02F0TBO
MEP8	SRR575725.241546.2 MS_VSBGE02F0TBO
MEP6	SRR575725.241546.2 MS_VSBGE02F0TBO
MEP12	SRR575725.241546.2 MS_VSBGE02F0TBO
MEP5	SRR575725.241546.2 MS_VSBGE02F0TBO
MEP9	SRR575725.241546.2 MS_VSBGE02F0TBO
MEP16	SRR575725.241546.2 MS_VSBGE02F0TBO
MEP17	SRR575725.241546.2 MS_VSBGE02F0TBO
MEP4	SRR575725.241546.2 MS_VSBGE02F0TBO
MEP7	SRR575725.244229.2 VS_VSBGE02FM033
MEP4	SRR575725.244229.2 VS_VSBGE02FM033

MEP14	SRR575725.244229.2 VS_VSBGE02FM033
MEP8	SRR575725.244229.2 VS_VSBGE02FM033
MEP2	SRR575725.244229.2 VS_VSBGE02FM033
MEP6	SRR575725.244229.2 VS_VSBGE02FM033
MEP12	SRR575725.244229.2 VS_VSBGE02FM033
MEP5	SRR575725.244229.2 VS_VSBGE02FM033
MEP9	SRR575725.244229.2 VS_VSBGE02FM033
MEP20	SRR575725.244229.2 VS_VSBGE02FM033
MEP22	SRR575725.244229.2 VS_VSBGE02FM033
MEP16	SRR575725.244229.2 VS_VSBGE02FM033
MEP11	SRR575725.244229.2 VS_VSBGE02FM033
MEP17	SRR575725.244229.2 VS_VSBGE02FM033
MEP15	SRR575725.244229.2 VS_VSBGE02FM033
MEP18	SRR575725.244229.2 VS_VSBGE02FM033
MEP23	SRR575725.244229.2 VS_VSBGE02FM033
MEP21	SRR575725.244229.2 VS_VSBGE02FM033

MEP3	SRR575725.244229.2 VS_VSBGE02FM033
MEP25	SRR575725.244229.2 VS_VSBGE02FM033
MEP1	SRR575725.253007.2 FS_VSBGE01EXOXP
MEP13	SRR575725.253007.2 FS_VSBGE01EXOXP
MEP4	SRR575725.253007.2 FS_VSBGE01EXOXP
MEP27 C-terminal	SRR575725.253453.2 MN_VSBGE01BWBBD
MEP7	SRR575725.28278.2 VN_VSBGE02IJPX7
MEP8	SRR575725.28278.2 VN_VSBGE02IJPX7
MEP2	SRR575725.28278.2 VN_VSBGE02IJPX7
MEP6	SRR575725.28278.2 VN_VSBGE02IJPX7
MEP5	SRR575725.28278.2 VN_VSBGE02IJPX7
MEP9	SRR575725.28278.2 VN_VSBGE02IJPX7
MEP22	SRR575725.28278.2 VN_VSBGE02IJPX7
MEP16	SRR575725.28278.2 VN_VSBGE02IJPX7
MEP11	SRR575725.28278.2 VN_VSBGE02IJPX7
MEP17	SRR575725.28278.2 VN_VSBGE02IJPX7

MEP15	SRR575725.28278.2 VN_VSBGE02IJPX7
MEP10	SRR575725.28278.2 VN_VSBGE02IJPX7
MEP21	SRR575725.28278.2 VN_VSBGE02IJPX7
MEP25	SRR575725.28278.2 VN_VSBGE02IJPX7
MEP4	SRR575725.28278.2 VN_VSBGE02IJPX7
MEP13	SRR575725.32281.2 FS_VSBGE02IGC9G
MEP17	SRR575725.56536.2 FN_VSBGE02GWL5E
MEP26	x
MEP27 central	x
MEP28	x
MEP24	x

Appendix 4. Sequences corresponding to the MC5E gene fragments amplified from *F. serratus* embryos. Sequenced PCR fragments showed 4 unique nucleotide sequences detected in the *F. serratus* embryos out of 7 reads initially aligned to the *F. vesiculosus* transcriptome (Martins et al., 2013).

>SRR575725.241546.2 MS_VSBGE02F0TBO

GATGGTCGTTCTTACATCAGCGCCGTGTCGGAGGTGTTGATCGAGGGCATGC
TGGGCTGCGAGGGCACCGCGAAGAATGAGATGGGCGAGGCTCGAATGGAC
GTGGTCAAGTCGGAGATCGCCTACATCGGGTACAAGGACAGCGAGAGCTAC
GGCCTGACCTGGAAGGTCCGAGGCTTCTGCAAGGACAAAGCAACCCGGAGA
TCTTCGACTACGTTGGTGTCTATGGGAACATCTACGACTCCCATCTTCACCAC
CTGAACTTCGCCGTCTACACGTACGGTCATCAGGGCGAGACTGGCNCCGTAA
NAAGTCCATCCAACTCCGGATACGGATTCGACCCTCACGATGACTCGGACTA
TCCTCACCATCCACGACAACGAAGTCTGGGACAACCACTGGCACGGGATTAT
CGCCTCCAAGCGATGC

>SRR575725.28278.2 VN_VSBGE02IJPX7

TACGACCAAGATGAGAGCGATGGTCGTTCTTACATCAGCGCCGTGTCGGAGG
TGTTGATCGAGGGCATGCTGGGCTGCGAGGGCACCGCGAAGAATGAGATGG
GGCGAGGCTCGAATGGACGTGGTCAAGTCGGAGATCGCCTACATCGGGTAC
AAGGACAGCGAGAGCTACGGCCTGACCTGGAAGGTCCGAGGCTTCTGCAAG
GCAAAAAGCAACCCGGAGATCTTCGACTACGTTGGTGTCTATGGGAACATCT
ACGACTCCCATCTTCACCACCTGAACTTCGCCGTCTACACGTACGGTCATCA
GGCGGAGACTGGCGCCGTAACAAGTCCACTCCAACTCCGGATACGGATTCG
ACCCTCACGATGACTCGGACTATCTCACCATCCACGACAACCGAAGTCCTGG
GACAACCACTGGCACGGGATTATCGCCTCCAAGCGATGCAACAACGTTTCCA
TCCAGAACATG

>SRR575725.244229.2 VS_VSBGE02FM033

TGGTTGTCTTGCACGAGGTTGTTGATCCAAACCCCTCCGATGTGGCCAAAAC
TGTACATACCGTACCACATGTGGTGGATGTTGCAGTTTATGATGTTGCCCCTG
ACATTCACACTGTCGAACAAATCGAGGTTGCTAAGGTCCAAGCAAAGCCCGC
GAACCTTCCACGAGAGTCCATACGACTCAGTGGCATAGTATCCCATGAAGCC

CAACTCGCTGTCCTCCATGTCCATGCGGCACTCGCCCATATTGTTCTTAGCCA
AGCCCTCGCAGGTCTCATCCTCGTCAACGTTCTCGCTGACGCAGGATATGTA
GGAGCGCGGCGTAGATCCGTCACTATCGATGCCGAGGTCGACCGGCCCCTC
GATATCCTCGTCCCAGCTCTGAATCTTTGTTTTATAGATGTCGATGTTTCCTCC
GTGGCCCATTACGAAGTGCATGTTCG

>SRR575725.56536.2 FN_VSBGE02GWL5E

CTTGAAATCCGCGCCCATGGAGGTGACCTCGACATCAGCTACATCCAGATCT
TTTCTTGGGACTTGCTGGCTGGGACGTACGATGTCAACACTGACGACGGCAG
AAGTTTCCTAAGCGCAATCACCGAGAAGATCACAGGACGCATCGAGGACACG
TGCCCCGACGACCCCGTTGATGAAAACGACGATCCGGATTACAGCAACGGC
AGCGCCAAGGAGGACATGGGGAATGCTCGAATGGACATCTTCCGCTCCGAG
ATCGCATACCTTGGGTACGATGCATCGGAGTCGTATGGCATCTCCTACAAGG
CTCGCGGACTGTGCAAGGACCTAAGTAACCTCGACATCTACGACGACGACAA
CGGGCTTAACG

>SRR575725.253007.2 FS_VSBGE01EXOXP

TCGTGAAGGTGTTGTCGTGGATATCAGCGTCGAAAGATTCCAGGATGGCCAG
ACCTGCGTCCTGCATGTCATATACCACGTTGTCGTAAATCTCGCAGCTAATCC
GAGCTGCGATGGAGGAAGATTCCCGCAGCCTGAGCACCACCGTCGTAGACC
TCGTTTTCGTATATTTTGAGGTTGTTGCAGCGCTTGGACGCGATGATACCATG
ATTAACGTTGTCGTAGACTTCGTTG

>SRR575725.32281.2 FS_VSBGE02IGC9G

TTTCGTGAAGGTGTTGTCGTGGATATCAGCGTCGAAAGATTACCAGGATGGC
CAGACCCTGCGTCCTGCATGTCATATACCACGTTGTCGTAAATCTCGCAGCTA
ATCCGAGCTGCGATGGAGGAAGATTCCCGCAGCCTGAGCACCACCGTCGTA
GACCTCGTTTTCGTATATTTTGAGGTTGTTGCAGCGCTTGGACGCGATGATAC
CATGATTAACGTTGTCGTAGACTTCGTTG

>SRR575725.253453.2 MN_VSBGE01BWBBD

GATCCGGATTACAGCAACGGCAGCGCCAAGGAGGACATGGGGAATGCTCGA
ATGGACATCTTCCGCTCCGAGATCGCATACCTTGGGTACGATGCATCGGAGT

CGTATGGCATCTCCTACAAGGCTCGCGGACTGTGCAAGGACCTAAGTAACCT
CGACATCTACGACGACGACAACGGGCTGGACTACGGAGTTTCCGGAGACAT
TTACCGATCCGAAATCCACCATAACTGGTTCGGGCACTACTCGTGGGGACAC
GACGGGGGCAAGTGGCAGTACAACGAGGTCCACGACAACGTCGGCTACGG
C

Appendix 5. Primer sequences used to amplify the mannuronan C-5 epimerases (MC5Es) regions for RT-PCR (and future qPCR experiments). The sequences were designed in the software Primer3 (http://bioinfo.ut.ee/primer3-0.4.0/), with a length 100-150 bp and Tm 58-60ºC.

Gene name	Forward primer name	Reverse primer name
MC5E_241546	GGCTTCTGCAAGGACAAAAG	CAGGTGGTGAAGATGGGAGT
MC5E_243453	AGTAGTGCCCGAACCAGTTG	CATCTACGACGACGACAACG
MC5E_244229	GCGATTCTCCTTGTCAACTCA	CAACTTCGCCCCAATACG
MC5E_32281	CTGCGGTGGAGGAAGATG	ATGGTATCATCGCGTCGAA
EFalpha	TGCCGGTGATCATGTTCTTG	AAGTTCGAGAAGGAGGCCG
TUB	GGATCCACTTCATGCTCACG	CCATGTACTTCCCGTGCCTA

Appendix 6. List of candidate 'Trinity genes' from *F. serratus de novo* transcriptome assembly encoding mannuronan C5 epimerases. BLAST analysis was performed on a protein level where known *Ectocarpus* MC5Es were aligned against the predicted proteins from the transcriptome. Percentage of identity relates to the portion of the query sequence (*E. siliculosus* MC5E sequence) and the alignment length represents the number of codons in the query sequence that align to the predicted proteins of the transcriptome. E-value shows the significance level of the alignment.

Trinity gene ID	% identity	alignment length	e-value
TRINITY_DN35335_c2_g2	85.714	126	2.43E-76
TRINITY_DN34703_c0_g1	79.825	114	3.07E-59

TRINITY_DN38589_c4_g1 (MC5E_32281)	78.696	230	1.23E-135
TRINITY_DN35211_c0_g1	78.333	120	2.59E-60
TRINITY_DN34703_c0_g2	77.186	263	4.00E-152
TRINITY_DN33964_c0_g1 (MC5E_241546)	75.824	364	0.00E+00
TRINITY_DN38517_c2_g1	73.636	220	6.63E-118
TRINITY_DN35335_c2_g3	72.093	215	1.29E-116
TRINITY_DN38177_c0_g2	70.701	314	6.49E-161
TRINITY_DN35335_c2_g1	70.345	290	2.17E-118
TRINITY_DN35335_c1_g1	70.222	225	4.08E-114
TRINITY_DN36843_c1_g1	69.853	136	4.06E-58
TRINITY_DN36696_c0_g1	67.634	448	0.00E+00
TRINITY_DN35084_c0_g4	67.236	702	0.00E+00
TRINITY_DN36843_c2_g1	61.814	474	0.00E+00
TRINITY_DN36843_c2_g3	61.37	365	2.34E-142
TRINITY_DN35664_c0_g1	61.29	403	2.80E-174

TRINITY_DN33101_c4_g2 (MC5E_244229)	59.498	279	1.16E-110
TRINITY_DN36825_c2_g1	57.556	311	2.09E-117
TRINITY_DN36528_c0_g3 (MC5E_253453)	55.346	318	1.77E-108
TRINITY_DN35355_c1_g1	53.961	467	3.95E-165

Appendix 7. Sequence alignment of mannuronan C5 epimerases. 31 epimerases *from E. siliculosus* and 21 candidate epimerases from *F. serratus*. Although not a perfect alignment between all of the sequences, similarities are found between amino acid 610 and 1020.

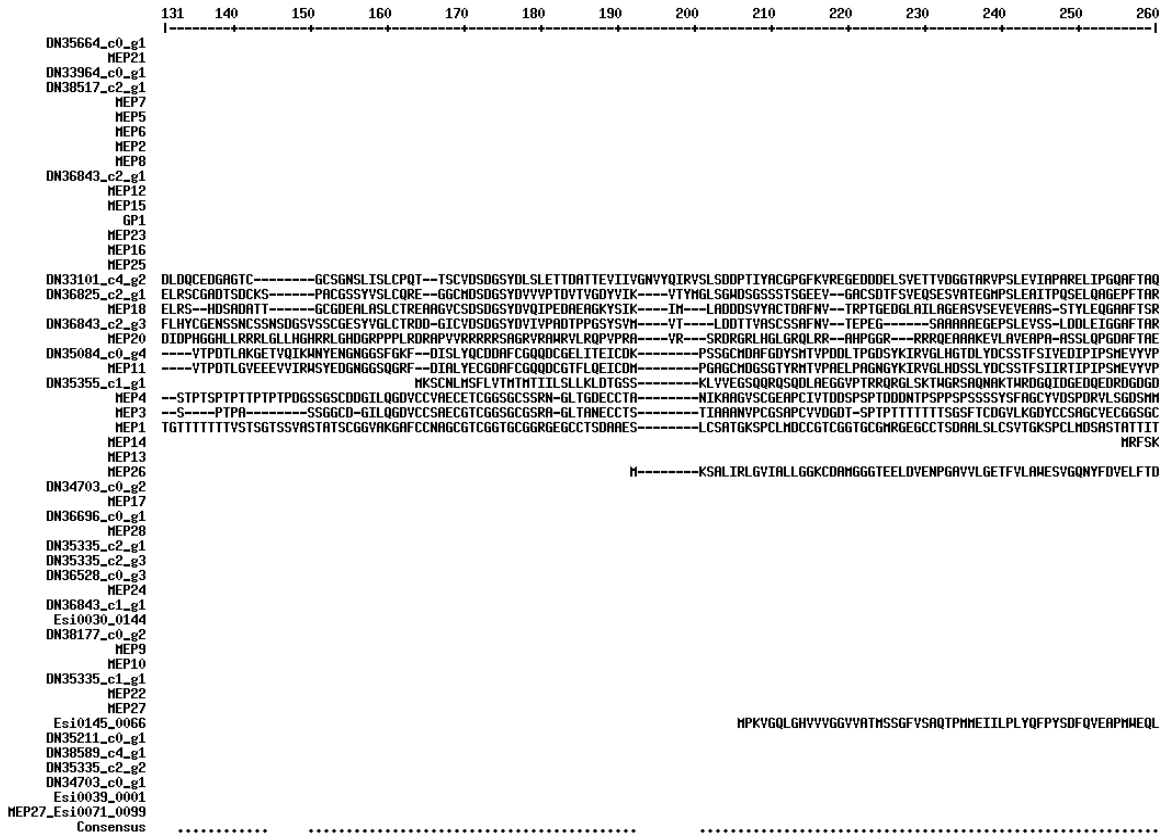

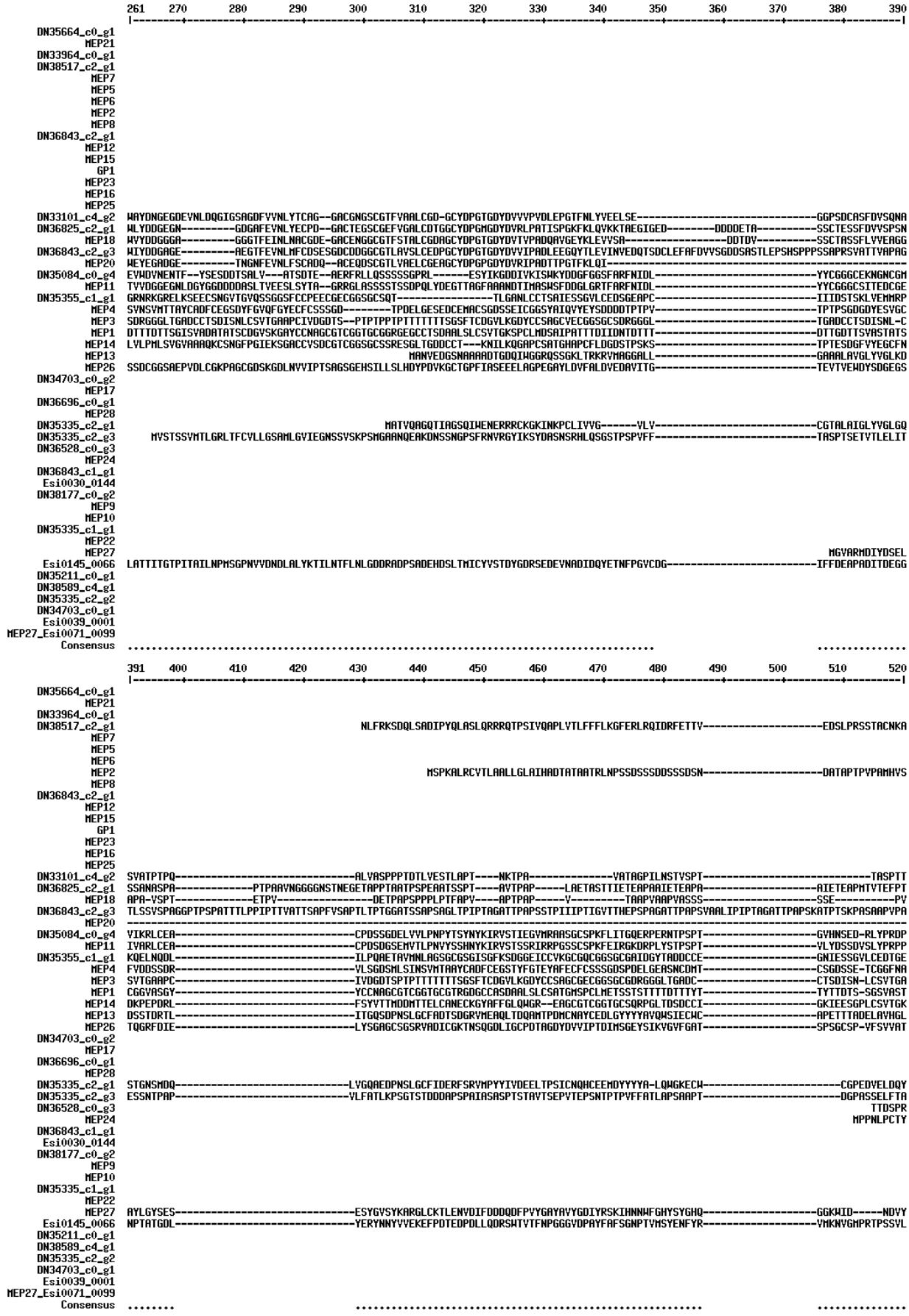

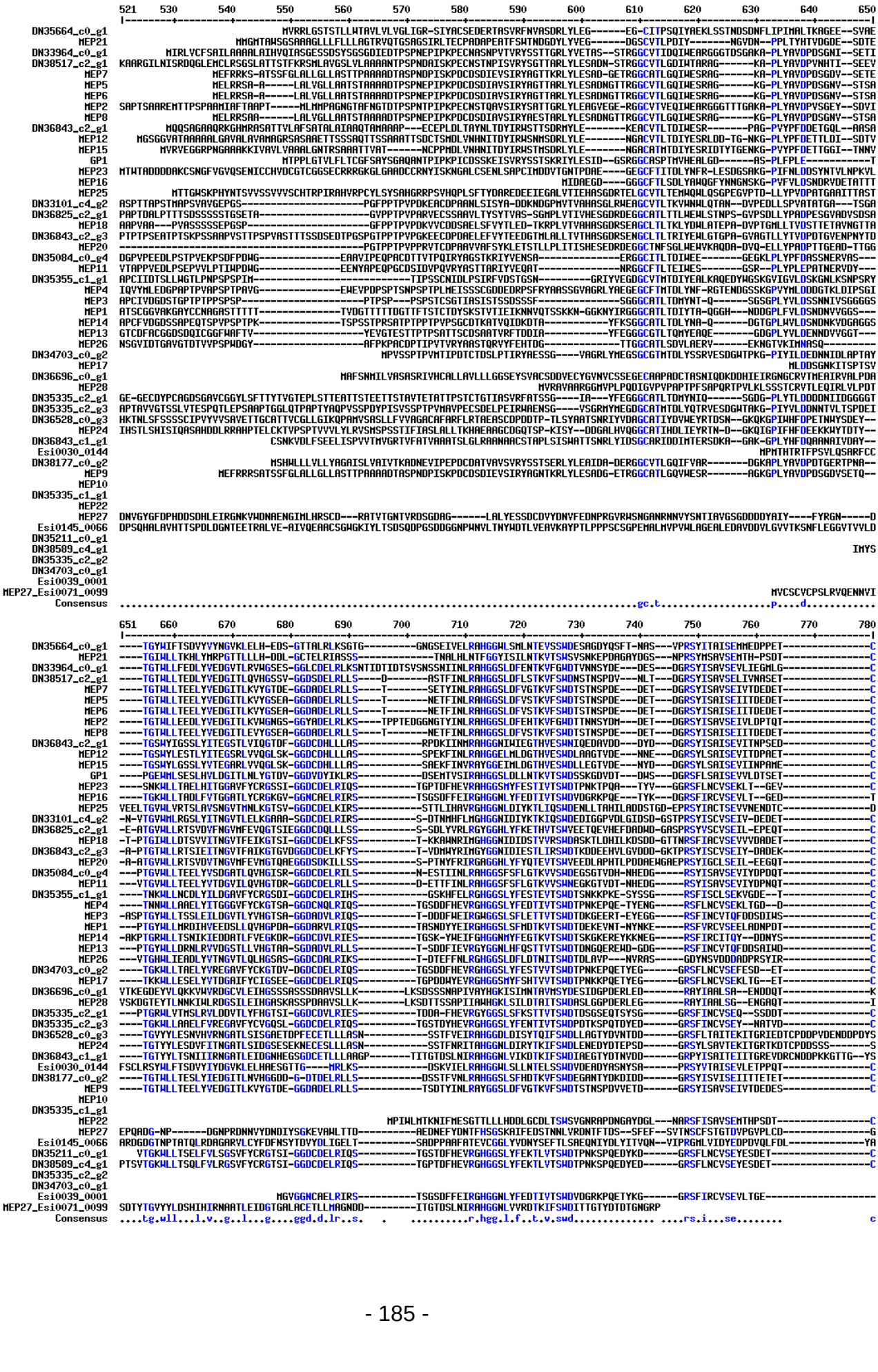

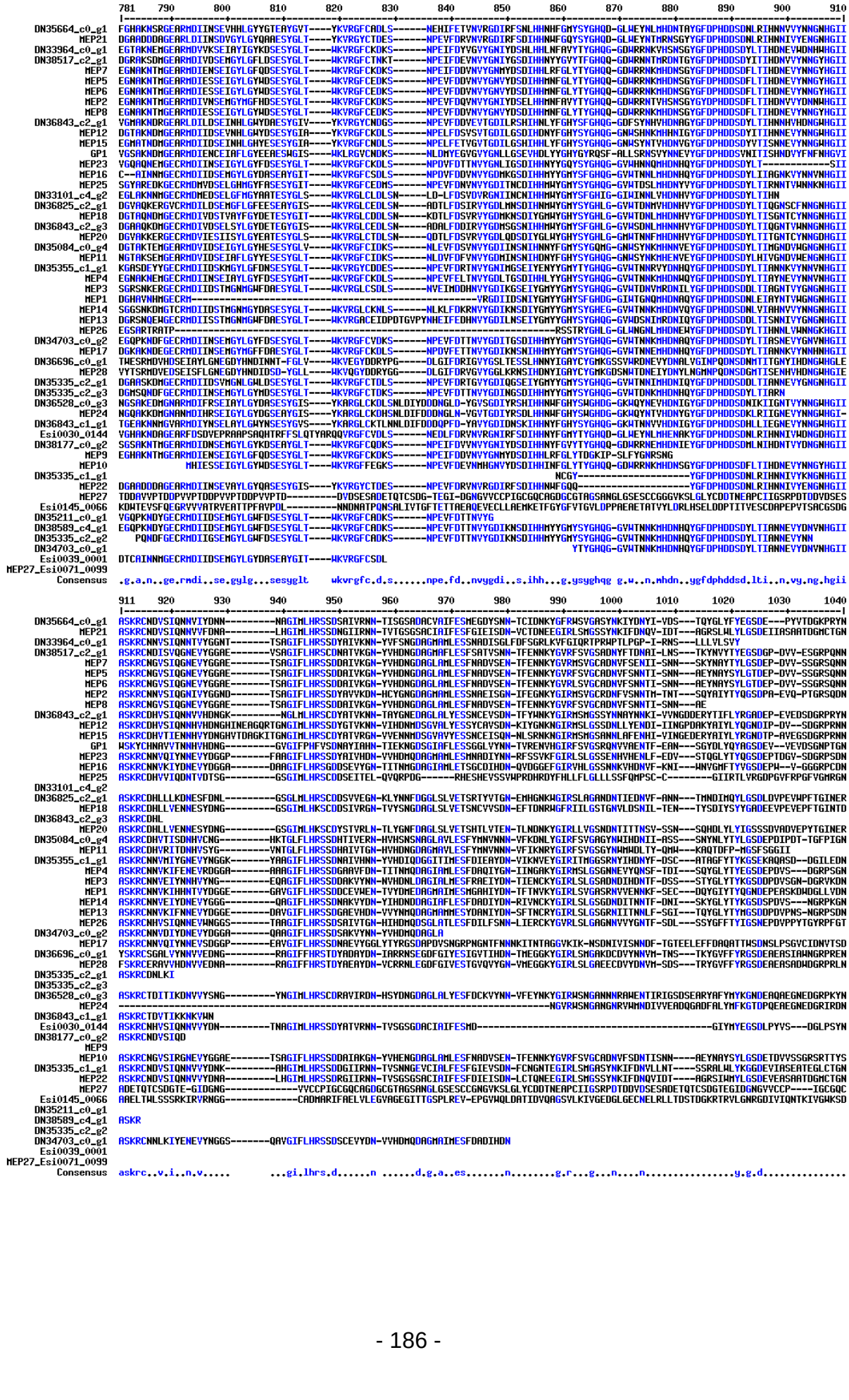

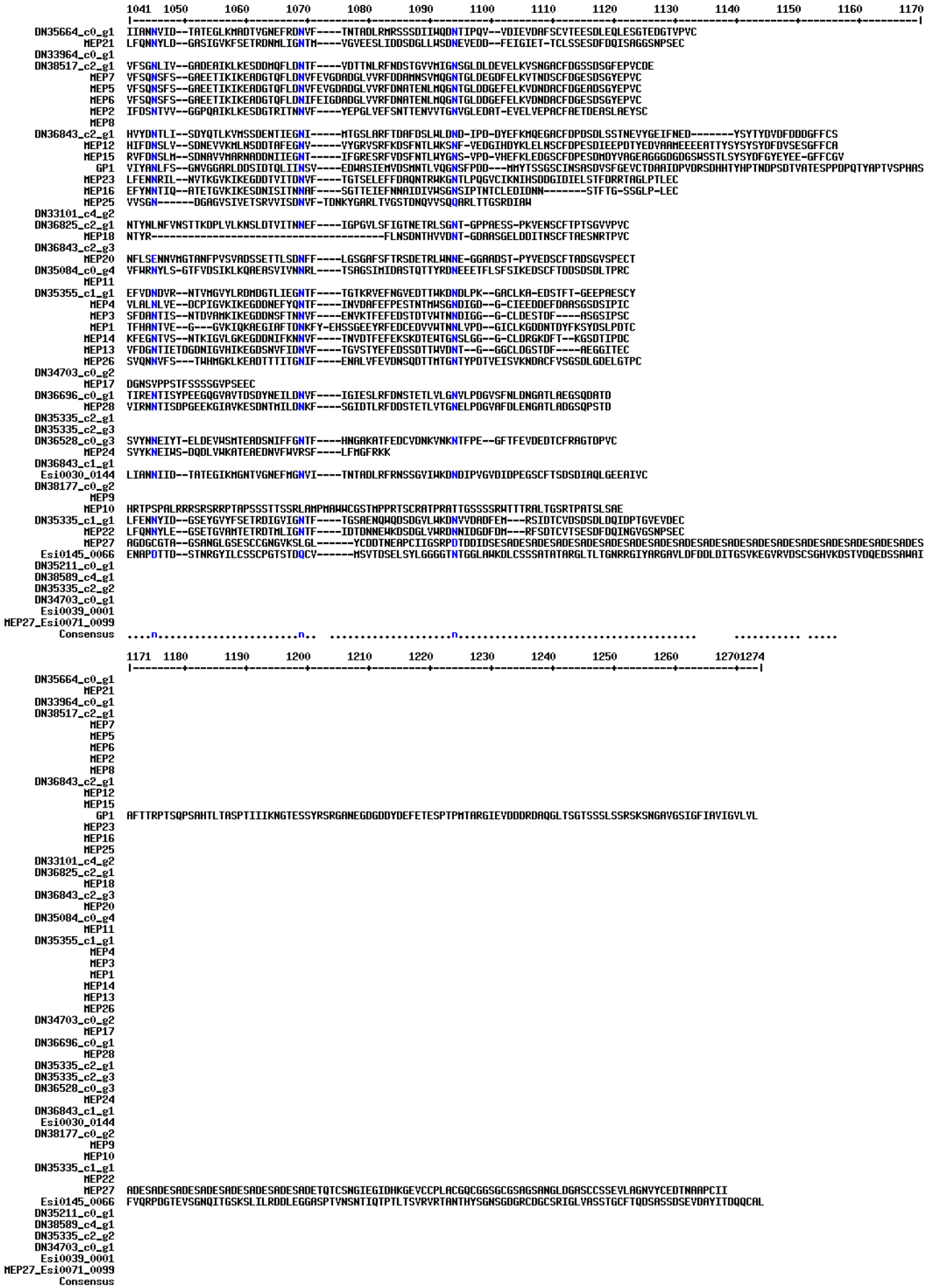

Appendix 8. Table of transcript expression values for *F. serratus* embryo developmental stages. R13, 14 and 15 represent three biological replicates.

MC5E candidate	R13_7h	R13_24h	R13_72h	R13_10d	R14_7h	R14_24h	R14_72h	R14_10d	R15_7h	R15_24h	R15_72h	R15_10d
TRINITY_DN35664_c0_g1	69.781	97.955	44.89	31.304	106.197	116.416	38.893	33.457	87.613	121.089	48.422	31.858
TRINITY_DN33101_c4_g2	10.938	37.374	55.935	51.61	18.653	44.486	55.131	52.957	16.261	49.52	58.777	47.699
TRINITY_DN33964_c0_g1	15.089	31.537	14.726	28.315	37.772	38.345	14.394	31.601	34.31	38.006	21.949	24.105
TRINITY_DN34703_c0_g1	3201.325	1092.459	341.885	167.548	4448.938	1088.93	114.04	165.626	3018.011	1240.784	187.121	210.039
TRINITY_DN34703_c0_g2	251.613	90.404	44.084	87.029	251.662	47.148	10.971	40.268	202.593	44.307	22.191	60.286
TRINITY_DN35084_c0_g4	14.601	18.372	8.562	6.893	23.042	26.542	11.133	7.483	19.739	27.152	11.022	6.656
TRINITY_DN35211_c0_g1	3720.535	1463.962	414.458	107.355	5927.075	1523.475	134.947	77.019	4466.14	1572.454	209.9	92.795
TRINITY_DN35335_c1_g1	12.591	12.276	9.741	9.65	15.965	16.757	11.068	8.798	19.702	17.315	11.108	7.697
TRINITY_DN35335_c2_g1	46.7	104.829	109.305	34.876	84.651	123.038	113.312	51.8	56.364	124.494	139.884	63.428
TRINITY_DN35335_c2_g2	561.56	233.932	108.87	175.065	182.688	58.888	23.472	174.237	144.038	51.008	32.088	201.682
TRINITY_DN35335_c2_g3	3.782	66.539	14.25	2.345	3.881	93.456	14.863	2.631	2.02	91.61	18.479	1.831
TRINITY_DN35355_c1_g1	14.054	105.867	5.077	24.693	41.214	147.544	4.79	27.225	41.829	153.003	5.355	19.187
TRINITY_DN36528_c0_g3	34.895	9.959	3.537	6.883	8.668	3.204	3.536	7.576	8.633	3.076	3.365	5.736
TRINITY_DN36696_c0_g1	44.072	135.848	80.526	42.202	56.233	151.147	53.569	42.125	45.233	142.928	63.38	45.17
TRINITY_DN36825_c2_g1	12.392	70.689	26.235	16.623	24.441	95.35	31.53	27.598	21.159	99.819	37.798	26.253
TRINITY_DN36843_c1_g1	0.358	0.825	0.259	14.148	0.343	0.43	0.138	10.776	0.453	0.769	0.104	10.44
TRINITY_DN36843_c2_g1	32.885	25.191	63.659	34.272	48.36	24.864	56.239	32.347	55.666	26.722	64.972	25.741
TRINITY_DN36843_c2_g3	10.57	16.297	16.639	35.53	9.217	16.368	16.894	36.853	5.596	21.619	18.998	31.561
TRINITY_DN38177_c0_g2	21.568	7.338	8.49	33.065	18.282	3.961	8.673	23.306	16.665	3.685	9.413	20.275
TRINITY_DN38517_c2_g1	285.612	69.744	43.619	12.9	482.271	29.183	5.016	3.769	408.579	20.581	3.443	9.175
TRINITY_DN38589_c4_g1	2490.768	991.901	301.927	173.193	3917.717	1036.204	102.252	158.703	2904.463	1060.169	156.382	178.804
TRINITY_DN38589_c4_g4	5.872	11.636	20.372	0.563	3.607	3.296	1.715	0.718	1.665	2.616	4.032	0.325

Appendix 9. Expression graphs of constantly expressed candidate MC5E Trinity genes. Graphs show Trinity genes with low probability of having a significant differential expression during *F. serratus* embryo development. Indicated under the Trinity gene name are the matching MC5E sequences described in Chapter 3.